

Josip Juraj Strossmayer University of Osijek
Faculty of Civil Engineering and Architecture Osijek

Postgraduate University Study Programme in Civil Engineering

Doctoral dissertation

Seismic behaviour of traditional rammed earth walls from eastern Croatia area

Ana Perić Fekete M. Sc. in Civ. Eng.

Osijek, mm gggg

Sveučilište Josipa Jurja Strossmayera u Osijek

Građevinski i arhitektonski fakultet Osijek

Doktorski studij Građevinarstvo

Doktorski rad

Potresno ponašanje tradicijskih zidova od nabijene zemlje s područja istočne Hrvatske

Ana Perić Fekete, mag. ing. aedif

U Osijeku, mm.gggg.

Prosudbena povjerenstva i bibliografski podaci

Povjerenstvo za prihvaćanje teme doktorskog rada

Povjerenstvo za prihvaćanje teme doktorskog rada imenovano na **n. redovitoj - izvarednoj** sjednici Fakultetskog vijeća Građevinskog fakulteta Osijek Sveučilišta Josipa Jurja Strossmayera u Osijeku, održanoj **dd.mm.gggg.** godine:

1. **ime, prezime, znanstveno-nastavno zvanje, akademski naziv i stupanj, visoko učilište i država (ukoliko je visoko učilište izvan Republike Hrvatske) prvog člana (predsjednik Povjerenstva)**
2. **ime, prezime, znanstveno-nastavno zvanje, akademski naziv i stupanj, visoko učilište i država (ukoliko je visoko učilište izvan Republike Hrvatske) drugog člana**
3. **ime, prezime, znanstveno-nastavno zvanje, akademski naziv i stupanj, visoko učilište i država (ukoliko je visoko učilište izvan Republike Hrvatske) trećeg člana**

Tema i mentori doktorskog rada prihvaćeni su odlukom Fakultetskog vijeća Građevinskog i arhitektonskog fakulteta Osijek Sveučilišta Josipa Jurja Strossmayera u Osijeku na **n. redovitoj - izvarednoj** sjednici održanoj **dd.mm.gggg.** godine.

Povjerenstvo za ocjenu doktorskog rada

Povjerenstvo za ocjenu doktorskog rada imenovano na **n. redovitoj - izvarednoj** sjednici Fakultetskog vijeća Građevinskog i arhitektonskog fakulteta Osijek Sveučilišta Josipa Jurja Strossmayera u Osijeku, održanoj **dd.mm.gggg.** godine:

1. **ime, prezime, znanstveno-nastavno zvanje, akademski naziv i stupanj, visoko učilište i država (ukoliko je visoko učilište izvan Republike Hrvatske) prvog člana (predsjednik Povjerenstva)**
2. **ime, prezime, znanstveno-nastavno zvanje, akademski naziv i stupanj, visoko učilište i država (ukoliko je visoko učilište izvan Republike Hrvatske) drugog člana**

3. ime, prezime, znanstveno-nastavno zvanje, akademski naziv i stupanj, visoko učilište i država (ukoliko je visoko učilište izvan Republike Hrvatske) trećeg člana

Doktorski rad prihvaćen je odlukom Fakultetskog vijeća Građevinskog i arhitektonskog fakulteta Osijek Sveučilišta Josipa Jurja Strossmayera u Osijeku na **n. redovitoj - izvarednoj** sjednici održanoj **dd.mm.gggg.** godine.

Povjerenstvo za obranu doktorskog rada

Povjerenstvo za obranu doktorskog rada imenovano na **n. redovitoj - izvarednoj** sjednici Fakultetskog vijeća Građevinskog i arhitektonskog fakulteta Osijek Sveučilišta Josipa Jurja Strossmayera u Osijeku, održanoj **dd.mm.gggg.** godine:

1. ime, prezime, znanstveno-nastavno zvanje, akademski naziv i stupanj, visoko učilište i država (ukoliko je visoko učilište izvan Republike Hrvatske) prvog člana (predsjednik Povjerenstva)
2. ime, prezime, znanstveno-nastavno zvanje, akademski naziv i stupanj, visoko učilište i država (ukoliko je visoko učilište izvan Republike Hrvatske) drugog člana
3. ime, prezime, znanstveno-nastavno zvanje, akademski naziv i stupanj, visoko učilište i država (ukoliko je visoko učilište izvan Republike Hrvatske) trećeg člana
4. ime, prezime, znanstveno-nastavno zvanje, akademski naziv i stupanj, visoko učilište i država (ukoliko je visoko učilište izvan Republike Hrvatske) trećeg člana (zamjena)

Doktorski rad javno je obranjen **dd.mm.gggg.** godine na Građevinskom i arhitektonskom fakultetu Osijek Sveučilišta Josipa Jurja Strossmayera u Osijeku.

Doktorski rad sadržava **n** stranica, **n** ilustracija, **n** tablica, **n** dodataka i **n** citiranih publikacija.

Prvi mentor doktorskog rada je ime, prezime, znanstveno-nastavno zvanje, akademski naziv i stupanj, visoko učilište i država (ukoliko je visoko učilište izvan Republike Hrvatske).

Drugi mentor doktorskog rada je ime, prezime, znanstveno-nastavno zvanje, akademski naziv i stupanj, visoko učilište i država (ukoliko je visoko učilište izvan Republike Hrvatske).

Istraživanje u okviru doktorskog rada pripada znanstvenom području tehničkih znanosti, znanstvenom polju građevinarstvo.

Evaluation committees and bibliographical data

Committee for the Recognition of the Doctoral Thesis Topic

The Committee for the Recognition of the Doctoral Thesis Topic was appointed at the **nth regular - irregular** session of the Faculty Council of the Faculty of Civil Engineering and Architecture Osijek of the Josip Juraj Strossmayer University of Osijek, held on **dd.mm.gggg**:

1. **name, surname, scientific-academic position, academic title and degree, institute of higher education and country (if the institute of higher education is outside of the Republic of Croatia) of the first Committee member (president of the Committee)**
2. **name, surname, scientific-academic position, academic title and degree, institute of higher education and country (if the institute of higher education is outside of the Republic of Croatia) of the second Committee member**
3. **name, surname, scientific-academic position, academic title and degree, institute of higher education and country (if the institute of higher education is outside of the Republic of Croatia) of the third Committee member**

The topic, mentor, first and second co-mentor of the doctoral thesis have been recognised by the decision of the Faculty Council of the Faculty of Civil Engineering Osijek of the Josip Juraj Strossmayer University of Osijek, at the **nth regular-irregular** session held on **dd.mm.gggg**.

Committee for the Evaluation of the Doctoral Thesis

The Committee for the Evaluation of the Doctoral Thesis was appointed at the **nth regular-irregular** session of the Faculty Council of the Faculty of Civil Engineering and Architecture Osijek of the Josip Juraj Strossmayer University of Osijek, held on **dd.mm.gggg**:

1. **name, surname, scientific-academic position, academic title and degree, institute of higher education and country (if the institute of higher education is**

outside of the Republic of Croatia) of the first Committee member (president of the Committee)

2. name, surname, scientific-academic position, academic title and degree, institute of higher education and country (if the institute of higher education is outside of the Republic of Croatia) of the second Committee member
3. name, surname, scientific-academic position, academic title and degree, institute of higher education and country (if the institute of higher education is outside of the Republic of Croatia) of the third Committee member

The doctoral thesis has been recognised by the decision of the Faculty Council of the Faculty of Civil Engineering and Architecture Osijek of the Josip Juraj Strossmayer University of Osijek, at the **nth regular-irregular** session held on **dd.mm.gggg**.

Committee for the Defence of the Doctoral Thesis

The Committee for the Defence of the Doctoral Thesis was appointed at the **nth regular - irregular** session of the Faculty Council of the Faculty of Civil Engineering and Architecture Osijek of the Josip Juraj Strossmayer University of Osijek, **dd.mm.gggg**:

1. name, surname, scientific-academic position, academic title and degree, institute of higher education and country (if the institute of higher education is outside of the Republic of Croatia) of the first Committee member (president of the Committee)
2. name, surname, scientific-academic position, academic title and degree, institute of higher education and country (if the institute of higher education is outside of the Republic of Croatia) of the second Committee member
3. name, surname, scientific-academic position, academic title and degree, institute of higher education and country (if the institute of higher education is outside of the Republic of Croatia) of the third Committee member
4. name, surname, scientific-academic position, academic title and degree, institute of higher education and country (if the institute of higher education is

outside of the Republic of Croatia) of the third Committee member (substitute)

The doctoral thesis has been publicly defended on dd.mm.gggg at the Faculty of Civil Engineering and Architecture Osijek of the Josip Juraj Strossmayer University of Osijek.

The doctoral thesis contains n pages, n illustrations, n tables, n annexes and n cited publications.

The mentor of the doctoral thesis is name, surname, scientific-academic position, academic title and degree, institute of higher education and country (if the institute of higher education is outside of the Republic of Croatia).

The co-mentor of the doctoral thesis is name, surname, scientific-academic position, academic title and degree, institute of higher education and country (if the institute of higher education is outside of the Republic of Croatia).

The research conducted as part of the doctoral thesis is from the scientific area of Technical Sciences, scientific field Civil Engineering.

Izjava o akademskoj čestitosti

Izjavljujem i svojim potpisom potvrđujem kako je doktorski rad isključivo rezultat mog vlastitog rada koji se temelji na mojim istraživanjima i oslanja se na objavljenu literaturu, a što pokazuje korištene bilješke i bibliografija. Izjavljujem kako nijedan dio rada nije napisan na nedozvoljen način, odnosno prepisan iz necitiranog rada te kako nijedan dio rada ne krši bilo čija autorska prava. Izjavljujem kako nisam prijavila doktorski rad s istovjetnom temom na drugom studiju Sveučilišta ili na drugom sveučilištu.

U Osijeku, dd.mm.gggg. godine

Ana Perić Fekete, mag. ing. aedif.

Statement on academic integrity

I hereby declare and confirm by my signature that this doctoral thesis is the exclusive result of my own work, which is based on my own research and which relies on published literature, which is demonstrated by the used notes and bibliography. I declare that no parts of this thesis were written in a manner that is not allowed, *i.e.*, that they were not copied from an uncited paper, and that no parts of this thesis violate anyone's intellectual property rights. I hereby declare that I have not applied a doctoral thesis with this identical topic at another study programme of this nor other university

Osijek, dd mm gggg

Ana Perić Fekete M. Sc. in Civ. Eng.



Ovaj doktorski rad izrađen je na Građevinskom i arhitektonskom fakultetu Osijek u sklopu HRZZ projekta „Nabijena zemlja za modeliranje i normizaciju u potresno aktivnim područjima“ (UIP-2020-02-7363) pod mentorstvom voditelja projekta izv. prof. dr. sc. Ivana Krausa.



This thesis was supported by Croatian Science Foundation, under the project UIP-2020-02-7363 "Rammed earth for modelling and standardisation in seismically active areas – RE-forMS", under the supervision of associate professor, Ph.D. Ivan Kraus.

Sažetak i ključne riječi

Drevne tehnike gradnje zemljanim kamenjem, nastale u dalekoj prošlosti, mnogo prije pojave konvencionalnih građevinskih materijala, ponovno su zaokupile pozornost znanstvene i šire javnosti početkom 21. stoljeća. Istraživanja su proteklih godina vršena u cijelom svijetu, ali hrvatski zemljani građevinski fond nije bio prepoznat zbog nedostatka informacija. Ovo je istraživanje provedeno u sklopu prvog znanstveno-istraživačkog projekta usmjerenog na razumijevanje seizmičkog ponašanja kuća od nabijene zemlje s područja istočne Hrvatske.

Kako bi se razumio napredak u razumijevanju zemljanih kuća napravljen diljem svijeta, izvršen je pregled literature nekoliko priručnika i normativnih dokumenata te više od 50 istraživačkih radova. Provedeno je istraživanje postojećih zemljanih kuća u istočnoj Hrvatskoj te je prikazano pet dokumentiranih kuća i raspravljen njihov raspored i uporaba, čime je stvorena mala baza podataka istočne Hrvatske zemljanih kuća. Ključna zapažanja odnose se na razlike u sastavu materijala između preporuka u literaturi i kuća od nabijene zemlje u istočnoj Hrvatskoj. S druge strane, plastičnost i tlačna čvrstoća tla u skladu su s većinom preporuka.

Saznanja stečena pregledom literature i terenskim promatranjem bila su vrijedan temelj za izvođenje eksperimentalne analize zidova od nabijene zemlje. Četiri zida od nabijene zemlje ispitana su u ravnini, variranjem režima pobude, sastava materijala i razdoblja sušenja. Međutim, utvrđeno je da razlike nisu značajno utjecale na nosivost zidova niti faktor ponašanja konstrukcije. Nadalje, rezultati eksperimenta su korišteni za provođenje validacije numeričkog modela u ANSYS Workbenchu. Provedena je parametarska analiza koja se sastoji od 54 numerička modela. Analizirano je ukupno 18 različitih zidnih sustava koji se mogu naći u tradicionalnim kućama od nabijene zemlje iz istočne Hrvatske, primjenom tri razine vertikalnog naprezanja na vrhu zida.

Parametarska analiza je pokazala da se zidovi od nabijene zemlje ne bi trebali smatrati samostojećim jedinicama, odvojenim od ostalih zidova u konstrukciji jer bi nosivost i potresna otpornost mogla biti precijenjena. Međutim, duljina bočnih zidova ne mora biti duža od 50% duljine stijenke. Faktor ponašanja konstrukcije od ca. 2.0 je određen, čime je za promatrane zidne sustave dokazano da se mogu koristiti

vrijednosti veće od 1.5. Primijenjena su dva pristupa za određivanje krivulja spektra odziva: trenutna i nova generacija Eurokoda 8. Stoga su razmotrane razlike u dvije generacije, u kontekstu zidova od nabijene zemlje. Naime, prema novoj generaciji Eurokoda 8, očekuje se da bi tradicionalni zidovi od nabijene zemlje mogli izdržati potresne aktivnosti koje se mogu očekivati u istočnoj Hrvatskoj. Međutim, trenutna verzija Eurokoda 8 daje potpuno suprotan zaključak, umanjujući potresni kapacitet takvih konstrukcija.

Ključne riječi: zidovi od nabijene zemlje, istočna Hrvatska, potresno ponašanje, ispitivanje zidova u ravnini, numerička analiza, ANSYS Workbench, faktor ponašanja konstrukcije

Abstract and keywords

Ancient earthen building techniques that originated in the distant past, long before the advent of conventional building materials, have regained the attention of the scientific and broader public with the beginning of the 21st century. Research has been performed throughout the world in the past few years. However, due to a lack of information, the Croatian earthen building fund was not widely recognised. This study was performed within the scope of the first scientific research project, which is directed at understanding the seismic behaviour of eastern Croatian rammed earth houses.

In order to understand the advancements in earthen houses made worldwide, a literature review of several manuals and normative documents, as well as more than 50 research papers, was performed. Observation of existing rammed earth houses in eastern Croatia was performed, and five documented houses were presented and their layout and usage discussed, thus creating a small database of eastern Croatian rammed earth houses. Key observations concern differences in granular composition between literature recommendations and eastern Croatian rammed earth houses. On the other hand, soil plasticity and compressive strength are in line with the majority of recommendations.

Knowledge gained through literature review and field observation was the valuable foundation for performing experimental analysis of rammed earth walls. Four rammed earth walls were tested in-plane by varying excitation regimes, material composition and drying periods. However, it was determined that differences did not majorly affect the load-bearing capacity of walls or structural behaviour factor. Results were further used to perform numerical model validation in ANSYS Workbench. A parametric analysis comprising 54 numerical models was performed. In total, 18 different wall systems found in traditional rammed earth houses from eastern Croatia were analysed by applying three levels of vertical stress on top of the wall.

Parametric analysis showed that rammed earth walls should not be considered free-standing units, separated from other walls in the structure, since the load-bearing and seismic capacity could be overestimated. However, the flange wall length

does not need to be longer than 50% of the wall length. A structural behaviour factor of ca. 2.0 was determined, thus proving that values greater than 1.5 can be used for wall systems observed. Two approaches for determining response spectrum curves were followed: current and new generation of Eurocode 8. Thus, differences between the two generations were considered in the context of rammed earth walls. Namely, according to the new generation of Eurocode 8, traditional rammed earth walls could withstand seismic activities that could be expected in eastern Croatia. However, the current version of Eurocode 8 yields an opposite conclusion by diminishing the seismic capacity of such constructions.

Keywords: rammed earth walls, eastern Croatia, seismic behaviour, in-plane wall testing, numerical analysis, ANSYS Workbench, structural behaviour factor

Contents

1	Introduction	1
1.1	Research hypothesis and aims	2
1.2	Methodology	3
1.3	Research significance and limitations	5
2	Literature overview	7
2.1	General overview	10
2.2	Rammed earth in Croatia	11
2.3	Standards overview	14
2.4	Construction soil	22
2.4.1	Particle size distribution	22
2.4.2	Optimum moisture content	35
2.4.3	Plasticity	39
2.4.4	Compressive strength	46
2.4.5	Hydro-mechanical behaviour	55
2.5	Experimental campaigns	58
2.6	Numerical analysis	61
2.7	Conclusion	64
3	Field observations	68
3.1	Rammed earth houses in eastern Croatia	69
3.2	<i>A-Z-73</i>	72
3.3	<i>A-ZS-1</i>	74
3.4	<i>BB-ZP-1</i>	77
3.5	<i>C-SR-38</i>	82

3.6	<i>K-SP-6</i>	84
3.7	Experimental tests of collected material	87
3.7.1	Moisture content	87
3.7.2	Particle size distribution	90
3.7.3	Plasticity	91
3.7.4	Unconfined compressive strength	93
3.7.5	Soil water retention behaviour	95
3.8	Conclusion	98
4	Seismic behaviour	101
4.1	Structural behaviour factor	103
4.2	Response spectrum	103
4.3	Conclusion	107
5	Experimental campaigns	108
5.1	Soil characterisation	108
5.1.1	Particle size distribution	109
5.1.2	Optimum moisture content	110
5.1.3	Plasticity	111
5.1.4	Tensile and compressive strength	112
5.2	Rammed earth walls	116
5.2.1	Test setup	119
5.2.2	Experimental results	122
5.2.3	Influence of excitation regime	128
5.2.4	Influence of material composition	128
5.2.5	Influence of drying period length	131
5.3	Conclusion	131
6	Numerical analysis	135
6.1	Constitutive model for rammed earth	135
6.2	Validation	137
6.3	Parametric analysis	144
6.3.1	C-walls	148
6.3.2	T-walls	152

6.4	Seismic behaviour	155
6.4.1	Characteristic seismic parameters	155
6.4.2	Seismic capacity	160
6.4.3	Superposition with response spectrum	161
6.5	Conclusion	169
7	Concluding remarks	174
7.1	Scientific contribution	177
7.2	Recommendations for future work	179
8	Appendices	181

List of Figures

2.1	Alhambra Palace in Grenada (Spain)	8
2.2	Great Wall of China, Jiayuguan Fort	9
2.3	Sustainable Development Goals	10
2.4	Process of building a rammed earth wall (author's graphic presentation)	11
2.5	Plan of three-room slavic house	12
2.6	Array of houses in a Slavonian street	13
2.7	Technical standard for adobe (Egypt, 1500 BC)	15
2.8	Lower limits for granular composition	25
2.9	Upper limits for granular composition	26
2.10	Envelopes for determining suitable soil in rammed earth construction	27
2.11	Compressive strength in function of modulus of elasticity - values from published articles	49
2.12	Compressive strength in function of density - values from published articles	50
3.1	Approximate locations of settlements containing rammed earth houses	70
3.2	Authors' photographs of A-Z-73 house	74
3.3	A-Z-73: Plan diagram	75
3.4	Authors' photographs of A-ZS-1 house	77
3.5	A-ZS-1: Plan diagram	78
3.6	Authors' photographs of BB-ZP-1 house	80
3.7	BB-ZP-1: Plan diagram	81
3.8	Authors' photographs of C-SR-38 house	83
3.9	C-SR-38: Disposition of the south façade	85
3.10	Authors' photographs of K-SP-6 house	86
3.11	K-SP-6: Disposition of the south façade	88

3.12	Particle size distribution of the material collected from rammed earth houses in eastern Croatia	91
3.13	Cutting rammed earth samples	93
3.14	Stress-strain curves of tested in-situ samples	94
3.15	Suction of samples collected from A-Z-73 house	97
3.16	The suction/compressive strength relationship	98
4.1	Locations of earthen construction overlapped with seismically prone areas (Thompson et al., 2022)	102
4.2	Map of earthquake epicentres in Croatia	102
4.3	Elastic response spectrum for the three ground types	106
5.1	Mixtures Soil-S and Soil-M compared to envelopes	110
5.2	Tensile strength of rammed earth samples	113
5.3	Compressive strength of rammed earth samples	115
5.4	Building of rammed earth walls	118
5.5	Schematic representation of the experimental setup	119
5.6	An overview of the experimental setup	121
5.7	Loading protocols used in the experiment	123
5.8	Von Mises strain at the point of yielding and after the final loading cycle	126
5.9	Comparison of seismic behaviour in walls tested with different loading protocols	129
5.10	Comparison of seismic behaviour in walls made of different material mixture	130
5.11	Comparison of seismic behaviour in walls tested at different moisture content	132
6.1	C-wall and T-wall systems as a part of a rammed earth house	136
6.2	Drucker-Prager model: uniaxial stress-strain relationship	137
6.3	Validation analysis performed by varying finite element size	140
6.4	Validation numerical model overlapped with experimental results . .	141
6.5	Different finite element (FE) sizes overlapped with experimental results	142
6.6	Comparison of small-scaled and full-scaled wall numerical test results	144

6.7	C-wall variations and load direction	146
6.8	T-wall variations and load direction	147
6.9	Numerical analysis results: 250_C_0	150
6.10	Bilinear idealisation: 250_C_0	151
6.11	Seismic capacity: 250_C	162
6.12	Superposition with response spectrum curves	163
8.1	Numerical analysis results: 250_C_0	183
8.2	Bilinear idealisation: 250_C_0	184
8.3	Numerical analysis results: 250_C_0.5	185
8.4	Bilinear idealisation: 250_C_0.5	186
8.5	Numerical analysis results: 250_C_0.25	187
8.6	Bilinear idealisation: 250_C_0.25	188
8.7	Numerical analysis results: 350_C_0	189
8.8	Bilinear idealisation: 350_C_0	190
8.9	Numerical analysis results: 350_C_0.5	191
8.10	Bilinear idealisation: 350_C_0.5	192
8.11	Numerical analysis results: 350_C_0.25	193
8.12	Bilinear idealisation: 350_C_0.25	194
8.13	Numerical analysis results: 450_C_0	195
8.14	Bilinear idealisation: 450_C_0	196
8.15	Numerical analysis results: 450_C_0.25	197
8.16	Bilinear idealisation: 450_C_0.25	198
8.17	Numerical analysis results: 450_C_0.5	199
8.17	Bilinear idealisation: 450_C_0.5	200
8.18	Numerical analysis results: 100_T_0	201
8.19	Bilinear idealisation: 100_T_0	202
8.20	Numerical analysis results: 100_T_0.5	203
8.21	Bilinear idealisation: 100_T_0.5	204
8.22	Numerical analysis results: 100_T_1	205
8.23	Bilinear idealisation: 100_T_1	206
8.24	Numerical analysis results: 150_T_0	207
8.25	Bilinear idealisation: 150_T_0	208

8.26	Numerical analysis results: 150_T_0.5	209
8.27	Bilinear idealisation: 150_T_0.5	210
8.28	Numerical analysis results: 150_T_1	211
8.29	Bilinear idealisation: 150_T_1	212
8.30	Numerical analysis results: 200_T_0	213
8.31	Bilinear idealisation: 200_T_0	214
8.32	Numerical analysis results: 200_T_0.5	215
8.33	Bilinear idealisation: 200_T_0.5	216
8.34	Numerical analysis results: 200_T_1	217
8.35	Bilinear idealisation: 200_T_1	218
8.36	Seismic capacity: 250_C	220
8.37	Seismic capacity: 350_C	221
8.38	Seismic capacity: 350_C	222
8.39	Seismic capacity: 100_T	223
8.40	Seismic capacity: 150_T	224
8.41	Seismic capacity: 200_T	225
8.42	Superposition with response spectrum: 250_C_0	227
8.43	Superposition with response spectrum: 250_C_0.25	228
8.44	Superposition with response spectrum: 250_C_0.5	229
8.45	Superposition with response spectrum: 350_C_0	230
8.46	Superposition with response spectrum: 350_C_0.25	231
8.47	Superposition with response spectrum: 350_C_0.5	232
8.48	Superposition with response spectrum: 450_C_0	233
8.49	Superposition with response spectrum: 450_C_0.25	234
8.50	Superposition with response spectrum: 450_C_0.5	235
8.51	Superposition with response spectrum: 100_T_0	236
8.52	Superposition with response spectrum: 100_T_0.5	237
8.53	Superposition with response spectrum: 100_T_1	238
8.54	Superposition with response spectrum: 150_T_0	239
8.55	Superposition with response spectrum: 150_T_0.5	240
8.56	Superposition with response spectrum: 150_T_1	241
8.57	Superposition with response spectrum: 200_T_0	242

8.58	Superposition with response spectrum: 200_T_0.5	243
8.59	Superposition with response spectrum: 200_T_1	244
8.60	Superposition with new response spectrum: 250_C_0	246
8.61	Superposition with new response spectrum: 250_C_0.25	247
8.62	Superposition with new response spectrum: 250_C_0.5	248
8.63	Superposition with new response spectrum: 350_C_0	249
8.64	Superposition with new response spectrum: 350_C_0.25	250
8.65	Superposition with new response spectrum: 350_C_0.5	251
8.66	Superposition with new response spectrum: 450_C_0	252
8.67	Superposition with new response spectrum: 450_C_0.25	253
8.68	Superposition with new response spectrum: 450_C_0.5	254
8.69	Superposition with new response spectrum: 100_T_0	255
8.70	Superposition with new response spectrum: 100_T_0.5	256
8.71	Superposition with new response spectrum: 100_T_1	257
8.72	Superposition with new response spectrum: 150_T_0	258
8.73	Superposition with new response spectrum: 150_T_0.5	259
8.74	Superposition with new response spectrum: 150_T_1	260
8.75	Superposition with new response spectrum: 200_T_0	261
8.76	Superposition with new response spectrum: 200_T_0.5	262
8.77	Superposition with new response spectrum: 200_T_1	263

List of Tables

2.1	An overview of rammed earth normative documents, standards and building codes	18
2.2	Particle size distribution used for rammed earth in literature	29
2.3	Optimum moisture content and maximum dry density of rammed earth in literature	36
2.4	Soil plasticity of rammed earth in literature	42
2.5	Compressive strength test specimen details in standards	47
2.6	Recommended minimal and design values for compressive strength . .	48
2.7	Compressive strength of rammed earth samples reported in reviewed articles	51
2.8	Rammed earth walls subjected to in-plane loading published in literature (updated table from Perić Fekete et al. (2024))	60
2.9	Software used in literature	63
3.1	Characteristic dimensions of eastern Croatian rammed earth houses .	71
3.2	Laboratory tests performed on collected samples	87
3.3	Soil plasticity of collected rammed earth samples	92
3.4	Average values of compressive strength and moisture content	95
5.1	Soil plasticity of used soil samples	111
5.2	Mechanical properties of Soil-S	114
5.3	Mechanical properties of Soil-M	116
5.4	Description of test parameters	124
5.5	Summary of experimental test results	127
6.1	Drucker-Prager parameters used for describing exponential softening in compression	139

6.2	Scale factors - Chauchy-Froude's similitude laws	143
6.3	Length variants characteristic for each tested system	145
6.4	C-walls: characteristic displacement and forces	153
6.5	T-walls: characteristic displacement and forces	156
6.6	C-walls: characteristic parameters determined from numerical results	158
6.7	T-walls: characteristic parameters determined from numerical results	159
6.8	Inter-story drift according to 1 st generation of Eurocode 8	164
6.9	Inter-story drift according to 2 nd generation of Eurocode 8	166

List of Symbols

μ	ductility factor
ρ	dry density
σ_v	vertical stress
ϕ	diameter
\mathbf{a}_w	water activity
$\mathbf{f}_{c,d}$	design value of compressive strength
$\mathbf{f}_{c,min}$	minimal allowed value of compressive strength
\mathbf{h}	height
\mathbf{l}	length
\mathbf{q}	structural behaviour factor
\mathbf{s}	suction
\mathbf{w}	width
\mathbf{w}_0	moisture content of in-situ material
\mathbf{w}_t	moisture content at the time of test
\mathbf{C}	clay
\mathbf{E}	Young's modulus of elasticity
\mathbf{G}	gravel
\mathbf{IDR}	inter-storey drift
\mathbf{K}_e	initial stiffness
\mathbf{LL}	liquid limit
\mathbf{M}	silt
\mathbf{M}_w	molecular mass of water
\mathbf{MDD}	maximum dry density
\mathbf{OMC}	optimum moisture content
\mathbf{PI}	plasticity index

PL	plastic limit
PSD	particle size distribution
R	gas constant
S	sand
T	temperature
UCS	unconfined compressive strength

Chapter 1

Introduction

Earthen construction has gained the interest of the scientific community in the past decades due to its potential as one of the options for sustainable buildings of the future (Hall et al., 2012). With the advent of Sustainable Development Goals proposed by the United Nations (2015), the increased use of rammed earth building techniques could help in achieving at least four Goals (*i.e.* No. 9 (Industry, innovation and infrastructure), 11 (Sustainable cities and communities), 12 (Responsible consumption and production) and 13 (Climate action)). Rammed earth structures owe their sustainability to building materials. Namely, the building techniques that ensured simplicity in the past make soil an extremely sustainable building material today (Jaquin, 2012). Rammed earth structures were traditionally built using locally available soil without any artificial binders. Traditional rammed earth houses in the eastern Croatia area were usually regular in shape and consisted of only one storey, with an attic as storage space (Lončar-Vicković and Stober, 2011; Silva et al., 2018). The desires of today's average person or family are bigger, even though the needs have not changed as much. Thus, modern rammed earth buildings are not always built in a sustainable manner. Instead, artificial stabilisers such as cement or gypsum (Toufigh and Kianfar, 2019) are added to the soil mixture to facilitate greater load resistance and a larger structure. Nonetheless, the use of artificial stabilisers will not be comprehended within this thesis to emphasise and promote the sustainable aspect of the rammed earth. Therefore, complete research will comprise unstabilised rammed earth structures with clay as the sole binder.

Earthen structures can be found on every continent except Antarctica (Thomp-

son et al., 2022). According to several authors, 30–50% of the population still lives in earthen houses today (Avrami et al., 2008; Kaluđer et al., 2022; Perić et al., 2021; Reyes et al., 2019; Thompson et al., 2022). Moreover, from more than 20 earthen construction techniques, rammed earth structures are the most common throughout the world (Houben and Guillard, 1994; Thompson et al., 2022). A significant portion of those structures is built in seismically active areas (Silva et al., 2014b; Thompson et al., 2022). In Croatia, rammed earth structures can be found mostly in eastern areas, *i.e.* Slavonia and Baranja, but also in Bjelovar-Bilogora County. Even though the greatest ground accelerations in Croatia are not in the eastern parts, the area of eastern Croatia has withstood several seismic activities of magnitude 4 to almost 6 (Savor Novak et al., 2019). Nonetheless, rammed earth structures, most of which were built a hundred or more years ago, have withstood the ravages of time and are generally still in use. However, even though their occurrence has been acknowledged in literature by several authors (Lončar-Vicković and Stober, 2011; Španiček, 1992; Živković, 2013), scientific research of rammed earth structures (*i.e.* determination of material properties and structural response) from the eastern Croatian area has not been previously conducted.

This research was conducted in the scope of the first scientific research project that encompasses rammed earth structures from eastern Croatia (*RE-forms*), supported by the Croatian Science Foundation, UIP-2020-03-7363. Thus, this first step consisted of investigating rammed earth houses on both a material and structural level.

1.1 Research hypothesis and aims

The lack of research on the seismic behaviour of rammed earth structures in general, but especially in the eastern Croatian area, motivated this thesis topic. Despite the high occurrence of rammed earth structures in eastern Croatia, knowledge regarding material properties, standard dimensions and load resistance is still limited. With that in mind, the aims and research hypotheses of this thesis were determined as follows:

Research hypotheses

H1: Rammed earth walls, the likes of which can be found in the eastern Croatian area, can withstand horizontal ground shaking with a minimum ground acceleration of $0.20g$, which is the design acceleration for the eastern Croatian area.

H2: The structural behaviour factor for rammed earth walls can be greater than 1.5, corresponding to the smallest allowed structural behaviour factor according to the current European standards for designing seismic resistance in masonry and concrete structures.

Aims

1. To create a database on locations, geometry, load, boundary conditions and material composition for physical and numerical models of traditional eastern Croatian rammed earth houses.
2. To evaluate the behaviour of the walls in existing rammed earth houses in eastern Croatia based on the results of destructive testing of physical models loaded with simulated gravity and earthquake loads.
3. To determine the seismic behaviour of rammed earth walls by performing parametric analysis on validated non-linear numerical models.

1.2 Methodology

The research was conducted on three levels. Firstly, a literature review was completed by studying domestic and foreign publications regarding rammed earth. The main focus was on seismic resistance, which is a known weak spot for rammed earth buildings. The seismic resistance in the published literature has been determined by means of experimental tests and numerical analysis. Both approaches were observed in the thesis. Moreover, testing material properties and soil composition in the literature were also evaluated. The recommendations in standards and handbooks for rammed earth structures were collected and exhibited, regarding both material properties and structural design. Moreover, field observation in eastern Croatia was conducted, and five rammed earth structures were documented. Existing rammed earth buildings were assessed by noting the locations of houses, boundary conditions, and standard dimensions of rammed earth walls and layers within the wall. Finally,

with the owners' permission, soil samples from rammed earth walls were collected for further examination in the laboratory.

Following that, the next level of research began. Laboratory testing was conducted on a material and structural level. On soil samples collected from rammed earth walls in eastern Croatia, material properties were identified. Namely, particle size distribution and soil plasticity were determined to assess the soil used for building rammed earth houses in eastern Croatia and compared to the literature. Furthermore, when it was possible without endangering the stability of the house, larger soil samples were collected. Regular prisms were cut from larger samples and tested for compressive strength to get an insight into the stress state of existing rammed earth houses.

The soil composition of rammed earth walls tested in the laboratory was decided upon with respect to the established soil composition of eastern Croatian rammed earth houses. One of the determining parameters in the construction of rammed earth walls is moisture content. The conventional procedure for determining optimum moisture content in soil is the standard Proctor test; however, according to Minke (2006), it is not an appropriate procedure for rammed earth. Instead, Minke (2006) and other authors (Keable and Keable, 1996; Walker et al., 2005), propose using the empirical *drop* test. Both approaches for determining optimum moisture content were used in this research, beginning with the Proctor test and *drop* test as a control. Following that, four models of rammed earth walls in scale 1:2 were constructed using traditional techniques. Rammed earth walls were tested in-plane using cyclic displacement paired with constant vertical load at the top of the wall. The experimental set-up was determined according to the literature review and per rammed earth structures exhibited in eastern Croatia, but also laboratory limitations. Experimental results were used to estimate the structural behaviour factor of a rammed earth wall and as a basis for performing numerical parametric analysis.

The final step in the research consisted of numerical analysis of various rammed earth walls using ANSYS Workbench software (v. 2022 R1). Numerical models were calculated using the finite element method. Firstly, experimental results were used for the validation of the numerical model and establishment of material properties.

A numerical model for validation purposes was made in the same dimensions as per the experiment, *i.e.* scaled model. Following that, a full-scale model was prepared and finally, parametric analysis on rammed earth walls of different geometry and loaded with three levels of vertical load was performed. In total, 54 variations were calculated and analysed. Based on numerical results, the seismic behaviour of rammed earth walls was observed on a larger scale. The structural behaviour factor was determined for every instance of the wall observed. Moreover, capacity curves were overlapped with response spectra and inter-storey drift was determined to assess the limit states of each observed wall system.

1.3 Research significance and limitations

This doctoral dissertation is the first attempt to scientifically comprehend rammed earth walls from eastern Croatia. Namely, in the past thirty years, research has been performed worldwide, but, not in Croatia. Due to that, when discussing the presence of earthen architecture throughout the world, Croatia was omitted due to the lack of information in the relevant literature. By this study, performed in the scope of the research project RE-forMS, funded by the Croatian Science Foundation, as well as all databases and scientific papers produced from the research project, Croatian rammed earth house will be placed on that map.

Furthermore, in order to understand the applicability of foreign standards and normative documents, soil material from existing rammed earth houses in eastern Croatia must be collected and tested. Therefore, field observation will serve as foundation for a database containing information regarding rammed earth houses in eastern Croatia, and it will also enable collecting material samples to better understand the material. Knowledge gathered from field observation and material testing will be implemented into constructing rammed earth walls for laboratory testing and numerical models in parametric analysis.

Experimental and numerical results will be used to evaluate the seismic behaviour of rammed earth walls characteristic for eastern Croatia. Namely, seismic capacity is still questionable when rammed earth structures are considered. Even though eastern Croatia is not the most seismically vulnerable part of the country,

design horizontal acceleration up to $0.2g$ could be observed and it should be verified whether rammed earth walls can sustain that. Therefore, by determining the seismic behaviour of rammed earth walls tested experimentally and numerically, the behaviour of existing rammed earth houses can be assumed. To place the walls analytically in eastern Croatia, seismic capacity curves will be overlapped with elastic response spectra. To the author's best knowledge, both the current and new generation of Eurocode 8 was used to determine the response spectrum curves and compared, in the context of rammed earth walls.

Finally, an important parameter in seismic analysis that enables one to perform a seismic design of a structure is surely the structural behaviour factor. In this study, the structural behaviour factor was determined as a ratio of a maximum and yielding force, based on bilinear idealisation of a structural capacity curve. The same procedure was utilised once previously for a rammed earth wall, but this study extends the calculations on rammed earth walls of different geometric proportions and vertical stresses. This analysis will give a better estimate of the structures and determine a range of the structural behaviour factors that can be expected in further analysis.

It should be noted that this thesis is concentrated solely on the seismic behaviour of rammed earth walls. Therefore, mechanical and physical properties reported in later chapters were determined only to support the research on the walls and no further analysis such as the influence of certain additives to the mixture was performed. Furthermore, all conclusions were drawn based on testing walls and should be comprehended as such. Further analysis ought to be performed to verify whether they are applicable to the rammed earth house as a whole.

Chapter 2

Literature overview

Rammed earth, as one of the most popular earthen building techniques, is one of the oldest building techniques. For example, Minke (2006) highlights the rammed earth foundations from 5000 BC in Assyria. Presumably, in different variations, earthen building techniques were developed alongside agriculture in the main cradles of civilization. The proximity of rivers made soil rich in clay and silt, which, consequently, makes the soil ideal for earthen structures. Seemingly, earthen building techniques spread throughout the world with migrations of people. Therefore, the earliest earth buildings might have been similar to caves and later developed as more permanent settlements emerged (Jaquin and Augarde, 2012).

Earth was historically used mostly for vernacular but also monumental buildings, such as Alhambra Palace in Granada (Figure 2.1) built around 1238 or parts of the Great Wall of China (Figure 2.2) built by the Ming dynasty. Further examples of rammed earth architecture across the world can be found in a book by Jaquin and Augarde (2012). However, the advent of modern construction materials with enhanced mechanical properties has diminished the use of earth for building (Jaquin, 2012). Namely, the Industrial Revolution influenced the improvement of manufacturing processes and transportation, and fired brick, concrete and steel displaced earth.

However, Europe rediscovered earthen building techniques following the World Wars. After the First World War, in the UK, an attempt to build with rammed earth was made by architect Clough Williams-Ellis (Jaquin and Augarde, 2012). Moreover, the first European contemporary technical standard devoted to earthen



Figure 2.1: Alhambra Palace in Granada (Spain) (source: <https://www.alhambradegranada.org/en/>, accessed on 23rd January 2024)

building techniques originated in Germany. At the culmination of the Second World War, the shattered industry was not able to facilitate the fast reconstruction of enormous losses in housing. Therefore, as usually the only available building material, the soil was intended as a fast and efficient solution for reconstruction after the war. However, even though the technical standard was drawn up in 1944, due to bureaucratic issues following the war, the code was put into effect seven years later, in 1951, as DIN 18951. In the 1970s, earthen building techniques were once again diminished by industrialisation in Germany, and DIN 18951 was withdrawn (Schroeder, 2012).

On a global scale, at the beginning of the 1970s, amidst the first global oil crisis, it became apparent that energy consumption ought to be reduced (Schroeder, 2016). In industrialised Europe, consumers began to value ecological aspects alongside established durability and strength. In the same period, in Australia and the southern United States, rammed earth was rediscovered as a sustainable building material (Jaquin, 2008). Today, consumption reduction has been expanded to resources in general (Schroeder, 2016), which is visible in the Sustainable Development



Figure 2.2: Great Wall of China, Jiayuguan Fort (source: <https://www.visitourchina.com>, accessed on 23rd January 2024)

Goals (Figure 2.3) proposed by the United Nations (2015). As Schroeder (2016) noted, a new perspective is given to earth-building techniques in light of these ecological advancements.



Figure 2.3: Sustainable Development Goals Nations (2015)

2.1 General overview

The rammed earth building technique is a fairly simple process that comprises compressing moist soil inside a formwork, resulting in a monolithic wall (Minke, 2006). Traditionally, a wall was built inside wooden formwork using manual rammers, but modern formwork is usually more sophisticated, and pneumatic rammers are commonly used (Keable and Keable, 1996; Krahn, 2019; Minke, 2006). Moreover, different variations of manual rammers were historically used in terms of the shape of the “head”, *i.e.* conic, wedged or flat, with a weight of 5 to 10 kg (Keable and Keable, 1996; Minke, 2006).

The very process of building a rammed earth wall is repetitive, as explained in several modern handbooks for earthen construction (Jaquin and Augarde, 2012; Keable and Keable, 1996; Krahn, 2019; Minke, 2006). Prior to the beginning of the building, soil is mixed with an appropriate amount of water and ideally stored inside a sealed container for up to 24 hours. The soil was traditionally mixed on the ground

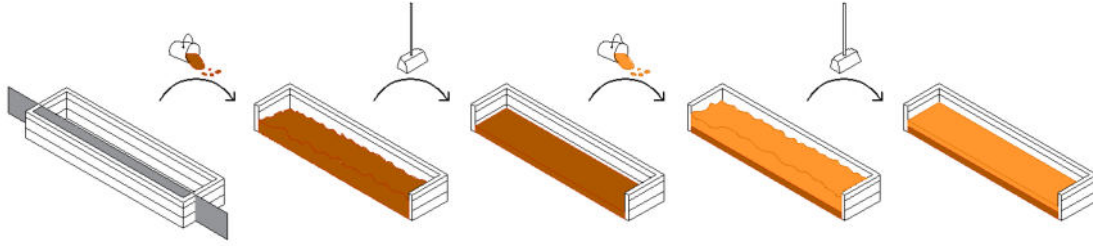


Figure 2.4: Process of building a rammed earth wall (author’s graphic presentation)

by shovelling or people and animals walking over it, while today it is usually mixed using electric mixers (Jaquin and Augarde, 2012). Following that, a portion of loose soil is poured into the formwork and compressed (or rammed), first ramming the outer parts of the wall and then the centre. After completion of the layer, another portion of loose soil is poured into the formwork, and ramming continues. The process is repeated for each layer until the desired wall height is reached (Minke, 2006). The process is graphically depicted on Figure 2.4. Moreover, the height of loose soil is usually halved after ramming, from around 100 mm to 50–70 mm (Keable and Keable, 1996). The process of ramming a layer is considered complete when a level of compaction of around 98% is reached (Walker et al., 2005), even though Schroeder (2012) claims that for most practical purposes, an acceptable compaction limit is achieved when around 90% of maximum dry density is achieved. One can recognise the *finish line* when the soil volume ceases to change after consecutive blows (Keable and Keable, 1996). Additionally, an experienced rammer will notice a “ringing” while compacting a finished layer (Krahn, 2019).

2.2 Rammed earth in Croatia

As Živković (2013) pointed out, Croatia is a relatively small area with various types of buildings, which indicates a richness in traditional building funds. Namely, the geographical position of Croatia enabled a collision of three cultures: the Pannonian, the Dinaric and the Mediterranean. The origin of the eastern Croatian house was just one room with a fireplace in the middle, which slowly developed into a two-room house by separating the sleeping area from the kitchen and *day area*. In the second half of the 18th century, during the reign of Maria Theresa and her son Joseph II, the

building of Slavonian villages was planned and legislated. The head of every house cooperative was given construction land 25 m wide and 100 m (or more) deep inside the yard. Therefore, houses were usually built with a shorter facade on the street side and a longer side in the yard, with auxiliary buildings below. Moreover, to ensure the equality of cooperative members, no additional separated sleeping areas were built. However, in the second half of the 19th century, when village cooperatives were not compulsory any more, another room was added to the house, creating a traditional Slavonian three-room house Figure 2.5. The house is comprised of a kitchen in the centre, a large room facing the street, and a smaller room on the other, yard, side. Moreover, with the abolishment of house cooperatives, land division among brothers was often implemented. Thus, 25 m wide land, was divided into two or even three narrow parts, about 10 m wide. That division resulted in a recognisable array of houses on Slavonian streets (Figure 2.6). Furthermore, the house plan development stopped at three rooms, but the house porch was gradually extended along the whole house (Živković, 2013).

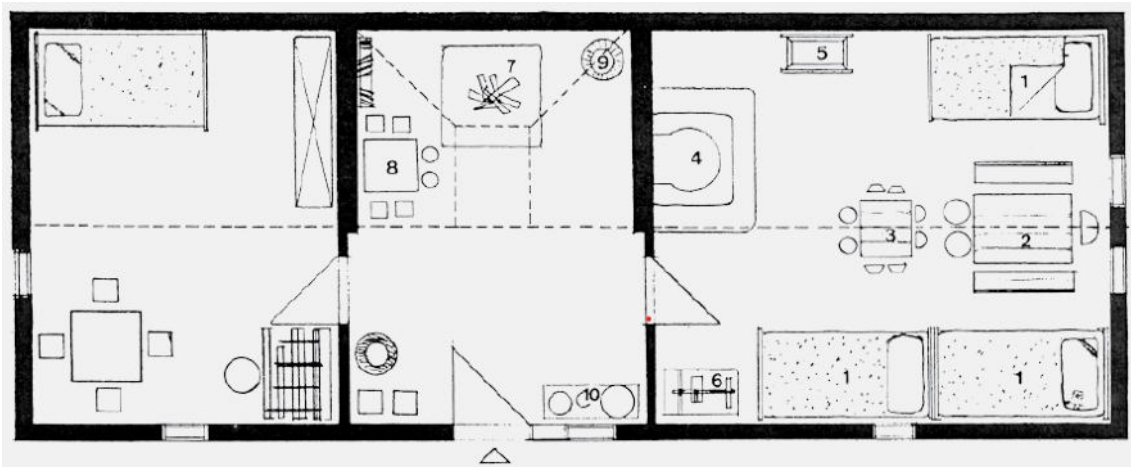


Figure 2.5: Plan of three-room Slavonian house (Živković, 2013)

Due to the large amount of loam in the area, rammed earth houses were historically a feature of eastern parts of Croatia (Lončar-Vicković and Stober, 2011; Živković, 2013). Throughout history, humans have been inclined to build with locally available materials from their surroundings. As opposed to stone (usually limestone) in the Adriatic area, eastern Croatian peasants used soil, commonly mixed



Figure 2.6: Array of houses in a Slavonian street (Živković, 2013)

with plant materials, to build their shelters. Another commonly used material for building houses in eastern Croatia was wood, until the 18th century, when the government prohibited using the then-pricey Slavonian oak for building, to gain more profit in sales across Europe. The Slavonian peasant was occasionally given the material for the timber frame from the government but was left to make infill per his own possibilities (Živković, 2013). It should be noted that Živković (2013) limits the usage of rammed earth in Croatia only to the Baranja area and attributes it to high Hungarian influence and a shortage of timber in the area. However, Lončar-Vicković and Stober (2011) mention the usage of rammed earth, among other traditional building techniques, in a wider area, including Slavonia, Baranja and Srijem. Finally, according to Španiček (1992), rammed earth houses in the Baranja area are one of the best achievements of village architecture in Croatia.

Material for building a rammed earth house was traditionally provided by digging a well or basement in proximity to the construction site. Low-quality soil was mixed with clay, and occasionally, the soil mixture was enriched with finely chopped straw or chaff. The soil in the excavation was mixed with the water and left for 12 to 24 hours prior to building. Moreover, Lončar-Vicković and Stober (2011) also report using different types of wooden rammers with flat, pointed or rounded heads. Approximately 10 to 15 cm of loose soil was rammed to 5–6 cm in the finished wall. It took from two to three weeks to finish ramming the walls of one house, and drying the structure could take up to two years.

Foundations were first made of rammed earth mixed with straw or chaff inside

excavations but were later replaced with fired brick and stone foundations. Walls around 50 cm (Živković, 2013) to 70 cm (Lončar-Vicković and Stober, 2011) thick were finished with oak beams on the top and plastered with a mixture of loam and chaff. Moreover, Lončar-Vicković and Stober (2011) mention the usage of fired brick or broken roof tiles in the lowest parts of the wall for waterproofing. Chopped straw, chaff or sawdust were added to the soil mixture to prevent cracking of the wall due to shrinkage, while corners were reinforced with vines or willow branches. Openings were cut out of the finished wall at least six months after building the wall, and gables of rammed earth houses were built after drying from adobe or fired brick (Lončar-Vicković and Stober, 2011). The ceiling construction was made of wooden beams. The space between the beams was filled with rolls of long straw and mud wrapped around wooden slats (cro. *vitlovi*). After ceiling construction was completed, it was coated with mud and chaff to flatten the surface. The attic area of the one-story houses was usually used as a granary or for other storage purposes. The roof construction was usually gable, covered with cane, straw and, in later instances, tile (Lončar-Vicković and Stober, 2011).

According to Živković (2013), traditional building techniques were utilised until the Second World War, when new materials emerged and new knowledge was applied. The processes of industrialisation and urbanisation marked traditional as outdated. As a result, people were ashamed of their traditions and demolished old buildings to build new and modern ones. However, at the end of the 19th century, among architects and ethnologists in the Croatian area, an interest in traditional buildings was awakened. Regardless, following the war years in the 1990s, major reconstruction took place, and many traditional houses were replaced by modern, fired brick houses. Lončar-Vicković and Stober (2011) also highlight the loss of cultural, social, demographic and rural aspects of Croatian villages in the 21st century.

2.3 Standards overview

Earthen structures were historically *non-engineered* building systems that required inexpensive and simple equipment. Basic quality control performed on-site yielded estimated values highly influenced by the subjectivity of the examiner. Therefore,



Figure 2.7: Technical standard for adobe (Egypt, 1500 BC) (Hassan, 1973; Schroeder, 2016)

the test conditions were not reproducible. The earliest rules were kept and transferred in the form of sketches and paintings (Hassan, 1973; Reddy et al., 2022; Schroeder, 2016), but contained only information regarding building techniques without quality control. However, increased interest in building with earth in the late 20th century moved earth building techniques from empirical handmade processes to industrial production. Thus, earth construction methods became *engineered* and regulated by standards and normative documents. *Engineered* constructions assume the industrial production of building materials, with defined parameters determined by reproducible laboratory testing procedures using standardised test equipment (Schroeder, 2012).

However, despite the existence of several standards and normative documents, uniform test procedures for determining material properties as well as design criteria for earthen constructions currently do not exist. Rather, test protocols from other disciplines are often utilised. The most common examples are using principles of soil mechanics for determining the suitability of the soil for earthen construction but also methods for testing tensile and compressive strength that originate in standards for concrete (Koutous and Hilali, 2021; Maniatidis and Walker, 2008; Toufigh and Kianfar, 2019), or less often masonry (Miccoli et al., 2016; Silva et al., 2014a). Despite the frequent use of these methods, their applicability was not proven on a larger scale. Schroeder (2012) pointed out the necessity of developing adequate test procedures on the same level as for other *conventional* building materials.

Schroeder (2012) gathered thirty-three building standards and normative documents from 10 countries, published over the last 40 years. Thirteen out of those thirty-three documents concern buildings with rammed earth. More recently, Thomp-

son et al. (2022) digested current construction guidelines, emphasising seismic recommendations. The Rilem Technical Committee (TC 247-TCE) published a report regarding the testing and characterisation of earthen building materials and elements (Reddy et al., 2022) that reflected codes and standards for earth construction techniques as well. A combined output of standards and normative documents regarding rammed earth constructions is given in Table 2.1. Twenty-nine documents from 20 countries in the world were listed, while half of those 29 documents contain recommendations regarding seismic-resistant design.

According to the International Standards Organisation (ISO), standards and normative documents are not the same. A standard is a *“document, established by consensus and approved by a recognised body, that provides, for common and repeated use, rules, guidelines, or characteristics of activities or their results, aimed at the achievement of the optimum degree or order in a given context”*, and it *“should be based on the consolidated results of science, technology, and experience and aimed at the promotion of optimum community benefits”*. In other words, a standard contains technical guidelines specifying minimum demands and directions for the construction process that should be adhered to (Heinsdorf, 2015; Thompson et al., 2022). If the standard is enacted into law by a local, regional or national authority, it becomes a code. All participants in the construction process are legally bound to comply with a building code (Heinsdorf, 2015; Thompson et al., 2022).

A normative document, on the other hand, does not have a scope or the endorsement of a standard, but it can become a standard should a government body adopt it (Schroeder, 2016). Therefore, normative documents provide instructions for building construction systems developed by non-government organisations, technical groups or academia. The purpose of creating normative documents, such as practical manuals, books and technical reports, is either to start standard development or to provide guidance for safe construction processes in developing countries (Thompson et al., 2022).

The documents in Table 2.1 were predominantly published in the form of standards or normative documents while only four instances of building codes were noted. Publications listed in Table 2.1 usually cover a variety of earthen building techniques, such as adobe, cob, compressed earth block, wattle and daub, and

rammed earth. Moreover, many of the guidelines regarding structural design apply to all types of earthen construction, while exceptions are indicated. Thompson et al. (2022) provided a review of structural design guidelines based on publications (Table 2.1), which concern the seismic resistance of the new rammed earth structure. Recommendations based on Thompson et al. (2022) are summarised below and can be further explored in the article and respective documents from Table 2.1.

In order to decrease seismic vulnerability, rammed earth buildings should be as regular and symmetric as possible. Publications that address a maximum number of storeys disagree on whether the rammed earth houses should be one-storey or two-storey. The reason for the disagreement possibly lies in the location where a specific guideline is applied. Namely, according to Arya 2014, recommendations regarding one-storey and two-storey houses relate to the seismic code classification in an individual location. All new rammed earth structures should be based on concrete foundations. Commonly, foundation strip footings from 0.5 to 0.7 m wide are recommended, while NBC 204:1994 implies a minimum width of wall thickness plus 0.3 m. Foundations should be at least from 0.3 to 0.6 m deep, in compliance with other codes in the respective country regarding the foundation design.

Wall dimensions are described by specifying either thickness, length or height. The recommended values for a minimum wall thickness differ greatly, according to Thompson et al. (2022): from 0.2 m (Lehmbau Regeln; EBAA) to 0.457 m (14.7.4 NMAC). Moreover, according to Minke (2006), a minimum wall thickness should be greater than the height of the construction divided by eight. The unsupported wall should not be longer than 15 times the wall thickness based on HB 195-2002 or 10 times the wall thickness according to NBC 204:1994. If the wall is supported, it should not be longer than 10 times the thickness according to Arya et al. (2014) and IS:13827, or 12 m as stated in NZS 4297. The most common recommendation for the wall height is the factor of the wall thickness. Besides that, NBC 204:1994 specifies a maximum wall height in the range of 3 to 3.6 m, while NZS 4297 and NZS 4299 differ the specification depending on the location's seismic zone.

Table 2.1: An overview of rammed earth normative documents, standards and building codes

No.	Country	Document ID	Type	Seismic recommendations
1	Afganistan	Guidelines for Earthquake Resistant Design, Construction and Retrofitting of Buildings in Afghanistan, 2003	ND	+
2	Africa	THC 03, SAZD 724, 2014	S	-
3	Australia	CSIRO Bulletin 5, 1995	ND	-
4	Australia	HB 195-2002, 2002	ND	+
5	Australia	EBAA, 2004	ND	-
6	Brazil	NBR 13553, 1996	S	-
7	Chile	Nch 3332, 2013	S	+
8	Columbia	AIS 610-EP-17, 2002	S	+
9	France	Guidelines for earthquake resistant non-engineered construction, 2004	ND	+
10	Germany	Construction manual for earthquake-resistant houses built of earth, 2001	ND	+
11	Germany	Lehmbau Regeln, 2009	S	-
12	India	IS:2110, 1998	S	-
13	India	IS:13827, 1998	S	+

Note: ND = Normative document, S = Standard, BC = Building code

Table 2.1 continued from previous page

No.	Country	Document ID	Type	Seismic recommendations
14	Kyrgyzstan	PCH-2-87, 1988	S	+
15	Nepal	NBC 204:1994, 1994	BC	+
16	New Zealand	NZS 4297, 1998	S	+
17	New Zealand	NZS 4298, 1998	S	+
18	New Zealand	NZS 4299, 1998	S	+
19	Nigeria	NBC 10.23, 2006	BC	-
20	Peru	NTE E. 080, 2000	S	+
21	Portugal	LNEC, 1953	S	-
22	Spain	MOPT Tapial, 1992	ND	-
23	Switzerland	Regeln zum Bauen mit Lehm, 1994	ND	-
24	UK	A Review of Rammed Earth Construction, 2003	ND	-
25	UK	Rammed Earth: Design and Construction Guidelines, 2005	ND	-
26	USA	Uniform Administrative Code Amendment for Earthen Material and Straw Bale Structures, 1997	BC	-
27	USA	14.7.4 NMAC, 2006	BC	+

Note: ND = Normative document, S = Standard, BC = Building code

Table 2.1 continued from previous page

No.	Country	Document ID	Type	Seismic recommendations
28	USA	ASTM E2392/E2392M, 2010	S	+
29	Zimbabwe	SAZS 724, 2001	S	-

Note: ND = Normative document, S = Standard, BC = Building code

Openings in the rammed earth walls for windows and doors are commonly limited by the percentage of the total wall area, in the range of $1/5$ to $1/3$ of the wall area (Arya, 2003; Houben and Guillard, 1994; ?). The maximum opening size is consistently limited, in all publications that consider the subject of openings, to a value of 1.2 m (Arya, 2003; Houben and Guillard, 1994; Minke, 2006; Walker, 2002). However, values for the minimum distance from the corner of the construction range from 0.75 to 1.2 m (Arya, 2003; Minke, 2006; Walker, 2002). Publications (Arya, 2003; Minke, 2006; Walker, 2002; Walker et al., 2005) also recommend a bearing length of lintels above openings as not less than 0.3 or 0.4 m. However, NBC 204:1994 recommends a significantly lower value of 0.05 m.

Reinforcement, a key element in the seismic resilience of a structure, is also mentioned by several publications. Vertical reinforcement should be cast into foundations, connected into plinth beams, of at least 300 mm height above ground, as per Arya et al. (2014); Minke (2006) and IS:13827, and run up through the wall to the horizontal bands. However, it should be noted that mentions of both concrete and timber horizontal bands were noted in publications. Specifications for vertical reinforcement are given in only two publications, *i.e.* IS:13827 and HB 195-2002, that recommend using 12 mm steel rebar. Obstructions during the ramming of the wall due to the reinforcement are recognised when using both vertical and horizontal reinforcement. Moreover, the negative effect of horizontal reinforcement bars on rammed earth walls reducing their ability to withstand shear forces due to cracking and weakening of the wall, was noted by Minke (2006). Indian standard IS:13827 also permits using bamboo canes as reinforcement.

The roof should be as light as possible, preferably made of timber or bamboo, and fixed to the rammed earth walls or horizontal band. The necessity of proper roof construction is emphasised due to its influence on the structural integrity of the building as well as seismic resistance (Keefe, 2005).

Most of the publications relate the seismic resistance of a rammed earth structure only to structural design. Formulas for seismic design are given in only two publications; Arya et al. (2014) and NZS 4297. Remaining publications usually merely reference another national code that is to be followed to ensure the seismic resilience of the structure. Therefore, one must read multiple publications simulta-

neously, which may lead to misinterpretation. To aid the problem, Thompson et al. (2022) propose the creation of one unified code, similar to Eurocode 8, Part 1: General Rules, Seismic Actions and Rules for Buildings. However, they acknowledge the lack of knowledge and research regarding material properties and structural behaviour of earthen materials that must precede the development of a specific standard. Most publications are developed from masonry codes and standards, despite the unproven applicability of the masonry codes for earthen materials. Thus, both earthen materials and the applicability of masonry codes should be further researched.

2.4 Construction soil

The rammed earth buildings of the past were built using empirically acquired knowledge, spread by word of mouth. However, if one wishes to utilise any form of building technique today, an appropriate standard or normative document should be followed. In order to enable the usage of traditional building techniques such as rammed earth in the same way as those used in contemporary construction, proper research ought to be conducted. The source material needs to be observed and tested following procedures as rigorous as those for conventional building materials (*e.g.* concrete, steel, masonry). However, since rammed earth needs to be understood as both soil and a construction element, a variety of analyses should be performed. In the reviewed research papers, the most commonly determined properties are particle size distribution, optimum moisture content, maximum dry density and compressive strength. However, a significant number of research papers also give information regarding plasticity and soil-water retention (*i.e.* suction). In the following sections, recommendations from the literature and previously conducted research regarding the mentioned most common material properties are summarised.

2.4.1 Particle size distribution

Soil is formed by weathering the bedrock and is usually divided into topsoil (with organic matter), subsoil (useful for building materials) and bedrock (Keable and Keable, 1996; Krahn, 2019). A construction soil (*i.e.* subsoil) is divided into boulders

(larger than 200 mm), cobbles (60–200 mm), gravel (2–60 mm), sand (0.06–2 mm), silt (0.002–0.06 mm) and clay (smaller than 0.002 mm) (Jonathan Knappett, 2012). Boulders and cobbles are not used for rammed earth construction, but the remaining four elements should comprise soil for earthen construction (McHenry, 1984). The skeleton is provided by gravel particles that are filled with sand and soil, while clay is used as a natural binder (Krahn, 2019; Minke, 2006). According to Jaquin and Augarde (2012), clay particles hold an electrostatic charge on their surface, which causes the attraction forces between the particles, providing an apparent cohesive strength in the soil. However, they deem the electrostatic bonding of particles not strong enough to generate strength and credit suction as a significant source of strength. The suction and unsaturated behaviour of soil in rammed earth structures will be further explained in section 2.4.5.

The construction soil was traditionally taken from the construction site without specific laboratory testing or determining the suitability of the soil. However, several preliminary field tests for determining the suitability of the soil have been proposed:

- Observation of the construction site (*e.g.* cracks in the dry soil indicate a high clay content, a loose dry soil indicates a high sand content) (Houben and Guillard, 1994; Keable and Keable, 1996)
- Rubbing the soil between the fingers or palms (Houben and Guillard, 1994; Keable and Keable, 1996; Walker et al., 2005) gives one an idea if particles are fine or coarse
- Smell test: used to determine the presence of organic matter in the soil (Houben and Guillard, 1994; Keable and Keable, 1996; Krahn, 2019; Minke, 2006; Walker et al., 2005)
- Taste test: used to determine the texture of the soil; the more coarse the soil is, the more irritating the texture is against one's teeth (Houben and Guillard, 1994; Krahn, 2019; Minke, 2006)
- Wash test is used to determine the predominant soil fraction (*i.e.* sand and gravel, silt or clay) by rubbing humid soil between palms and observing the soil residue on palms (Houben and Guillard, 1994; Minke, 2006)

- Cutting test: if the cut surface of the wet soil ball is shiny, the mixture has a high clay content; otherwise, it indicates high silt content (Keable and Keable, 1996; Minke, 2006)
- Simplified sedimentation using a jar (Houben and Guillard, 1994; Keable and Keable, 1996; Krahn, 2019; Minke, 2006; Walker et al., 2005) to get an estimation of particle size distribution
- Inquiring the locals or builders in the area of the construction site (Houben and Guillard, 1994; Walker et al., 2005)

However, engineering design cannot rely solely on simple field tests, despite their applicability for the initial selection of the soil. Instead, thorough laboratory testing should be performed (Walker et al., 2005). According to Schroeder (2012), the suitability of the soil for earthen construction depends on the granular composition of the mixture (influencing the “skeleton”) and the amount and type of clay particles (responsible for plasticity and cohesion). Determining a complete particle size distribution (PSD) curve requires using laboratory procedures such as sieving and hydrometer methods (Avrami et al., 2008; Houben and Guillard, 1994; Maniatidis and Walker, 2003; Minke, 2006; Reddi et al., 2012).

A soil mixture containing both fine and coarse particles without organic matter present is usually recommended (Hall and Djerbib, 2004; Houben and Guillard, 1994; Walker et al., 2005). According to Keable and Keable (1996), good soil is crucial for adequate performance of rammed earth construction, and it should be rich in sand and gravel content, with just enough clay acting as a binder, while more than 30% of clay in the mixture could cause shrinkage cracks (Reddi et al., 2012). On the other hand, some researchers diminish the influence of the particle size distribution on the suitability of the soil for rammed earth construction (Gomes et al., 2014). The Rilem Technical Committee (TC 247-TCE) recommended using a performance-based approach for determining the suitability of the soil rather than solely the composition of the material (Reddy et al., 2022).

Despite the disagreements on the role of the material composition in soil suitability, particle size distribution is one of the key parameters describing the soil and therefore cannot be omitted due to its impact on mechanical performance (Ávila

et al., 2021). Therefore, in previously published guidelines and normative documents regarding rammed earth construction, recommendations for choosing the appropriate soil based on composition were given. From eleven recommendations plotted in Figure 2.8 and Figure 2.9, only one recommends a soil with the majority of clay particles (Alley, 1948), while all others propose mainly sand and gravel particles in the mixture. Moreover, in two publications (McHenry, 1984; Schrader, 1981), mixtures containing only clay, sand and gravel without silt are recommended. Remaining publications (Doat et al., 1979; Houben and Guillard, 1994; Keable and Keable, 1996; Keefe, 2005; Norton, 1997; of Zimbabwe, 2001; Walker, 2002; Walker et al., 2005) propose a similar particle size distribution, with a majority proportion of sand and gravel particles.

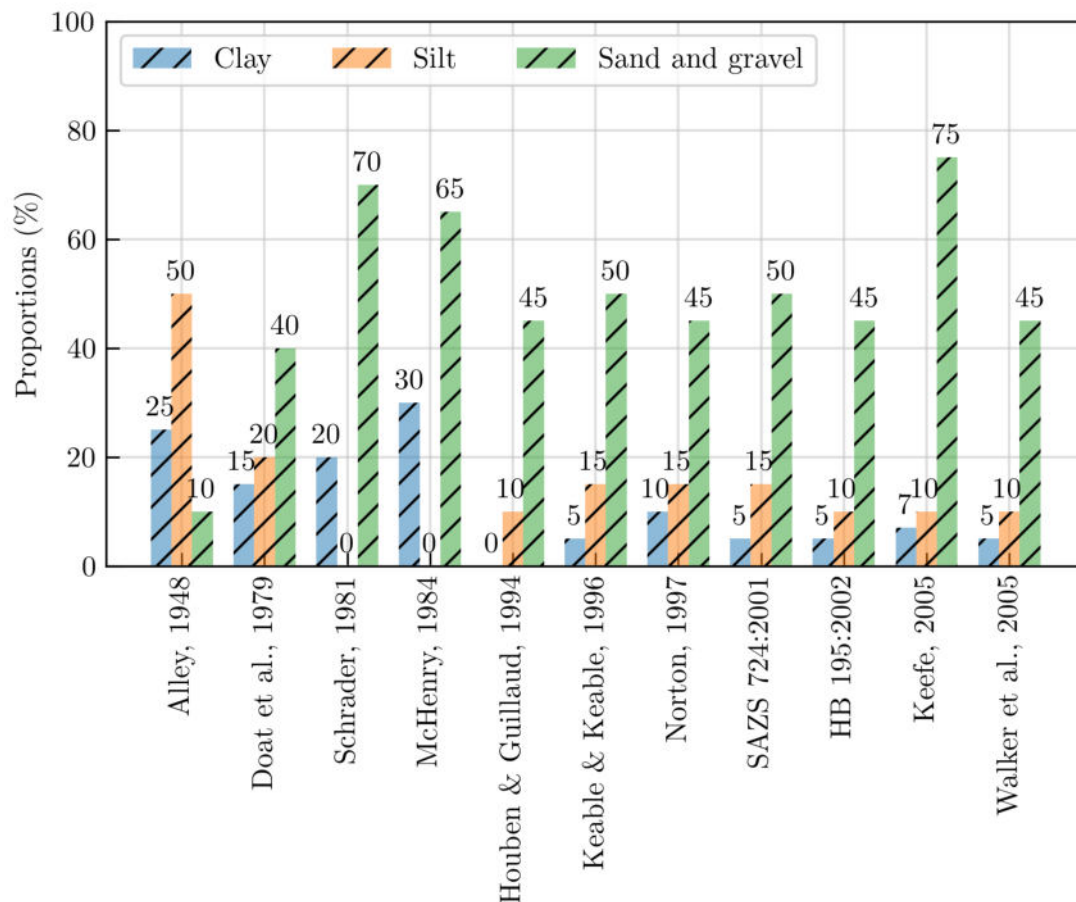


Figure 2.8: Lower limits for granular composition

One of the commonly used envelopes for determining the suitability of the soil for rammed earth construction was proposed by Houben and Guillard (1994),

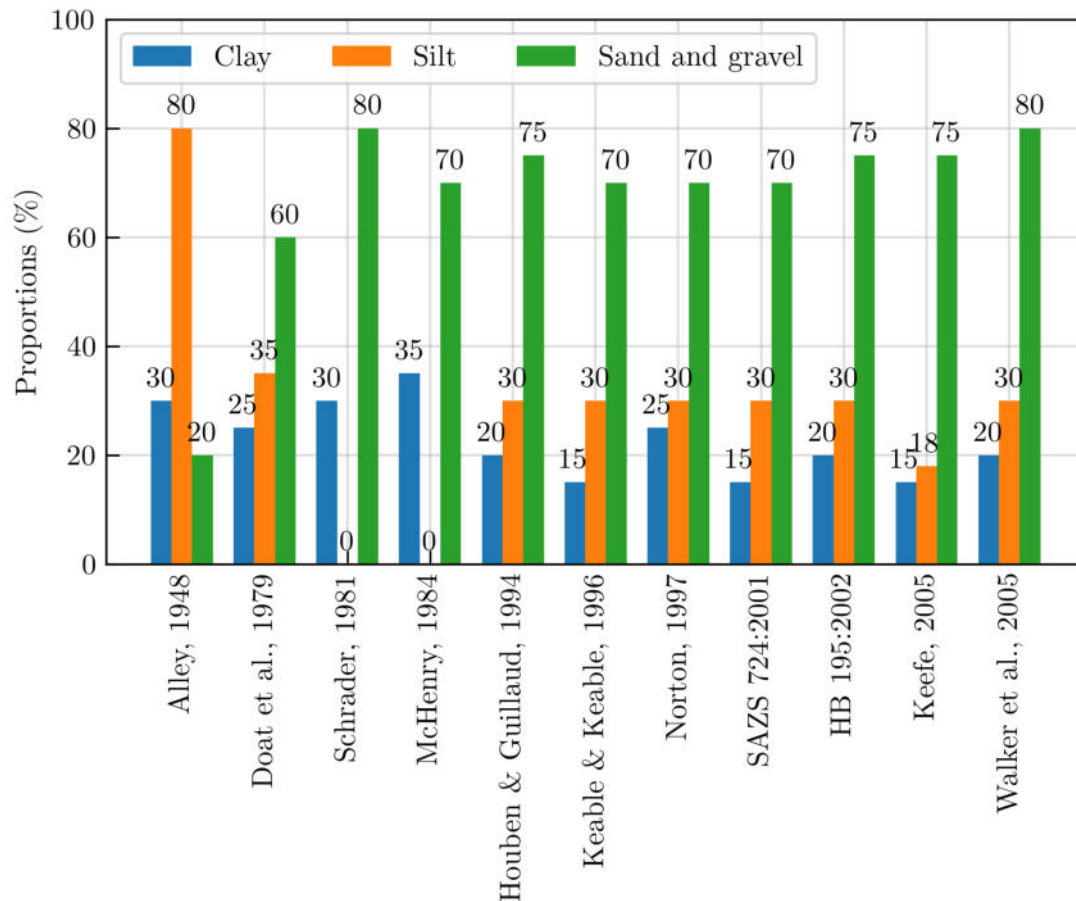


Figure 2.9: Upper limits for granular composition

but only as guidance. According to them, the envelope is intended to be applied as a flexible frame. Despite that, research published in articles regarding rammed earth construction is often conducted with soil chosen based on the envelope (Ávila et al., 2022; Lin et al., 2017; Romanazzi et al., 2022a; Silva et al., 2016a). In Figure 2.10, the envelope proposed by Houben and Guillaud (1994) is plotted, with two recommendations used by Walker et al. (2005) and HB 195-2002, as those were in the biggest percentage throughout considered research papers. It should be noted that the recommendations presented by Walker (2002) and Houben and Guillaud (1994) are essentially the same, with a small difference regarding the minimal limit of fine soil particles. The plot will be used in the following chapters for comparison with the local soil collected from rammed earth houses in eastern Croatia.

In published articles concerning rammed earth structures, the particle size distribution of used mixtures is commonly reported. According to the report by The Rilem Technical Committee (TC 247-TCE) (Aubert et al., 2022), particle size dis-

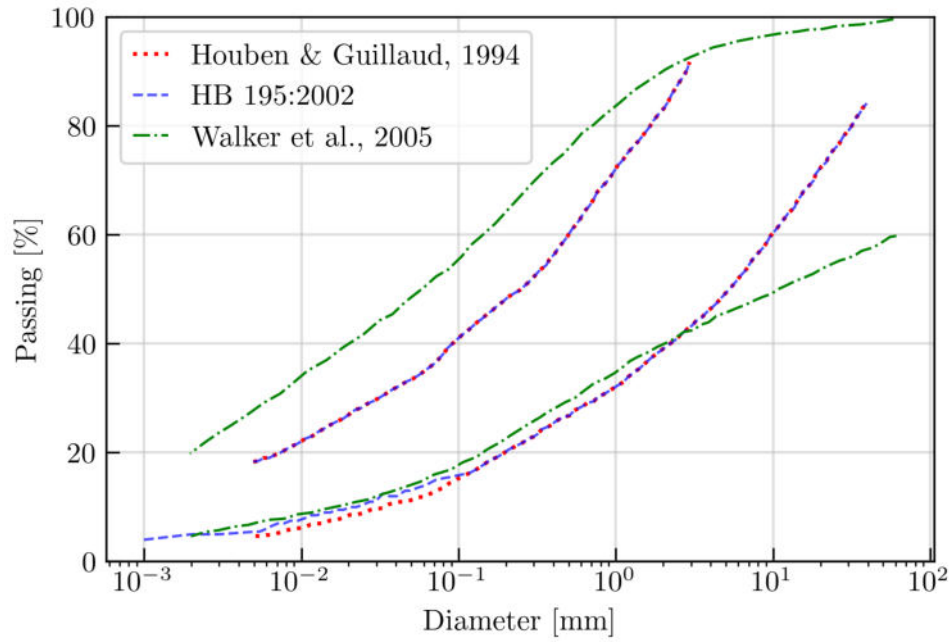


Figure 2.10: Envelopes for determining suitable soil in rammed earth construction

tribution was mentioned in all observed articles (19 in total), while other properties were mentioned in less than 50% of the articles. In Table 2.2, 50 articles published in the last 15 years were reviewed, and 80 different granular compositions were noted. In the majority of articles, all four groups of particles (clay, silt, sand, and gravel) are reported separately. However, in three articles (Miccoli et al., 2014; Michiels et al., 2017; Silva et al., 2014c), the amount of sand and gravel was summarised, while clay and silt were summarised in only one article (Barrera et al., 2023). Moreover, based on the 80 mixture compositions observed, the minimum and maximum amounts of each particle group were determined, and very high variability was observed. Fine particles, clay and silt, appear in ranges of 1 to 48% and 1 to 83%, respectively, while large particles, sand and gravel, were used in ranges of 6 to 90% and 1 to 55%, respectively. The high variability of particle proportions in soil mixtures used for rammed earth constructions indicates that different kinds of soils can be used for building elements. Moreover, it could also support the view presented by Gomes et al. (2014), regarding the lack of effect of particle size distribution on soil suitability for rammed earth constructions. On the other hand, Dialmy et al. (2023) proved that by adjusting the granular proportions in the rammed earth mixture, compactness is increased, and, by extension, the unconfined compressive strength and stiffness are increased. It should be noted that, according to them, one must

perform extensive laboratory tests to achieve the optimum granular composition, and thus they give no recommendations similar to those presented in Figure 2.8 and Figure 2.9.

Finally, the granular compositions of mixtures presented in articles (Table 2.2), were compared with the upper and lower limits in the normative documents and standards (Figure 2.8 and Figure 2.9). For each mixture, an abbreviation was noted in the last column in Table 2.2, or N/A was written if the mixture corresponded to none of the recommendations. 80 mixtures were gathered, half of which complied with no recommendations. Moreover, from eleven suggestions plotted in Figure 2.8 and Figure 2.9, the one made by Alley (1948), with a major intake of clay particles in the mixture, corresponded with none of the mixtures presented in the articles. Furthermore, recommendations in Schrader (1981) and McHenry (1984) agreed with only one of the presented mixtures (Ciancio et al., 2013), which corresponded to no other suggestions. On the other hand, of the 40 mixtures that agree with at least one of the recommendations, 75% of them comply with all three most common recommendations by Houben and Guillard (1994), HB 195-2002 and Walker et al. (2005). What is more, 90% of the mixtures made by recommendations were in line with Walker et al. (2005), while 78% and 75% of them were in correspondence with Houben and Guillard (1994) and HB 195-2002, respectively.

Table 2.2: Particle size distribution used for rammed earth in literature

Particle size distribution					Reference	The regulations with which it complies		
C (%)	M (%)	S (%)	G (%)					
12	13	45	30		(Maniatis and Walker, 2008)	HG, HB, Kf, W		
16	49	35	0		(Bui et al., 2009a)	N/A		
8	27	49	16			HG, SATZ, HB, W, Kb		
4	31	48	17		(Bui and Morel, 2009; Bui et al., 2009b)	N/A		
10	15	54	16		(Jaquin et al., 2009)	HG, N, SATZ, HB, W, Kb		
8	4	60	28		(Nowamooz and Chazallon, 2011)	N/A		
5	25	50	20		(Ciancio et al., 2013)	HG, SATZ, HB, W, Kb		
30	0	50	20			S, McH		
15	15	50	25			HG, HB, Kf, W		
30	20	40	10			N/A		
40	20	20	20			N/A		
6	14	45	35		(Silva et al., 2013)	W		
5	15	59	21			W		
4	14	60	22			N/A		
12	12	53	23			W		

Table 2.2 continued from previous page

The regulations with which it complies					The regulations with which it complies		
C (%)	M (%)	S (%)	G (%)	Reference	C (%)	M (%)	S (%)
5	30	49	16	(Bui et al., 2014a)	5	30	49
4	35	59	2		4	35	59
9	38	50	3		9	38	50
10	30	12	48		10	30	12
10	22	43	25		10	22	43
10	25	18	47	(Bui et al., 2014b)	10	25	18
5	30	49	16		5	30	49
8	34	8	50		8	34	8
0	0	90	10	(Ciancio et al., 2014)	0	0	90
9	16	67	8	(Gomes et al., 2014)	9	16	67
27	20	23	30		27	20	23
18	31	17	34		18	31	17
10	18	47	25		10	18	47
13	24	29	34		13	24	29
17	23	33	27		17	23	33
11	25	65		(Miccoli et al., 2014; Silva et al., 2014c)	11	25	65

Table 2.2 continued from previous page

	C (%)	M (%)	S (%)	G (%)	Reference	The regulations with which it complies
14	16	32	38		(Silva et al., 2014a, 2016b)	HG, N, SATZ, HB, W, Kb
8	28	48	13		(Bui and Morel, 2015)	HG, SATZ, HB, W, Kb
13	64	26	0		(Gerard et al., 2015)	N/A
16	22	56	6		(Araki et al., 2016)	HG, N, HB, W
16	46	38	0		(Champiré et al., 2016)	N/A
17	27	54	2			Do, HG, N, HB, W
6	16	42	36			W
20	66	14	0		(Arrigoni et al., 2017a)	N/A
20	8	59	13		(Arrigoni et al., 2017b)	N/A
48	2	6	44		(Arslan et al., 2017)	N/A
2	12	79	7		(Lin et al., 2017)	N/A
10	40	49	1			N/A
4	11	66	19			N/A
5	83	12	0		(Liu and Tong, 2017)	N/A
10	79	11	0			N/A
15	74	11	0			N/A

Table 2.2 continued from previous page

C (%)	M (%)	S (%)	G (%)	Reference	The regulations with which it complies
20	70	10	0		N/A
25	66	9	0		N/A
15	24		61	(Michiels et al., 2017)	HG, N, SATZ, HB, W, Kb
20	64	16	0	(El-Nabouch et al., 2018)	N/A
34	41	25	0	(Xu et al., 2018)	N/A
17	19	64	0		HG, N, HB, W
26	30	44	0		N/A
18	27	54	1	(Abhilash and Morel, 2019)	Do, HG, N, HB, W
24	66	10	0		N/A
7	53	40	0	(Chauhan et al., 2019)	N/A
23	27	30	20	(Tinsley and Pavía, 2019)	Do, N
5	0	40	55	(Toufigh and Kianfar, 2019)	N/A
0	1	51	48	(Kosarimovahed and Toufigh, 2020)	N/A
20	18	48	14	(Shrestha et al., 2020a)	HG, N, HB, W
10	12	33	45	(Chitimbo et al., 2022)	W
10	24	46	20	(Ramezanpour et al., 2021)	HG, N, SATZ, HB, W, Kb

Table 2.2 continued from previous page

	C (%)	M (%)	S (%)	G (%)	Reference	The regulations with which it complies
0		15	61	24	(Ávila et al., 2022)	N/A
7		51	30	12	(Chauhan et al., 2022)	N/A
1		12	47	40	(Gil-Martín et al., 2022)	N/A
19		28	53	0	(Misseri and Rovero, 2022)	Do, HG, N, HB, W
18		27	55	0		Do, HG, N, HB, W
8		11	26	55	(Pelé-Peltier et al., 2022)	N/A
6		9	38	47	(Romanazzi et al., 2022b)	N/A
43		39	18	0	(Sen and Saha, 2022)	N/A
		82	13	5	(Barrera et al., 2023)	N/A
10		11	33	46	(Baleca et al., 2023; Barsotti et al., 2023)	W
1		20	36	43	(Dialmy et al., 2023)	N/A
2		28	53	17		HG
19		30	25	25	(Koutous and Hilali, 2023)	Do, HG, N, HB, W
15		22	41	22		HG, N, SATZ, HB, W, Kb
10		17	32	41		HG, HB, W
15		15	54	16	(Losini et al., 2023)	HG, N, SATZ, HB, W, Kb

Table 2.2 continued from previous page

C (%)	M (%)	S (%)	G (%)	Reference	The regulations with which it complies
6	9	38	47	(Romanazzi et al., 2023)	N/A
1	1	6	1	MIN	
48	83	90	55	MAX	
13	28	40	19	MEAN	
10	19	18	17	STANDARD DEVIATION	
6	15	26	1	1 st QUARTILE	
18	32	52	30	3 rd QUARTILE	

Note: Do = (Doat et al., 1979), HG = (Houben and Guillard, 1994), Kb = (Keable and Keable, 1996), HB = (HB 195-2002), KF = (Keeffe, 2005), McH = (McHenry, 1984), N = (Norton, 1997), S = (Schrader, 1981), SATZ = (SAZS 724), W = (Walker et al., 2005), N/A = not applicable

2.4.2 Optimum moisture content

In order to make a rammed earth construction, suitable soil must be mixed with water, which activates the binding forces (Minke, 2006). However, the amount of water added to the mix is crucial; too dry or too wet soil cannot be properly compacted. The optimum moisture content depends on the soil mix; however, experienced builders can estimate if the soil is too wet or dry (Keable and Keable, 1996).

The optimum moisture content for building rammed earth construction can be easily determined on-site, without any sophisticated laboratory equipment, by performing the *drop* test. What is more, a *drop* test enables builders to quickly and frequently check the moisture content during the building process. According to Houben and Guillard (1994); Keable and Keable (1996), a ball (40 mm in diameter) should be formed from damp soil and dropped from shoulder level to the ground. If the ball flattens and the soil stays in one piece without much cracking, the soil mixture is too wet, and if it breaks into many small pieces, it is too dry. The optimum moisture content is indicated by breaking the ball into only a few larger pieces.

It should be noted that when assessing the state of the ball, one should consider the clay content as well. Namely, the soil that appears too dry could lack clay, and *vice versa*, seemingly too wet soil could have excessive clay content (Keable and Keable, 1996; Minke, 2006).

Although Krahn (2019) urges that the *drop* test has not been proven precise and repeatable, the author recognises its efficiency and marks the test as compulsory in his manual. Maniatidis and Walker (2003) also mention the *drop* test, which is suited for a good first approximation of the optimum moisture content and for monitoring the moisture content during construction.

The standard procedure for determining the optimum moisture content at which a maximum dry density is achieved is the Proctor test (BS 1377-4:1990). In cylindrical moulds soil mixtures with different moisture contents are compacted using a standardised Proctor hammer (Houben and Guillard, 1994; Maniatidis and Walker, 2003; Minke, 2006). Keable and Keable (1996) and Krahn (2019) propose using a variety of a standardised Proctor test, using a square mould and a constant amount of compaction, to find the maximum dry density. It should be noted that the

standard Proctor test, with lower compaction energy, is more suitable for manually compacted rammed earth structures (Keable and Keable, 1996). The modified Proctor test could result in an overestimated optimum moisture content (Walker et al., 2005) and it is more suitable for pneumatically compacted rammed earth structures (Ávila et al., 2021; El Nabouch, 2017). However, according to Minke (2006), the compaction at optimum moisture content does not necessarily lead to the maximum density and compressive strength. Hence, Minke (2006) advocated using higher than the optimum moisture content, which he characterised as a minimum moisture content, and the same is repeated by Schroeder (2012). Walker et al. (2005) proposed using the soil at $\pm 1\text{--}2\%$ from the optimum moisture content determined by the experiment, while (NZS) allows using the water content within 3% of the optimum moisture content.

In 38 out of 50 articles reviewed articles (76%), information regarding optimum moisture content (OMC) and dry density (MDD) was given (Table 2.3). However, in a few instances, one of the pieces of information was omitted, usually the maximum dry density, thus N/A was written. A wide range of optimum moisture content reported in the literature was noticed, from 5.8% to 26.4%, but most values lay in the range of 8 to 12%. The range of maximum dry density values is slightly less dispersed. Values from 1526 to 2190 kg/m³ were reported in the reviewed literature.

Table 2.3: Optimum moisture content and maximum dry density of rammed earth in literature

OMC [%]	MDD [kg/m ³]	Reference
12.5	1850	(Maniatidis and Walker, 2008)
12	2017	(Jaquin et al., 2009)
9	2060	(Nowamooz and Chazallon, 2011)
5.8	N/A	(Ciancio et al., 2013)
8.3	N/A	
6.4	N/A	
7.4	N/A	

Table 2.3 continued from previous page

OMC [%]	MDD [kg/m ³]	Reference
9.6	N/A	
12	1920	(Silva et al., 2013)
12	1840	
12	1710	
10	2010	
11	1920	(Bui et al., 2014a,b)
7.6	2190	(Ciancio et al., 2014)
8	2018	(Gomes et al., 2014)
17.8	1733	
21.5	1651	
11.2	1600	
15.6	1814	
8	2018	
10.1	2100	(Silva et al., 2014a, 2016b)
15	1876	(Gerard et al., 2015)
10.1	1997	(Araki et al., 2016)
11	1950	(Champiré et al., 2016)
11	1970	
9	1980	
N/A	1870	(Arrigoni et al., 2017a)
8	2160	(Arrigoni et al., 2017b)
14	1820	(Lin et al., 2017)
16	1820	
11	1950	
16.3	1779	(Liu and Tong, 2017)
19.4	1697	

Table 2.3 continued from previous page

OMC [%]	MDD [kg/m ³]	Reference
20.9	1657	
24.2	1586	
26.4	1526	
12	1850	(El-Nabouch et al., 2018)
12.5	1950	(Xu et al., 2018)
9.8	2000	(Abhilash and Morel, 2019)
12.3	1860	
12.5	1900	(Chauhan et al., 2019)
14.1	1840	(Tinsley and Pavía, 2019)
12	N/A	(Toufigh and Kianfar, 2019)
9	1940	(Kosarimovahhed and Toufigh, 2020)
9.6	2060	(Chitimbo et al., 2022)
9	2055	(Ramezanpour et al., 2021)
12.5	1900	(Chauhan et al., 2022)
8	2165	(Gil-Martín et al., 2022)
8	1900	(Pelé-Peltier et al., 2022)
12	2020	(Romanazzi et al., 2022b)
19.7	1726	(Sen and Saha, 2022)
16	1700	(Barrera et al., 2023)
11.1	2020	(Baleca et al., 2023; Barsotti et al., 2023)
9.9	1872	(Dialmy et al., 2023)
9.6	1850	
12	2020	(Romanazzi et al., 2023)

Table 2.3 continued from previous page

OMC [%]	MDD [kg/m ³]	Reference
5.8	1526	MIN
26.4	2190	MAX
12.2	1896	MEAN
4.3	153.2	STANDARD DEVIATION
9.6	1820	1st QUARTILE
12.5	2015	3rd QUARTILE

2.4.3 Plasticity

The dependency of water content on soil state is a fairly familiar concept in soil mechanics, introduced by a Swedish soil scientist, Albert Atterberg (Reddi et al., 2012). Hence, the plasticity of the soil is usually characterised by testing the Atterberg limits: the liquid limit (LL), the plastic limit (PL), the shrinkage limit (SL), and the plasticity index (PI), which are commonly reported in the literature, except shrinkage limit. The transition between the limits is gradual, without abrupt changes (Reddi et al., 2012). Essentially, the liquid limit is a boundary between liquid and plastic states, the plastic limit is the boundary between plastic and semi-solid states, and the shrinkage limit is the boundary between the semi-solid and solid states (Minke, 2006).

The liquid limit (LL) can be determined using the Casagrande apparatus (Houben and Guillard, 1994; Reddi et al., 2012) as the minimum water content at which two parts of the soil sample separated by a standardised tool will come together at a distance of 13 mm, after 25 blows in the apparatus. Another commonly used method, that is the preferred procedure in literature, is the cone penetration test which defines the liquid limit as the water content at which a standardised cone (weight 80 g, angle 30°) sinks precisely 20 mm into the soil during a 5 s period (Reddi et al., 2012). The plastic limit (PL) is the minimum water content at which soil rolled into a cylindrical thread, 3 mm in diameter, does not crumble (Houben and Guillard, 1994; Reddi et al., 2012). The shrinkage limit is the minimum water content at which drying will not cause a volume decrease (Reddi et al., 2012). The

plasticity index, specified as the difference between the liquid and the plastic limit, indicates the potential deformation of the material (Avrami et al., 2008). Moreover, according to Maniatidis and Walker (2003), the plasticity index also indicates clay content, *i.e.* soil with a high clay content yields a higher plasticity index, which indicates a higher shrinkage rate of a dry soil sample. Additional information and a detailed description of the procedures can be found in standard BS 1377-2:1990 or publications regarding earthen construction requirements (Minke, 2006; Reddi et al., 2012).

Moreover, in standards and normative documents, several recommendations were given regarding upper and lower limits for liquid and plastic limits, or the plasticity index for rammed earth soil mixtures. Walker (2002) recommended using soil with a liquid limit in the range of 35 to 45% and a plasticity index ranging from 10 to 30%. Walker et al. (2005) limited only the upper value of the liquid limit to 45% but allowed the plasticity index in a wide range from 2 to 30%. Houben and Guillard (1994) recommended using the soil with a liquid limit of 25 to 45%, and a plasticity index also in the range of 2 to 30%. Doat et al. (1979) allowed the largest value of liquid limit, ranging from 25 to 50%, while their recommendation for the plasticity index was from 7 to 29%. Finally, Delgado and Guerrero (2007) suggested the narrowest range of liquid limit and plasticity index for soil mixtures suitable for rammed earth construction. Namely, they proposed a liquid limit in the range of 32 to 46% and a plasticity index ranging from 16 to 28%.

In 24 out of 50 reviewed articles (48%), information regarding soil plasticity, *i.e.* liquid limit and plasticity index, was given (Table 2.4). Moreover, liquid limit is reported in all reviewed articles, while information regarding plasticity index and plastic limit was omitted from two articles (Gomes et al., 2014; Silva et al., 2013). Missing values were denoted as N/A (not applicable) in Table 2.4. A high dispersion of values was observed, with the liquid limit and plastic limit ranging from 14.8 to 51.8% and 7.0 to 76.9%, respectively. The plasticity indexes presented in the reviewed articles ranged from 3.0 to 29%.

Furthermore, the values presented in the articles were compared with the literature recommendations described in the previous paragraph. Since recommendations were given separately for liquid limit and plasticity index, in Table 2.4 distinction

was made regarding complying with recommendations only for liquid limit, plasticity index, or both. If the category complied with none of the recommendations, non-applicable (N/A) was written. It was observed that more than 81% of reported data agree with recommendations given by Walker et al. (2005), for values of both liquid limit and the plasticity index. The remaining data corresponded to recommendations for either liquid limit or plasticity index in Walker et al. (2005). Furthermore, recommendations given by Doat et al. (1979) and Houben and Guillard (1994) complied with both values in more than 65%. The recommendations given in HB 195-2002 and Delgado and Guerrero (2007) corresponded to less than 20% of the data of liquid limit and plasticity index values as a group. However, more than 65% of the data agreed with the recommendation in HB 195-2002 regarding the minimum and maximum value of the plasticity index as an individual value. Finally, if both values did not correspond to a recommendation, the value for the plasticity index complied with literature recommendations in more cases than the liquid limit.

Table 2.4: Soil plasticity of rammed earth in literature

LL [%]	PL [%]	PI [%]	Reference	The regulation with which it complies		
				Only LL	Only PI	Both
49	25	24	(Maniatis and Walker, 2008)	N/A	HG, HB, W, DG	Do
27	19	8	(Bui et al., 2009a)	N/A	N/A	Do, HG, W
16	13	3	(Ciancio et al., 2013)	N/A	HG	W
26	12	14		N/A	HB	Do, HG, W
18	8	10		N/A	Do, HG, HB	
25	11	13		N/A	HB	Do, HG, W
35	16	18		N/A	N/A	Do, HG, HB, W, DG
34	N/A	N/A	(Silva et al., 2013)	Do, HG, W, DG	N/A	N/A
27	N/A	N/A		Do, HG, W	N/A	N/A
28	N/A	N/A		Do, HG, W	N/A	N/A
30	19	11		N/A	HB	Do, HG, W
26	20	6	(Gomes et al., 2014)	Do	N/A	HG, W
41.2	25.1	16.1		N/A	N/A	Do, HG, HB, W, DG
46.1	26.7	19.4		N/A	HG, HB W, DG	Do

Table 2.4 continued from previous page

				The regulation with which it complies		
LL [%]	PL [%]	PI [%]	Reference	Only LL	Only PI	Both
35.5	22	13.5		DG	HG, HB, W, DG	Do
17	N/A	N/A		W	N/A	N/A
14	N/A	N/A		W	N/A	N/A
23	16	7	(Silva et al., 2014a, 2016b)	N/A	Do, HG	W
32.5	15	17.5	(Gerard et al., 2015)	N/A	HB	Do, HG, W DG
24	18	7	(Champiré et al., 2016)	N/A	Do, HG	W
29	16	14		N/A	HB	Do, HG, W
20	16	4		N/A	HB	W
24	7	17	(Lin et al., 2017)	N/A	Do, HG, HB, DG	W
43	14	29		DG	N/A	Do, HG, HB, W
26	8	18		N/A	HB, DG	Do, HB, W
26.3	13.7	12.6	(Liu and Tong, 2017)	N/A	HB	Do, HG, W
28.1	14.7	13.4		N/A	HB	Do, HG, W
30.9	16.4	14.5		N/A	HB	Do, HG, W

Table 2.4 continued from previous page

LL [%]	PL [%]	PI [%]	Reference	The regulation with which it complies		
				Only LL	Only PI	Both
33.4	18	15.4		DG	HB	Do, HG, W
37.8	20.9	16.9		N/A	N/A	Do, HG, HB, W
43	21	22	(Xu et al., 2018)	N/A	N/A	Do, HG, HB, W, DG
27.4	16.4	11	(Chauhan et al., 2019, 2022)	N/A	HB	Do, HG, W
35	19	17	(Tinsley and Pavia, 2019)	N/A	N/A	Do, HG, HB, W, DG
30	19	11	(Chitimbo et al., 2022)	N/A	HB	Do, HG, W
26.1	14.8	11.3	(Ramezanpour et al., 2021)	N/A	HB	Do, HG, W
39.8	21.6	18.2	(Sen and Saha, 2022)	N/A	N/A	Do, HG, HB, W, DG
32	19	12	(Barrera et al., 2023)	DG	HB	Do, HG, W
25	21	4	(Baleca et al., 2023; Barsotti et al., 2023)	Do,	N/A	HG, W
28	36	8	(Dialmy et al., 2023)	N/A	N/A	Do, HG, W
27	35	8		N/A	N/A	Do, HG, W
51.8	76.9	25.1	(Koutous and Hilali, 2023)	N/A	Do, HG, HB, W, DG	N/A

Table 2.4 continued from previous page

				The regulation with which it complies		
LL [%]	PL [%]	PI [%]	Reference	Only LL	Only PI	Both
32.8	43.4	10.6		DG,	HB	Do, HG, W
30	19.1	10.9	(Romanazzi et al., 2023)	N/A	HB	Do, HG, W
14.8	7	3	MIN			
51.8	76.9	29	MAX			
30.2	20.2	13.4	MEAN			
8.3	11.8	5.9	STANDARD DEVIATION			
26	14.9	10.3	1 st QUARTILE			
34	21	17	3 rd QUARTILE			

Note: Do = (Doat et al., 1979), HG = (Houben and Guillard, 1994), HB = (HB 195-2002),

W = (Walker et al., 2005), DG = (Delgado and Guerrero, 2007)

N/A = not applicable

2.4.4 Compressive strength

Rammed earth, similar to concrete, can predominantly resist compressive loads and is troubled by tension and shear loads, particularly if the element is still moist (Maniatidis and Walker, 2003). However, as Houben and Guillard (1994) pointed out, soil can be considered a low-strength concrete due to its low compressive strength coupled with high specific gravity. According to Keable and Keable (1996), all parts of the building process contribute to the compressive strength of the rammed earth construction. Namely, they indicate the importance of soil mixture and optimum moisture content, but also mixing and ramming inside a well-constructed formwork. Therefore, the strength of a rammed earth element is unattainable to predict without performing testing (Maniatidis and Walker, 2003). However, a uniform procedure for testing mechanical properties has still not been developed. Instead, procedures from concrete and masonry standards have been adopted. The applicability of the adopted test procedures has not been reliably proven. The latter is necessary for increasing the competitiveness of earthen building techniques and raising them to the level of commonly used concrete and masonry structures (Schroeder, 2012). Furthermore, one cannot identify a universal value for the compressive strength of rammed earth due to the high variability of the raw earth material properties. Thus, Abhilash et al. (2022) suggested that the compressive strength should be evaluated individually for each rammed earth construction. Also, Keable and Keable (1996) suggest that the simplest way of determining soil suitability is to prepare a small rammed earth sample and use it to test compressive strength. It should be noted that they suggest using a simple, non-destructive compressive strength field tester. Nonetheless, if the compressive strength of the rammed earth cube, at least eight hours after production, is 0.5 to 0.75 MPa, after a week it should be two or three times bigger and in compliance with requirements. However, they urge the reader to perform a full set of laboratory tests for a more detailed identification of the soil.

Due to the similar nature of rammed earth and concrete (*i.e.* high compressive and low tensile strength), compressive strength is usually determined by laboratory tests corresponding to concrete standards or less frequent masonry (Maniatidis and Walker, 2003). Therefore, test samples (cylinders, prisms or cubes) are loaded until failure, and compressive strength is determined according to the maximum ap-

Table 2.5: Compressive strength test specimen details in standards

Cylinder		Prism			No. of required specimens	Reference
ϕ	h	l	w	h		
[mm]	[mm]	[mm]	[mm]	[mm]		
150	110	150	$1.3 \times h$	150	5	(CSIRO Bulletin 5)
150	300	N/A	N/A	N/A	1 sample every 25-100 m ²	(HB 195-2002)
N/A	N/A	102	102	102	N/A	(14.7.4 NMAC)
N/A	N/A	N/A	$2 \times h$	N/A	5	(NZS 4298)
N/A	N/A	200	200	200	3	(Lehmbau Regeln)
N/A	N/A	300	300	300	10	(MOPT Tapial)

plied load. Moreover, Maniatidis and Walker (2003) recommend avoiding designing rammed earth elements for pure tension and assuming bending and shear strength to be zero without experimental data proving otherwise. According to Schroeder (2016), compressive strength, which is usually the only one determined, is abundant.

Houben and Guillard (1994) pointed out that even though for a single-story, a downward thrust equals around 0.1 MPa, one should require a much higher compressive strength, in total 24 times larger, due to several safety factors: the construction process, material quality, loading, and the ratio of wet and dry strength. Therefore, an earthen sample should have a compressive strength of at least 2.4 MPa after 28 days of drying. Moreover, without any special information regarding a structure height, a specimen compressed to 90–95%, according to standard Proctor, should have a compressive strength of about 2 MPa, which should increase by about 40% after 1 year and by about 50% after 2 years. Other sources proposed significantly smaller values for the safety factor, *i.e.* 6.7 to 8 (Lehmbau Regeln; Regeln zum Bauen mit Lehm) and even 3 to 6 (MOPT Tapial; Rammed Earth: Design and Construction Guidelines). What is more, even though researchers usually condition samples for 28 days, following the concrete standards, Schroeder (2016) recommends drying specimens until equilibrium moisture content is reached (no weight change) – at least 6 weeks, without artificial acceleration. Also, a decrease in specimen dimensions leads to an increase in compressive strength. In (Table 2.5) details regarding

Table 2.6: Recommended minimal and design values for compressive strength

$f_{c,min}$ [MPa]	$f_{c,d}$ [MPa]	Reference
N/A	0.7	(CSIRO Bulletin 5)
1	N/A	(EBAA)
1	0.4 - 0.6	(HB 195-2002)
2.07	N/A	(14.7.4 NMAC)
N/A	0.5	(NZS 4298)
1.5/2 ^a	N/A	(Keable and Keable, 1996) & (SAZS 724)
N/A	0.3 - 0.5	(Lehmbau Regeln)
N/A	0.2/0.13 ^b	(MOPT Tapial)
N/A	0.3 - 0.5	(Regeln zum Bauen mit Lehm)
1	N/A	(Walker et al., 2005)
2	N/A	(Houben and Guillard, 1994)

Note: ^a = for two-storey walls, ^b = in wet environment

test specimens for compressive strength tests were reported. In six standards, various specimen dimensions and shapes were noted. Cylindrical specimens were noted only in Australian standards (CSIRO Bulletin 5; HB 195-2002). Moreover, the number of specimens required for each case ranges from 3 to 10. Recommended minimal and design values also vary from one source to another (Table 2.6), though there is no big dispersion. Minimal recommended values of compressive strength do not appear to be less than 1 MPa or more than 2 MPa, while design values range from 0.2 to 0.7 MPa.

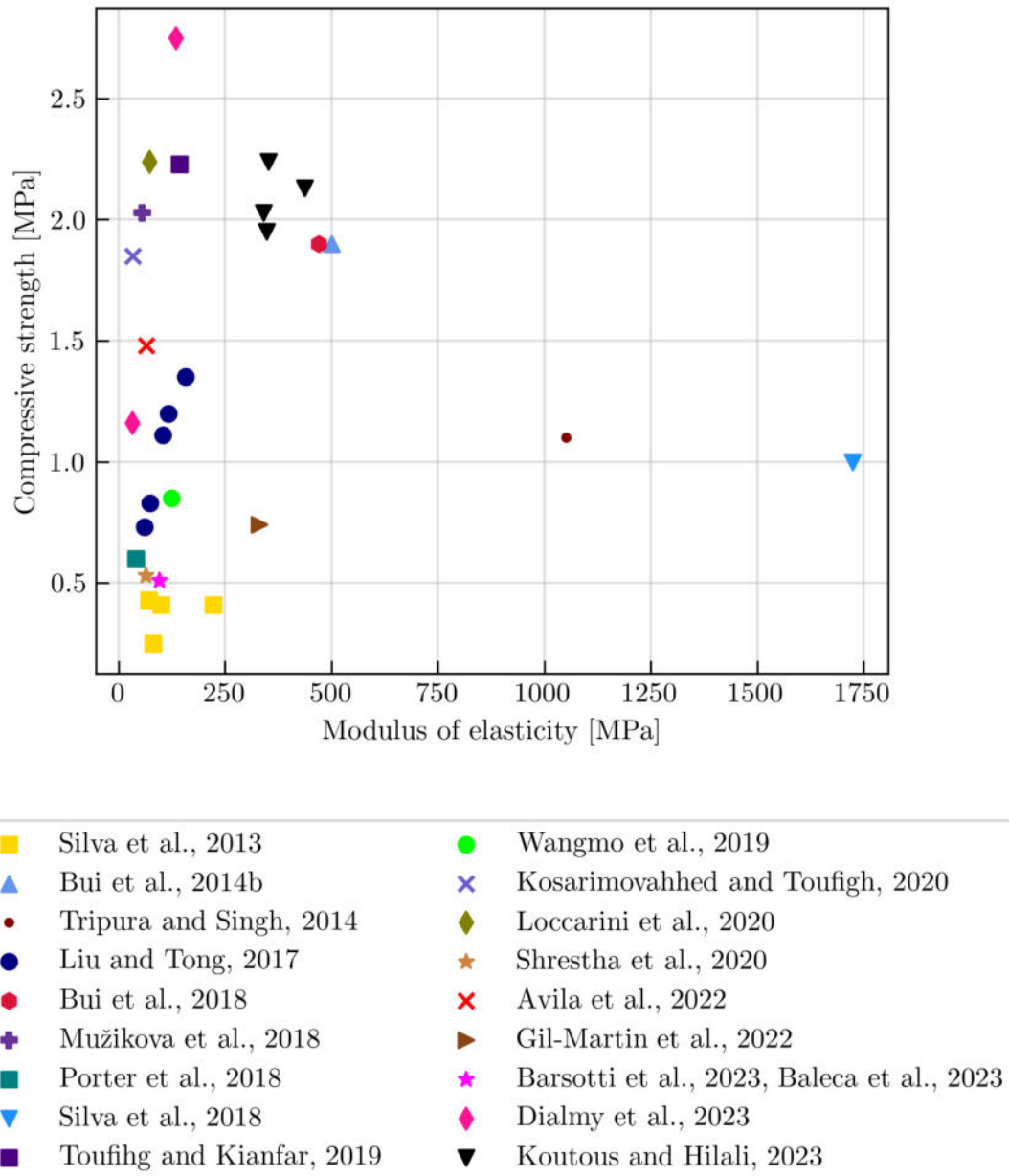


Figure 2.11: Compressive strength in function of modulus of elasticity - values from published articles

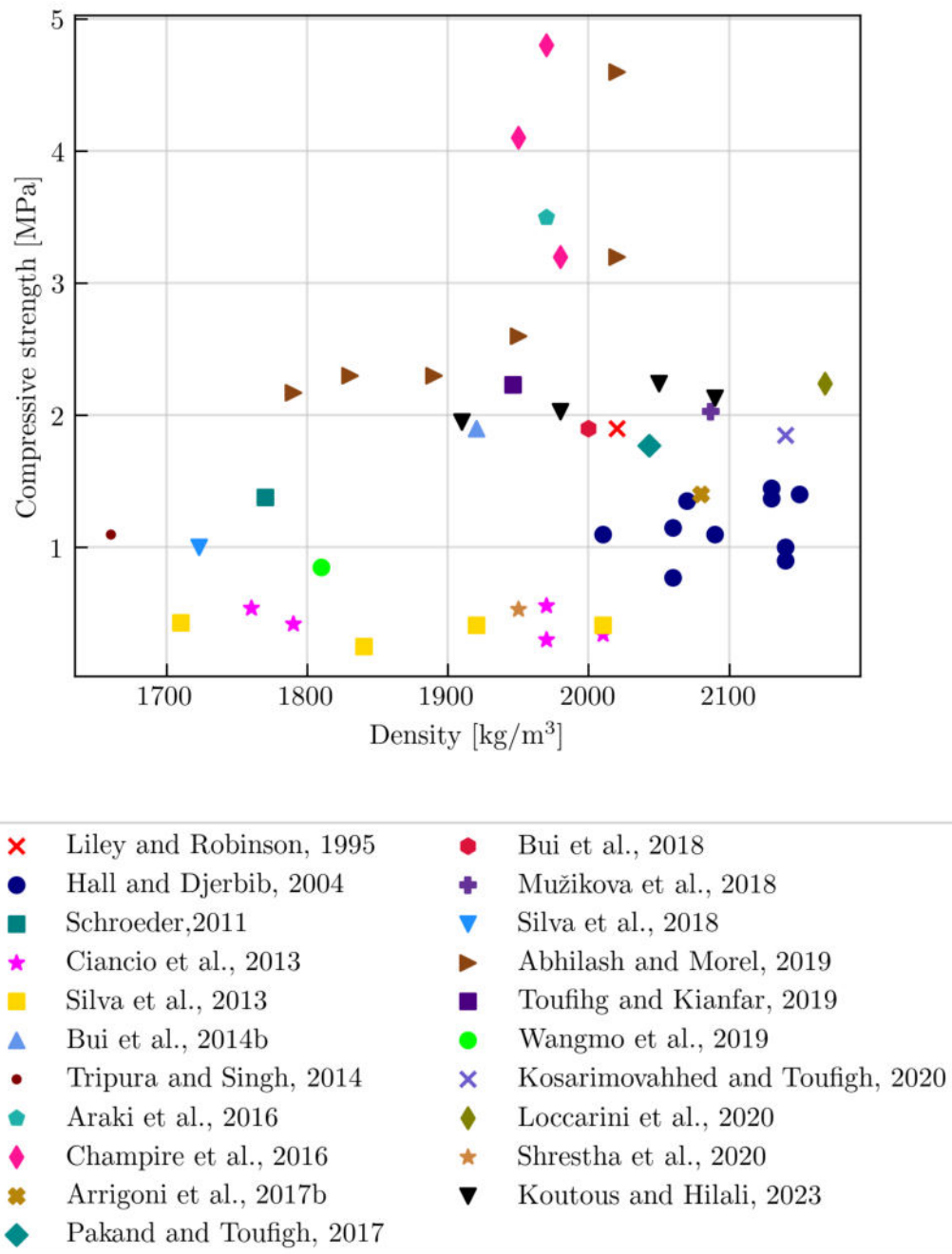


Figure 2.12: Compressive strength in function of density - values from published articles

Table 2.7: Compressive strength of rammed earth samples reported in reviewed articles

Sample [mm]	UCS [MPa]	E [MPa]	ρ [kg/m ³]	Reference
150 × 150 × 150	1.9	N/A	2020	(Liley and Robinson, 1995)
150 × 150 × 150	0.9	N/A	2140	(Hall and Djerbib, 2004)
	1	N/A	2140	
	0.77	N/A	2060	
	1.1	N/A	2010	
	1.4	N/A	2150	
	1.37	N/A	2130	
	1.45	N/A	2130	
	1.15	N/A	2060	
	1.35	N/A	2070	
	1.1	N/A	2090	
ϕ 160, h = 265	2.2	N/A	N/A	(Bui et al., 2009b)
200 × 200 × 200	1.38	N/A	1770	(Schroeder, 2011)
ϕ 100, h = 200	0.3	N/A	1970	(Ciancio et al., 2013)
	0.56	N/A	1970	
	0.34	N/A	2010	
	0.42	N/A	1790	

Table 2.7 continued from previous page

Sample [mm]	UCS [MPa]	E [MPa]	ρ [kg/m ³]	Reference
	0.54	N/A	1760	
ϕ 100, h = 200	0.41	100	1920	(Silva et al., 2013)
	0.25	80.5	1840	
	0.43	70.6	1710	
	0.41	221.6	2010	
ϕ 160, h = 300	1.9	500	1920	(Bui et al., 2014b)
100 \times 100 \times 100	1.1	1050	1660	(Tripura and Singh, 2014)
ϕ 50, h = 100	3.5	N/A	1970	(Araki et al., 2016)
ϕ 64.4, h = 140	4.8	N/A	1970	(Champiré et al., 2016)
	4.1	N/A	1950	
	3.1	N/A	1980	
ϕ 100, h = 200	1.4	N/A	2080	(Arrigoni et al., 2017b)
ϕ 39, h = 80	1.35	157.3	1649	(Liu and Tong, 2017)
	1.2	117.6		
	1.11	103.7		
	0.83	74.3		
	0.73	60.5		

Table 2.7 continued from previous page

Sample [mm]	UCS [MPa]	E [MPa]	ρ [kg/m ³]	Reference
ϕ 75, h = 150	1.77	N/A	2043	(Pakand and Toufigh, 2017)
150 \times 150 \times 150	1.9	470	2000	(Bui et al., 2018)
100 \times 20 \times 20	2.03	54.6	2087	(Mužiková et al., 2018)
150 \times 150 \times 150	0.6	40	N/A	(Porter et al., 2018)
ϕ 150, h = 230	1	67	1723	(Silva et al., 2018)
ϕ 160, h = 300	2.3	N/A	1890	(Abhilash and Morel, 2019)
	2.6	N/A	1950	
	3.2	N/A	2020	
ϕ 110, h = 220	2.17	N/A	1790	
	2.3	N/A	1830	
	4.6	N/A	2020	
ϕ 75, h = 150	2.23	143	1946	(Toufigh and Kianfar, 2019)
ϕ 92, h = 180	0.85	123.5	1810	(Wangmo et al., 2019)
ϕ 75, h = 150	1.85	34	2140	(Kosarimovahed and Toufigh, 2020)
80 \times 80 \times 80	2.24	71.9	2168	(Loccarini et al., 2020)
ϕ 92 - 96, h = 163 - 200	0.53	63.4	1950	(Shrestha et al., 2020a)
ϕ 100, h = 200	2.03	340	1980	(Koutous and Hilali, 2021)

Table 2.7 continued from previous page

Sample [mm]	UCS [MPa]	E [MPa]	ρ [kg/m ³]	Reference
100 × 100 × 100	1.48	65	N/A	(Ávila et al., 2022)
ϕ 150, h = 300	0.74	330	N/A	(Gil-Martín et al., 2022)
60 × 210 × 60	2.57	N/A	N/A	(Misseri and Rovero, 2022)
h: ϕ = 2:1	0.51	96	N/A	(Baleca et al., 2023; Barsotti et al., 2023)
ϕ 150, h = 300	2.07	N/A	N/A	(Barrera et al., 2023)
ϕ 150, h = 200	1.16	31.4	N/A	(Dialmy et al., 2023)
	2.75	133.5	N/A	
ϕ 100, h = 200	1.95	348	1910	(Koutous and Hilali, 2023)
	2.03	340	1980	
	2.13	437	2090	
	2.24	352	2050	

Values of compressive strength, modulus of elasticity, and dry density reported in the published articles were gathered and reported in Table 2.7. Firstly, both cylindrical and prismatic specimens were used in a high variety of sizes, as could be assumed based on Table 2.5. The compressive strength was reported to range from 0.25 to 4.8 MPa, while the modulus of elasticity ranged from 31.4 to 1050 MPa. Moreover, of the more than 30 research papers reviewed, modulus of elasticity is reported in 19 of them. It should be noted, however, that due to difficulties regarding placing measuring instruments on the rammed earth sample, the modulus of elasticity is usually estimated based on the stress-strain curve and not measured. Density values were slightly less widespread, ranging from 1649 to 2168 kg/m³.

A high level of scatter is even more obvious if Figure 2.11 and Figure 2.12 are observed. What is more, no apparent relationship between compressive strength and modulus of elasticity or density can be recognised. It supports the opinion of Abhilash et al. (2022) that excessive laboratory testing should be carried out for each rammed earth construction. However, caution should be taken when transferring laboratory test results to real construction due to differences in test and site conditions, such as the size of the test specimen and compaction energy (Schroeder, 2012). Laboratory-tested samples usually yield higher compressive strength and bulk density, reflecting short-term strength (*i.e.* fast load application) as opposed to the creep strength in the structural element (Schroeder, 2016).

2.4.5 Hydro-mechanical behaviour

Depending on the amount of voids between soil particles (*i.e.* degree of saturation), one can distinguish between saturated and unsaturated soil. Saturated soil contains only soil particles and water, while unsaturated soil assumes at least a portion of the voids are filled with air. In analysis and design, engineers usually assume saturated soil, even though it is not correct in all applications (Augarde, 2012). Moreover, unsaturated soil exhibits greater strength than saturated soil, thanks to suction. According to Augarde (2012), water between two grains of unsaturated soil is “pulling” them together, as opposed to saturated soil when grains are “pushed” apart by water. Hence, in unsaturated soil, the normal force at contact is greater, which leads to a greater frictional force and, finally, a greater shear strength. Con-

sequently, the difference between the air pressure and the pore water pressure is what is commonly referred to as suction. Unstabilised earthen constructions owe their stability precisely to suction. Even though they appear dry, a small amount of water is always present, and, according to Augarde (2012), they can never be completely dry. Practically, a wall will dry until humidity in pores between soil particles and relative humidity in the air surrounding the wall equalize (Bui et al., 2011b). Due to the small amount of water, suction is present and deserving of the strength of a structure. Even though it is known that suction is the sum of matric and osmotic suction, Jaquin et al. (2009) proposed that rammed earth owes its strength to matric suction. Furthermore, they pointed out that suction highly depends on relative humidity (RH), especially in rammed earth structures due to a large area of wall exposed to air. Especially in areas of high RH (100–95%), small changes can lead to fluctuations in total suction up to 1 MPa, while variations of RH below 95% cause much smaller changes. And since the majority of historic rammed earth structures are located in arid parts of the world with low RH, changes in suction over time will be small, eventually resulting in stability.

Principles of unsaturated soil mechanics were used for the mechanical characterisation of rammed earth for the first time by Jaquin et al. (2009). The relationship between suction and strength was determined in reviewed articles on several occasions by testing both properties at different moisture levels (Jaquin et al., 2009). According to Walker et al. (2005), the final value of compressive strength in a construction is estimated to be at least 50% higher than that of a moist sample. Moreover, it was shown that in sandy clay (soil comparable to one in a rammed earth structure), suction contributes to strength to a certain degree, upon which suction rises but strength remains at a plateau (Toll, 1990; Toll and Ong, 2003).

As mentioned, Jaquin et al. (2009), tested compressive strength and suction on samples whose moisture content varied between 5.5 and 10%, while Bui et al. (2011b, 2014a) increased the moisture content range (from 11–13% to 1–2%). Moreover, they tested different soils and concluded that, albeit compressive strength rises with a decrease in moisture content, the rate of increase depends on soil. Araldi et al. (2018) did not determine suction; instead, they concentrated on determining compressive strength at different moisture contents, among other properties. Three

different moisture contents were observed: naturally dry specimens (2%), dry specimens kept inside boxes under conditions of 97% RH and 21 °C to increase moisture content (4%) and specimens tested 24h after manufacturing (8%). They found the difference between the compressive strength of the sample with 4% and 2% moisture content to be around 30%, while the difference rises to 49% when 4% and 8% of moisture content are taken into consideration. The same trend was noticed when the modulus of elasticity was taken into consideration.

Champiré et al. (2016); Chauhan et al. (2019, 2022); Chitimbo et al. (2022); François et al. (2017); Gerard et al. (2015); Hajjar et al. (2018) all used special saline solutions to impose different RH levels and thus determine the relationship of suction and strength. Champiré et al. (2016) found that the compressive strength of samples conditioned at 95% RH was 60-80% of the strength of samples conditioned at 25% RH. Gerard et al. (2015) and François et al. (2017) found that samples conditioned at 97% RH (moisture: 6%) achieved 50% smaller compressive strength than samples conditioned at 40% RH (moisture: 2%). Moreover, Gerard et al. (2015) observed that the compressive strength of a saturated sample (moisture 14.5%) is 10% of the compressive strength at 40% RH. Chauhan et al. (2019, 2022); Hajjar et al. (2018) and Chitimbo et al. (2022) conditioned samples using seven saline solutions to impose RH from 9 to 97.3% and corresponding suction values. It was observed that compressive strength increases after additional compaction by performing unload-reload cycles during the compression strength test (Chauhan et al., 2019; Hajjar et al., 2018). Moreover, Hajjar et al. (2018) found that for RH around 60%, compressive strength is around 3 MPa, while Chauhan et al. (2019) and Chitimbo et al. (2022) observed a brittle failure in samples at higher suction states. Chitimbo et al. (2022) dried larger rammed earth prismatic samples (15 × 15 × 45 cm) over a longer period (0, 2, 3, 4, 6, 8, and 19 weeks) prior to performing the compressive strength test. They noticed that compressive strength increased by 60% in the 3-week drying period, while maximum strength was achieved after 6 weeks of drying. Moreover, Chauhan et al. (2022) developed a methodology for determining the required drying period for the rammed earth wall and concluded that 3-4 months of drying during the summer are needed, while a 6-month period is necessary during the winter conditions.

Beckett et al. (2018) on the other hand, conditioned samples at different temperatures (15 °C, 20 °C, 30 °C, and 40 °C) along different RH (30%, 50%, 70% and 90%). With a reduction in RH and a temperature increase, moisture content reduces, hence suction and compressive strength increase. Also, for the corresponding RH, compressive strength increased with temperature increase.

2.5 Experimental campaigns

The seismic behaviour of rammed earth constructions is still a matter of question. One could assume that ancient rammed earth buildings such as Alhambra Palace in Spain or The Great Wall of China have encountered seismic activities during their lifespan, which they have apparently withstood without serious damage. Silva et al. (2018) suggested that old rammed earth buildings successfully withstood seismic load by virtue of the traditional way of building. Namely, ancient buildings were usually one-story and had thick walls with a regular floor plan. However, today, traditional rammed earth buildings are more sensitive to earthquakes than conventional buildings such as concrete or masonry structures. According to Ortega et al. (2018), the reason for that lies in poor quality of building materials and workmanship, while Arto et al. (2020) believe that lack of maintenance and time deepen the deterioration, increasing the seismic vulnerability.

When it comes to modern rammed earth buildings, they should comply with standards and norms such as those presented in Table 2.1. Bui et al. (2011a) explained that Eurocode 8 can be utilised, but after them, to the author's best knowledge, no other researcher supported the claim with further research. Therefore, experimental testing of rammed earth walls is still a necessity in order to gain a better understanding of their seismic behaviour. Table 2.8 contains data regarding rammed earth walls subjected to in-plane loading published in reviewed articles. In-plane loading is applied as monotonically increasing (*i.e.* pushover method) in 40% of cases, while cyclic loading is used in 60% of articles. In one instance, presented in articles by Bui et al. (2014a,b), only vertical load was applied in the absence of horizontal displacement. It should be noted that in a few instances, the out-of-plane behaviour of walls was tested as well (Romanazzi et al., 2022b; Wangmo et al., 2019).

However, this being the first research of this scope regarding rammed earth walls from eastern Croatia, it was decided to focus only on in-plane load behaviour.

Furthermore, rammed earth walls are usually quadratic, with the same height and width, with just a few instances of a different geometry. The biggest deviation from the norm was presented in Romanazzi et al. (2022a) when an I-shaped wall was tested (a flat wall with two flanges) to understand side walls' contributions to the in-plane load resistance. It was observed that although wall dimensions correspond to a scaled model, the scale factor is reported in only four instances: 1:1 (Reyes et al., 2018), 1:1.25 (Romanazzi et al., 2022a), 1:2 (El-Nabouch et al., 2016, 2017) and 1:3 (Ramezanpour et al., 2021). However, it should be noted that the scale of the wall is usually determined by laboratory conditions and the size of the test rig. As for the number of tested walls per research, it usually ranges from one to three, while in only one instance, nine walls were tested per study (Wangmo et al., 2021).

For each rammed earth wall, when it was possible, the inter-story drift (IDR) was obtained. Therefore, comparison of this research with previously published research in articles would be easier, despite differences in geometry proportions. The test setup is usually a cantilever, with reinforced concrete beams under and above the rammed earth wall. However, another type of test setup was used, when a rammed earth panel was placed inside a steel (Arslan et al., 2017) or wooden frame (Baleca et al., 2023; Barsotti et al., 2023). The frame, with hinges in corners, enabled a rammed earth wall to endure much higher forces. In particular, walls with reinforced concrete beams showed IDR from 0.06 to 1.82%. On the other hand, a rammed earth wall inside a steel frame exhibited IDR from 2.49 to 2.64%, while a wooden frame enabled even higher IDR (5.1-5.8%). Finally, a vertical load in most cases was applied in ranges of 0.1 to 0.3 MPa. However, extremes were also present: Miccoli et al. (2016, 2017) applied a vertical load of 0.56 MPa, exaggerating on purpose to impose a desired failure behaviour, while Romanazzi et al. (2022a) applied an extremely low vertical load (0.0067 MPa) by virtue of placing only cement bags on top of the wall and not using hydraulic presses for additional load. Data published in research papers was used to determine the experimental setup for rammed earth walls presented in this thesis.

Table 2.8: Rammed earth walls subjected to in-plane loading published in literature (updated table from Perić Fekete et al. (2024))

Wall [m]	Testing method	σ_v [MPa]	IDR [%]	Reference
$1.0 \times 1.0 \times 0.3$	vertical load	MI	N/A	(Bui et al., 2014a,b)
$1.3 \times 1.05 \times 0.25$	cyclic load	0.56	0.47 - 0.55	(Miccoli et al., 2016, 2017)
$1.5 \times 1.5 \times 0.25$	pushover	0.10, 0.20, 0.30	0.73 - 1.06	(El-Nabouch et al., 2016, 2017)
$1.0 \times 1.5 \times 0.2$	pushover	0.10, 0.20, 0.30	0.60 - 0.70	
$1.5 \times 1.5 \times 0.2$	cyclic load	0	2.49 - 2.64	(Arslan et al., 2017)
$1.8 \times 2.5 \times 0.4$	cyclic load	0.018, 0.048, 0.067	1.16 - 1.82	(Reyes et al., 2018)
$1.2 \times 1.2 \times 0.6$	pushover	0	0.28 - 0.33	(Shrestha et al., 2020a,b)
$0.5 \times 0.5 \times 0.11$	pushover	0.10, 0.15, 0.20	1.06 - 3.54	(Wangmo et al., 2021)
$1.0 \times 0.9 \times 0.2$	cyclic load	0.10, 0.20, 0.30	1.24 - 1.49	(Ramezanpour et al., 2021)
$1.8 \times 2.8 \times 0.4^a$	cyclic load	0.0067	0.06 - 0.17	(Romanazzi et al., 2022a)
$1.5 \times 1.5 \times 0.25$	pushover	0.13	5.4 - 5.6	(Barsotti et al., 2023)
$1.5 \times 1.5 \times 0.25$	cyclic load	0.13	5.1 - 5.8	(Baleca et al., 2023)

Note: MI = monotonically increasing

^a = a wall with two wing walls at the end ($1.8 \times 1.2 \times 0.4$ m)

2.6 Numerical analysis

In this literature review, focus was put on numerical analysis performed using the finite element method (FEM), which can be carried out either as a micro-model or a macro-model (Bui et al., 2022). The micro-modelling strategy leads to accurate simulation at the local level of the model but requires high computational time and resources. Mesh needs to be refined on a higher level, and the analysis usually requires inputting computational parameters that need to be estimated. The latter leads to a considerable amount of uncertainty in the analysis. Therefore, according to Bui et al. (2022), macro-modelling might be a better approach for larger structures. That assumes utilising homogenous and continuous material with parameters that can be obtained directly from performing tests on specimens. Furthermore, other idealisations in terms of simpler geometry and elements can be implied. It should be noted, however, that the use of FEM analysis has not yet been adequately adapted for evaluating earthen structures (Bui et al., 2022). Despite that, FEM is commonly used for modelling rammed earth walls following laboratory testing. Another approach, discrete element modelling (DEM), did not show precedence to FEM in the case of modelling rammed earth (Bui et al., 2022), even though it was used in several instances (Bui et al., 2016, 2018, 2017).

Numerical models of rammed earth structures presented in articles were mainly developed using a macro-modelling approach, which does not take the layered structure of the rammed earth wall into consideration. A high variety of software was reported in the literature. *Diana* was mentioned in the highest percentage (Alahvirdizadeh et al., 2019; Miccoli et al., 2015, 2016; Shrestha et al., 2020b; Silva et al., 2014a,c; Wangmo et al., 2019, 2021), while *Abaqus* is the second most used software (Bui et al., 2019, 2020; Loccarini et al., 2020; Nguyen et al., 2021) for modelling rammed earth structures. Other software was used in much fewer instances: *ANSYS*: (Liu et al., 2014; Loccarini et al., 2020), *Adina*: (Loccarini et al., 2020) and *SAP2000*: (Gomes et al., 2011). Also, the usage of different computational codes is mentioned in three instances: CASTEM code (Bui et al., 2014b), Aster code (El-Nabouch et al., 2015) and CAST 3M code (Nowamooz and Chazallon, 2011). It should be noted that, although rammed earth walls are analysed in most cases, other types of structures were mentioned as well, such as arches (Loccarini et al.,

2020) and whole buildings (Gomes et al., 2011).

A complete description of models is presented in Table 2.9. As was explained in the previous paragraph, the majority of research papers report using Diana software. What is more, software usually governs the choice of constitutive model, *i.e.* TSRCM constitutive model is usually used when Diana software is applied. Also, it was determined that about half of the analysis comprises micro modelling, which implies each rammed earth layer is modelled separately. The testing method reported in Table 2.9 depended on experimental research previously performed based on which numerical analysis was modelled.

Table 2.9: Software used in literature

Software/code	Constitutive model	Micro-/macro-modelling	Testing method	Reference
SAP2000	N/A	macro-modelling	modal analysis	Gomes et al. (2011)
CAST 3M code	N/A	macro-modelling	pushover	Nowamooz and Chazallon (2011)
CASTEM code	N/A	macro-modelling	pushover IP	Bui et al. (2014b)
Diana	TSRCM + MC	micro-modelling	diagonal compression	Silva et al. (2014a,c)
ANSYS	MC	macro-modelling	pushover IP	Liu et al. (2014)
Aster code	DP	macro-modelling	pushover IP	El-Nabouch et al. (2015)
Diana	TSRCM + MC	micro-modelling	cyclic IP	Miccoli et al. (2015, 2016)
Abaqus	CDP + MC	micro-modelling	pushover IP	Bui et al. (2019)
Diana	TSRCM + MC	micro-modelling	pushover OoP	Wangmo et al. (2019)
Abaqus	CDP + MC	micro-modelling	pushover OoP	Bui et al. (2020)
ANSYS	DP	macro-modelling	vertical load of RE arch	Loccarini et al. (2020)
Abaqus	CDP	macro-modelling	vertical load of RE arch	Loccarini et al. (2020)
Adina	Concrete model	macro-modelling	vertical load of RE arch	Loccarini et al. (2020)
Diana	TSRCM + MC	micro-modelling	Pushover IP	Wangmo et al. (2021)
Diana	TSRCM + MC	both	pushover OoP	Allahvirdizadeh et al. (2019)
Diana	TSRCM + MC	micro-modelling	pushover IP	Shrestha et al. (2020a)
Abaqus	CDP	macro-modelling	RE house	Nguyen et al. (2021)

Note: TSRCM = total strain rotating crack model, MC = Mohr Coulomb

DP = Drucker Prager, CDP = Concrete Damage Plasticity, N/A = not applicable

Even though numerical analysis of rammed earth structures was the subject of more than 15 published articles, no consensus was reached on the optimal process of building a numerical model. The debate is still ongoing regarding the choice of software, using micro-modelling or macro-modelling strategy and the type of non-linear material used. However, the approaches used in published articles were used as a tool to understand the modelling approaches suitable for performing analyses of rammed earth structures. The selection of software was not based on the frequency of appearances in published articles but on the availability of software at the home university and previous knowledge. Based on that, the ANSYS software was chosen, since instances of using the ANSYS software for modelling rammed earth structures have appeared in the literature.

2.7 Conclusion

Even though rammed earth structures, along with other earthen buildings, have existed since ancient times, the research regarding their behaviour is still fairly new. Excessive research has begun yet in the 21st century. Several notable publications were written in the 20th century as well, but not as frequently. In recent decades, there has been an increase in awareness of the extent of climate change. That led to an increase in the popularity of earthen structures due to their low ecological impact. However, since earthen structures were built empirically in the past, there is not sufficient scientific knowledge regarding their mechanical and physical properties, as well as seismic behaviour. In this chapter, an overview of published manuals and guides was given, with emphasis on recommendations regarding minimum requirements for material and structure. A section was devoted to standards overview and another to the history of rammed earth houses in Croatia. Finally, more than 50 articles published on the topic of rammed earth structures were reviewed, and their key information was noted.

Rammed earth houses in Croatia were previously digested in three publications, that concentrated mostly on architectural aspects of structures, without reviewing structural capacity. However, the information is crucial in comprehending the circumstances and approximation of a time period in which still existing rammed

earth houses in eastern Croatia were built. What is more, an explanation of traditional building practices was given as well.

Standards and normative documents reviewed in this chapter give recommendations regarding construction design. Namely, wall dimensions are usually described by a function of thickness, which can range from 0.2 to 0.5 m, while openings should not exceed more than 1/3 of the total wall area. Reinforcement is mentioned in several publications, regarding foundations, plinth beams and wall bands. Also, concrete or wooden frame is usually mentioned as necessary, especially in danger of seismic activity. It should, however, be mentioned that for seismic design reader is usually referenced to explore more in the corresponding national normative document.

When construction soil is considered, in published research papers, particle size distribution, optimum moisture content and dry density and compressive strength were usually reported. However, in more than a few instances, plasticity and suction were presented as well. In this chapter, a short digestion of all material properties was given. Also, several recommendations were presented, regarding choosing an appropriate soil by performing simple field tests.

Particle size distribution in literature is usually described in permissible proportions of each soil particle size. The most commonly used envelope by Houben and Guillard (1994) was plotted. However, the particle size distribution presented in research papers was compared with ten more recommendations. It was determined that other than Houben and Guillard (1994), the majority of research agrees with recommendations by Walker et al. (2005) and HB 195-2002 as well. Also, it was determined based on 80 different granular compositions that high dispersion of particles can be observed. Namely, the proportions of particles range: 1-48% (clay), 1-83% (silt), 6-90% (sand) and 1-55% (gravel).

Optimum moisture content determined by the standard Proctor test and corresponding maximal dry density was presented in 38 out of 50 reviewed research papers. It was determined that a wide range of optimum moisture content was reported in the literature (5.8 to 26.4%), while maximum dry density ranged from 1526 to 2190 kg/m³. Plasticity was slightly less frequently reported since it was usually determined only to confirm the applicability of the soil for rammed earth

building. Again, a high range of values was reported: 14.8 to 51.8% (LL), 7.0 to 76.9% (PL) and 3.0 to 29.0% (PI). Most values corresponded to recommendations given by Doat et al. (1979) and Houben and Guillard (1994). Also, no apparent relationship between compressive strength and modulus of elasticity or dry density could be recognised.

Compressive strength was determined on samples of various shapes and sizes. It should also be mentioned that standards regarding rammed earth also do not agree on test samples and high variation was reported in that area as well. While compressive strength was usually tested, the modulus of elasticity is commonly determined based on the stress-strain curve. Values of compressive strength in research papers range highly from 0.25 to 4.8 MPa. However, despite the value of compressive strength, most samples yield a modulus of elasticity around 100 to 300 MPa.

Suction was determined in several research papers by following a variety of test methods. The most commonly used method implies using different saline solutions that impose different RH levels. What is more, suction was usually reported along with compressive strength, thus describing the changes in rammed earth sample behaviour with changed moisture content.

Experimental testing of rammed earth structures usually implies testing rammed earth walls. The majority of performed tests comprised testing the in-plane behaviour of rammed earth walls. However, the loading regime varied from monotonically increased (*i.e.* pushover) and cyclic loading. Also, vertical stress applied to the top of the wall ranged from very low values (0 and 0.0067 MPa) to very high and unexpected values for a rammed earth structure (0.56 MPa). Also, IDR values were determined for rammed earth walls reported in published articles. When the test set-up characteristic for testing masonry was implied (*i.e.* test specimen placed between two concrete beams), which was used most frequently in published articles, IDR values ranging from 0.28 to 1.06% were reported. However, changes in test set-up, geometry and vertical load implied major changes in IDR values.

Numerical analysis was performed several times in published research papers, however in fewer quantities than experimental testing of rammed earth walls. Due to that, no uniformity in approaches was recognised. Namely, the usage of several

software was observed, with each of them usually governing the decision regarding the constitutive model used for modelling. Also, micro and macro modelling approaches were recognised in equal proportions.

Knowledge gained through reviewing published articles and recommendations regarding rammed earth building practices was used in later phases of research. Namely, traditional building practices were supplemented with modern recommendations in normative documents, standards and manuals. Values reported in research papers were used as a reference for analysing values determined on produced samples. Also, test set-up and numerical analysis approaches were employed as a guide as well.

Chapter 3

Field observations

Earthen houses in Croatia are a traditional feature in the eastern parts of the country. Slavonia and Baranja were described as locations holding an important part of cultural heritage by Lončar-Vicković and Stober (2011) and Živković (2013). What is more, publications of both issues were supported by Croatian ministries, showing their recognition of earthen architecture. The Croatian Ministry of Culture and Media has also drawn up a *Strategy for the protection, preservation, and sustainable economic use of the cultural heritage of the Republic of Croatia*. The Strategy makes the protection and preservation of building heritage in Croatia compulsory. On a much higher scale, earthen constructions throughout the world make up 15% of UNESCO's world heritage list (Arto et al., 2020; Saidi et al., 2018).

Despite the recognition of earthen architecture on a local and global scale, there is no legal framework for building with earth in Croatia since no standards or normative documents have been developed. In order to open the possibility of standards development, exhaustive research on earthen architecture in eastern Croatia should be performed. This study was performed within the scope of the research project RE-forMS, which is the first attempt to scientifically comprehend rammed earth houses from eastern Croatia (Kraus et al., 2022). The focus of the project is the seismic behaviour of traditional rammed earth structures, but other properties, such as material composition, strength, and thermal properties, are researched as well.

To comprehend the current state of rammed earth houses in eastern Croatia, the frequency of their occurrence, and their characteristic geometrical proportions, field observation was conducted. Houses were documented and, with the owners'

permission, photographed, measured, and the material was collected according to the procedure in Gomes et al. (2014). In this chapter, five documented houses are presented in detail. Houses were observed in early spring, from the end of March until the end of April. When material collection was possible, laboratory tests were performed and reported. This knowledge gathered through field observation was used for determining experimental settings. Moreover, by noting information on rammed earth houses from eastern Croatia, a database regarding rammed earth houses worldwide was supplemented. It should be noted that the observed rammed earth constructions in eastern Croatia were mainly residential. Therefore, all buildings, whether their application was residential or industrial (*i.e.* outbuildings, storage spaces, or stable), are hereafter denoted *houses*.

3.1 Rammed earth houses in eastern Croatia

The field observation comprised more than thirty villages and two towns in Osijek-Baranja County and one village in Vukovar-Srijem County. Furthermore, 19 villages were screened entirely, *i.e.* all streets were analysed and visually identified rammed earth houses were noted. It should be noted that in approximately half of the settlements, only adobe houses were observed. A visual observation was possible due to the deteriorated state of the houses, owing to a lack of maintenance. Damaged rammed earth houses were usually still used for storage, while those in a better state are still in use for living or occasional occupancy (*e.g.* tourism). On Figure 3.1, settlements in which rammed earth houses were observed are noted, while settlements containing only adobe houses are omitted. Even though both rammed earth and adobe are techniques of building with earth, due to the different nature of the structure and material demands, adobe was not considered in this study.

In 15 settlements marked on Figure 3.1, more than 90 rammed earth houses were noted. Most of the houses were observed in Baranja (59%), while the remaining are located in Slavonia. Features observed in houses are in agreement with those described in Lončar-Vicković and Stober (2011) and Živković (2013). Encountered houses were usually elongated inside yards, with shorter façades and gable walls facing the street. Moreover, most of the houses contained porches inside the yard,



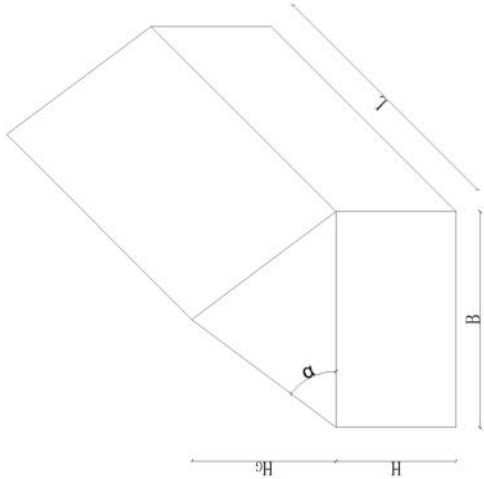
Figure 3.1: Approximate locations of settlements containing rammed earth houses (source: <https://croatia.eu/>, accessed on 25th January 2024)

from which one could enter the middle room of the house. The other two rooms could be entered from the middle room. Characteristic dimensions measured on ten observed rammed earth houses in eastern Croatia are presented in Table 3.1.

Dimensions are graphically explained in the sketch inside the table. The length of the houses (L) varies highly, but other dimensions are much more uniform. Namely, wall thickness (d_{wall}) varies from 40 to 55 cm, while the height of the wall from ground to gable wall (H) from 227 to 344 cm was measured. The width of the houses (B) from 450 to 657 cm was measured in the ten observed houses. However, it should be noted that width was measured as outer dimension and it is not the same as the largest span of the house.

Table 3.1: Characteristic dimensions of eastern Croatian rammed earth houses

No.	Geographical coordinates	B [cm]	L [cm]	H [cm]	H _G [cm]	α [°]	d _{wall} [cm]
1	45°39'50.5"N 18°46'19.6"E	450	532	267	N/A	N/A	40
2	45°47'55.9"N 18°47'57.6"E	513	800	270	270	46.47	55
3	45°45'09.5"N 18°44'26.1"E	527	1212	227	300	48.71	47
4	45°45'06.3"N 18°43'53.9"E	542	1530	340	N/A	N/A	50
5	45°45'07.3"N 18°44'06.6"E	550	1783	320	276	45.10	50
6	45°41'06.1"N 18°40'35.4"E	534	1710	344	309	49.17	N/A
7	45°31'13.3"N 18°52'20.6"E	505	1280	290	335	52.99	50
8	45°31'41.3"N 18°56'44.3"E	657	995	N/A	N/A	N/A	45
9	45°31'47.1"N 18°57'10.6"E	500	1451	239	273	47.52	50
10	45°31'38.7"N 18°56'33.9"E	515	1379	270	250	44.15	50
<hr/>							
MIN		450	532	227	250	44.15	40
MAX		657	1783	344	350	52.99	55
MEAN		529.3	1267.2	285.2	287.6	47.7	48.6
STANDARD DEVIATION		52.8	396.3	41.8	28.7	2.9	4.2
1 st QUARTILE		507	1049.3	267	271.5	45.8	47
3 rd QUARTILE		540	1510.3	320	304.5	48.9	50



In the following sections, five selected rammed earth houses from eastern Croatia are described with photographs and architectural plans. Based on the amount of material that was collected, physical and mechanical properties were determined. The labels for each house in the following sections were created based on the address of the house, which was purposely omitted from the text, to adhere to the privacy of the owners.

3.2 A-Z-73

The one-story rammed earth house is located in Aljmaš, a village in Osijek-Baranja county, and is in private ownership. The year of construction is estimated to be the 1930s, according to the owners. The house is uninhabited and in a fairly deteriorated state (Figure 3.2), hence it is not in use. One column of the porch is missing, making the roof structure unsafe for frequent use (Figure 3.2a). With the owners' permission, the house was documented, and a large amount of earthen material was collected. Therefore, it was possible to perform a great number of laboratory tests.

The layout of the house corresponds to a three-room house connected by the porch (Figure 3.3), as described in the literature (Lončar-Vicković and Stober, 2011; Živković, 2013). The external dimensions of the house are roughly 5×14 m, or 6.5×14 m if a porch is included. The first and third rooms have similar dimensions (ca. 4.15×4.5 m), while the middle room is significantly smaller (ca. 4.15×2.8 m). The remains of the fired brick chimney in the middle room indicate that the room was used as a kitchen area. Following the spatial organisation of the traditional earthen houses in the area, one could presume that the front room was the main room, serving as the living room, bedroom, and dining room, while the back room was the guest room.

The porch was presumably flanked by four columns; however, today only three remain. Two of the columns are constructed of fired brick, while the third one is wooden. Due to the deteriorated state of the porch and the house, one cannot, with security, presume how the communication through the rooms was organised. Namely, at the time the house was documented, the first door leading to the front room, which faces the street, was serviceable. However, the double door leading to

the third room was barricaded. What is more, owing to the damage to the inside walls, one could not be certain regarding the placement of the door that leads to the middle room in the house (Figure 3.3).

The gable is facing the street, and the street façade is characterised by two small windows (75×100 cm). Even though the majority of the traditional earthen houses were built on the edge separating the plot and street, this house is slightly indented into the yard. Outer, load-bearing walls are around 50 cm thick, while inner walls are a bit thinner (40 cm). All walls comprise approximately 10 cm of rammed earth layers and were originally completely covered with plaster. Ravages of time took a toll on the house, which is visible by the missing plaster and parts of the wall missing as well (Figure 3.2b).

The ceiling was constructed traditionally by filling the space between wooden beams using rolls of long straw and mud wrapped around wooden slats (cro. *vitlovi*). The largest span between load-bearing walls is 415 cm. The traditional gable roof is covered with flat clay tiles (cro. *biber crijep*) and is in a fairly deteriorated state, while the gable wall is constructed of wood planks.



(a) North-East façade in deteriorated state

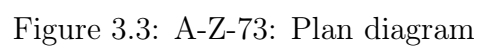


(b) South-West façade in deteriorated state

Figure 3.2: Authors' photographs of A-Z-73 house

3.3 *A-ZS-1*

This Aljmaš located rammed earth house was originally “U” shaped in plan view (Figure 3.5). However, the northern part of the building collapsed (Figure 3.4a). It appears like the core building was the usual three-room house with a porch, and *flange* buildings were added subsequently. The house is placed on top of a small hill, in close proximity to the Danube River. Due to the deteriorated state of the house, it is not in use for living or storage purposes. The year of construction is unknown,



and ownership is private.

Despite the unique layout of the house, the roof construction is a traditional gable roof, covered with flat clay tiles. However, unlike the majority of traditional earthen houses in the area, the roof runs parallel to the street. The yard entrance is placed along the northern façade, while the house entrance is placed inside the yard, on the west façade (Figure 3.4a).

Prior to the entrance, a small porch is covered with a roof, thus protecting the user from rain while walking between the rooms. Moreover, the porch ceiling and roof construction are supported by three square columns made of a combination of adobe and fired brick. The core building (*i.e.* the main living area) consisted of three connected rooms. The middle room was presumably the kitchen area since the fired brick chimney is still visible today. From the kitchen, one could enter the main room, which would traditionally face the street. However, in this house, the two windows in the main room face the yard entrance. The third room, which could be used as the guest room, could be entered only from the porch, as is the case with the two *flange* rooms, which presumably served as storage or as a room for young married couples (cro. *kijeri*).

The walls in the elongated part of the house are 50 cm thick, while in the subsequently built *flange* building, the thickness of the walls made of rammed earth and fired brick is 38 cm. Gable walls are built of adobe, while the northern wall of the house is protected by building a fired brick wall on the outer side of the house (Figure 3.4b). The fired brick wall was presumably built to secure the building from further collapse. The largest span between the load-bearing walls is 400 cm, while the ceiling construction was traditional, made of wooden beams and rolls of long straw and mud wrapped around wooden slats (cro. *vitlovi*).



(a) West façade in deteriorated state



(b) Fired brick wall built to support collapsed rammed earth wall

Figure 3.4: Authors' photographs of A-ZS-1 house

3.4 *BB-ZP-1*

This rammed earth house located in the village Bijelo Brdo, in Osijek-Baranja County, was used as a stable, but now it is only a storage space. The location of the BB-ZP-1 house inside the yard can indicate the original spatial organisation

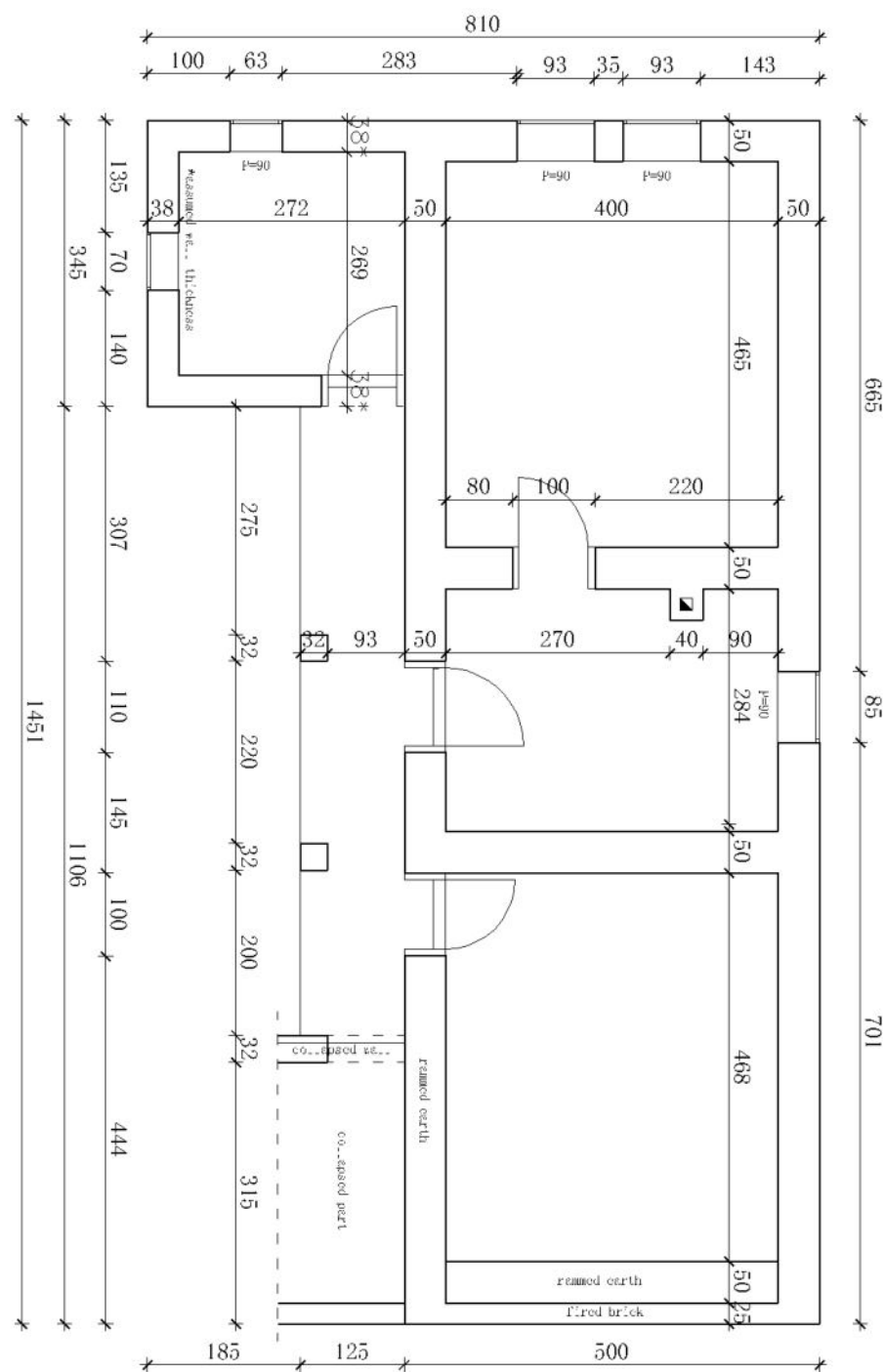


Figure 3.5: A-ZS-1: Plan diagram

of the house plot. Specifically, traditional earthen houses were usually located in the front portion of the yard, while utility buildings were placed below. Today, the modern residential building is located in the front portion of the yard. One could presume it was built in the place of the old, traditionally built house. The ownership of the building is private, but the year of construction is unknown.

Despite the non-residential use of the building, the layout is similar: three rooms connected by a porch (Figure 3.6a, Figure 3.7). Six circular columns flank the porch and support the roof construction, thus protecting the user from environmental influences such as rain, snow, and sunshine. The traditionally constructed ceiling is extended to the end of the porch. As is the case with previously presented rammed earth houses, wooden slats wrapped with mud and straw (cro. *vitlovi*) are used to fill the space between the two wooden beams. Above the ceiling, attic space was used as storage space. The gable roof is covered with flat clay tiles.

The dimensions of the building are roughly 5×13 m, while the porch adds an additional ca. 1.5 m to the width. The largest span between the load-bearing walls, which is essentially the inside width of each room, is 405 cm. All three rooms have similar dimensions.

The columns in the porch are all built of fired brick and are in fairly good condition, as is the majority of the load-bearing construction. The plaster, however, is missing from most of the façade, and the gable walls have collapsed (Figure 3.6b).

Rammed earth walls are 50 cm thick and made of layers from 6 to 10 cm high. Chopped straw could be identified in wall portions without plaster. Vines and thin branches were also used between the layers as simple reinforcement. According to the owner, the walls were constructed on a fired brick foundation, constructed by laying fired brick and then pouring a fine soil fraction over them. Due to the way the building was used, no windows were observed, and only three doors, for entering three rooms.



(a) South façade



(b) East façade

Figure 3.6: Authors' photographs of BB-ZP-1 house

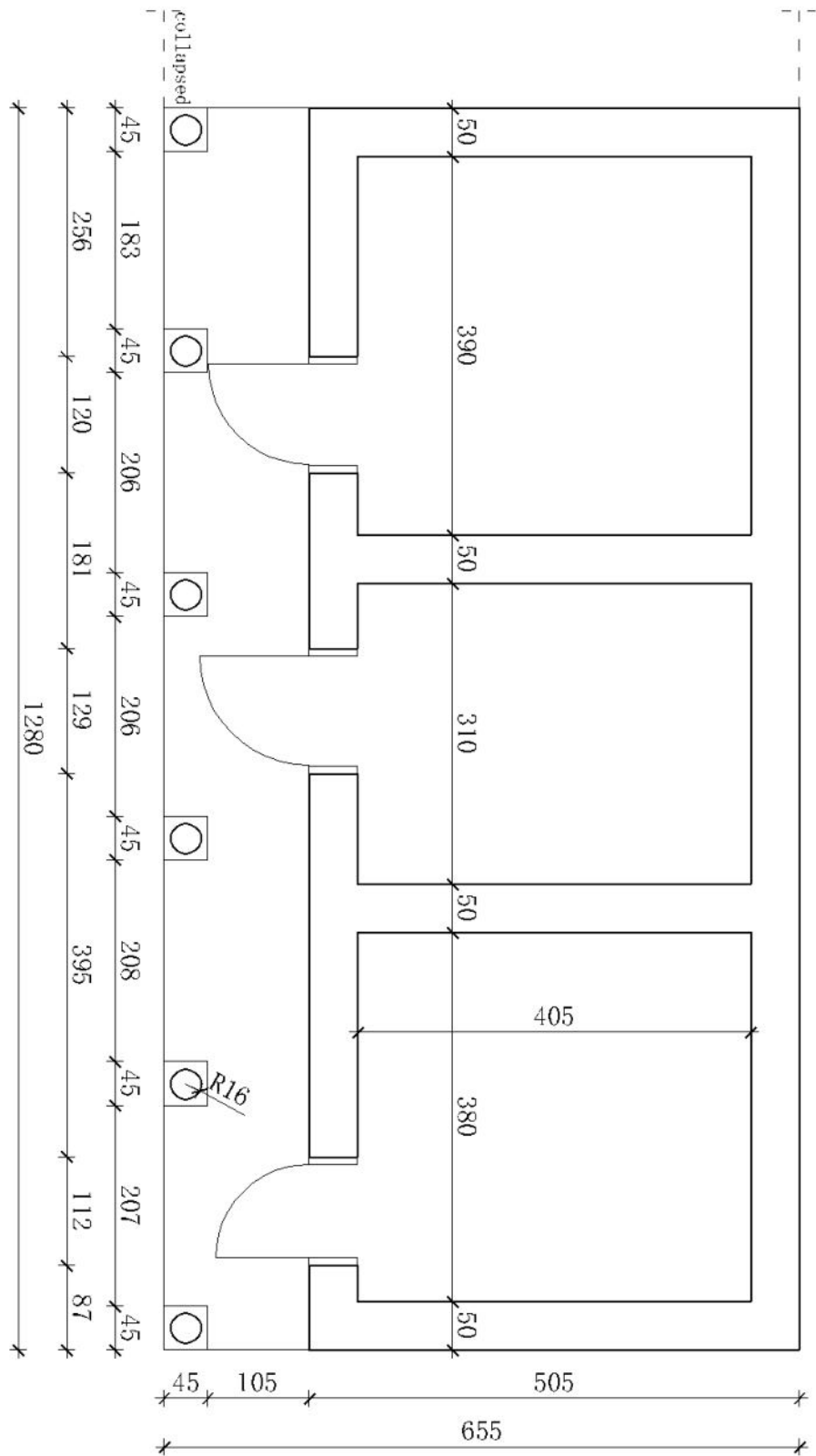


Figure 3.7: BB-ZP-1: Plan diagram

3.5 *C-SR-38*

The one-storey rammed earth house is located in Čeminac, a village in Osijek-Baranja County. It appears to be a classic example of a three-room house with a porch inside a yard (Lončar-Vicković and Stober, 2011; Živković, 2013), as it can be observed in Figure 3.8a and Figure 3.9. The year of construction is unknown, and the ownership is private. Moreover, it was not possible to enter the house, but based on the surroundings, one could assume it is not inhabited. It may be used for storage purposes. Deterioration is apparent, especially on the yard side.

The external dimensions of the house are roughly 6.8×17 m, with a porch included. Moreover, the house is located at the street line, and the 1.5 m wide porch contains an arched entrance from the street. Two windows (ca. 95×130 cm) are also facing the street. The porch is flanked by fired-brick columns. Today, five columns remain; however, following their arrangement, one could presume that the additional two columns are missing. The deterioration of the roof beam due to their absence is apparent.

The porch, being the major communication element in the traditional three-room house system, is extended along the house and ends with the same arched passage that leads further into the yard. Two doors lead from the porch into the house. If the traditional three-room house system is assumed, one of the doors presumably leads inside the middle room (usually the kitchen), from which the user can enter the front room. The other door leads inside the back room, which is usually used as the guest room.

Thanks to the roof construction, the porch is covered, preserving the house façade and protecting the user from weathering conditions. The roof is gabled and covered with traditionally used flat clay tiles. As is usually the case, the gable is oriented towards the street, while the other utility building is presumably located deeper inside the yard.

Rammed earth walls are made up of layers 10 cm high. The corners of the house are strengthened using fired brick (Figure 3.8b). Between fired bricks, layers of approx. 25 cm of rammed can be recognised. Moreover, fired brick can be found in the footings of the walls and porch columns as well. The gable wall is built from an adobe, and the largest span is 440 cm if 50 cm thick walls are assumed.



(a) South façade



(b) A detail of corner strengthened with fired brick

Figure 3.8: Authors' photographs of C-SR-38 house

3.6 *K-SP-6*

The rammed earth house is located in Karanac, an Ethno-village in Osijek-Baranja County. Moreover, Karanac is a part of Kneževi Vinogradi municipality, in which the largest percentage of rammed earth houses was observed. The house is presumably a three-room house with a porch (Lončar-Vicković and Stober, 2011; Živković, 2013). It could be deduced that the house is uninhabited, even though it was not possible to enter the rooms. Moreover, based on the surroundings, one could presume that the house is still in use for storage purposes. On the street fa

The house is located almost on the line on the neighbouring (northern) side of the plot. However, the street façade is slightly indented inside the yard (ca. 1 m). Two windows (ca. 80×150 cm) are facing the street, enabling light into, presumably, a main room if the three-room house is assumed. Moreover, on the street facade, a distinctive column creates the arched entrance to the porch.

The porch is covered by the roof, as is usual in traditional earthen buildings. Columns that typically flank the porch are missing in this house, except the first one (Figure 3.10a, Figure 3.11). However, one can assume the columns were a part of the original house but were demolished at some point and never rebuilt. Despite that, the roof is in quite a preserved state. even though some mending of the ceiling construction on the porch is visible.

According to the owner, the ceiling was constructed traditionally, using wooden slats wrapped in muddy straw (cro. *vitlovi*). Moreover, the attic floor was then covered with a layer of poured soil material, upon which oak planks were placed. That form of ceiling construction served as thermal insulation. The roof construction is, as expected, a gable roof, with the ridge oriented perpendicular to the street.

The external dimensions of the house are roughly 6.5×18 m, with an about 1 m wide porch. Two doors lead from the porch inside the house, presumably inside the kitchen and the back room (usually the guest room). The majority of the house is built of rammed earth walls, presumably 50 cm thick. The back rooms, however, are made of adobe walls, 50 cm thick. The privately owned house was built in 1883. Considering the long life span of the house, it is in a good state. However, plaster is missing from most parts of the northern façade and cracks can be observed (Figure 3.10b).

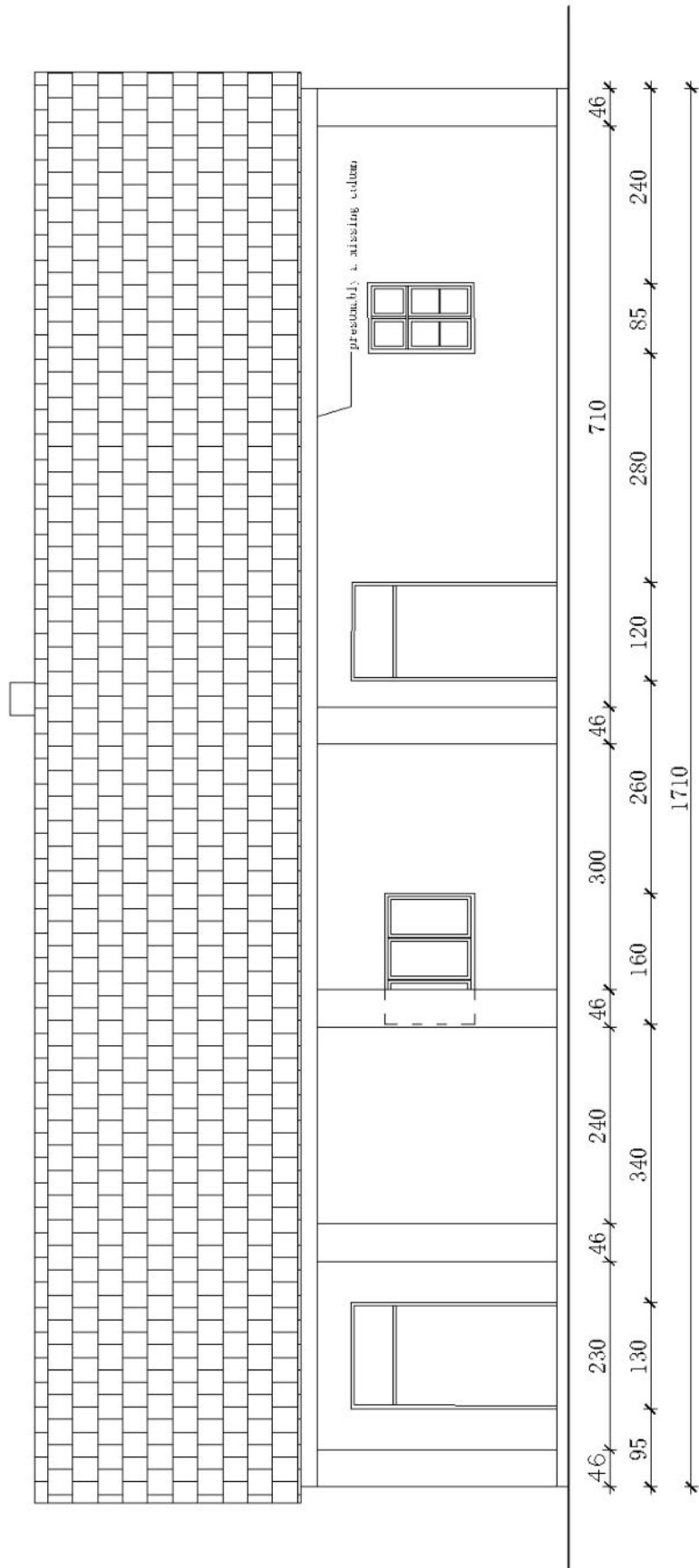


Figure 3.9: C-SR-38: Disposition of the south façade



(a) South façade



(b) Northern façade

Figure 3.10: Authors' photographs of K-SP-6 house

3.7 Experimental tests of collected material

Depending on the amount of collected material, a different range of laboratory tests could be performed. For example, for all houses presented in sections section 3.2 through section 3.6, the moisture content of the in-situ material was determined, while suction was determined for only one of them presented in section 3.2.

The reason for the different amounts of material collected during the field observation is the state of the construction, usage and accessibility. Specifically, if the building was in use for, at least, storage purposes and the construction was in a rather good state, it was decided not to collect an excessive amount of material to protect the construction. On the other hand, if the building was out of use and construction was already in an extremely deteriorated state, with the owners' permission, larger amounts of material were collected. Tests performed on material collected from each house are presented in Table 3.2, along with the standard according to which the test was conducted.

Table 3.2: Laboratory tests performed on collected samples

	A-Z-73	A-ZS-1	BB-ZP-1	C-SR-38	K-SP-6	Standard
w_0	+	+	+	+	+	HRN EN ISO 17892-1:2015
PSD	+	+	+	+	-	HRN EN ISO 17892-4:2016
LL, PL, PI	+	+	+	-	-	BS 1377-2:1990
UCS	+	+	+	-	-	BS EN 196-1:2005
s	+	-	-	-	-	ASTM S 6836-02

3.7.1 Moisture content

The moisture content of the in-situ material (w_0) was determined for all collected samples according to HRN EN ISO 17892-1:2015. The test was performed by drying a portion of earthen material in the oven at 105 °C, for 24 hours. The moisture content is then determined according to the mass of wet (m_{wet}) and completely dry

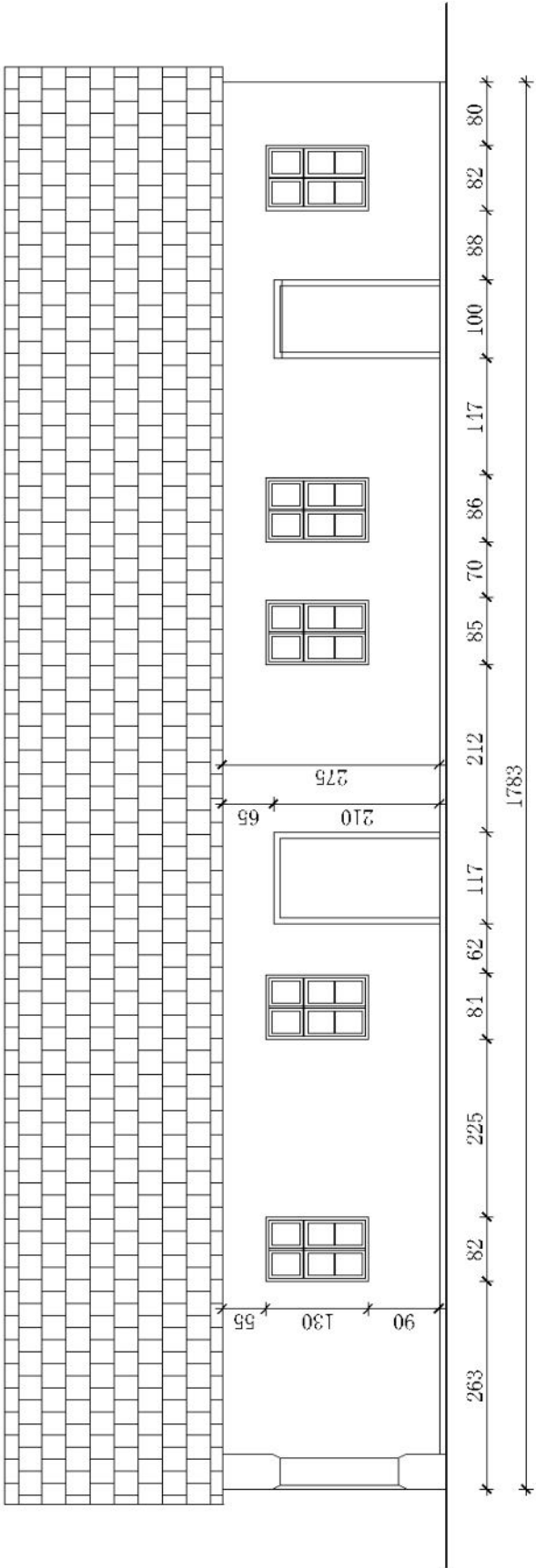


Figure 3.11: K-SP-6: Disposition of the south façade

material (m_{dry}), as exhibited in Equation 3.1:

$$w = \frac{m_{wet} - m_{dry}}{m_{dry}} \cdot 100\% \quad (3.1)$$

From house A-Z-73, two samples were collected at the end of April, during sunny weather. One from the outer part of the wall, at 2 m height, while the other one was collected from the inside, at 0.6 m height. Moisture content was determined for both samples as an average value from three specimens. Samples collected from the higher part of the wall showed an average moisture content of 2.8%, while samples collected closer to the ground had a moisture content of 3.6%. The latter exhibited a higher moisture content, presumably due to its proximity to the ground. Since traditional rammed earth houses had primitive waterproofing systems, and sometimes not even that, it is not surprising that capillary moisture made its way into the wall.

From house A-ZS-1, three samples were collected at the end of April, during sunny weather. Again, the moisture content of each sample was determined as the average of three values determined for each specimen. All three collected samples were exposed to the environment and weathering due to the highly deteriorated state of the house. Two samples collected from the pile of a previously collapsed rammed earth wall had moisture contents of 3.9% and 2.8%. A sample collected from the intact wall at 0.5 m height had a moisture content of 2.4%. It can be observed that the intact wall was at least slightly better protected from moisture from the ground than soil material from the collapsed wall, as could be expected.

Two samples collected from the BB-ZP-1 house were both collected from approximately 0.5 m in height. However, one was collected from the inside of the room and the other from the outer part of the rammed earth wall. The house was observed at the end of April on a cold but sunny day. Moisture content was determined as an average value from three specimens taken from each sample as two close values. Namely, the sample collected from the inside of the room had a moisture content of 6.7%, while the other sample collected outside had a moisture content of 6.5%. No difference between the moisture content on the inside and the outside parts of the wall could be determined. What is more, the values determined on samples from this house were undoubtedly the highest.

From house C-SR-38, two samples were collected as well, at the end of March, during a cloudy day. Both samples were collected from the outside part of the rammed earth wall since access to the interior was not possible. The first sample was collected from an approximate height of 0.6 m, while the second sample was collected from an approximate height of 1 m. Three specimens were taken from each sample to determine the average moisture content of each sample. Moisture content was determined as 3.6% and 2.6% for samples collected from heights of 0.6 m and 1 m, respectively. Again, as it was observed on samples collected from the A-Z-73 house, samples collected closer to the ground exhibited a higher value of moisture content, presumably due to the capillary moisture.

House K-SP-6 was observed on the same day as house C-SR-38. Due to the limited accessibility to the interior of the house, samples were also collected only from the outside parts of the rammed earth wall, from heights of 1.3 m and 1.7 m. As with other samples collected, three specimens were taken from each sample to get an average moisture content. For the sample collected from 1.3 m, a moisture content of 3.1% was determined, while the other sample, collected from a height of 1.7 m showed a moisture content of 3.0%. If these results are put into perspective with other results presented in this subsection, it can be assumed that the influence of the moisture from the ground ceases as the height of the wall increases.

3.7.2 Particle size distribution

Particle size distribution was determined for four out of five collected samples by a combination of wet sieving and sedimentation (hydrometer method), in accordance with HRN EN ISO 17892-4:2016. In four observed samples the proportions of particle sizes were determined as follows: clay (5.32% to 12.0%), silt (19.28% to 49.5%), sand (19.28% to 49.5%) and gravel (0.5-4.7%).

All grading curves were compared with envelopes presented in the Figure 2.10, subsection 2.4.1. Moreover, the envelope developed according to local mixtures from eastern Croatia, presented in Perić Fekete et al. (2024), was also plotted and compared to the other envelopes in the literature. The granular composition of the four collected samples exhibited in Figure 3.12, agrees with the local envelope (Perić Fekete et al., 2024), as expected. The other three literature suggestions

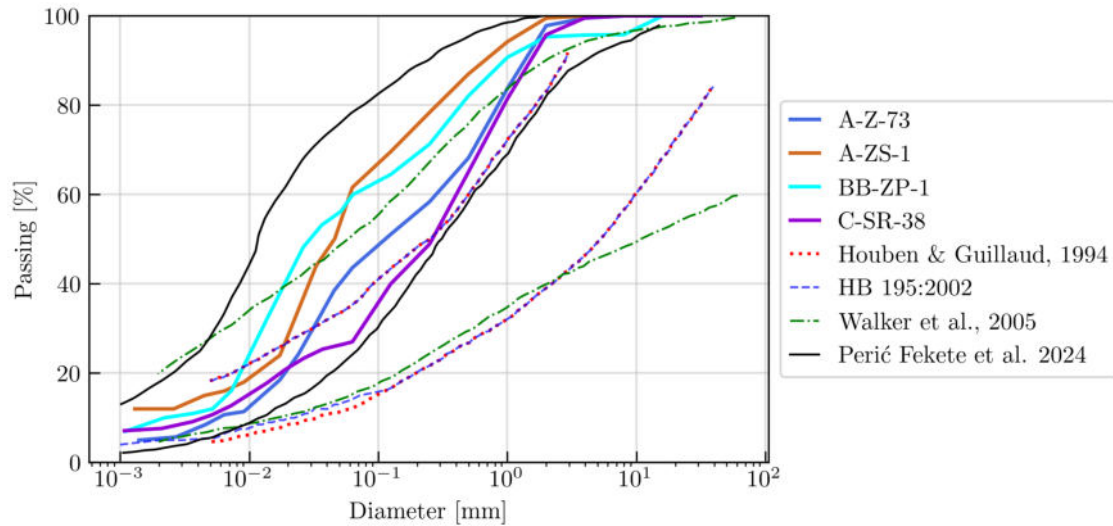


Figure 3.12: Particle size distribution of the material collected from rammed earth houses in eastern Croatia

(Houben and Guillaud, 1994; Walker, 2002; Walker et al., 2005), on the other hand, only partially align with the gathered samples' particle size distribution. The fine particle proportion of all PSD curves corresponds to the recommendations, while A-Z-73 and C-SR-38 correspond to the recommendation envelopes even more. What is more, all four PSD curves also agree with the clay recommendation given by Keable and Keable (1996) and SAZS 724, while three of them, except A-Z-73, agree with the clay recommendation by Keefe (2005). If sand and gravel are considered together, as is usually defined by reviewed guides and normative documents, the particle size distribution of material collected from house C-SR-38 corresponds to all three recommendations given in Figure 3.12.

3.7.3 Plasticity

Plasticity properties (LL, PL and PI) were determined for three out of five samples, according to BS 1377-2:1990. The soil sample was previously prepared by wet sieving, limiting the largest particle size to 0.425 mm. The liquid limit (LL) was determined using a cone penetration test. The plastic limit (PL) was determined by rolling soil into a cylindrical thread (ϕ 3 mm). Finally, the plasticity index (PI)

Table 3.3: Soil plasticity of collected rammed earth samples

House	LL [%]	PL [%]	PI [%]	The regulations with which it complies		
				only LL	only PI	both
A-Z-73	32	20	12	N/A	HB	Do, HG, W
A-ZS-1	32.4	18.8	13.6	Dg	HB	Do, HG, W
BB-ZP-1	36.4	19.7	16.7	N/A	N/A	Do, HG, HB, W, Dg
MIN	32	18.8	12			
MAX	36.4	20	16.7			

Note: *Do* = (Doat et al., 1979), *HG* = (Houben and Guillard, 1994),

HB = (HB 195-2002), *W* = (Walker et al., 2005),

DG = (Delgado and Guerrero, 2007)

was determined as a difference between the liquid and plastic limits (Equation 3.2).

$$PI = LL - PL \quad (3.2)$$

In Table 3.3, plasticity properties determined on samples collected from three houses in eastern Croatia are reported. According to USCS classification (ASTM D 2487-17), all three samples collected from houses in Aljmaš (A-Z-73 and A-ZS-1) and Bijelo Brdo (BB-ZP-1) are classified as low-plasticity. According to the ESCS classification (HRN EN ISO 14688-2), the limit between low and medium plasticity is 35%, while the limit between medium and high plasticity is 50%. Following that, samples from houses in Aljmaš (A-Z-73 and A-ZS-1) would remain classified as low-plasticity, while sample BB-ZP-1 would become medium-plasticity.

All samples comply with recommendations by Doat et al. (1979); Houben and Guillard (1994) and Walker et al. (2005) in both LL and PI, while sample BB-ZP-1 complies with all five recommendations considered. Minimum and maximum values of limits fall between the extreme values in published articles (Table 2.4). Hence, according to determined soil plasticity, samples collected from rammed earth houses in eastern Croatia agree with soil used worldwide, even though differences in particle size distribution exist.

3.7.4 Unconfined compressive strength

Unconfined compressive strength (UCS) was determined by following the standard for testing compressive strength in cement samples (BS EN 196-1:2005). That standard was chosen because, due to the size and shape of the collected samples, it was not possible to cut cylindrical or cubical samples characteristic for testing compressive strength in concrete (*i.e.* diameter (ϕ) 15 cm, $h = 30$ cm, or $15 \times 15 \times 15$ cm), as is common for rammed earth samples.

Therefore, samples resembling those on which compressive strength in cement and mortar is tested (*i.e.* 4×4 cm in cross-section) were cut using a circular saw from collected pieces of material (Figure 3.13). Loading was performed with a stress control of 0.01 MPa/s using a Shimadzu AG-X plus 50 kN testing machine.

Testing was performed on samples collected from three rammed earth houses in eastern Croatia (A-Z-73, A-ZS-1, and BB-ZP-1). Because houses were out of use and in a deteriorated state, a large number of samples could be collected. What is more, owing to the size of the samples, several small specimens could be cut for testing the UCS. From each sample, between two and five specimens were cut. Results are presented as stress-strain curves (Figure 3.14) and in Table 3.4, where average values of compressive strength and moisture content at the time of the test were also presented.

Five specimens tested from sample 1 obtained in the A-Z-73 house showed remarkably higher compressive strength than other samples, despite moisture content in the same range as other samples. Moreover, samples collected from house



Figure 3.13: Cutting rammed earth samples

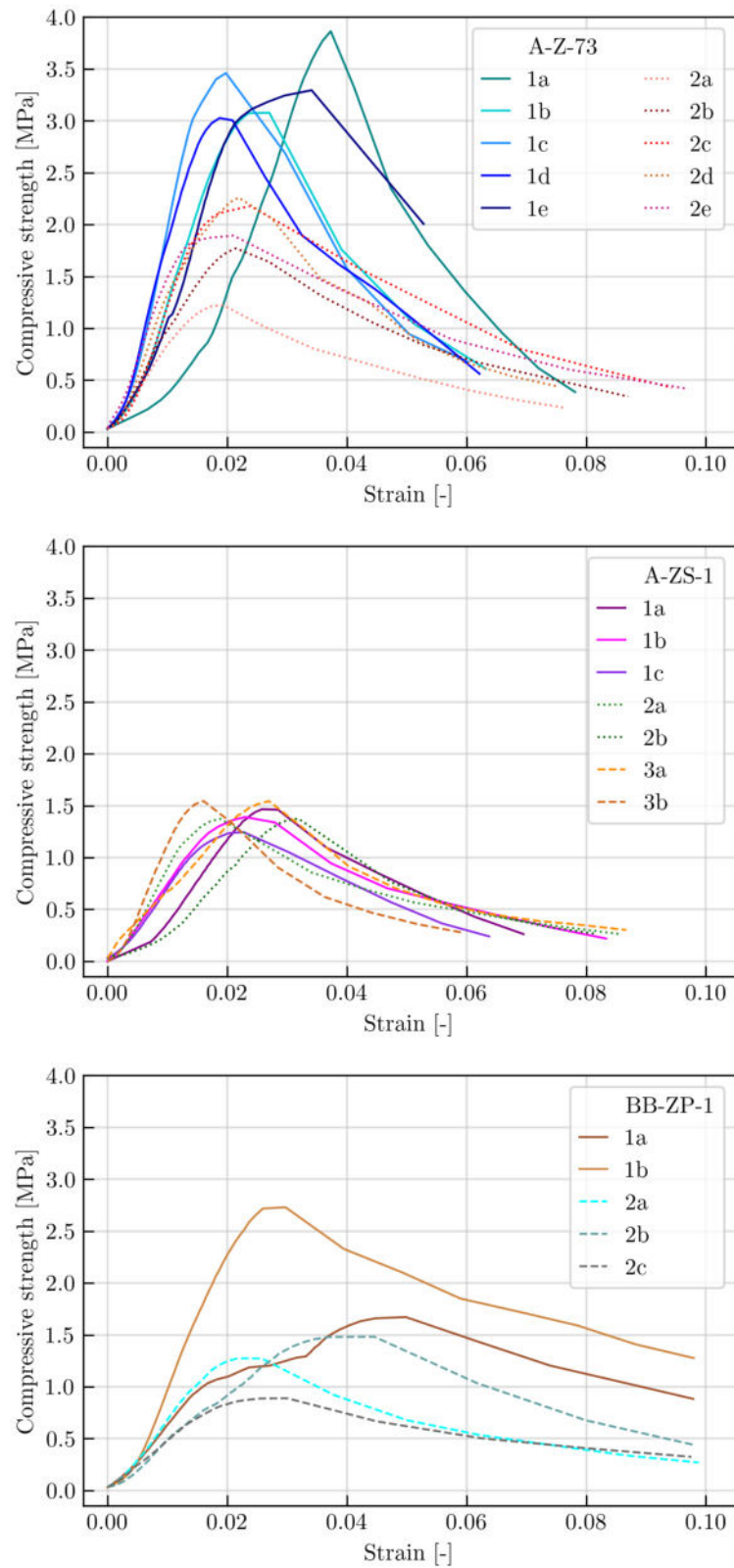


Figure 3.14: Stress-strain curves of tested in-situ samples

Table 3.4: Average values of compressive strength and moisture content

House	Sample	No. of specimen tested	UCS [MPa]	w_t [%]
A-Z-73	1	5	3.38	2.23
	2	5	1.88	2.82
A-ZS-1	1	3	1.40	2.90
	2	2	1.37	1.95
	3	2	1.57	1.87
BB-ZP-1	1	2	2.22	5.59
	2	3	1.22	4.80

BB-ZP-1 with extremely high moisture content (compared to other samples, see subsection 3.7.1) showed compressive strength in the same range, or even higher, than less moist samples. All of the samples showed compressive strength in line with recommendations for minimal compressive strength by EBAA, HB 195-2002, and Walker et al. (2005), as presented in Table 2.6 in subsection 2.4.4.

3.7.5 Soil water retention behaviour

Due to lacking appropriate testing machines, soil water retention behaviour was determined at Durham University (UK), during a research visit. That limited the amount of material to be tested. Thus, soil water retention behaviour (suction) was determined on only one sample, collected from a house labelled A-Z-73 (section 3.2), according to Method D in ASTM S 6836-02. Suction was determined using a Decagon Water Potential 4C (WP4C) apparatus, following the chilled mirror hygrometer method. Method D in ASTM S 6836-02 is used for suctions above 1000 kPa, while the chilled mirror hygrometer method determines suction based on the water potential of the soil specimen. The procedure for measuring the soil suction using the WP4C apparatus in detail is described in Rahardjo et al. (2019). According to them, after a specimen is equilibrated inside the WP4C apparatus, the water potential of the air in the chamber and the specimen becomes the same. Inside the apparatus, condensation appears on the mirror above the soil specimen, and a thermocouple reads the temperature at which condensation occurs. After 20-30 minutes, the final water potential (total suction) and temperature of the soil

specimen are displayed on the apparatus screen. Total suction is calculated using the Kelvin equation (Equation 3.3) (Gerard et al., 2015).

$$s = \frac{\rho_w RT}{M_w} \cdot \ln(RH) \quad (3.3)$$

where:

ρ_w = bulk density of water (1000 kg/m³)

R = universal gas constant (8.3143 J/mol/K)

T = absolute temperature

M_w = molar mass of water (0.018 kg/mol)

RH = relative humidity

Suction was determined on small disc samples (approx. diameter (ϕ) 35 mm, h = 8 mm) at different moisture contents, ranging from 2 to 12%. A set of preliminary samples was made to determine the drying rate of test samples by weighing samples every 5 to 10 minutes during 8 hours. Following that, samples were oven-dried, and the drying pace was determined. 50 test specimens were made in the special mould using a hydraulic press and kept in plastic cups for 24 hours prior to the drying process to achieve equilibration inside the sample (Beckett and Augarde, 2012). Specimens were air-dried inside a temperature-controlled chamber, where WP4C apparatus was placed as well. After each sample group of five specimens was dried for the previously set period, plastic cups were covered with lids for at least an hour prior to testing for equilibration. After the test, samples were oven-dried at 105 °C, for 24 hours to determine the test moisture for each specimen.

Three samples in an undisturbed state, *i.e.* not crushed or oven-dried, were tested as well. Small pieces of rammed earth wall were placed in the WP4C apparatus and tested. Moisture content, determined by drying samples after the test in the oven, ranged from 1.95 to 2.10%. In Figure 3.15, a decrease in moisture content, followed by an increase in suction, can be observed. The undisturbed samples fit well with the produced samples, which could indicate that the crushing and drying of material for disc samples did not influence the soil water retention behaviour. What is more, by air-drying disc samples, conditions close to those in an existing rammed earth house were achieved.

To get a better understanding of the relationship between compressive strength and suction, as described in the reviewed articles (Bui et al., 2014a; Jaquin et al.,

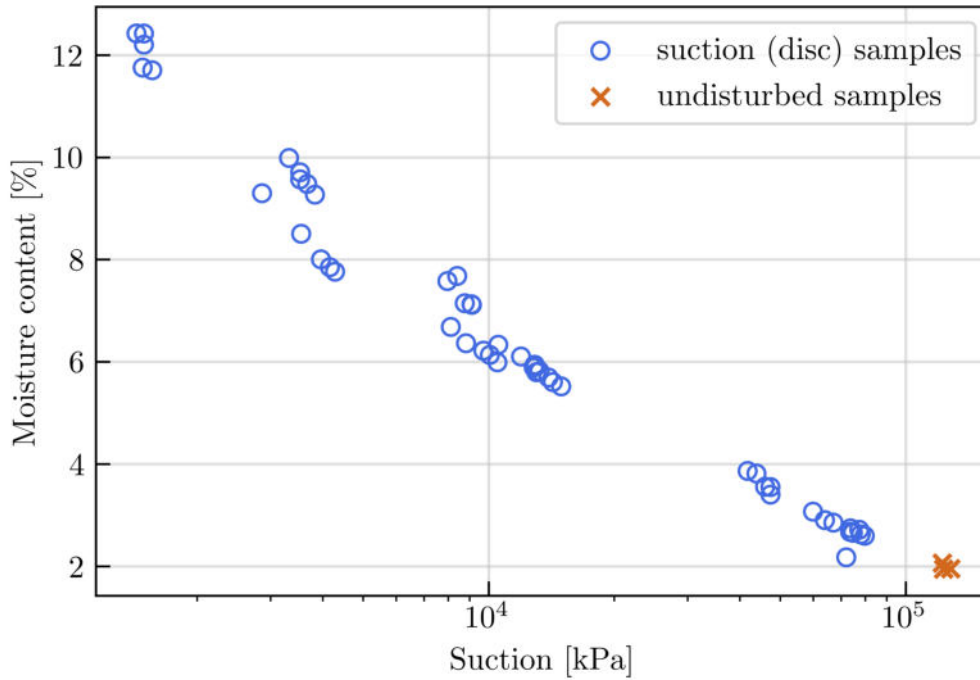
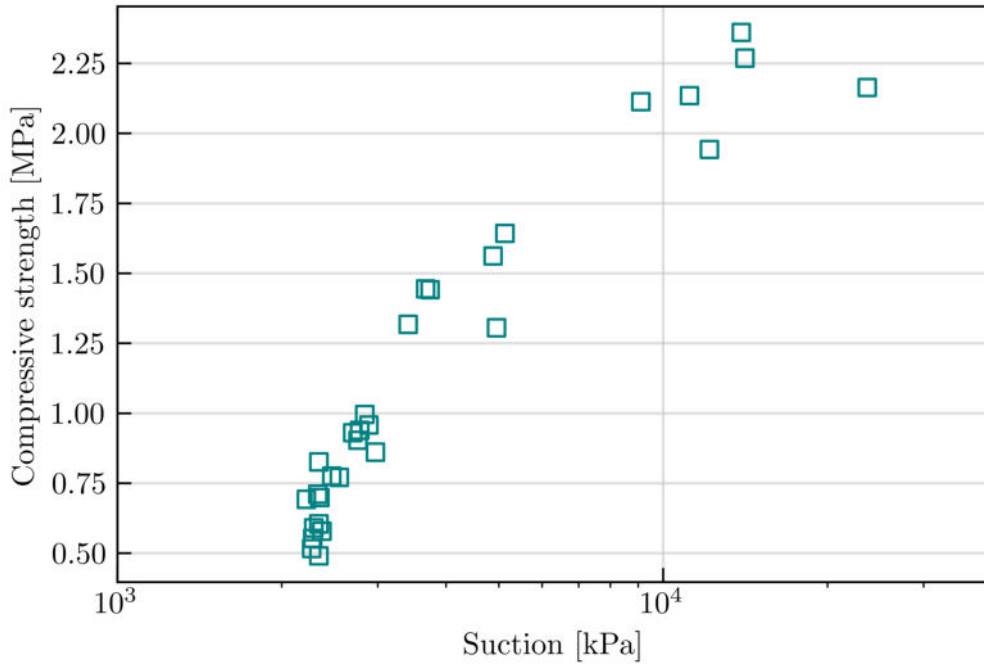


Figure 3.15: Suction of samples collected from A-Z-73 house

2009), a set of small cylindrical samples was produced and tested using a Lloyd test machine with a load cell of 5 kN capacity and a loading rate of 0.1 mm/min. Samples (approx. diameter (ϕ) 38 mm, $h = 76$ mm) were produced and cured in the same way as disc suction samples but were wrapped in plastic film and kept in sealed plastic bags instead of plastic cups. In total, 30 samples were produced at ca. 12% moisture content and air-dried. The moisture content of test samples groups ranged from 4.5 to 12.25%. Following the UCS test, a small portion was taken from each sample and placed in the WP4C apparatus to get information regarding suction. The two pieces of information are presented in Figure 3.16. As expected, with an increase in suction, the compressive strength increased as well. However, the contribution of suction to the strength ceased after about 10⁴ kPa. The same plateau behaviour was observed earlier by other researchers (Jaquin et al., 2009; Toll, 1990; Toll and Ong, 2003).



68.92% of sand, and 0.5-4.7% of gravel. Grading curves plotted against literature recommendations corresponded to them in fine particle proportion. Also, if sand and gravel proportions were combined, the material collected from C-SR-38 corresponded perfectly with the recommendations given in Houben and Guillard (1994); Walker et al. (2005) and HB 195-2002.

Soil plasticity properties (LL, PL, and PI) were determined on samples collected from three houses (A-Z-73, A-ZS-1, and BB-ZP-1). The liquid limit, determined using the cone penetration test, ranged from 32 to 36.4%. The plastic limit was determined to be 18.8 to 20%, while the plasticity index was between 12 and 16.7%. According to the ESCS classification (HRN EN ISO 14688-2), two samples (A-Z-73 and A-ZS-1) were classified as low-plasticity, while the remaining sample from BB-ZP-1 was classified as medium-plasticity. On the other hand, if UCSC classification is considered (ASTM D 2487-17), all samples would be classified as low-plasticity. It should be noted that all three samples agree with recommendations with which most samples from published articles agree (Doat et al., 1979; Houben and Guillard, 1994; Walker et al., 2005).

The compressive strength was determined on a small specimen cut from large collected samples. From each sample, between two and five specimens were tested. Most specimens exhibited compressive strength of around 1.5 MPa. One sample, collected from the outer part of the wall in house A-Z-73, had an average strength of 3.38 MPa, but moisture content was in line with other samples of lesser strength. On the other hand, samples collected from the BB-ZP-1 house exhibited average values of compressive strength but had a much higher moisture content. Based on the results, moisture content in this case did not significantly affect the value of compressive strength.

Soil water retention behaviour was determined on samples from only one house (A-Z-73), due to the amount of the collected material. Testing on disc samples and fragments from the UCS test samples was performed using the WP4C apparatus, and undisturbed samples were tested as well. As expected, based on a literature review, a drop in moisture content causes an increase in suction. Moreover, the relationship between suction and compressive strength is proportional until reaching suction of *ca.* 10^4 kPa, when compressive strength reaches a plateau despite the continued growth

of suction.

The information regarding the design, boundary conditions, and geometry of rammed earth houses in eastern Croatia that creates this database helps place Croatia on the earthen construction map of the world. Moreover, the valuable knowledge gained through field observations will be used in defining the experimental and numerical parts of the research. Laboratory testing performed on collected samples aids in determining similarities, like soil plasticity and soil water retention behaviour, with the material used for building rammed earth structures in other parts of the world. Equally important, differences in the material from published articles and recommendations given in handbooks and guidelines prove the variety of the material that can be utilised for the rammed earth technique.

Chapter 4

Seismic behaviour

Poor material properties of rammed earth, *i.e.* brittleness and low tensile strength, accompanied by the large weight of the structure add up to high vulnerability to strong loads such as earthquakes. The susceptibility rises even more in traditional buildings, due to the low quality of building caused by the empiric approach to building (Morris, 2012). Despite that, many earthen houses are built in seismically prone areas (Figure 4.1) (Thompson et al., 2022).

According to a literature review and field observations, traditional rammed earth houses in eastern Croatia were empirically built around one hundred years ago. Being built in a seismically prone area with a design ground acceleration of $0.20g$, one can presume they encountered seismic events of magnitudes 4 to 6 (Figure 4.2). Despite that, as described in the chapter 3, encountered houses are in a deteriorated state, but since construction is in a mainly good state, one could presume that deterioration is a result of a lack of maintenance. However, the seismic resistance of rammed earth structures is still a matter of research, as explained in section 2.5. The first attempt to seismically comprehend rammed earth walls from eastern Croatia was published in Perić Fekete et al. (2024) and will be presented in the next chapter (chapter 5) in greater detail. In this chapter, a short introduction to analysis for determining the seismic behaviour of rammed earth walls is given.

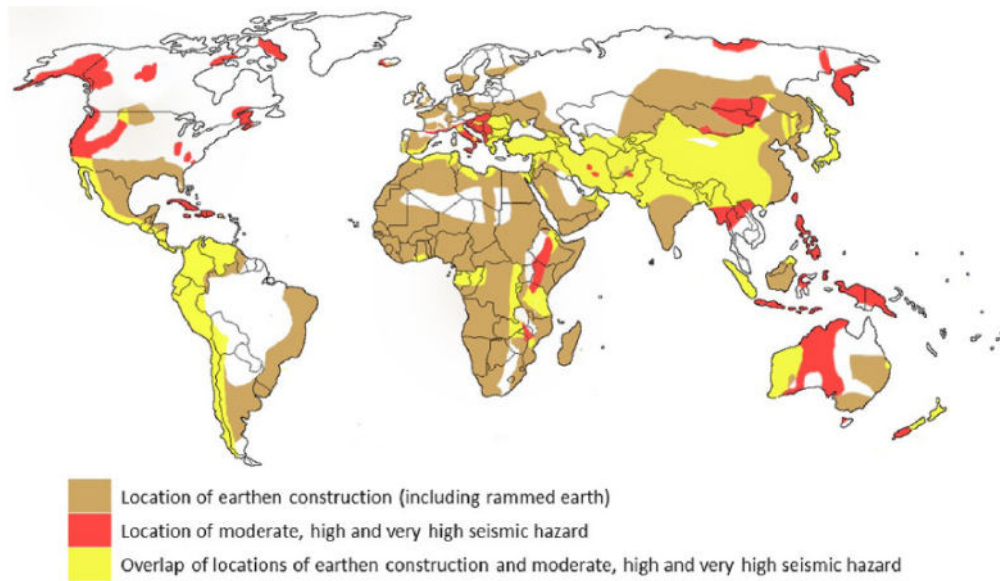


Figure 4.1: Locations of earthen construction overlapped with seismically prone areas (Thompson et al., 2022)

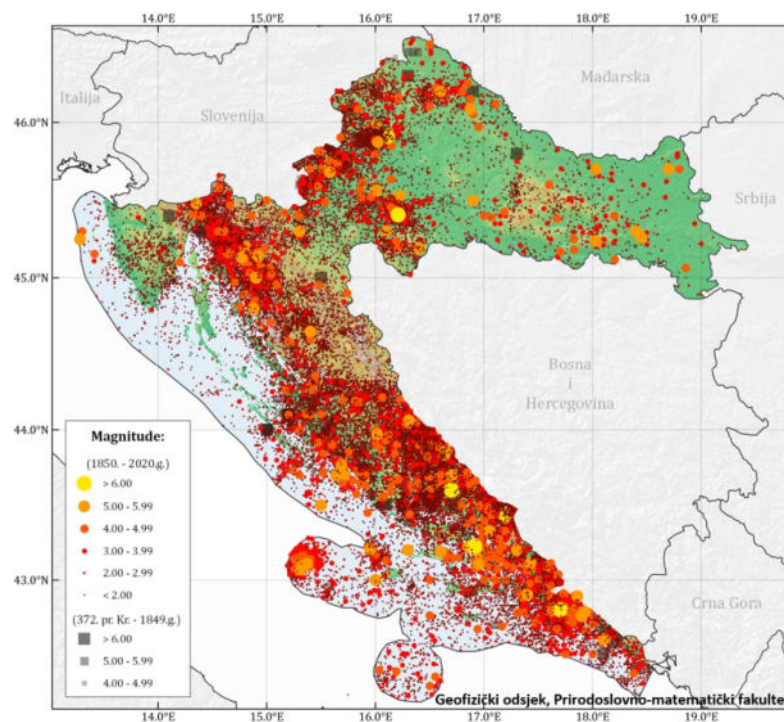


Figure 4.2: Map of earthquake epicentres in Croatia (source: https://www.pmf.unizg.hr/geof/seizmoloska_sluzba/seizmicnost_hrvatske, accessed on 31st January 2024; Savor Novak et al. (2019))

4.1 Structural behaviour factor

The structural behaviour factor is based on the assumption that structural systems have a significant amount of ductility (Chourasia et al., 2021). According to EN 1998-1, the structural behaviour factor (q) is “*an approximation of the ratio of the seismic forces that the structure would experience if its response is completely elastic with 5% viscous damping to the minimum seismic forces that may be used in the design with a conventional elastic analysis model.*”

Following the definition, the structural behaviour factor can be calculated from the maximum seismic force in an elastic structure (F_{max}) and the ultimate design seismic force (F_u) (Chourasia et al., 2021; Tomažević, 2006). Both values of force ought to be determined according to the bilinear idealisation of the capacity curve. Maximum force in an idealised elastic structure ($F_{max} = F_e$) corresponds to 40% of the peak load, whereas ultimate seismic force F_u is the force at the end of the loading phase (*i.e.* the ultimate base shear capacity of the rammed earth wall).

In the absence of proper standards for rammed earth constructions in Europe, a comparison with recommendations for URM was made previously in published articles. EN 1998-1 proposes the structural behaviour factor for URM in the range of 1.5 to 2.5. Following the same recommendations, Bui et al. (2016) mention that for rammed earth walls, a value of at least 1.5 should be used. To the author’s best knowledge, the sole attempt to determine the structural behaviour factor of a rammed earth wall was performed by Romanazzi et al. (2022a), in the same manner as presented in this section, in the amount of 2.63 and 2.71 for an I-shaped wall.

In this study, the structural behaviour factor was determined based on experimental and numerical analysis data and compared with minimal value according to EN 1998-1, which was previously assumed correct for rammed earth structures.

4.2 Response spectrum

One of the objectives of this study is to determine the seismic behaviour of rammed earth walls characteristic of the eastern Croatia area. Thus, from performed experimental analysis, settings for performing numerical analysis were acquired. A parametric analysis comprising several wall systems was performed and capacity curves

were determined. From determined base shear forces and horizontal displacement at the top of the wall, seismic acceleration and displacement were determined. Spectral acceleration was determined as a ratio of horizontal force at the base of the wall and mass supported by the wall. In contrast, spectral displacement was equal to the yield displacement of the top of the wall (Bui et al., 2016). By knowing the spectral acceleration and displacement, the seismic capacity of each wall could be estimated. In order to determine the target displacement, seismic capacity curves were overlapped with response spectrum curves.

For that purpose, the elastic response spectrum was determined for ground types A, B, and C. Ground types B and C can be encountered in eastern Croatia (Pavić, 2023). Ground type A was considered as a referent response spectrum, representing a situation when rammed earth walls were built on the rock or ground of excellent quality. What is more, the elastic response spectrum was determined according to the current Eurocode 8 standard (EN 1998-1) and the second generation of the standard, according to the explanation in Čaušević and Bulić (2020) and Čaušević et al. (2023). The elastic response spectrum was calculated for three limit states corresponding to a different return period:

- DL: Damage Limitation
- SD: Significant Damage (this state is necessary to achieve according to Čaušević and Bulić (2020))
- NC: Near Collapse

In the past few years, the general standard for the design of earthquake-resistant structures, *i.e.* Eurocode 8 (EN 1998-1) has been renewed with a new generation that carries significant changes. According to Čaušević and Bulić (2020), the fact that the technical committee in charge of making the standard did not make corrections to the previous version but opted for making a completely new document divided into two parts indicates the depth of the changes in the second generation. However, since the first generation of the standard is still in use in Croatia, seismic capacity in this study was compared with the response spectra determined according to both generations. However, a complete set of changes that the second generation

brings will not be discussed in this study, and an interested reader can further explore the topic in the relevant literature, *e.g.* Čaušević and Bulić (2020), Labbé and Paolucci (2022) or Čaušević et al. (2023).

The elastic response spectrum, according to the current Eurocode 8 (in graphs denoted as “*1st gen EC8*”), was determined based on peak ground acceleration (PGA) for the location of eastern Croatia. Namely, a PGA of $0.125g$ was utilised that corresponds to the Baranja area in eastern Croatia to determine the response spectrum for ground types A, B and C. Damping of 5% was assumed due to the lack of appropriate knowledge of damping in rammed earth structures.

In the second generation of the Eurocode 8 (in graphs denoted as “*2nd gen EC8*”), the elastic response spectrum is defined by two probabilistically determined spectral ordinates (S_α and S_β). S_α is the reference spectral acceleration of the elastic response spectrum for a ground type A, with a return period of 475 years and 5% of damping, while the S_β is the spectral acceleration for the period of 1 s, at the same elastic response spectrum (Čaušević et al., 2023). Both parameters should be determined according to the national hazard maps that will need to be created for each country by seismologists. Also, according to Čaušević and Bulić (2020), the difference between the PGA and S_α around 2.5 should be considered. However, it should be noted that since the National Annex and seismic hazard maps are still not available, this analysis will rely on assumptions and simplifications, similar to Brandis (2022). For this study, the parameters were determined by picking a location in eastern Croatia (Baranja, near Kneževi Vinogradi) using the European Seismic Hazard Model 2020 (<http://hazard.efehr.org/en/home/>, accessed: 10th May 2024).

In the following figures (Figure 4.3), the elastic response spectra for three limit states (DL, SD and NC) determined according to the two generations of Eurocode 8 are presented. In both cases, consequence class 2 is considered since it is assumed that rammed earth walls from this study are members of residential buildings. It should be noted that only the SD limit state corresponds to the same return period (475 years) in both generations, while the other two differ. Precisely, the NC limit class corresponds to a 2475 and 1600 years return period, while the DL limit state corresponds to 225 and 60 years return period for 1st and 2nd generations of Eurocode

8, respectively (Figure 4.3).

Furthermore, the return period is not the only difference between the two generations of a standard. The change in length of a plateau characteristic for response spectra curves is obvious. Also, differences in spectral acceleration and displacement corresponding to each limit state can be observed. If curves for a return period of 475 years are compared between the two generations, significant changes of spectral acceleration at which plateau occurs can be observed. The influence of the differences on the seismic response of rammed earth walls will be discussed in more detail in the chapter 6.

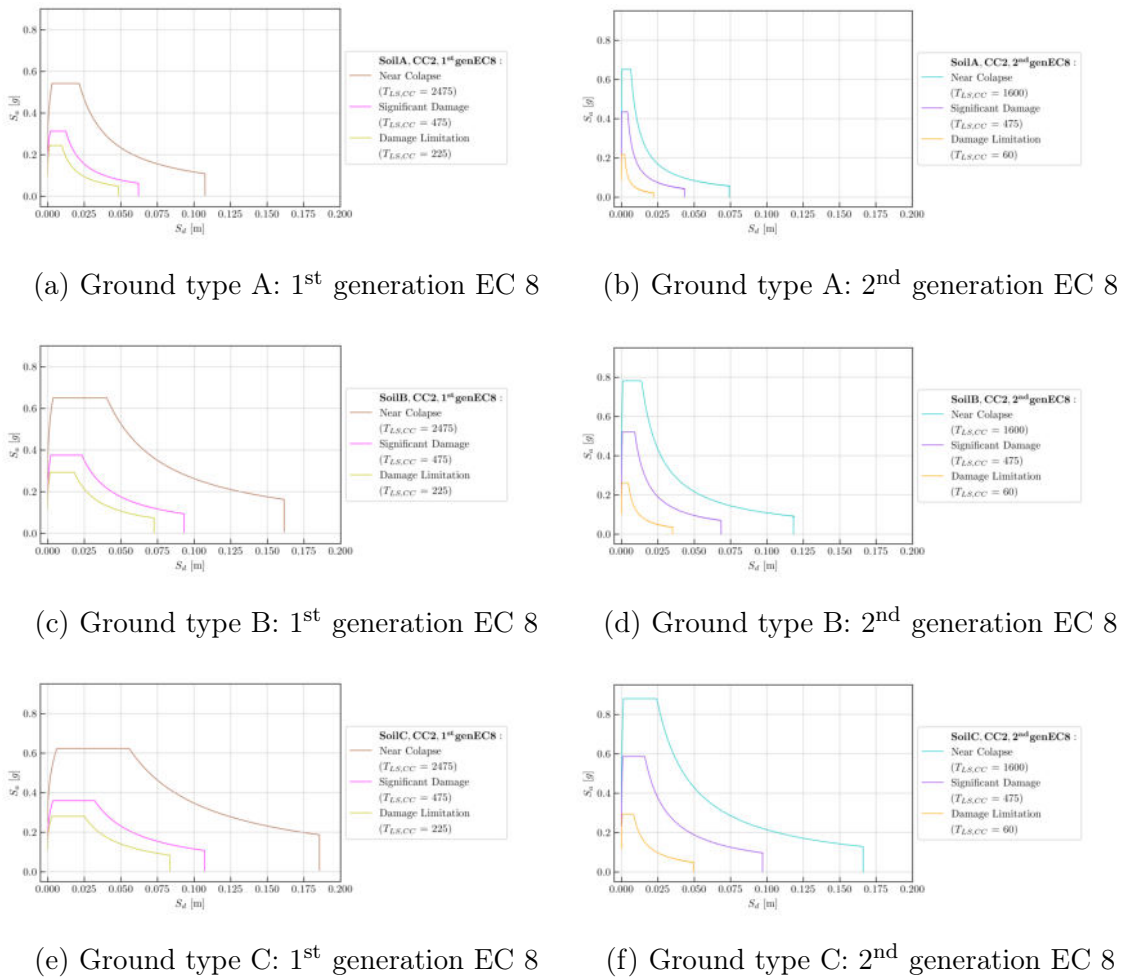


Figure 4.3: Elastic response spectrum for the three ground types

The target displacement of every analysed wall was determined as an intersection point by overlapping the response spectrum corresponding to the three limit states and return periods with capacity curves. Thus, inter-storey drift (IDR_{dT}) and

damage state of each wall could be determined. According to Calvi (1999), there are four limit states:

- LS1: no damage
- LS2: minor structural and moderate non-structural damage; a proposed drift limit of 0.1%
- LS3: significant structural and extensive non-structural damage; a proposed drift limit of 0.3%
- LS4: structural collapse; a proposed drift limit of 0.5%

However, when rammed earth walls are taken into consideration, El-Nabouch et al. (2016) and Bui et al. (2016) suggest LS3 (0.3% IDR) should be the end limit.

In this study, only the elastic response spectrum was observed since the aim is to study the behaviour of the traditionally built rammed earth walls found in existing houses in eastern Croatia and not to perform the design of such structures.

4.3 Conclusion

The topic of this study assumed the determination of the seismic behaviour of rammed earth walls. In this chapter, the method for determination of structural behaviour factor, which was previously used for rammed earth walls, was explained. Moreover, in order to get the seismic capacity of a wall, analysis results should be overlapped with elastic response spectra to determine the target displacement on the respective ground type. That enables one to analytically place structure in the desired location, but even then it should be taken *with a grain of salt*, due to the unpredictability of any seismic event.

Moreover, the 2nd generation of Eurocode 8 is going to undergo major changes in many aspects, one of which is the procedure for determining the response spectrum. Since the procedure was already explained in detail in several research papers, it was used in this study to evaluate the rammed earth walls. To the author's best knowledge, the comparison of the response spectra from 1st and 2nd generation of Eurocode 8 standard, in the context of rammed earth walls has not been performed earlier.

Chapter 5

Experimental campaigns

Conflicts of interest disclosure: Please note that the research presented in this chapter has been published in Perić Fekete et al. (2024) thus there are many similarities and cross-referencing between this chapter and the paper.

Experimental research was concentrated on testing the seismic resistance of flat, square-rammed earth walls by performing in-plane cyclic loading. Four rammed earth walls were constructed by following traditional building techniques and from the material corresponding to the local envelope presented in Figure 3.12 in chapter 3. The geometry of the tested walls was also determined according to the houses encountered during the field observation but was scaled (1:2) to ease the testing in the laboratory and reduce the cost of construction.

All four model walls were made in the same dimension; however, two different material compositions were used, and the drying period was varied in one of the walls, as was the loading protocol. Further research involving different geometric proportions, construction systems, and vertical pressure was performed numerically, based on knowledge gained on experimental analysis, and is presented in the chapter 6.

5.1 Soil characterisation

Existing rammed earth houses encountered during field observation prove the usability of the material composition characteristic of eastern Croatia. However, this

experiment was performed with two different material compositions, both in compliance with the local envelope, to get a better understanding of the influence granular composition has on seismic response. What is more, due to the traditional approach chosen for constructing the walls, soil material was chosen solely according to the local envelope without considering recommendations in the literature.

Soil material was collected from two building sites in eastern Croatia, south and west of Osijek. One of them, denoted as Soil-S, due to the majority of sand particles in the mixture, was used in its original state, as found at the building site. The other soil material (Soil-M, with the majority of silt particles) fell out of the envelope in its original state and was therefore mixed with 40% of the fine gravel collected from the Drava River.

For both soil mixtures, particle size distribution (HRN EN ISO 17892-4:2016) and plasticity (BS 1377-2:1990) were determined. What is more, optimum moisture content was determined by the standard Proctor test (BS 1377-4:1990) and controlled by the *drop* test. Following that, samples for testing compressive (EN 12390-2:2019) and tensile strength (BS EN 196-1:2005) were made and tested after drying for 28 days.

5.1.1 Particle size distribution

Soil composition was determined for both mixtures according to HRN EN ISO 17892-4:2016 and compared to envelopes presented in Figure 3.12, chapter 3. However, the local envelope from Perić Fekete et al. (2024) was considered a determining factor. In Figure 5.1, the granular composition of the mixtures is presented and compared with the envelopes. As it can be observed, both Soil-S and Soil-M fit well in the local envelope. However, mixtures comply with other recommendations only in a portion of fine particles but have a much smaller intake of gravel, as is the case with samples collected from rammed earth houses in eastern Croatia. Soil-M, however, deviates only slightly from the envelope by Walker et al. (2005).

As explained above, the mixture Soil-S contained the majority of sand particles, in particular: 7.8% of clay, 30.1% of silt, 57.3% of sand, and 4.9% of gravel. The second mixture (Soil-M) contained 8.9% of clay, 46.9% of silt, 33.9% of sand, and 10.3% of gravel. Two model walls were made of Soil-S and the other two of Soil-

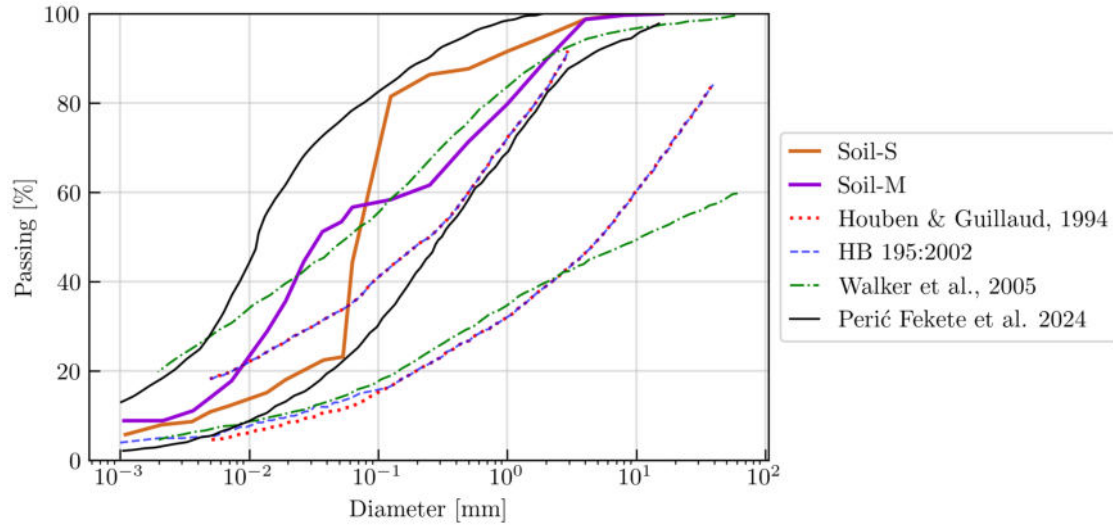


Figure 5.1: Mixtures Soil-S and Soil-M compared to envelopes

M to test whether the soil composition has an impact on their seismic behaviour. Moreover, despite eastern Croatia being a rather small area, different soil compositions were used for building rammed earth houses, as is evident by the range of the envelope (Perić Fekete et al., 2024).

5.1.2 Optimum moisture content

The optimal moisture content was tested by performing the *drop* test, as recommended by Houben and Guillaud (1994); Keable and Keable (1996); Krahn (2019); Minke (2006) and Maniatidis and Walker (2003). However, due to the empirical nature of the test, the standard Proctor test was performed as well, according to BS 1377-4:1990.

The *drop* test results showed a big difference in the optimum moisture content between the soil mixtures. The optimum moisture content of the Soil-S was estimated to be 21.4%. For Soil-M, it was estimated to be 13.5%. However, standard Proctor test results differ from the *drop* test results. The optimal moisture content (OMC) and maximum dry density (MDD) of the Soil-S were determined to be 16.7% and 1690 kg/m³, respectively. Soil-M showed OMC and MDD in the amount of 8.5% and 2033 kg/m³.

Table 5.1: Soil plasticity of used soil samples

Soil	LL [%]	PL [%]	PI [%]	The regulations with which it complies		
				only LL	only PI	both
Soil-S	37.4	21.1	16.3	N/A	N/A	Do, HG, HB, W, Dg
Soil-M	32.4	19.4	13.0	Dg	HB	Do, HG, W

Note: *Do* = (Doat et al., 1979), *HG* = (Houben and Guillard, 1994),

HB = (HB 195-2002), *W* = (Walker et al., 2005),

DG = (Delgado and Guerrero, 2007)

5.1.3 Plasticity

The plasticity of the soil mixtures was determined to verify the applicability for building with rammed earth. Thus, results were compared with literature recommendations and field observations. Samples were prepared by sieving and mixing with distilled water, and soil plasticity was determined following the same procedures that were used to test samples collected from the rammed earth houses. The liquid limit (LL) was determined by a cone penetration test, while the plastic limit (PL) was determined by rolling soil into a cylindrical thread. The plasticity index (PI) was determined as a difference between the liquid and plastic limits.

The results were compared with recommendations from the literature. Soil-S agreed with all of the five recommendations presented in subsection 2.4.3, while Soil-M slightly differed. The values of soil plasticity determined on samples collected from the existing rammed earth houses in eastern Croatia were also compared to soil samples. Soil-S showed less than 2% greater values of liquid and plastic limit from maximum values observed on field samples, while the plasticity index falls in the extreme interval. On the contrary, Soil-M agreed with field sample intervals. Both soils can be classified as low-plasticity, according to USCS classification (ASTM D 2487-17), similar to field values and were thus considered appropriate for building rammed earth walls. If ESCS classification (HRN EN ISO 14688-2) is considered, Soil-M remains classified as low-plasticity, while Soil-S becomes medium-plasticity.

5.1.4 Tensile and compressive strength

The strength properties were determined on three sets of rammed earth samples, made from each soil mixture. Tensile strength was determined on prismatic samples ($40 \times 40 \times 160$ mm) using a three-point bending test, according to BS EN 196-1:2005. Compressive strength was determined on sample halves that remained after testing tensile strength as well as on cubic ($150 \times 150 \times 150$ mm) and cylindrical (ϕ 150, $h = 300$ mm) samples. All samples were prepared by manual compression of the moist rammed earth material, mixed according to the *drop* test and standard Proctor test results (subsection 5.1.2), in the same manner as rammed earth walls. The curing time of 28 days was determined based on the standard for testing concrete samples, such as EN 12390-2:2019 since the same principle was used in published articles as well (Koutous and Hilali, 2021; Maniatidis and Walker, 2008; Toufigh and Kianfar, 2019). For each mixture, six prismatic samples and three cubic and cylindrical samples were tested.

Prismatic samples were tested to ease the comparison with the compressive strength of the samples collected from existing rammed earth walls. Cubic and cylindrical samples were chosen according to rammed earth standards and published articles. By testing compressive strength on three different sample shapes and sizes, their influence on the value of compressive strength could be assessed as well.

Tensile strength was determined on prismatic samples only, due to the high brittleness of the samples and the difficulty of performing the test. The average values of tensile strength were similar for both mixtures: 0.87 ± 0.08 and 0.89 ± 0.11 MPa for samples made of Soil-S and Soil-M, respectively. The coefficient of variation (CV) was also determined and presented in Table 5.2 and Table 5.3. Even though the mean values of the tensile strength are close for the two soil mixtures, Soil-M exhibited a bigger range of tensile strength values (Figure 5.2).

As mentioned above, compressive strength was determined on prismatic, cubic, and cylindrical samples and listed in Table 5.2 and Table 5.3. Moreover, to get a better perspective on differences in compressive strength between sample shapes and the two soils, values were plotted on a box-whisker plot (Figure 5.3). Soil-S showed remarkably higher values of compressive strength determined on prismatic samples (2.25 ± 0.21 MPa) than on cubic and cylindrical samples. On the other

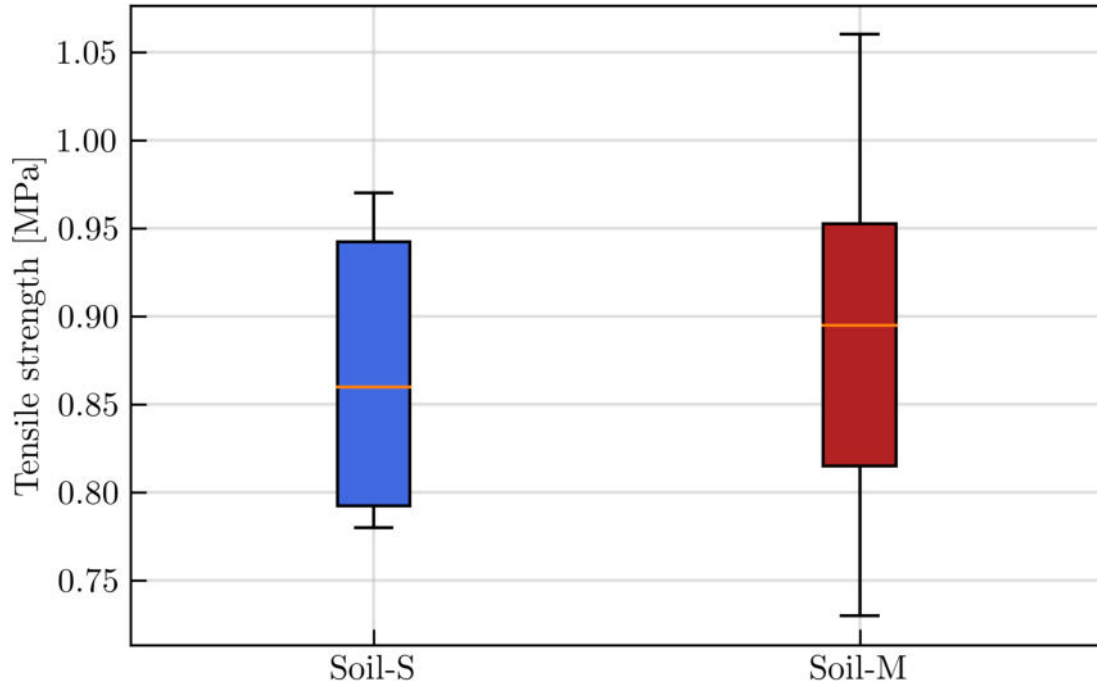


Figure 5.2: Tensile strength of rammed earth samples

hand, the values of compressive strength determined on cubic and cylindrical samples were close: 1.25 ± 0.14 MPa and 1.10 ± 0.07 MPa, respectively. Soil-M, however, exhibited mean values of compressive strength on all three sample shapes in a much closer range. Despite that, the compressive strength of cubic samples was the lowest (1.90 ± 0.10 MPa), while prismatic and cylinder samples had similar compressive strength; 2.19 ± 0.20 MPa and 2.11 ± 0.08 MPa, respectively. Moreover, cubic and cylindrical samples of both soil mixtures did not show a high range of values, as is evident by the whiskers in the plot (Figure 5.3). That could be expected due to the low number of tested samples, *i.e.* 3 samples per batch. Prismatic samples, on the other hand, exhibited a higher range of values, but the test was performed on four times more samples.

Based on the results of the tensile and compressive strengths, no evident influence of mixture composition on the mechanical properties could be determined. Sample shape also did not exhibit a pronounced influence on the results, even though prismatic samples showed higher values, but not in the same range for both mixtures. To get a clearer picture of the sample shape's influence on strength value, further tests should be conducted. However, since the use of prismatic, cubic, and cylindrical samples is mentioned in the reviewed literature and normative documents, one

Table 5.2: Mechanical properties of Soil-S

	Prism		Cube	Cylinder
	ft [MPa]	fc [MPa]	fc [MPa]	fc [MPa]
Soil-S	0.78	1.93	1.13	1.00
	0.89	2.51	1.43	1.17
	0.96	2.09	1.13	1.12
	0.78	2.45		
	0.83	2.15		
	0.97	2.25		
		1.89		
		2.56		
		2.13		
		2.29		
		2.42		
		2.33		
Mean	0.87	2.25	1.23	1.10
σ	0.08	0.21	0.14	0.07
CV	0.09	0.09	0.11	0.07

could assume that no regularity could be observed. Nonetheless, it could be useful to mention the sample shape and size when discussing the strength properties of the rammed earth to ease comparison with other research.

The compressive strength determined on samples collected from the existing rammed earth houses in eastern Croatia can be compared to the test results of Soil-S and Soil-M prismatic samples. It can be observed that the values of compressive strength on test samples corresponds well with values observed on samples collected in the field and even surpasses the average value of 1.86 ± 0.70 MPa.

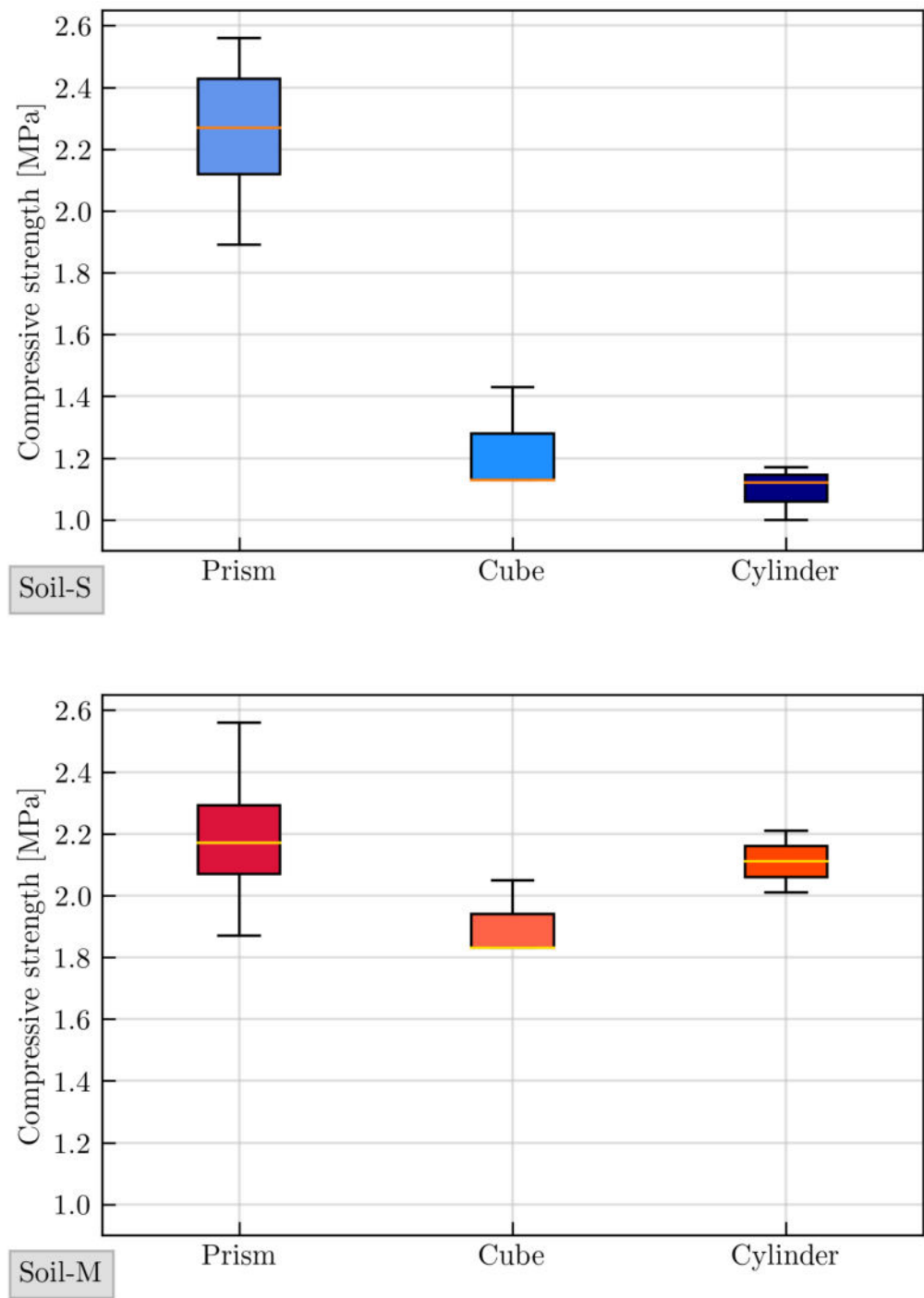


Figure 5.3: Compressive strength of rammed earth samples

Table 5.3: Mechanical properties of Soil-M

	Prism		Cube	Cylinder
	ft [MPa]	fc [MPa]	fc [MPa]	fc [MPa]
Soil-M	0.90	2.56	1.83	2.01
	0.79	2.36	1.83	2.21
	0.73	2.27	2.05	2.11
	1.06	1.87		
	0.97	2.13		
	0.89	2.20		
		2.44		
		2.07		
		2.14		
		1.88		
		2.07		
		2.23		
Mean	0.89	2.19	1.90	2.11
σ	0.11	0.20	0.10	0.08
CV	0.12	0.09	0.05	0.04

5.2 Rammed earth walls

The experimental testing of rammed earth walls was designed according to boundary conditions and geometry encountered during field observation and literature review. Thus, four rammed earth walls were constructed as flat square walls, $125 \times 125 \times 25$ cm, representing a two-times bigger wall. Scaling was performed in order to adhere to laboratory size limitations and reduce the cost of labour and material. Wall dimensions were chosen based on field observation, as the most common values of thickness and height. The literature review was also considered, and square walls were tested to ease the comparison. Scaling laws were implied based on recommendations for pseudo-dynamic testing by Carvalho (1998) and Harris and Sabnis (1999) and scaling factor 1:2 was chosen since it does not require scaling the material properties. Moreover, square flat walls were also chosen as the optimal shape

for validating the numerical model since further analysis of rammed earth walls was performed numerically (chapter 6).

Walls were constructed following traditional building techniques by experienced local masons. To ease the transportation inside the laboratory and to ensure that the wall is connected to the hard surface during testing, the wall was constructed on a reinforced concrete beam ($250 \times 45 \times 25$ cm). Moreover, prior to assembling the formwork, a thin layer of lime mortar was applied to the beam covering the area of the wall's cross-section. A previously moistened soil material was poured inside the wooden formwork and compressed using manual rammers. The moisture content of the earthen material was controlled during the building with a *drop* test.

The two walls made from the Soil-S were built at $15 \pm 1\%$ moisture content, while the other two walls, made from the Soil-M were built with a moisture content of $12 \pm 1\%$. It should be noted that all four walls were made with material within 3% of the OMC determined with the standard Proctor test, as proposed in the reviewed literature (Minke, 2006; , NZS; Schroeder, 2012; Walker et al., 2005).

Each layer was compacted as per recommendation (Keable and Keable, 1996; Krahn, 2019; Walker et al., 2005), until no volume change was noticeable with further blows. After reaching the desired height, the formwork was kept for five to seven days to minimise the creep and then air-dried in the laboratory before conducting the experiment. Walls were built in May and dried at 25 ± 2 °C and RH $50 \pm 5\%$ until testing was commenced in July.

Three walls were dried for 60 days, while the fourth wall was dried for 45 days, to test the influence of the drying period and the moisture content of the wall on the seismic behaviour. The drying period was chosen in compliance with the information regarding previously tested rammed earth walls presented in published articles (Table 2.8 in section 2.7). The drying period in the articles varied, from one month to more than five months. However, since a two-month drying period was used several times in previously conducted research (El-Nabouch et al., 2016, 2017; Miccoli et al., 2016, 2017), it was decided to follow the same approach.



Figure 5.4: Building of rammed earth walls

5.2.1 Test setup

Walls were tested within a cantilever boundary condition, which means that the bottom of the wall was rigidly connected to the massive concrete floor using bolts and nuts. Moreover, the in-plane movement of the foundation beams was fixed using hydraulic presses as well. Another reinforced concrete beam ($200 \times 35 \times 20$ cm) was placed on top of the wall to ensure the even distribution of vertical load on the wall and glued using high bond strength adhesive. A similar experimental setup was used in the previously conducted research on rammed earth walls (El-Nabouch et al., 2016, 2017; Miccoli et al., 2016, 2017; Ramezanpour et al., 2021), based on what was proposed for masonry walls by Tomažević (2009). The experimental setup is shown schematically in Figure 5.5, in the same way as it was represented in Perić Fekete et al. (2024).

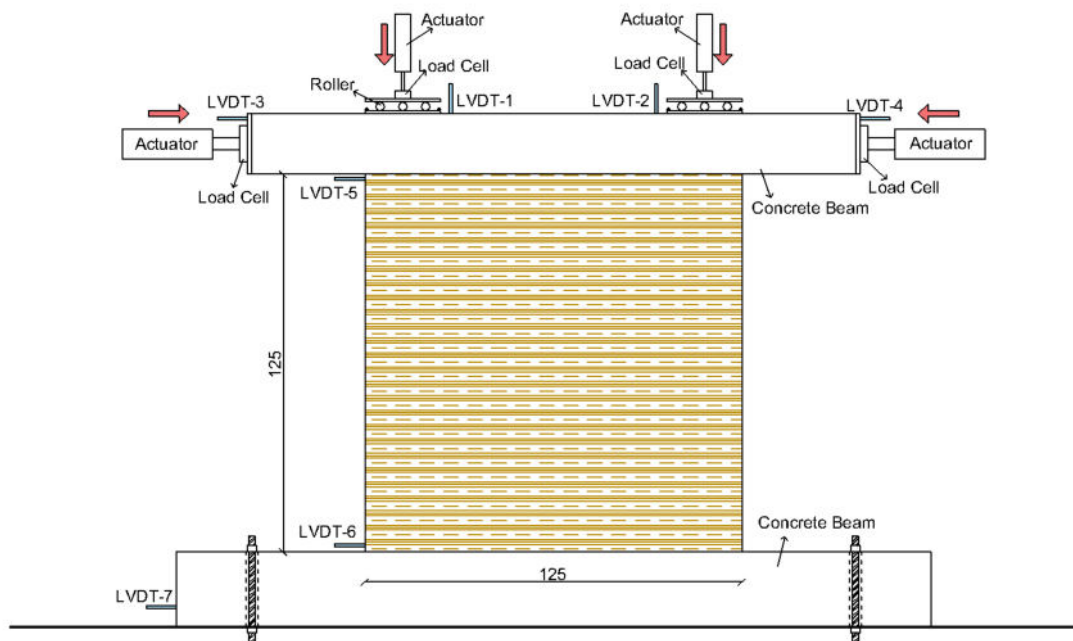


Figure 5.5: Schematic representation of the experimental setup (Perić Fekete et al., 2024)

In the following paragraphs, the elements of the test setup, as enumerated in Figure 5.6, are referenced in brackets (). Test walls were placed next to the reaction wall (1) to enable the application of load using hydraulic actuators (2). Horizontal displacement on the left and right sides was induced by two Yale YCS-33/150 actuators with a 150 mm stroke and a 500 kN capacity. Actuators were placed in the centre of the reinforced concrete beam sides. Vertical stress was applied on top of the upper reinforced concrete beam with two Yale YLS-50/60 actuators with a stroke of 60 mm and capacity of 500 kN, with the upper reinforced concrete beam taken into consideration as well. All hydraulic actuators have been manually operated (6). The applied loads were measured using load cells. Horizontal load was measured using two class 1 AEP TC4 load cells with a capacity of 500 kN and linearity of 0.05%. Two class 2 Burster 8438-6200 load cells at the top, with a capacity of 200 kN and a linearity of 1%, were used to measure vertical load. Load cells were calibrated according to ISO 376:2012.

Deformation was measured using linear variable differential transformers (LVDTs) (3), positioned as exhibited in Figure 5.5. LVDTs with range of ± 75 mm (RDPE DCTH3000A), ± 50 mm (RDPE DCTH2000A) and ± 25 mm (RDPE DCTH1000A) with a linearity of 0.1% were used to measure displacements at characteristic segments of the wall. Namely, LVDTs 1 and 2 measured vertical displacement of the wall, while LVDTs 3 and 4 controlled horizontal displacement. Sliding of the upper and lower beam along the wall was controlled as well, with LVDTs 5 and 6, respectively, while sliding of the wall along the floor slab was measured with LVDT 7.

All values were recorded using the DEWESoft Sirius HD-LV data acquisition system (4) with a sampling frequency of 1 Hz. What is more, a spatial digital image correlation system, the GOM Aramis system (GOMmbH, 2007a,b), was used to record the displacement and Von Mises strains. Two cameras with lenses of 12 mm focal length set at an angle of 25° were placed at a specific distance from the wall and from one another to get a complete picture (5). The software on the device tracks the 0.01% systemic strain precision through an intersection deviation of less than 0.1 pixels. To create a stochastic surface with high contrast, the faces of each wall and beam were painted white and then randomly scattered with black dots, as can be observed in the test specimen in Figure 5.6.

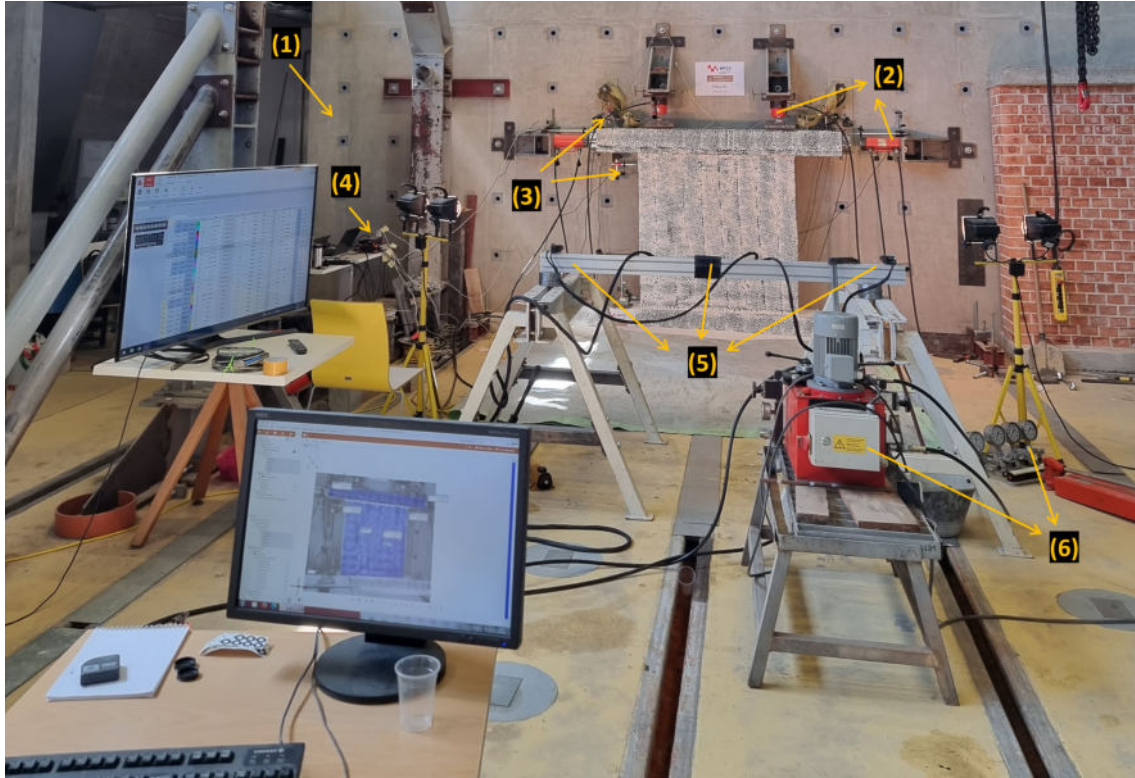


Figure 5.6: An overview of the experimental setup (Perić Fekete et al., 2024)

The first step of the test was applying a vertical stress of 0.18 MPa, simulating a constant and live load in a traditional rammed earth house from eastern Croatia. Based on field observations, a traditional two-sided roof was assumed, in which the attic space is used for storing grains. The value of vertical stress is close to the mean value of vertical stress used in the majority of experimental work in reviewed articles (Table 2.8 in section 2.7) if extreme values of extremely high value or those close to zero are excluded. Such high values of vertical stress can in reality rarely be expected in traditional rammed earth houses, even though their positive effect on the shear behaviour of the wall was demonstrated for earthen walls in the past (Mirjalili et al., 2020; Ramezanzpour et al., 2021). Moreover, a vertical stress of 0 MPa (or close to zero), despite being used in previously conducted research (Arslan et al., 2017; Romanazzi et al., 2022a; Shrestha et al., 2020a,b), would correspond to a free-standing rammed earth wall without a beam, roof or any live load. Therefore, a vertical stress of 0.18 MPa was determined to be a good representation.

After applying vertical stress, horizontal displacement was applied following two sets of a loading protocol (Figure 5.7) to determine how different excitation regimes influence the seismic behaviour of rammed earth walls. Therefore, one of

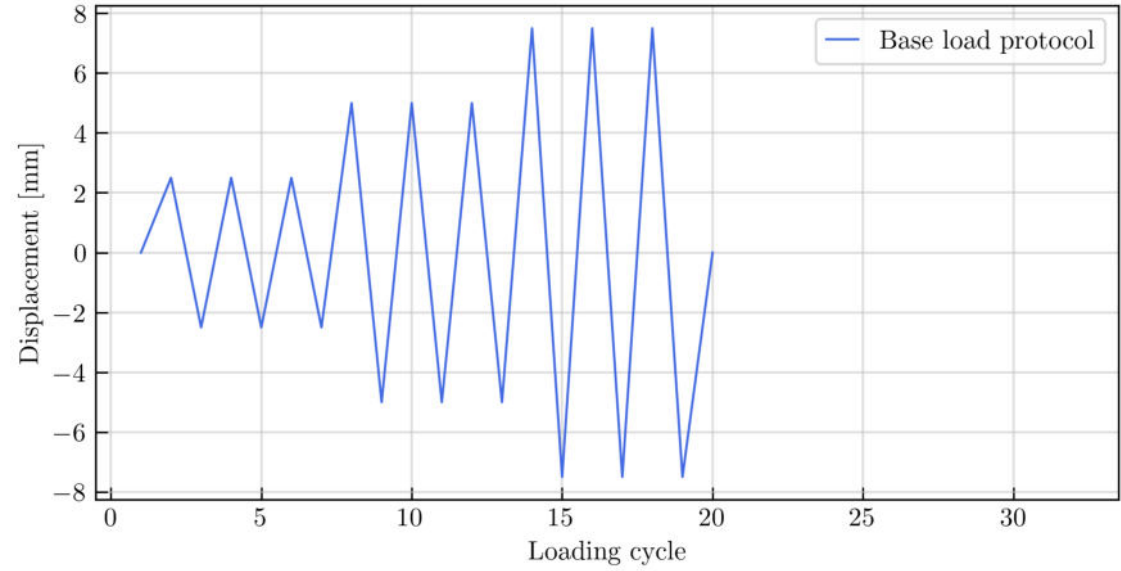
the walls was tested with a different loading protocol than the other three walls. In previously conducted experiments published in the literature, three loading protocols were recognised. The most frequently used protocol comprises loading steps of 2.5, 5, and 7.5 mm, repeating three times in positive and negative directions. It was utilised by Miccoli et al. (2016, 2017) and Ramezanpour et al. (2021) for rammed earth walls, masonry (Hračov et al., 2016) and adobe walls (Mirjalili et al., 2020) as well. The two other loading protocols were used on walls tested inside a different test setup when a rammed earth wall was tested inside a steel (Arslan et al., 2017) or a wooden (Baleca et al., 2023) frame. It was decided to use the loading protocol that was used for testing rammed earth walls within the same setup chosen for this experiment, containing loading steps of 2.5, 5, and 7.5 mm (Figure 5.7a). From the base loading protocol, a variation was developed, with a more gradual loading at the beginning of the experiment. The modified loading protocol started with a peak amplitude of 0.625 mm repeated three times in positive and negative directions, followed by an amplitude of 1.25 mm, ending with the complete base protocol (Figure 5.7b).

The endpoint of the experiment was critically determined when a decrease in the horizontal load accompanied by increasing horizontal displacement was observed (Miccoli et al., 2016). All tested walls endured horizontal displacement of ± 7.5 mm without collapse. However, severe cracks in every wall indicated the necessity to terminate the experiment due to the protection of the equipment attached to the wall.

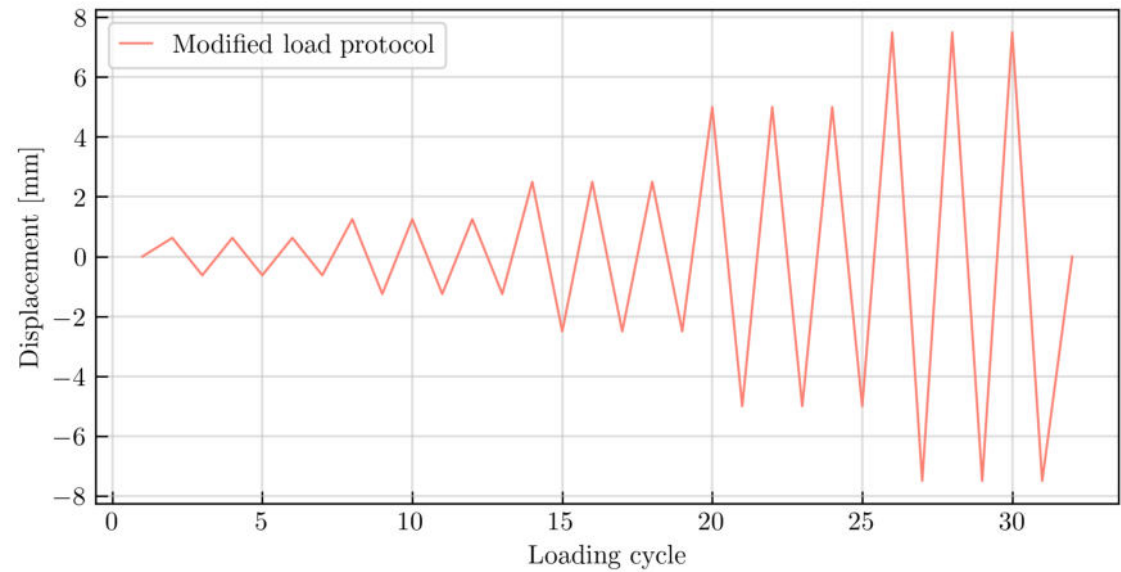
5.2.2 Experimental results

Even though the four rammed earth walls were all constructed in the same manner using traditional building techniques, the differences among them enabled comparison, as presented in the following paragraphs. In Table 5.4, test parameters varied with each wall are presented, along with wall IDs in format E:125-X, where X represents variations, *i.e.* L stands for loading protocol, M for soil mixture, and D for drying period. What is more, ID format E:125 was chosen to emphasise that walls of 125 cm in length were tested experimentally, not numerically.

For each wall, horizontal displacement measured with LVDTs was plotted against horizontal force to create hysteresis. Moreover, IDR was determined accord-



(a) Base loading protocol



(b) Modified loading protocol

Figure 5.7: Loading protocols used in the experiment

Table 5.4: Description of test parameters

Wall	Soil mixture	Drying period	Cyclic loading protocol
E:125	Soil-S	60 days	Modified
E:125-L	Soil-S	60 days	Base
E:125-M	Soil-M	60 days	Modified
E:125-D	Soil-M	45 days	Modified

ing to maximum displacement and the corresponding ultimate load-bearing capacity. Due to insufficient experience and knowledge in analysing the seismic behaviour of rammed earth walls from eastern Croatia, results were validated according to previously published data, using a value that is independent of the scale, the IDR (Petry and Beyer, 2014). Moreover, results were evaluated according to procedures common for unreinforced masonry walls, as was previously done by other researchers (El-Nabouch et al., 2016, 2017; Ramezanpour et al., 2021; Romanazzi et al., 2022a).

Moreover, the damage state was assessed according to drift limits for masonry structures (Calvi, 1999), previously used for rammed earth walls by El-Nabouch et al. (2016) and Bui et al. (2016). It was determined that the IDR values of the tested walls were similar to those of other rammed earth walls tested in the same experimental setup, ranging from 0.28 to 0.7% (El-Nabouch et al., 2016, 2017; Miccoli et al., 2016, 2017; Shrestha et al., 2020a). Different setup and boundary conditions (Arslan et al., 2017; Baleca et al., 2023; Barsotti et al., 2023) as well as the geometry and scale of the wall (Reyes et al., 2018; Romanazzi et al., 2022a) influenced the IDR values ranging from 1.16 to 5.8%. Therefore, the experimental results of the four walls considered here do not correspond to the results of testing those walls. A complete set of IDR values corresponding to each article was reported previously, in Table 2.8 in section 2.7.

Experimental results gathered from experimental data after testing each wall are presented in Table 5.5. For each wall, maximum horizontal force and displacement, as well as the IDR, were determined separately for push and pull directions. It should be noted that the IDR is determined according to the displacement at the maximum force, and was therefore denoted accordingly in the table (IDR_{dmax}). The behaviour was predominantly symmetrical in both directions for all tested walls.

The only exception was the wall E:125, in which maximum force in the push and pull directions was not achieved at the same level of horizontal displacement. Moreover, ductility, initial stiffness, and structural behaviour factors were determined according to the bilinear curve calculated for the positive (push) direction.

The bilinear curve was determined based on the backbone curve according to ASTM E2126-19, as previously used by Ramezanpour et al. (2021). The criteria for determining the bilinear curve was the equality of the areas under both curves until the ultimate displacement was reached. Also, the bilinear curve and the backbone curve coincided until reaching 40% of the maximum load.

Characteristic displacement values were determined: the idealised elastic limit displacement d_e at 40% of the peak load, the yield displacement d_y where the bilinear curve changes direction, and the ultimate displacement d_u once the loading process has concluded. The ratio between the ultimate and yield displacements was used to calculate the ductility. Initial stiffness was determined for all observed walls. However, the value determined for the wall tested with a different loading protocol (E:125-L) should be treated with caution since the initial elastic behaviour was not completely grasped.

The structural behaviour factor, also presented in Table 5.5, was determined as the maximum seismic force in an elastic structure and the ultimate seismic design force ratio (Chourasia et al., 2021; Tomažević, 2006), as previously explained in chapter 4. Both characteristic values were determined according to the bilinear curve and can be observed in Figure 5.9 through Figure 5.11.

The ARAMIS system was used to record the Von-Mises strain (Figure 5.8). According to the strain representation, the failure mode was determined and analysed following the analogy for the unreinforced masonry walls (Tomažević, 2009). For each wall, the Von Mises strain at the transition from elastic to plastic behaviour was compared with the strain at the end of the experiment. E:125-L exhibited the highest strain at the yield point, while other walls exhibited similar behaviour to a lesser extent, *i.e.* lower strain values at the same loading point. At the final stage, all four test walls showed X-shaped fractures on the front face of the wall. The most severe cracks were observed at E:125-D, which was tested after a shorter drying period.

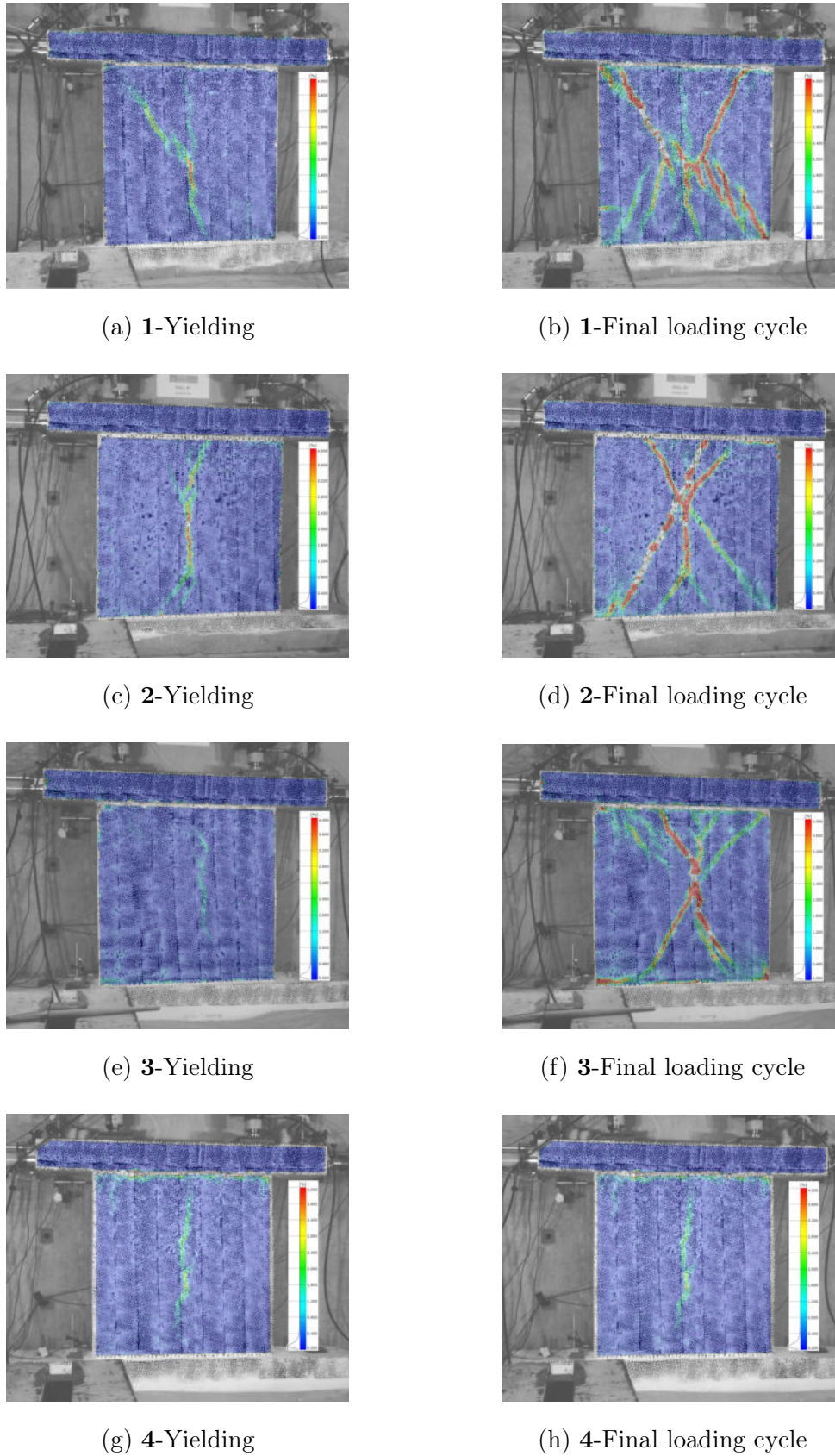


Figure 5.8: Von Mises strain at the point of yielding and after the final loading cycle; **1** E:125, **2** E:125-L, **3** E:125-M, **4** E:125-D

Table 5.5: Summary of experimental test results

	F_{max} [kN]		d_{max} [mm]		$IDR_{d_{max}}$ [%]		μ [-]	K_e [kN/m]	q [-]
	push	pull	push	pull	push	pull			
E:125	18.32	19.22	4.82	7.35	0.39	0.59	6.91	14974.67	2.15
E:125-L	19.73	19.92	4.74	4.99	0.38	0.40	6.65	16163.38	2.11
E:125-M	18.18	19.27	7.31	7.23	0.59	0.58	7.30	15334.93	2.03
E:125-D	18.36	17.38	4.94	4.94	0.40	0.40	6.26	13261.04	2.31

If the shape of the fractures on the face of the wall at the end of the experiment and their location are taken into consideration, the failure mode can be determined. According to Wilding and Beyer (2017), after the initial linear elastic behaviour is surpassed, cracks appear in unreinforced masonry walls. Based on the nature and location of the cracks, the non-linear behaviour can either be flexure-dominated or shear-dominated. They report that the flexure cracks appear in the bearing joint; thus, flexural-dominated behaviour is characterised by rocking of the wall and toe crushing. On the other hand, shear deformations are usually concentrated in a single diagonal fracture. Moreover, Tomažević (2009) further differentiates shear collapse into sliding and diagonal shear collapse. The former occurs when the wall horizontally slides at the bottom due to too low vertical stress and poor material quality. It should be noted that both research papers cited in this paragraph consider the non-linear behaviour of unreinforced masonry walls and not rammed earth walls. However, as stated above, the lack of appropriate directions for rammed earth forced other studies as well as this study to evaluate rammed earth using recommendations for unreinforced masonry.

According to the failure mode criteria previously mentioned, a diagonal shear caused the collapse of all four of the tested rammed earth walls. Moreover, by following the definition of shear collapse by Tomažević (2009), one could assume that the vertical stress and the material properties of the tested walls were adequate since no horizontal sliding at the bottom of the walls was observed.

Values presented in Table 5.5 are digested in the following subsections (subsection 5.2.3 through subsection 5.2.5), with respect to the influence of excitation regimes, material composition, and drying period length on seismic behaviour.

5.2.3 Influence of excitation regime

Two rammed earth walls tested with a different regime of applying horizontal loading were labelled E:125 and E:125-L. Base and modified loading protocols exhibited in Figure 5.7 were used in E:125-l and E:125, respectively. Due to differences in the initial part of the loading protocols, elastic behaviour was not pronounced in the E:125-L wall results (Figure 5.9b). On the other hand, when the initial horizontal load was applied more gradually, the elastic behaviour of the rammed earth wall could be grasped more easily (Figure 5.9a).

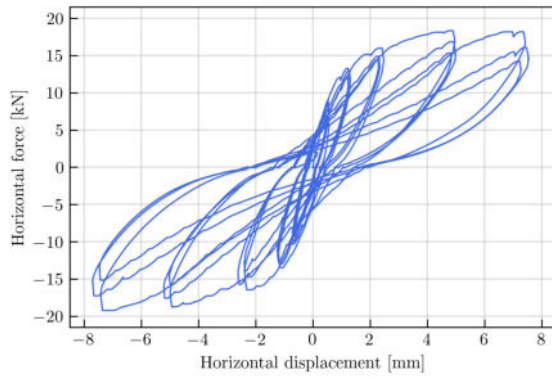
However, different loading regimes did not influence the maximum horizontal force the walls endured. The horizontal displacement corresponding to the maximum horizontal force was similar in both walls (Table 5.5). Owing to the distinctions in displacement at maximum force, differences in IDR are present as well. It should be noted that both walls reached the LS3 damage state, and E:125 even surpassed the LS4 damage state in the pull direction without collapsing.

The ductility of both walls was essentially the same, determined according to the bilinear idealised curve in Figure 5.9c and Figure 5.9d. Initial stiffness was higher for an E:125-L wall since the initial part of the loading protocol was changed. However, as mentioned earlier, the value should be cautiously concerned. Moreover, dissipated energy in both walls was essentially the same, 666 kNmm and 712 kNmm in E:125 and E:125-L, respectively. Structural behaviour factor values were also pretty close for both walls observed in this subsection, with values of 2.15 and 2.11 for walls E:125 and E:125-L, respectively.

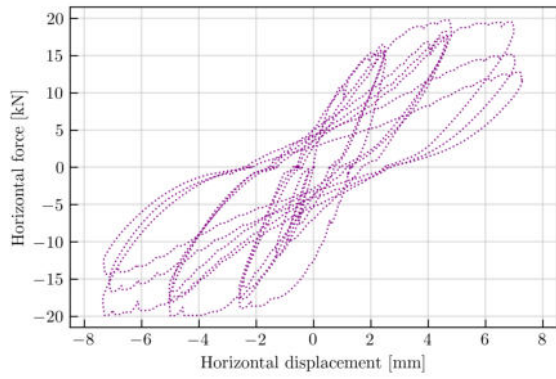
5.2.4 Influence of material composition

Two rammed earth walls made of different material mixtures were indexed E:125 and E:125-M. The material composition did not influence the hysteresis or backbone curve (Figure 5.10). However, despite the similitude of the two hysteresis, E:125-M exhibited 26% more dissipated energy. In particular, walls E:125 and E:125-M dissipated 666 and 901 kNmm of energy, respectively.

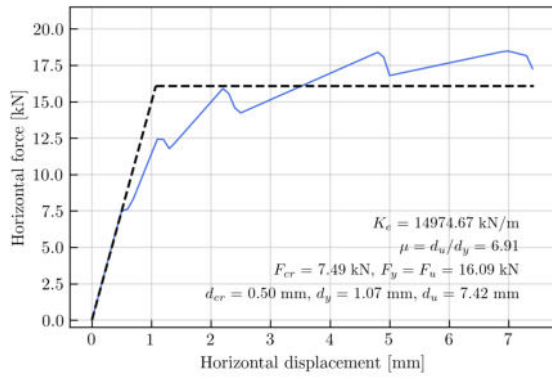
Furthermore, the similitude of backbone curves is mirrored in the load-bearing capacity as well. Both walls achieved 18-19 kN of horizontal force. However, E:125-M reached the maximum horizontal load at a much higher displacement, around



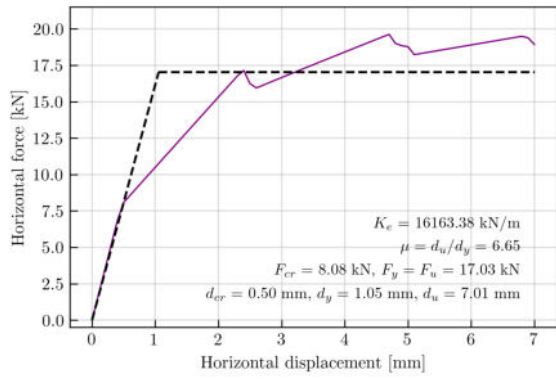
(a) Hysteresis (E:125)



(b) Hysteresis (E:125-L)



(c) Backbone curve and bilinear idealization (E:125)



(d) Backbone curve and bilinear idealization (E:125-L)

Figure 5.9: Comparison of seismic behaviour in walls tested with different loading protocols

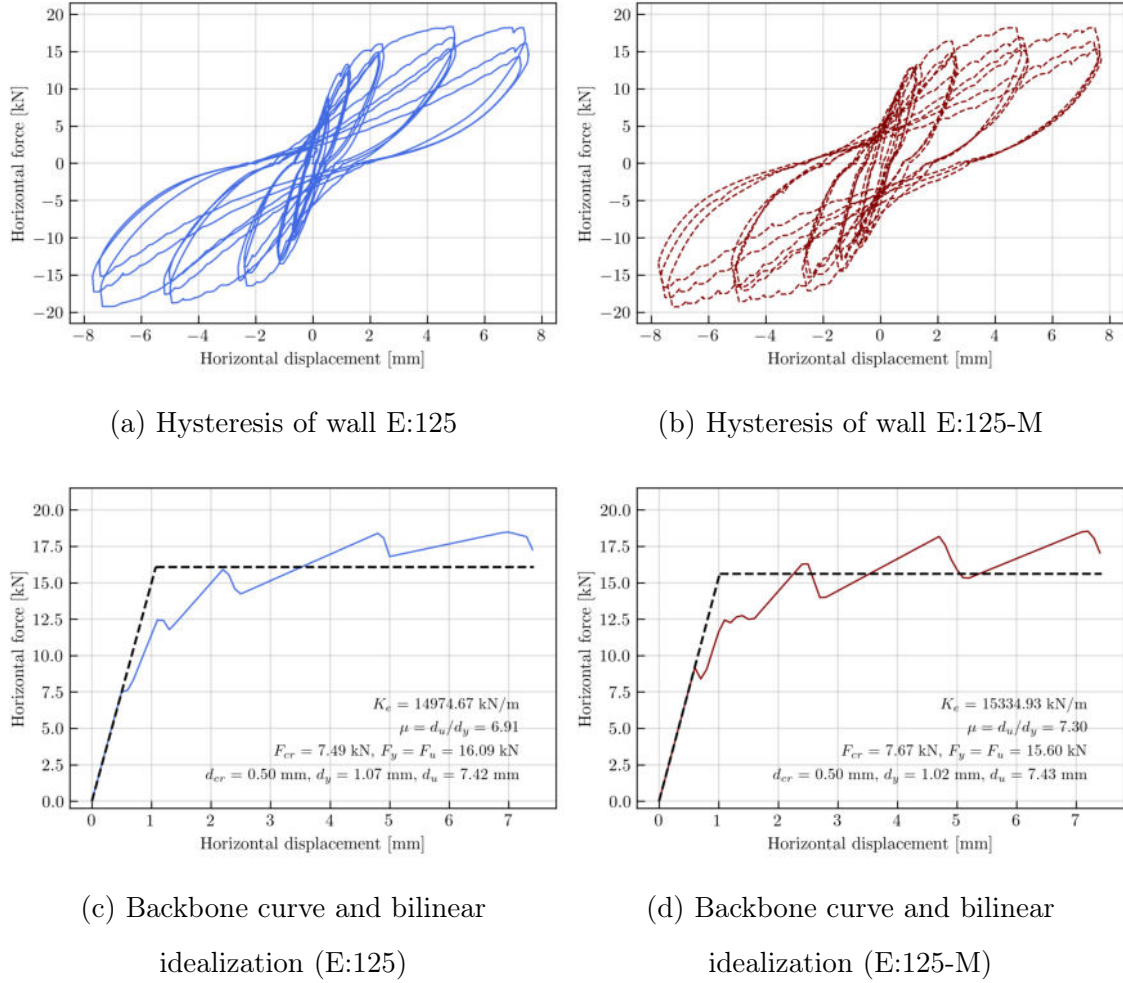


Figure 5.10: Comparison of seismic behaviour in walls made of different material mixture

7.3 mm. Hence, the IDR was bigger in E:125-M as well (Table 5.5). E:125-M wall surpassed the LS4 damage state by Calvi (1999), by reaching 0.59% and 0.58% of the IDR in the push and pull directions, respectively, while E:125 surpassed the LS4 only in the pull direction. Despite reaching the damage state characterised by the collapse of the masonry structure, both walls remained whole, but with major cracks reaching from one side of the wall to the other.

E:125-M showed slightly greater ductility and initial stiffness, while the structural behaviour factor was almost 6% lower. Precisely, for wall E:125, the structural behaviour factor was determined in a value of 2.15, while for E:125-M, it was 2.03.

5.2.5 Influence of drying period length

Two rammed earth walls that dried for a different period were indexed E:125-M and E:125-D. Even though E:125-D was dried for 15 days less, hysteresis and backbone curves were essentially the same (Figure 5.11). Despite that, E:125-M dissipated 23% more energy than E:125-D; 901 kNmm and 693 kNmm, respectively.

The load-bearing capacity of E:125-D was slightly smaller, and E:125-M reached maximum horizontal force at much higher horizontal displacement. Therefore, the IDR was greater in E:125-M, which, as mentioned in the previous subsection, surpassed the LS4, while E:125-D surpassed the LS3, completely symmetrical in the push and pull direction (Table 5.5). As was previously stated for other rammed earth walls presented in this study, walls did not collapse even after reaching the load-bearing capacity and surpassing the drift limit states proposed by Calvi (1999).

Furthermore, E:125-M showed 14% greater ductility and 13.5% greater initial stiffness. Moreover, the structural behaviour factor of E:125-M was 12% lower than that of E:125-D.

5.3 Conclusion

The rammed earth walls that are characteristic of eastern Croatia were tested on material and structural levels. Two soil mixtures were chosen according to the local granular envelope. Both mixtures fit well inside the local envelope but differ from the recommendations given in the literature. However, the mixtures differ in granular composition. First of all, Soil-S looks less uniform than Soil-M. What is more, Soil-S consisted mainly of sand particles (57.3%), while Soil-M had a majority of silt particles (46.9%).

The optimal moisture content was determined by performing the empirical *drop* test and the standard Proctor test. The values of optimal moisture content differed highly between the two test methods. Namely, the standard Proctor test showed 22% lower OMC of Soil-S and even 37% lower OMC of Soil-M. Moreover, soil plasticity, *i.e.* liquid and plastic limits and the plasticity index were determined to get a better understanding of the plastic behaviour of the two soils and compare it

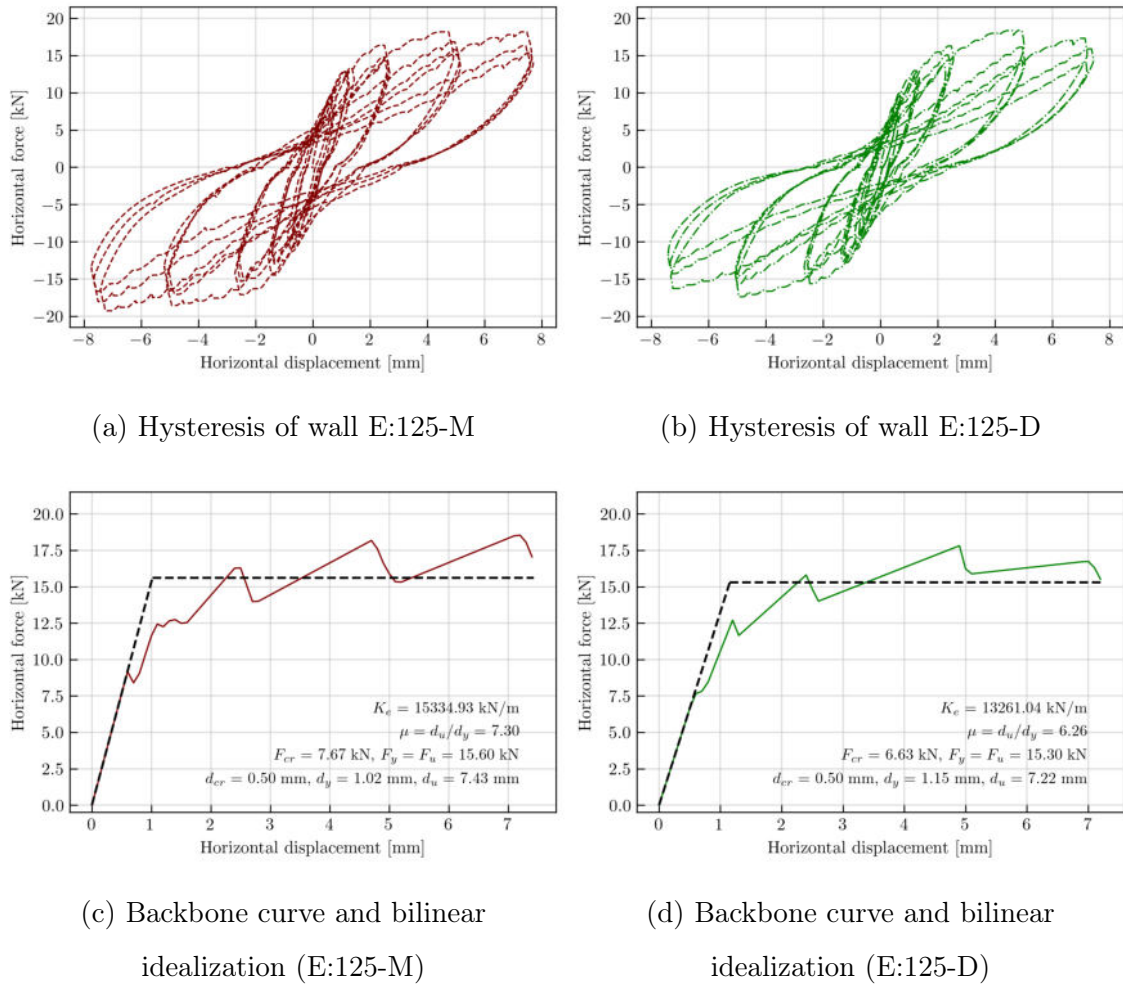


Figure 5.11: Comparison of seismic behaviour in walls tested at different moisture content

to the soil samples collected from existing rammed earth houses in eastern Croatia. Soil-S exhibited liquid and plastic limit values 2% greater than the maximum values in field samples. However, the plasticity index of the Soil-S and Soil-M agreed with field samples and was thus decided that both mixtures were appropriate for rammed earth.

Tensile and compressive strengths were determined on rammed earth samples made of the two soil mixtures. Tensile strength was determined on prismatic samples using a three-point bending test. Compressive strength was determined on halved samples following the tensile strength test and on cubic and cylindrical samples as well. All samples were prepared in the same manner, manually compressed and air-dried for 28 days. The tensile strength of both mixtures was similar. However, compressive strength differed between the mixtures and sample shapes. Soil-M exhibited a more uniform compressive strength between the sample shapes, than Soil-S. Furthermore, the values of compressive strength determined on the halves of prismatic samples were close for both mixtures. However, Soil-S cubic and cylindrical samples showed remarkably smaller values than those of Soil-M.

The seismic behaviour of flat rammed earth walls was experimentally evaluated on four scaled-rammed earth walls. By testing the walls using different excitation regimes, building them from two different soil mixtures, and drying them for different time periods, their effect on the seismic resistance was analysed.

It was determined that the excitation regime does not influence greatly the seismic response of the wall, except for the omission of linear behaviour if loading was performed less gradually in a wall E:125-L. Due to the stochastic nature of the seismic load, one can presume that two separate seismic events would differentiate even more than the two loading protocols used in this study. However, to enable the comparison, only the initial portion of the loading regime was altered, portraying two events that broke out with different starting intensities.

The second altering parameter, soil mixture, showed a greater influence on the wall's seismic response. Namely, failure mode and load-bearing capacity were the same for the two walls made of different materials (E:125 and E:125-M). However, in other tested properties, the wall (E:125-M) made of material with more a uniform particle size distribution (Soil-M), performed better. In particular, the wall endured

higher IDR, even surpassing the final limit state for masonry (LS4) while remaining upright, albeit with major fractures. Moreover, E:125-M showed greater ductility and higher initial stiffness while dissipating 26% more energy. Finally, the structural behaviour factor of the E:125-M was 6% lower than that of the wall E:125, made of Soil-S, which contained more than 50% of sand.

The drying period prior to testing the rammed earth wall is still a matter of question. To this day, there has been no consensus among the researchers in the field regarding the drying conditions of smaller samples and walls. All four walls were dried in the same laboratory conditions during the late spring and early summer, from May to July. However, one of the walls (E:125-D) was dried for 15 days less and compared with the wall made of the same source material that was dried for a full two months (E:125-M). It was determined that the reduction of the drying period affected all properties considered in the study, apart from the failure mode. Namely, the wall that was dried for 45 days performed lower than the wall dried for 60 days, as one could expect. The additional two weeks of drying the wall enabled the E:125-M wall to dissipate 23% more energy, have greater ductility and initial stiffness while having a 12% lower structural behaviour factor. Moreover, even though the E:125-M exhibited greater IDR, surpassing the LS4, the more humid wall (E:125-D) surpassed the LS3, the same as walls made of a different soil mixture, dried for a full two months.

The experimental study was limited to flat, rammed earth walls at a 1:2 scale due to laboratory limitations and cost. However, it is necessary to comprehend the behaviour of full-scale walls as part of the construction. Therefore, in the following chapter, different wall systems were analysed numerically after making a validated model based on the experimental results. Knowledge gathered in this experimental analysis is a valuable source and base point from which the numerical analysis should be built.

Chapter 6

Numerical analysis

Due to the limitations of the experimental work, further numerical analysis was necessary in order to get a better understanding of the rammed earth walls. ANSYS software (v. 2022 R1) was used for performing the numerical analysis. As the first step, experimental data obtained from the wall E:125, presented in chapter 5, was used to validate a numerical model. After establishing the numerical model's analysis settings and material properties, parametric analysis on full-scale models was conducted. It was extended to rammed earth walls that are part of construction because the experimental analysis only included flat, free-standing rammed earth walls, the kind of which are rarely found in real construction. Two systems were analysed, C-wall and T-wall, as parts of the traditional three-room rammed earth house from eastern Croatia (Figure 6.1). In total, 54 numerical models were analysed by varying the length of the walls and the intensity of the vertical load.

6.1 Constitutive model for rammed earth

The literature review revealed the need for more consensus regarding the applied software and the computer modelling process itself. In this analysis, ANSYS software (v. 2022 R1) was chosen due to the level of familiarity with the software and the licence availability at the *Alma mater*. This study adopted a previously used constitutive model by Loccarini et al. (2020). Namely, the Drucker-Prager Concrete constitutive model was used due to the similitude of rammed earth with con-

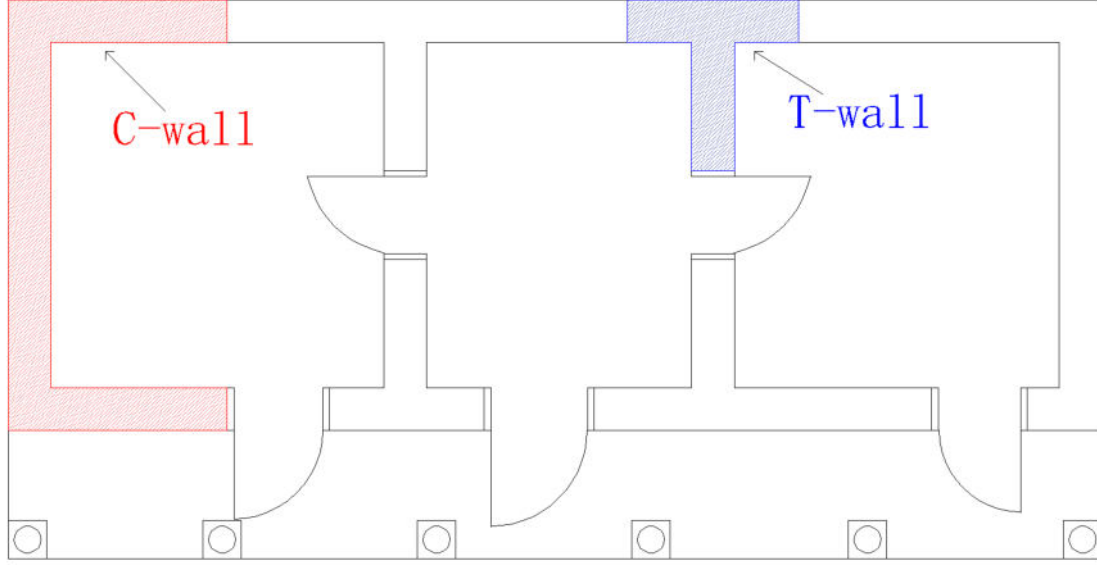


Figure 6.1: C-wall and T-wall systems as a part of a rammed earth house

crete. The plasticity type model contains strain-softening behaviour, which makes it appropriate for low-tensile materials such as concrete and rammed earth. The Drucker-Prager material model assumes a yield domain in the space of principal stress as represented by a circular composite cone around the hydrostatic pressure line, which is also the axis (Kossa, 2012; Loccarini et al., 2020). Moreover, ANSYS offers several hardening-softening-dilatation (HDS) behaviour models: exponential, steel reinforcement, fracture energy and linear. For exponential behaviour, hardening in compression and softening in both compression and tension is defined by the yield functions Ω_c (Equation 6.1) and Ω_t (Equation 6.2) which depend on the hardening variable κ , as it can be observed in Figure 6.2.

$$\Omega_c = \begin{cases} \Omega_{ci} - (1 - \Omega_{ci}) \sqrt{2 \frac{\kappa}{\kappa_{cm}} - \frac{\kappa^2}{\kappa_{cm}^2}} & \text{for } \kappa < \kappa_{cm} \\ 1 - (1 - \Omega_{cu}) \left(\frac{\kappa - \kappa_{cm}}{\kappa_{cu} - \kappa_{cm}} \right)^2 & \text{for } \kappa_{cm} < \kappa < \kappa_{cu} \\ \Omega_{cr} + (\Omega_{cu} - \Omega_{cr}) \exp \left(2 \frac{\Omega_{cu} - 1}{\kappa_{cu} - \kappa_{cm}} \cdot \frac{\kappa - \kappa_{cm}}{\Omega_{cu} + \Omega_{cr}} \right) & \text{for } \kappa > \kappa_{cu} \end{cases} \quad (6.1)$$

where:

κ_{cm} = plastic strain at uniaxial compressive strength

κ_{cu} = plastic strain at transition from power law to exponential softening

Ω_{ci} = relative stress at start of non-linear hardening

Ω_{cu} = residual relative stress at κ_{cu}

Ω_{cr} = residual compressive relative stress

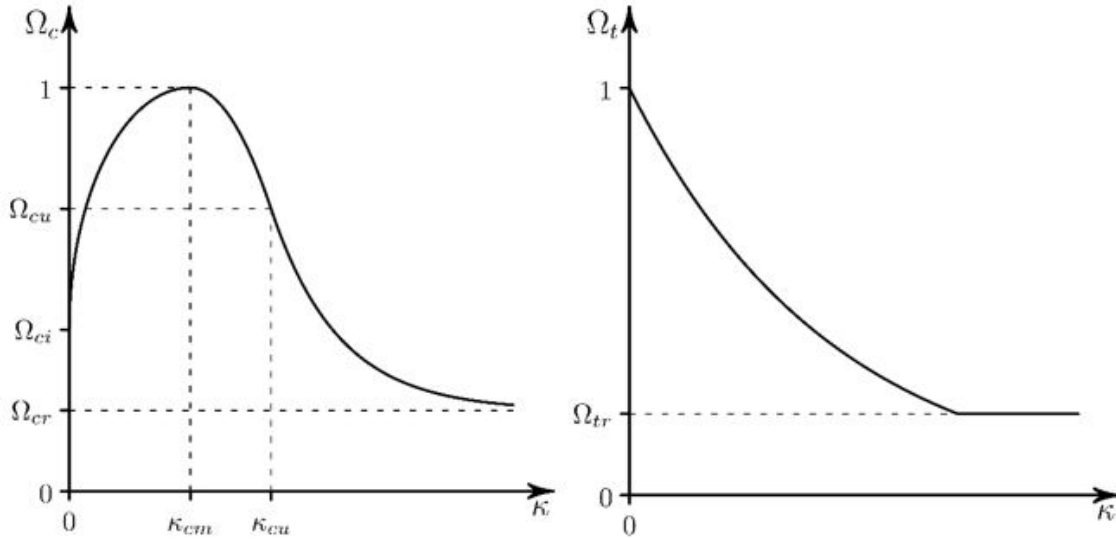


Figure 6.2: Drucker-Prager model: uniaxial stress-strain relationship (left: compression, right: tension) (ANSYS)

$$\Omega_t = \exp\left(-\frac{\kappa}{\alpha_t}\right) \quad \alpha_t = \frac{g_{ft}}{R_t} \quad g_{ft} = \max\left(\frac{G_{ft}}{L_i}, \frac{R_t^2}{E}\right) \quad (6.2)$$

where:

R_t = tensile strength

G_{ft} = mode I area-specific fracture energy

L_i = effective element length

E = Young's modulus

6.2 Validation

As a first step towards the parametric analysis, a numerical model was developed in the same manner as the tested rammed earth wall. Thus, the numerical model was validated based on the experimental data. It was decided to use the results obtained after testing the wall E:125, made of Soil-S. Its counterpart, E:125-M, made of Soil-M, performed better in terms of ductility, stiffness and energy dissipation ability. Therefore, a more critical case was chosen for further examination since both soil mixtures correspond to the local envelope and are thus expected to be found in eastern Croatia.

To better comprehend the behaviour of a rammed earth wall, a micro-modelling approach was applied by modelling a rammed earth wall constructed of consecutive

layers, even though that procedure was not the norm in the observed literature. A numerical model was developed with the exact dimensions of the tested wall, *i.e.* $125 \times 125 \times 25$ cm, consisting of layers 5 cm thick. Material properties were the same in each layer. However, a cohesive zone model with slip tangent to the interface was applied between the layers to enable stiffness reduction with the load progression. Moreover, the normal stiffness of the contact surface between the layers was characterised by a factor equal to 0.1. The analysis was distributed into two load steps that were further divided into substeps. Vertical stress was applied during the first load step, while the second was reserved for applying displacement at a constant amount of vertical stress. The second load step also utilised stabilisation with a constant energy dissipation ratio of 1^{-10} .

Material properties that could not be reliably determined experimentally were chosen according to the literature review. Namely, a density of 2000 kg/m^3 was chosen as most of the literature values are concentrated around that amount (Abhilash and Morel, 2019; Baleca et al., 2023; Barsotti et al., 2023; Champiré et al., 2016; Chitimbo et al., 2022; Gomes et al., 2014; Ramezanpour et al., 2021; Romanazzi et al., 2022b; Silva et al., 2014a, 2016a), and the greatest compressive strength values correspond to that value of density (Figure 2.12 in section 2.7). Young's modulus of 300 MPa was also chosen as a value corresponding to the literature (Gil-Martín et al., 2022; Koutous and Hilali, 2021), but it also agrees with the wall stiffness exhibited during the experimental testing. Poisson's ratio of 0.2 was reported by Bui et al. (2014a) as experimentally determined on dry rammed earth samples. Uniaxial compressive and tensile strength were experimentally determined on prismatic samples as 2.25 MPa and 0.87 MPa, respectively (Table 5.2 in chapter 5). In the validation process, values of compressive strength determined on cubic and cylindrical samples were also considered; however, load-bearing capacity did not correspond to the experimental results. The Drucker-Prager constitutive model's exponential behaviour that implies exponential compression softening was adopted according to the experimental results (Table 6.1). In contrast, tensile softening parameters (Mode 1 Area Specific Fracture energy = 0.004 N/mm; Residual Tensile Relative Stress = 0.1) were assumed based on the literature review (Loccarini et al., 2020). Moreover, two more parameters were required to define the Drucker-Prager model

in ANSYS: tensile and tension-compression dilatancy and compression dilatancy, which were both assigned a value of 1, the same as in Loccarini et al. (2020).

Table 6.1: Drucker-Prager parameters used for describing exponential softening in compression

Parameter		Value
Plastic strain at uniaxial compressive strength	κ_{cm}	0.012
Plastic strain at transition from power law to exponential softening	κ_{cu}	0.062
Relative stress at start of non-linear hardening	Ω_{ci}	0.8
Residual relative stress at κ_{cu}	Ω_{cu}	0.45
Residual compressive relative stress	Ω_{cr}	0.25

Even though the wall dimensions in the numerical model were the same as in the experimental testing, a few differences in the modelling approach were made. Reinforced concrete beams were not modelled to make the numerical model less complicated. Instead, the lower beam was replaced by imposing fixed support at the bottom surface of the wall, while the appropriate amount of vertical stress replaced the upper beam. Horizontal displacement was applied at the top surface of the wall. However, to reduce the computational time and cost while making the parametric analysis more efficient, it was decided to continue the analysis with a pushover method instead of cyclic loading. It was decided that pushover analysis was appropriate based on two reasons. Namely, the behaviour of experimentally tested walls and numerical models analysed in the validation process was essentially the same in both push and pull directions. Also, the primary outcome of the numerical analysis was determining the structural behaviour factor and the level of resistance to seismic excitations, both of which can be determined solely based on pushover or bilinear curves. The horizontal displacement applied at the top of the validation numerical models monotonically increased until reaching the final displacement of 7.5 mm. Moreover, as previously mentioned, it was applied after the vertical stress was applied.

A sensitivity analysis regarding the finite element (FE) size was performed. Numerical models were divided into square finite elements of a linear order (SOLID185)

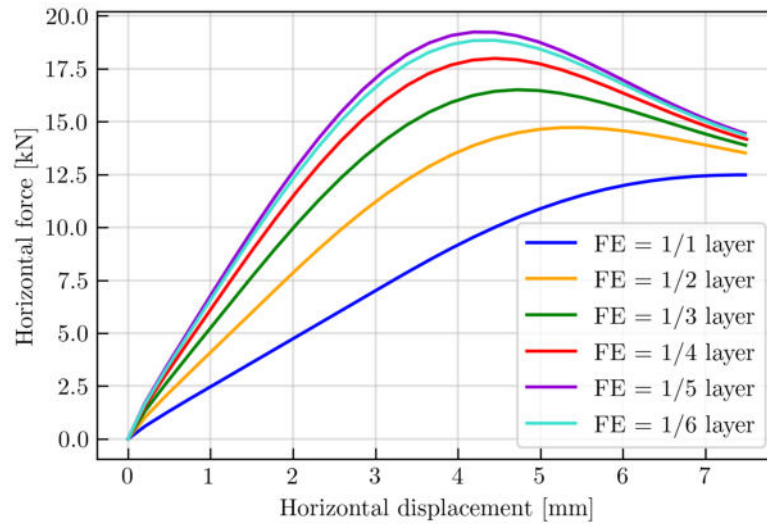


Figure 6.3: Validation analysis performed by varying finite element size

(ANSYS). The size of the finite elements varied depending on the function of the layer height (50 mm). Therefore, the parametric analysis performed on full-scale models could be performed by modelling walls following the same procedure, *i.e.* dividing the wall into finite elements as a function of the layer height. Moreover, by dividing the model into finite elements whose size is in function of the layer height, it was ensured that each layer would begin and end with finite elements of equal size. Six variants were computed, with finite elements size equal to the height of the layer (50 mm), 1/2 of the layer (25 mm), 1/3 of the layer (16.67 mm), 1/4 of the layer (12.5 mm), 1/5 of the layer (10 mm) and 1/6 of the layer (8.33 mm).

All six analyses were performed using the same material and analysis settings. The finite element size greatly influenced the numerical model's structural capacity (Figure 6.3). It was observed that the load-bearing capacity and stiffness in the models divided into finite elements of 1/5 of the layer and 1/6 of the layer is close enough. Thus, it was decided that further reduction of the finite elements is not necessary. The validation numerical model divided into finite elements of 1/5 of layer height has proved accurate enough (Figure 6.4). Therefore, the finite element size in parametric analysis was chosen to be 1/5 of layer height. Further reduction of finite element size in parametric analysis models would only increase the computational time and memory without providing significantly more accurate results.

Cyclic numerical analysis was also performed, even though it was decided to perform the parametric analysis using the pushover method. That way, it was

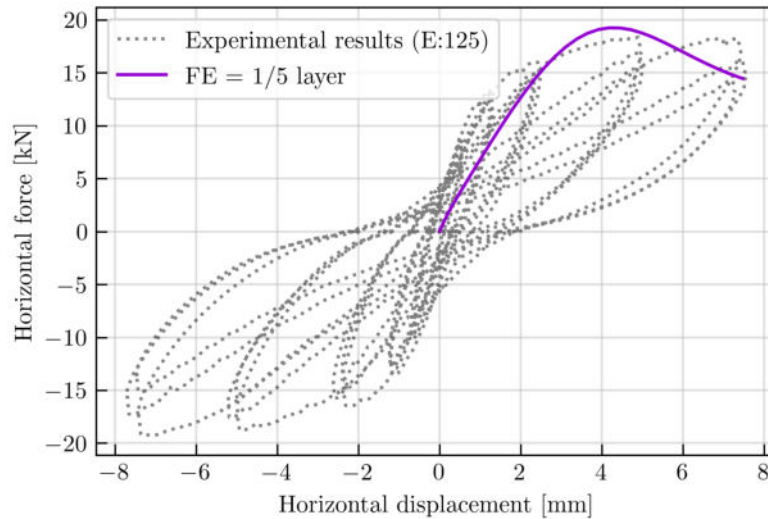


Figure 6.4: Validation numerical model overlapped with experimental results

possible to check whether the changes in capacity with finite element size changes would appear in hysteresis as well. The validation model was loaded in the same manner as the experimentally tested wall by applying cyclic horizontal displacement at the top surface of the wall. Modified load protocol, starting with a displacement of ± 0.625 mm, was applied since the same protocol was utilised at the experimentally tested wall, which was the basis of the validation process (E:125).

According to the results, the change in the finite element size did not influence the load-bearing capacity in a grand manner (Figure 6.5). Even though differences are present, all five hysteresis look similar. Therefore, the cyclic numerical analysis did not influence the decision regarding the finite element size explained in previous paragraphs.

The modelling approach determined on validation numerical models was followed for building parametric analysis numerical models. However, the experimental testing was performed on a small-scaled rammed earth wall (1:2 scale). Therefore, it was necessary to first perform a numerical analysis on the wall represented by the experimental sample. Chauchy-Froude's similitude laws for scaling were considered since the same principle was previously used for rammed earth walls (Romanazzi et al., 2022a). Following the scale factors presented in Carvalho (1998), only geometry was scaled by the scale factor $\lambda = 2$, while material properties remained the same (Table 6.2). Namely, a 50 cm thick wall with 250 cm height and width was modelled. The layer thickness was also doubled, from 5 cm in the small-scale

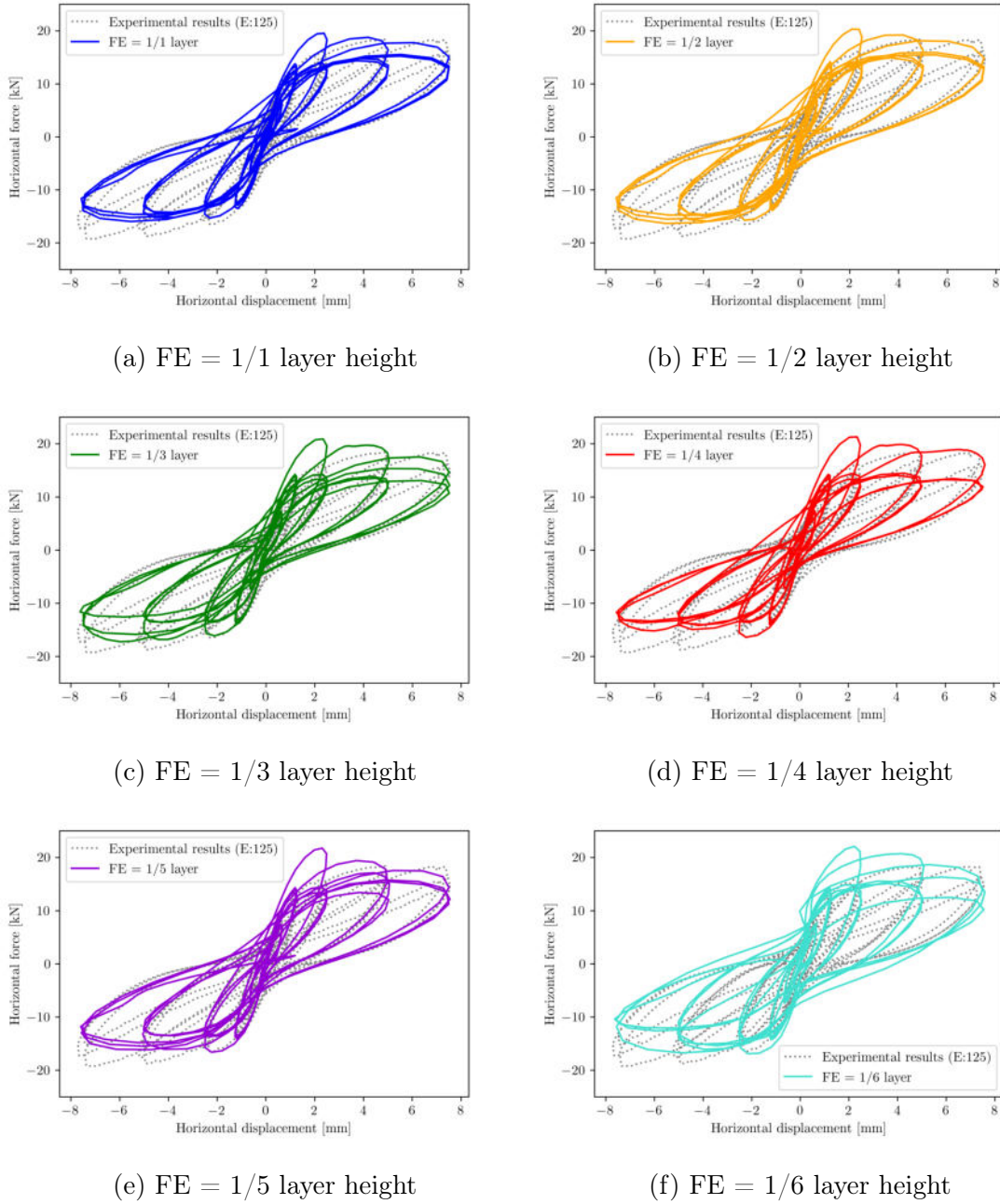


Figure 6.5: Different finite element (FE) sizes overlapped with experimental results numerical model to 10 cm in the full-scale model.

The vertical stress applied to the top surface of the wall was not scaled. However, the horizontal displacement was scaled by the scale factor $\lambda = 2$. Thus, vertical stress of 0.18 MPa and horizontal displacement of 15 mm were applied at the top of the full-scale numerical model, in the direction as presented in Figure 6.7 and Figure 6.8. It should be mentioned that a horizontal displacement of 15 mm is equal to 0.6% of the IDR, which is higher than the final limit state proposed by Calvi (1999).

Table 6.2: Scale factors - Chauchy-Froude's similitude laws

Parameter	Cauchy-Froude scale factor
Length	λ
Modulus of elasticity	1
Specific mass	λ^{-1}
Area	λ^2
Volume	λ^3
Mass	λ^2
Displacement	λ
Force	λ^2
Moment	λ^3
Stress	1
Strain	1

The results of both small-scaled and full-scaled numerical models were overlapped in Figure 6.6. A similar behaviour could be observed, with the expected difference in load-bearing capacity. If scale factors in Table 6.2 are considered, the force in the full-scale model should be λ^2 larger than in the small-scale model. In this case, the force in the full-scale model should be about four times larger. If the maximal forces of both models are divided, it is apparent that the maximum force in the full-scale model is 3.94 times larger than that of the small-scale model (Figure 6.6). It was concluded that the deviation of 1.5% from the expected scale factor is permissible and that the parametric analysis can be performed following the established procedure. It should be noted that greater stiffness could also be observed in the full-scale model. However, differences in stiffness were also observed between different sample shapes and sizes, which were thus expected in this case as well.

This study is the first attempt to numerically analyse the rammed earth walls from eastern Croatia on this level. Therefore, the procedure for developing numerical models was based on previously published research and experimental tests that could be reliably conducted due to the limited guidelines and appropriate equipment. Since the gathered information was validated by experimental results, the same approach

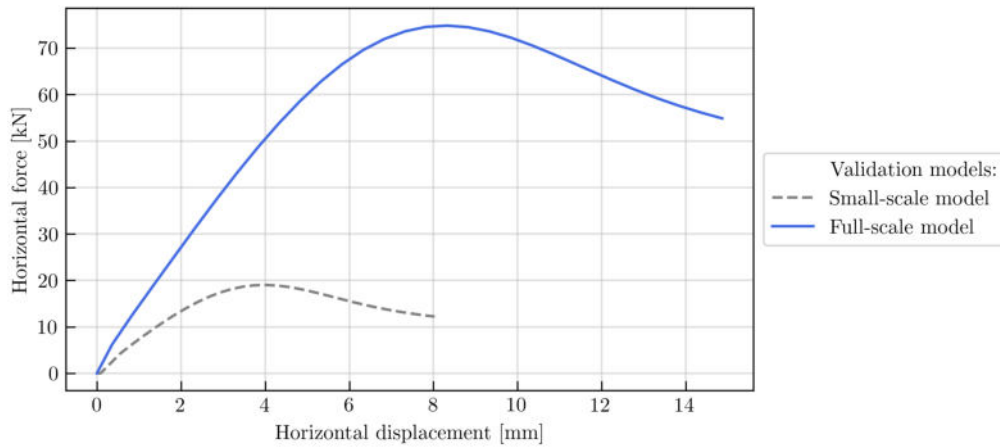


Figure 6.6: Comparison of small-scaled and full-scaled wall numerical test results

was followed for further research steps. The following sections explain the systems covered by parametric analysis in detail before the results are reported.

6.3 Parametric analysis

Following the principles determined on the validated numerical model tested using the pushover method, parametric analysis was expanded to different systems and vertical loads. Experimentally tested walls represented flat square rammed earth walls, even though walls in the actual construction rarely occur alone, without other walls connected to them. However, since traditional rammed earth houses are simple, regular constructions, one can presumably separate them into independent elements, *i.e.* walls (EN 1998-1), thus justifying the experimental work. The nature of the numerical analysis enables one to investigate different systems more efficiently than by performing experimental testing. Therefore, experimental work served as the basis for performing the numerical analysis on more samples. Namely, if the traditional rammed earth house plan from eastern Croatia is analysed, two systems stand out (Figure 6.1). The experimental approach accuracy, *i.e.* whether walls can be observed as separate units, will also be examined by performing numerical analysis on the two systems.

C-type is a wall connected to two transverse walls on the edge. The length of the transverse walls (flanges) that needs to be considered is a matter of question. What is more, the necessity of making flanges an inherent part of the wall also needs

Table 6.3: Length variants characteristic for each tested system

Characteristic length	Length variant [cm]			
L_C	250	350	450	see Figure 6.7
L_T	100	150	200	see Figure 6.8

Note: L_C = length of the C-type wall,

L_T = length of the T-type wall

to be verified. Therefore, a C-type wall was tested as a flat wall without flanges and with two lengths of flanges, determined in function of the wall length (L_C), as seen in Figure 6.7. Three wall lengths were considered (Table 6.3) based on the information collected from the traditional rammed earth houses during field observation.

T-type is a part of the wall extended from the opening to the house's outer wall. Namely, if the plan of the traditional rammed earth house is considered, three rooms stacked one after another, connected by doors, can be distinguished. Both inside walls are separated into two sections by the door. Therefore, it was decided to analyse the T-type of the wall instead of an I-type that would represent an inside wall with two flanges at the end, a kind which was previously tested by Romanazzi et al. (2022a). The variations of the numerical models were similar to the C-type. Namely, three wall lengths were considered (Table 6.3) and were the basis of determining the flange length (Figure 6.8). A flat wall without flanges with length L_T and two flange lengths were considered. Wall lengths were also determined according to the field observation and traditional rammed earth houses encountered.

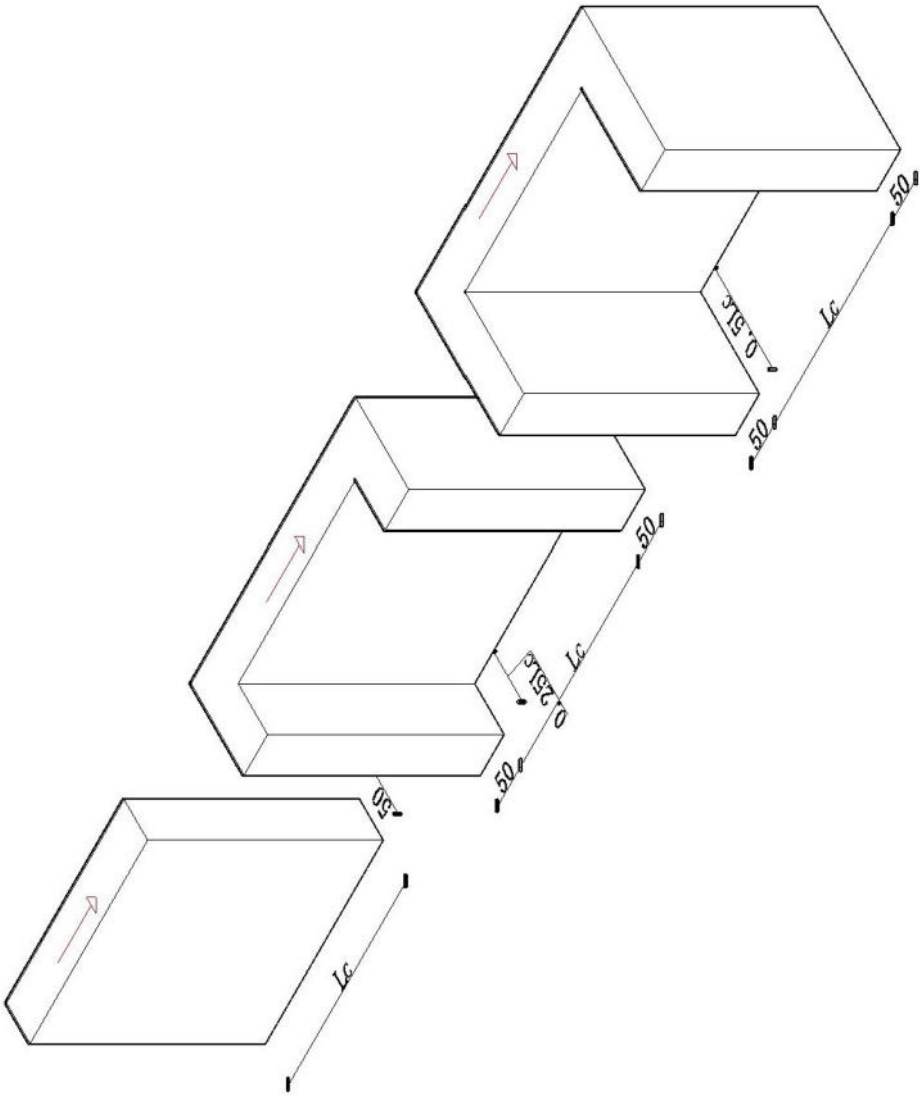


Figure 6.7: C-wall variations and load direction

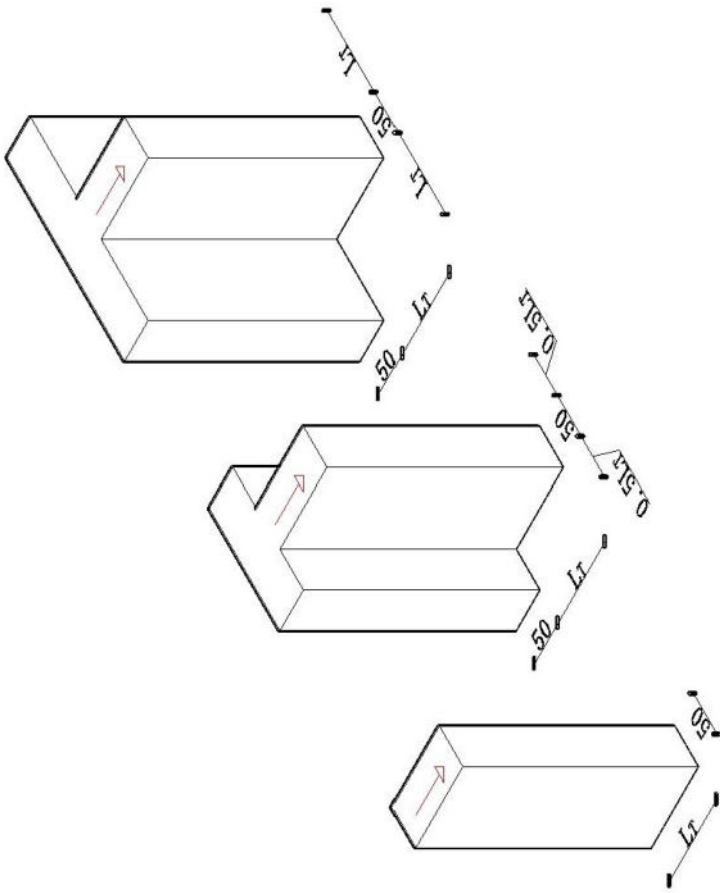


Figure 6.8: T-wall variations and load direction

The influence of vertical load intensity was also analysed numerically. Namely, even though experimental results showed that the vertical load of 0.18 MPa was adequate (Tomažević, 2009), two other intensities were considered to analyse their influence on the seismic response. Vertical stress equal to 0.18 MPa, 0.22 MPa and 0.25 MPa was applied at the top surface of the numerical models. The load was determined according to the house measurements during the field observation by considering the weight of the roof construction and live load by assuming the attic was used as storage space or granary. The three values correspond to a minimum, average and maximum load, depending on the span length and the gable height. In the experimental work, a minimum value of 0.18 MPa was applied. The numerical analysis consisted of applying all three levels of vertical load to all 18 geometry variations, totalling 54 analysed numerical models.

6.3.1 C-walls

Wall systems corresponding to the shorter outer wall with flanges of various lengths were modelled in ANSYS Workbench in the same manner as determined by the validation process. All analysed walls were 50 cm thick and 250 cm high, while the length was variable. Namely, walls of 250 cm, 350 cm and 450 cm in length were modelled by stacking 10 cm thick layers. The horizontal load was applied in-plane in all cases considered (Figure 6.7), while the vertical load was varied, as was previously explained.

In this subsection, only graphs containing results for one wall system (250_C_0) were plotted, to ease the description of different colours and styles of plotting corresponding to different numerical models. Complete numerical results, as well as bilinear idealisations, are plotted in Figure 8.1 through Figure 8.16 in Appendix A (starting at pg.182).

As can be seen in Figure 6.9, different graph styles are plotted for each wall system: a solid line for a straight wall, a dotted line for a wall with shorter flanges, and a dashed line for a wall with more extended flanges. The different intensities of vertical load are colour-coded. The highest intensity (0.25 MPa) is plotted with a red line, 0.22 MPa is plotted with a green line, while the lowest intensity (0.18 MPa) is plotted with a blue line. All the graphs representing C-type wall results are

plotted using the same x and y axes to ease the comparison.

Moreover, critical values of displacement and force were extracted for each system observed (Table 6.4). Critical force (F_{cr}), yield force (F_y) and ultimate force (F_u) were determined from bilinear idealisation, along with corresponding displacements. Bilinear idealisation was performed in the same manner as explained in chapter 5 for experimentally tested walls (Figure 6.10). On the other hand, maximum force (F_{max}) was determined from the actual pushover curve, plotted from numerical results. It corresponds to the maximum force each numerical model had endured.

It was observed that the increase in wall length and the addition of flange walls increased the load-bearing capacity. Thus, a 450 cm long wall with flanges equal to 50% of the wall length exhibited the greatest load-bearing capacity (Figure 8.17). However, the intensity of vertical stress did not influence the behaviour.

If different systems of the same length are compared, namely a wall with no flanges and the two flange lengths, a difference in load-bearing capacity and endured displacement is apparent. Flat walls without flanges (250_C_0, 350_C_0 and 450_C_0) all endured displacement close to 15 mm, while numerical models of walls with flanges all exhibited convergence issues due to the material failure much earlier. Namely, the ultimate displacement of those walls ranged from around 9 mm and 11 mm for walls 250 cm and 450 cm in length, respectively. It should be noted, however, that 250 cm long walls endured slightly greater displacement if shorter flanges were considered, while the opposite can be observed for 450 cm long walls. On average, 350 cm long walls showed the same behaviour regardless of the flange length.

The maximum force each numerical model had endured (F_{max}) was highly influenced by the wall length and the presence of flanges. Namely, 250 cm long straight walls without flanges endured around 40% lower force than those with flanges, while 350 cm long walls and 450 cm long walls exhibited around 32% and 26% lower force, respectively. Thus, the difference between the systems decreased as the wall length decreased. However, the length of the flanges did not cause such a great difference in load-bearing capacity, only around 2-3%.

If different wall lengths are compared, walls with 450 cm in length managed

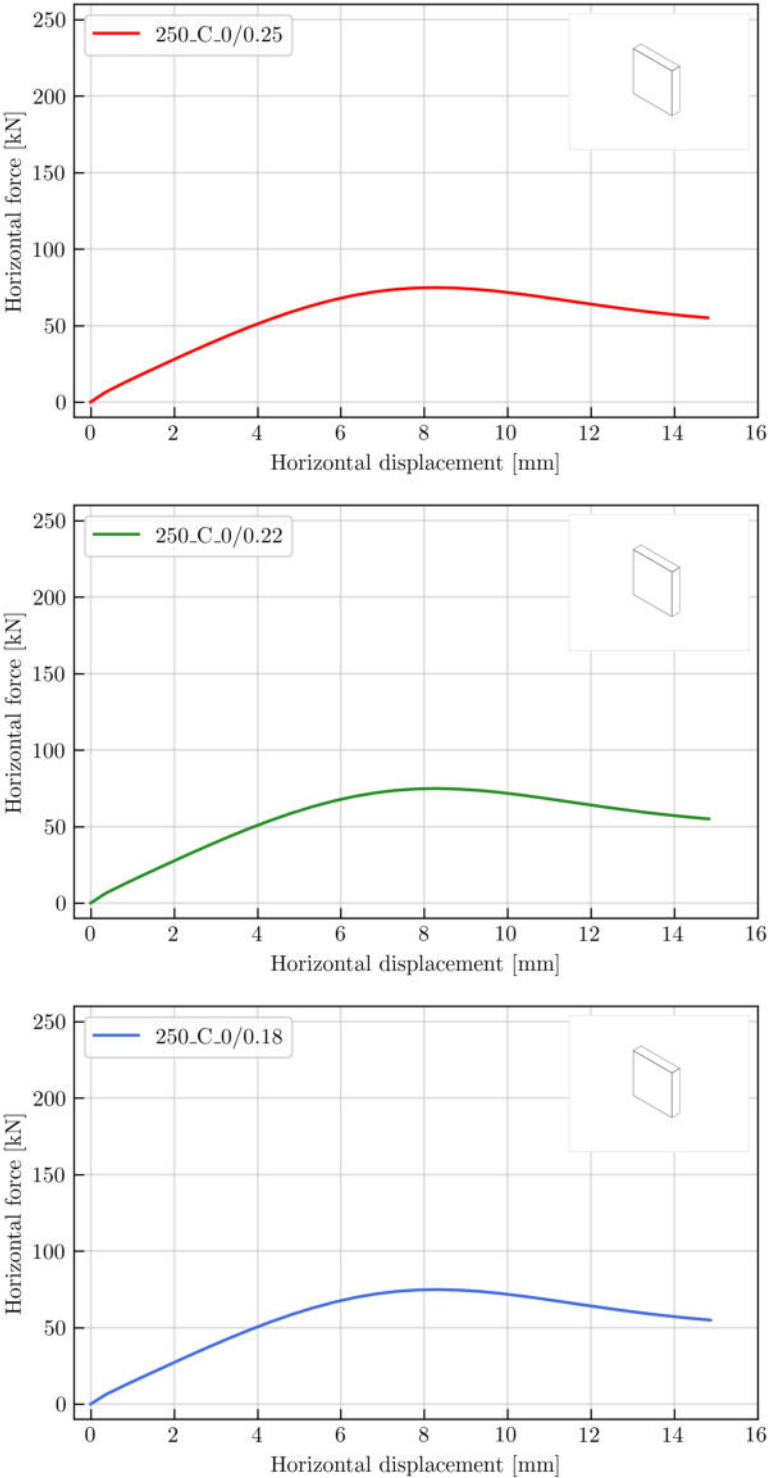


Figure 6.9: Numerical analysis results: 250_C_0

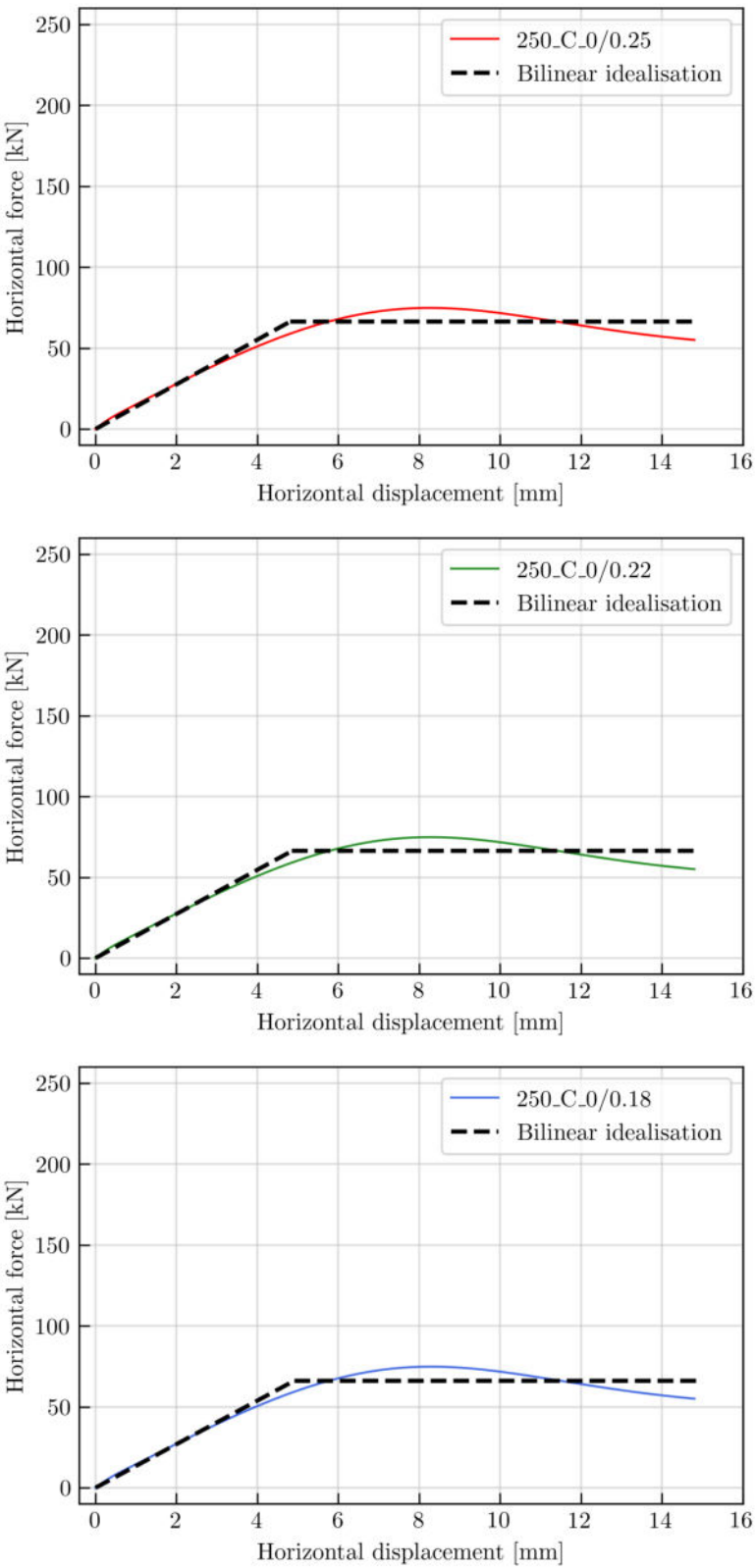


Figure 6.10: Bilinear idealisation: 250_C_0










to endure the greatest forces. To be more specific, 450 cm long straight walls had around 50% bigger load-bearing capacity than 250 cm long straight walls and around 25% bigger capacity than 350 cm long straight walls. The differences between the lengths subsided for walls with flanges, and it was the same for both flange lengths. Namely, 450 cm long walls with both flange lengths endured around 40% and 20% bigger force than 250 cm and 350 cm long flanged walls, respectively.

6.3.2 T-walls

Wall systems corresponding to the inner wall connecting the outside wall and the door were modelled in ANSYS Workbench per conclusions within the validation process. As with C-wall systems, all analysed walls were 50 cm thick and 250 cm high, while the length was variable. Namely, walls of 100 cm, 150 cm and 200 cm in length were modelled by stacking 10 cm thick layers. Three variants were tested for each length group to determine whether the outside wall (flange) has to be considered and in which range. Namely, a wall of length L_T without any flanges and systems with a flange wall in the function of the L_T (*i.e.* 50% and 100%) were tested. It should be noted that the same length of the flange wall is extended to each side of the wall (Figure 6.8). As with C-walls, the horizontal load was applied in-plane in all cases (Figure 6.8), while the vertical load was varied (0.18 MPa, 0.22 MPa and 0.25 MPa).

Results were plotted in the same manner as C-wall results, with line style corresponding to a geometry system and the colour of the line corresponding to the vertical load. Both pushover curves and bilinear idealisations are plotted in Figure 8.18 through Figure 8.35 in Appendix A. Different graph styles are plotted for each wall system: a solid line for a straight wall, a dotted line for a wall with a flange wall equal to 50% of the wall length (L_T), and a dashed line for a wall with a flange wall equal to L_T . The different intensities of vertical load are colour-coded. The highest intensity (0.25 MPa) is plotted with a red line, 0.22 MPa with a green line, and the lowest intensity (0.18 MPa) is plotted with a blue line. From numerically obtained data, bilinear idealisation was performed in the same manner as for C-wall results. It was exhibited that, similar to C-walls, the length of the wall and flanges influences the load-bearing capacity of the walls in question, while

Table 6.4: C-walls: characteristic displacement and forces

	Wall ID	d_{cr} [mm]	d_y [mm]	d_u [mm]	F_{max} [kN]	F_{cr} [kN]	$F_y = F_u$ [kN]
	250_C_0/0.25	2.20	4.48	14.80	74.84	30.36	66.43
	250_C_0/0.22	2.20	4.85	14.83	74.86	30.05	66.31
	250_C_0/0.18	2.20	4.91	14.86	74.83	29.62	66.10
	250_C_0.25/0.25	1.30	2.92	9.76	125.00	50.33	113.08
	250_C_0.25/0.22	1.30	2.98	10.30	125.00	49.43	113.20
	250_C_0.25/0.18	1.40	3.12	9.84	125.00	51.21	114.00
	250_C_0.5/0.25	1.30	2.94	9.26	128.00	51.65	116.81
	250_C_0.5/0.22	1.30	2.98	9.30	128.00	50.73	116.25
	250_C_0.5/0.18	1.40	3.15	9.34	128.00	52.43	117.90
	350_C_0/0.25	1.50	3.13	14.72	114.00	45.73	95.41
	350_C_0/0.22	1.50	3.17	14.76	114.00	45.02	95.23
	350_C_0/0.18	1.60	3.29	14.80	114.00	46.52	95.69
	350_C_0.25/0.25	1.10	2.47	9.72	167.00	66.89	150.06
	350_C_0.25/0.22	1.10	2.46	10.76	168.00	65.65	146.71
	350_C_0.25/0.18	1.20	2.63	10.31	168.00	68.27	149.61
	350_C_0.5/0.25	1.10	2.48	10.20	172.00	68.02	153.64
	350_C_0.5/0.22	1.10	2.49	10.74	172.00	66.85	151.56
	350_C_0.5/0.18	1.20	2.63	10.29	172.00	69.73	152.77
	450_C_0/0.25	1.20	2.44	14.67	155.00	61.56	124.94
	450_C_0/0.22	1.20	2.49	14.71	155.00	60.50	125.50
	450_C_0/0.18	1.30	2.59	14.75	155.00	62.89	125.29
	450_C_0.25/0.25	1.00	2.17	10.69	210.00	83.60	181.79
	450_C_0.25/0.22	1.00	2.26	10.22	211.00	81.89	185.05
	450_C_0.25/0.18	1.10	2.34	10.78	211.00	85.79	182.58
	450_C_0.5/0.25	1.00	2.18	11.18	216.00	85.24	186.12
	450_C_0.5/0.22	1.00	2.24	11.22	216.00	83.65	187.21
	450_C_0.5/0.18	1.10	2.34	11.27	217.00	87.89	186.87

vertical stress had negligible impact.

All T-wall results plotted in Appendix A had the same x and y axis to facilitate the comparison between different geometry systems. It was observed that walls with L_T equal to 200 cm (cases with the longest walls) exhibited the greatest load-bearing capacity, specifically a wall with the largest flanges (200_T_0.5). Also, as for C-walls, critical force and displacement values were extracted from bilinear idealisation and presented in Table 6.5, along with the maximum force each of the numerical models withstood.

Like C-type walls, straight walls with no flanges endured close to 15 mm horizontal displacement. On the other hand, when a transverse (flange) wall was added, numerical models had convergence issues and failed due to material failure at horizontal displacement ranging from 9.8 to 13.4 mm. Also, shorter walls 100 cm long endured larger displacement values than longer walls of 200 cm in length. Furthermore, the exact behaviour of walls with transverse walls exhibited in C-walls was noticed. Namely, in short walls (100 cm long), when the transverse wall (flange) was longer, the ultimate horizontal displacement was lower, but the other two walls did not show a distinguished difference between the flange lengths.

Again, the maximum force highly depended on the length and flange wall. When 100 cm long walls were considered, walls had 63 to 66% lower load-bearing capacity without a transverse wall. 150 cm long walls endured 42 to 46% lower maximum force without a transverse wall, while 200 cm long walls endured 35 to 39% lower force. If the two transverse wall lengths were observed, the load-bearing capacity differed from 5 to 8%.

Wall length also influenced the load-bearing capacity, *i.e.* the longest wall considered (200 cm) showed the greatest load-bearing capacity. If straight walls without a transverse wall were observed, shorter walls of 100 cm and 150 cm in length had 70 and 32% lower load-bearing, respectively. When a transverse wall was added, the difference between the longest and the shorter walls was slightly reduced. Specifically, a 100 cm long wall endured 47 to 49% lower force, while a 150 cm long wall withstood around 23% lower force.

All results are plotted in graphs and can be observed in Appendix A (Figure 8.18 through Figure 8.35). It should be noted that the shortest walls observed,

100 cm in length, did not exhibit pronounced plastic behaviour, especially a wall without a transverse wall (100_T_0), whose behaviour remained linear until the end of the analysis.

6.4 Seismic behaviour

Capacity curves presented in the last section show the load-bearing capacity of each system. However, further analysis had to be performed to fathom how those systems would behave when encountering a seismic event. Therefore, bilinear idealisation of the capacity curve had to be performed in the same manner as it was performed for experimentally obtained results. Namely, a bilinear idealisation of the capacity curves was performed according to ASTM E2126-19, previously used by Ramezani-pour et al. (2021) in the field of rammed earth structures. According to them, the bilinear curve should overlap with the original curve until reaching 40% of the load-bearing capacity. Also, the area under both curves should remain the same until reaching the ultimate displacement. One can quickly determine the characteristic displacements and belonging forces from the bilinear curve. In the same manner as capacity curves, bilinear idealisation is graphically presented in Appendix A. It should be noted that since no pronounced difference in structural capacity between the three vertical stress intensities was observed, as previously stated, the bilinear curves of all three vertical stresses are incredibly close. Thus, the vertical stress differences had little impact on the values of the determined parameters presented in the following paragraphs.

6.4.1 Characteristic seismic parameters

The structural behaviour factor was determined from the characteristic force values visible in the bilinear curves, following the same procedure used on experimentally obtained data. Despite the shape of the system and vertical load, the structural behaviour factor (Table 6.6 and Table 6.7) in all observed numerical models was around 2 (values ranging from 1.99 to 2.43). Those values agree with previously reported structural behaviour factors determined on experimentally obtained data despite the difference in scale. Moreover, parametric analysis results of 54 numerical

Table 6.5: T-walls: characteristic displacement and forces

	Wall ID	d_{cr} [mm]	d_y [mm]	d_u [mm]	F_{max} [kN]	F_{cr} [kN]	$F_y = F_u$ [kN]
	100_T_0/0.25	5.80	13.66	14.91	17.12	6.79	15.98
	100_T_0/0.22	5.90	13.61	14.92	17.09	6.88	15.86
	100_T_0/0.18	5.90	13.52	14.94	17.06	6.85	15.69
	100_T_0.5/0.25	3.40	7.87	12.83	46.26	18.50	42.79
	100_T_0.5/0.22	3.40	7.94	13.35	46.25	18.40	42.97
	100_T_0.5/0.18	3.40	7.96	13.38	46.24	18.28	42.80
	100_T_1/0.25	3.30	7.60	12.83	50.35	20.32	46.78
	100_T_1/0.22	3.30	7.55	12.34	50.32	20.21	46.23
	100_T_1/0.18	3.30	7.56	12.37	50.27	20.08	45.98
	150_T_0/0.25	4.30	9.94	14.87	38.75	15.53	35.90
	150_T_0/0.22	4.30	9.94	14.89	38.66	15.47	35.75
	150_T_0/0.18	4.30	10.15	14.91	38.48	15.38	36.30
	150_T_0.5/0.25	2.20	5.10	11.28	65.46	26.16	60.60
	150_T_0.5/0.22	2.20	5.21	10.81	65.48	25.93	61.41
	150_T_0.5/0.18	2.30	5.28	10.84	65.50	26.69	61.25
	150_T_1/0.25	2.20	5.04	10.28	69.99	28.18	64.58
	150_T_1/0.22	2.20	5.18	11.30	70.00	27.96	65.86
	150_T_1/0.18	2.20	5.19	10.33	69.97	27.66	65.28
	200_T_0/0.25	2.90	6.69	14.83	56.19	22.57	52.08
	200_T_0/0.22	2.90	6.72	14.85	56.13	22.41	51.94
	200_T_0/0.18	2.90	6.75	14.87	55.98	22.20	51.70
	200_T_0.5/0.25	1.70	3.90	10.24	86.04	34.64	79.43
	200_T_0.5/0.22	1.70	3.91	10.80	86.10	34.23	78.66
	200_T_0.5/0.18	1.70	4.05	10.31	86.16	33.64	80.05
	200_T_1/0.25	1.70	3.99	10.25	91.20	36.00	84.40
	200_T_1/0.22	1.70	4.02	9.77	91.20	35.64	84.23
	200_T_1/0.18	1.80	4.16	9.80	91.20	36.98	85.45

models showed that the structural behaviour factor of rammed earth walls bigger than 1.5 can be used, which is a minimum value for unreinforced masonry according to EN 1998-1 and previously used by Bui et al. (2016) and El-Nabouch et al. (2017). Nonetheless, the parametric analysis results agree with a previously reported value of the structural behaviour factor of an I-shaped rammed earth wall (Romanazzi et al., 2022a).

However, it should be noted that despite the variety of shapes and sizes of the wall systems and the range of vertical stress acting on the wall, the parametric analysis was performed with material properties validated by experimental data from traditionally built walls. Thus, the study is limited to the eastern Croatian area and traditional building techniques, presumably affecting the properties' strength. Further analysis of rammed earth houses should be performed to validate whether the structural behaviour factor determined on wall systems can be used for a complete structure such as a house.

Elastic stiffness and ductility are also reported in Table 6.6 and Table 6.7. Both characteristics were determined according to the characteristic forces and displacement in bilinear idealisation curves (Table 6.4 and Table 6.5). Elastic stiffness was determined according to the slope of the first branch in a bilinear curve, *i.e.* as a ratio of the force and displacement at the yielding point. Ductility was determined as a ratio of the ultimate and yield displacements.

If C-walls are observed, flange walls significantly increase the elastic stiffness. Specifically, for 250 cm long walls, elastic stiffness increased by ca. 35% when flange walls were added, while the increase was even higher for 350 cm and 450 cm long walls, ca. 50% and 60%, respectively. However, the length of the flange walls did not influence the elastic stiffness. Also, the elastic stiffness of T-walls was significantly lower than that of C-walls, but a flange wall also had a grand influence. Again, the difference in elastic stiffness between the wall with a flange and the free-standing wall subsided as the wall length decreased. Namely, a 100 cm long wall showed ca. 18% higher elastic stiffness if a flange wall was added, while a 150 cm long wall and 200 cm long wall exhibited ca. 30% and ca. 35% higher elastic stiffness, respectively. Again, the flange wall length did not significantly influence the elastic stiffness.

However, if ductility is observed, no such pronounced difference between walls

Table 6.6: C-walls: characteristic parameters determined from numerical results








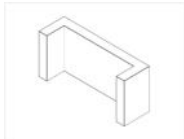










	Wall ID	q [-]	K_e [kN/m]	μ [-]	IDR_{du} [%]
	250_C_0/0.25	2.19	13802	3.08	0.592
	250_C_0/0.22	2.21	13658	3.05	0.593
	250_C_0/0.18	2.23	13464	3.03	0.595
	250_C_0.25/0.25	2.25	38716	3.34	0.391
	250_C_0.25/0.22	2.29	38022	3.46	0.412
	250_C_0.25/0.18	2.23	36579	3.16	0.394
	250_C_0.5/0.25	2.26	39730	3.15	0.370
	250_C_0.5/0.22	2.29	39021	3.12	0.372
	250_C_0.5/0.18	2.25	37452	2.97	0.374
	350_C_0/0.25	2.08	30484	4.70	0.589
	350_C_0/0.22	2.12	30014	4.65	0.590
	350_C_0/0.18	2.06	29078	4.50	0.592
	350_C_0.25/0.25	2.43	60812	3.94	0.389
	350_C_0.25/0.22	2.23	59680	4.38	0.430
	350_C_0.25/0.18	2.19	56891	3.92	0.412
	350_C_0.5/0.25	2.26	61838	4.11	0.408
	350_C_0.5/0.22	2.27	60772	4.31	0.430
	350_C_0.5/0.18	2.19	58111	3.91	0.412
	450_C_0/0.25	2.03	51299	6.02	0.587
	450_C_0/0.22	2.07	50413	5.91	0.588
	450_C_0/0.18	1.99	48380	5.70	0.590
	450_C_0.25/0.25	2.17	83600	4.91	0.427
	450_C_0.25/0.22	2.26	81890	4.52	0.409
	450_C_0.25/0.18	2.13	77992	4.61	0.431
	450_C_0.5/0.25	2.18	85236	5.12	0.447
	450_C_0.5/0.22	2.24	83649	5.01	0.449
	450_C_0.5/0.18	2.13	79901	4.82	0.451

Table 6.7: T-walls: characteristic parameters determined from numerical results

	Wall ID	q [-]	K_e [kN/m]	μ [-]	IDR_{d_u} [%]
	100_T_0/0.25	2.35	1170	1.09	0.597
	100_T_0/0.22	2.31	1166	1.10	0.597
	100_T_0/0.18	2.29	1161	1.10	0.598
	100_T_0.5/0.25	2.31	5440	1.63	0.513
	100_T_0.5/0.22	2.34	5413	1.68	0.534
	100_T_0.5/0.18	2.34	5376	1.68	0.535
	100_T_1/0.25	2.30	6156	1.69	0.513
	100_T_1/0.22	2.29	6126	1.64	0.494
	100_T_1/0.18	2.29	6085	1.64	0.495
	150_T_0/0.25	2.31	3613	1.50	0.595
	150_T_0/0.22	2.31	3598	1.50	0.595
	150_T_0/0.18	2.36	3578	1.47	0.596
	150_T_0.5/0.25	2.32	11891	2.21	0.451
	150_T_0.5/0.22	2.37	11785	2.07	0.432
	150_T_0.5/0.18	2.29	11603	2.05	0.434
	150_T_1/0.25	2.29	12810	2.04	0.411
	150_T_1/0.22	2.36	12709	2.18	0.452
	150_T_1/0.18	2.36	12573	1.99	0.413
	200_T_0/0.25	2.31	7783	2.22	0.593
	200_T_0/0.22	2.32	7729	2.21	0.594
	200_T_0/0.18	2.33	7655	2.20	0.595
	200_T_0.5/0.25	2.29	20374	2.63	0.410
	200_T_0.5/0.22	2.30	20136	2.76	0.432
	200_T_0.5/0.18	2.38	19790	2.55	0.412
	200_T_1/0.25	2.34	21176	2.57	0.410
	200_T_1/0.22	2.36	20967	2.43	0.391
	200_T_1/0.18	2.31	20544	2.36	0.392

with or without flanges can be highlighted. Different wall lengths, however, did influence the ductility and range of ductility values observed. C-walls with a length of 250 cm showed ductility ca. 3 to 3.5; 350 cm long walls had ca. 4 to 4.7, while 450 cm long walls had ductility of ca. 4.5 to 6. T-walls exhibited smaller ductility values, but wall length also had an effect. Namely, ductility in T-walls ranged: from ca. 1.1 to 1.7 (100 cm long walls); from ca. 1.5 to 2.2 (150 cm long walls); from ca. 2.2 to 2.75 (200 cm long walls).

Inter-storey drift (IDR) was also determined as a ratio of the ultimate displacement that can be observed in Table 6.4 and Table 6.5 and a wall height of 250 cm. Each cell's colour in Table 6.6 and Table 6.7 represents the IDR's intensity and corresponding damage state according to Calvi (1999). Namely, red indicates surpassing the last limit state with $IDR > 0.5\%$, while yellow cells correspond to the LS3 (significant damage) and IDR between 0.3 and 0.5%. It was observed that all C-walls without flanges surpassed 0.5% of the IDR, which is the last limit state (LS4) connected to the collapse of the building, according to Calvi (1999). Furthermore, walls with flanges, regardless of their length, all showed the IDR values corresponding to the LS3 (significant damage), which was previously considered to be the final limit for the rammed earth structures (Bui et al., 2016; El-Nabouch et al., 2017). Also, the IDR values slightly increased as the wall length increased from 250 cm to 450 cm. T-walls exhibited similar behaviour, except walls 100 cm long, in which case only two flanged walls had IDR lower than 0.5%.

6.4.2 Seismic capacity

Before overlapping the seismic capacity curves with the response spectrum, they were plotted alone to verify whether all examined wall systems can withstand horizontal acceleration of at least $0.20g$. Also, since the superposition of curves and response spectrum is performed following the bilinear idealisation, idealised curves are plotted for all capacity curves as well. In this case, bilinear idealisation was performed according to EN 1998-1 by sustaining the maximum value of spectral acceleration, as was previously done for observing the seismic response of rammed earth walls in El Nabouch (2017). In contrast with force-displacement curves, seismic capacity curves had different capacities for all three vertical stress intensities,

i.e. an increase in vertical stress decreased the spectral acceleration achieved. The difference occurred due to taking vertical stress into account as an additional equivalent mass while determining seismic capacity curves. Moreover, plotting was done similar to with force-displacement curves, colour-coded for vertical stress and line styles corresponding to different wall systems. Also, a sketch of each wall system is plotted in the corner of the graph, to make results easier to comprehend and compare (Figure 6.11). In Figure 6.11, a graphical representation of the seismic capacity of only one wall system is presented, to clarify different line colours and styles connected to different numerical models. A complete set of seismic capacity curves can be found in Appendix B (Figure 8.36 through Figure 8.41). All curves were plotted with the same axes to ease the comparison.

All C-walls have presented the same behaviour, regardless of the wall length. Namely, walls without flanges all endured spectral acceleration greater than $0.20g$, while the behaviour of walls with flanges depended on the amount of vertical stress. Namely, for shorter flanges, walls loaded with 0.22 and 0.18 MPa achieved spectral acceleration above $0.20g$, while that is true only for walls with more extended flanges loaded with 0.18 MPa of vertical stress. T-walls exhibited slightly different behaviour. Firstly, wall length had a more significant influence on the spectral acceleration. None of the 100 cm long walls achieved a spectral acceleration of $0.20g$, and neither did the walls with flanges despite their length. However, some 150-cm and 200-cm long walls without flanges did. Specifically, all straight 200 cm long walls surpassed the $0.20g$ and two 150 cm long walls (with vertical stress of 0.18 and 0.22 MPa).

6.4.3 Superposition with response spectrum

To put the structural capacity determined by the pushover method into the context of seismic behaviour, force and displacement were transformed into seismic acceleration and seismic displacement. However, without the superposition of the seismic capacity curves with the response spectrum, one can hardly know how a structure would behave at a location of interest. Even then, one cannot assume it is undoubtedly true due to the stochastic nature of seismic events, but it gives an adequate estimate.

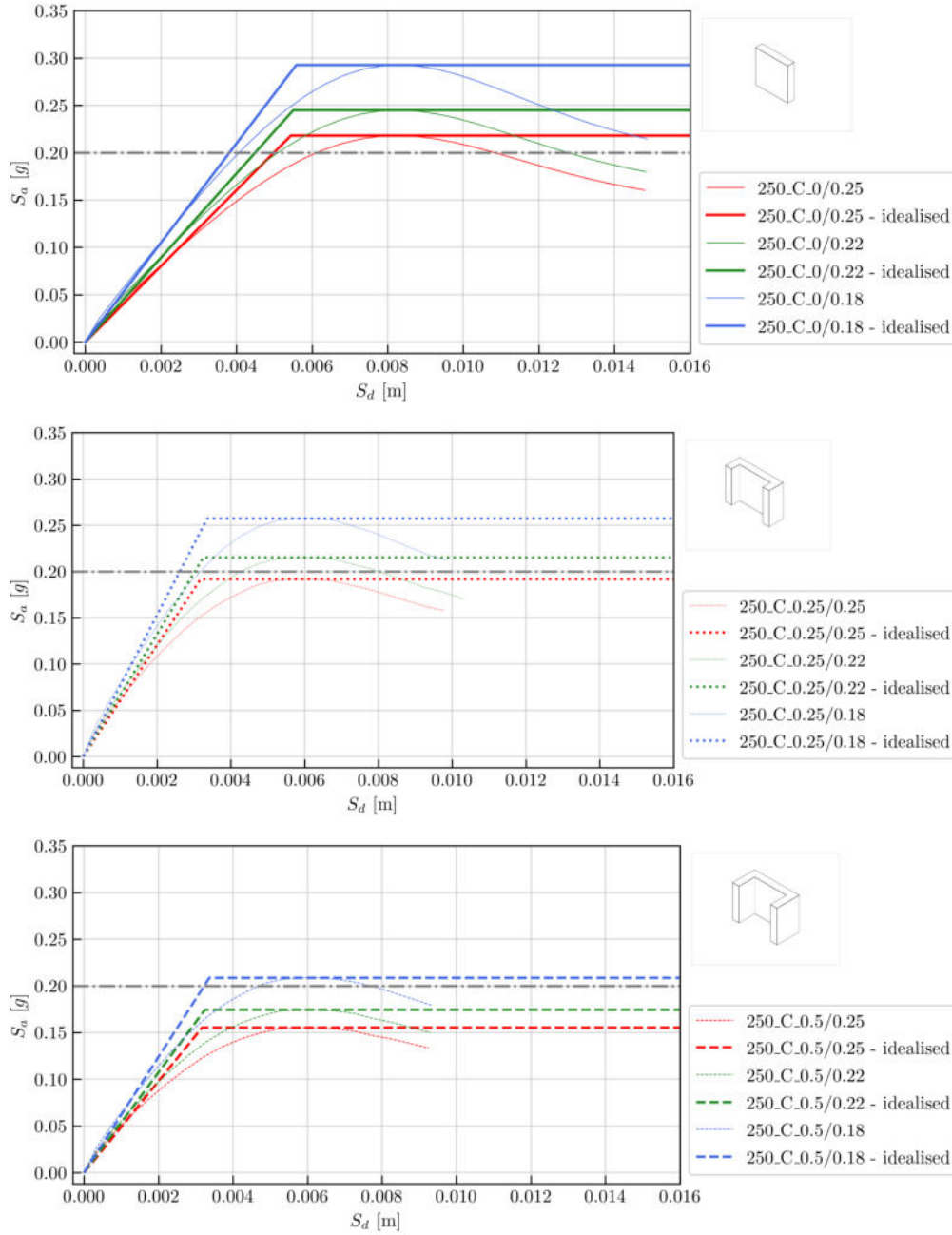


Figure 6.11: Seismic capacity: 250_C

The bilinear idealisation of each seismic curve, performed according to EN 1998-1, was overlapped with the elastic response spectrum curves. Bilinear curves are plotted assuming that maximum spectral acceleration is retained until a response spectrum's end maximal spectral displacement is reached. That idealisation enables one to get information for all limit states, even though numerical models, in reality, achieved lower spectral displacement (*e.g.* the model failed due to convergence problems). The same approach was applied earlier by Bui et al. (2016), El Nabouch (2017) and El-Nabouch et al. (2017).

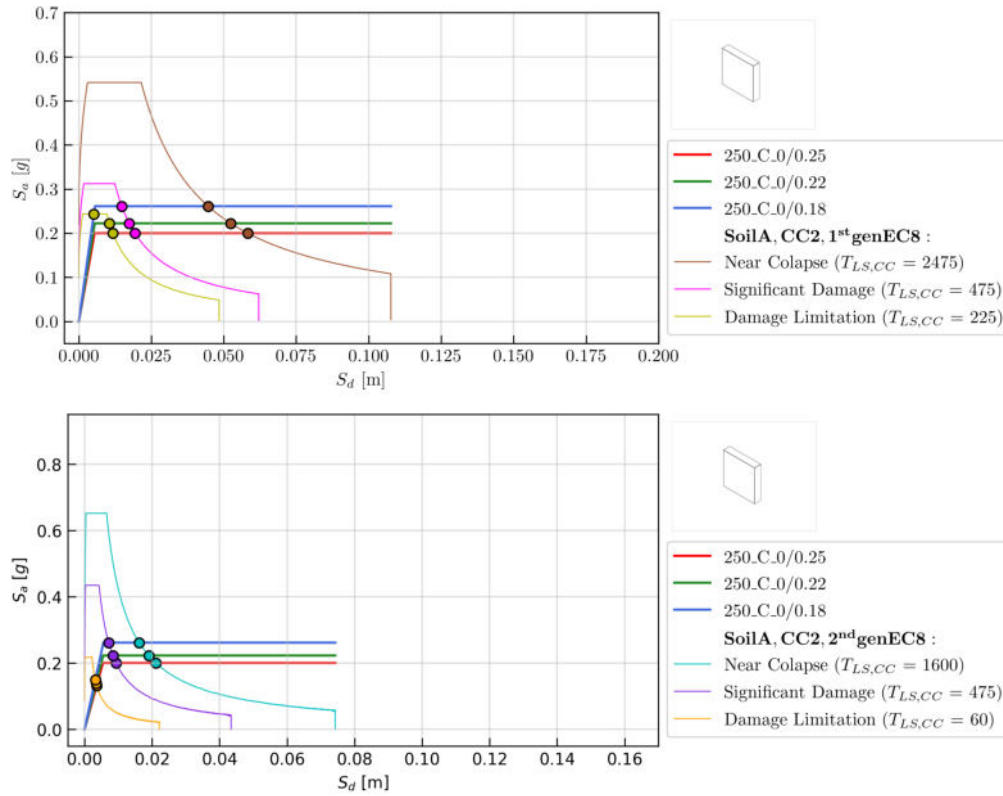


Figure 6.12: Superposition with response spectrum curves

Graphs are all grouped and exhibited in Appendix C and Appendix D to make the text of this subsection more fluid and easier to read, while in this subsection only two graphs were plotted (Figure 6.12). Bilinear curves were colour-coded and plotted in different line styles in the same manner as other graphs corresponding to one wall system exhibited by parametric analysis. The intersection point of each bilinear curve with an elastic response spectrum is marked and colour-coded to correspond to a specific limit state. Response spectrum curves were defined following the approach explained in more detail in chapter 4. Response spectrum curves were plotted by varying line colours between different return periods and Eurocode 8 generations.

Target displacement determined according to each intersection point was used to determine the inter-story drift (IDR_{RS}) each wall system would experience based on a different elastic response spectrum (Table 6.8 and Table 6.9). In contrast to inter-story drift (IDR_{du}) presented in the previous subsection in Table 6.6 and Table 6.7, the IDR_{RS} puts every wall system into seismic context by adding information regarding the location and ground type, on which a rammed earth wall is built.

Table 6.8: Inter-story drift according to 1st generation of Eurocode 8

Wall ID	IDR _{RS} [%]								
	Ground type A			Ground type B			Ground type C		
	NC	SD	DL	NC	SD	DL	NC	SD	DL
250_C_0/0.25	2.331	0.776	0.471	5.244	1.745	1.060	6.935	2.308	1.402
250_C_0/0.22	2.096	0.698	0.424	4.717	1.569	0.954	6.238	2.076	1.261
250_C_0/0.18	1.785	0.594	0.208	4.017	1.337	0.812	5.312	1.767	1.074
250_C_0.25/0.25	2.651	0.882	0.536	5.965	1.985	1.206	7.429	2.625	1.595
250_C_0.25/0.22	2.385	0.794	0.482	5.367	1.786	1.085	7.098	2.362	1.435
250_C_0.25/0.18	2.031	0.676	0.411	4.569	1.520	0.924	6.043	2.011	1.222
250_C_0.5/0.25	3.271	1.088	0.661	6.460	2.448	1.488	7.429	3.238	1.968
250_C_0.5/0.22	2.942	0.979	0.595	6.460	2.203	1.339	7.429	2.913	1.770
250_C_0.5/0.18	2.505	0.833	0.506	5.636	1.875	1.140	7.429	2.480	1.507
350_C_0/0.25	2.142	0.713	0.433	4.820	1.604	0.974	6.374	2.121	1.289
350_C_0/0.22	1.927	0.641	0.390	4.336	1.443	0.877	5.735	1.908	1.159
350_C_0/0.18	1.641	0.546	0.136	3.692	1.228	0.746	4.882	1.624	0.15
350_C_0.25/0.25	2.611	0.869	0.528	5.875	1.955	1.188	7.429	2.585	1.571
350_C_0.25/0.22	2.335	0.777	0.472	5.254	1.748	1.062	6.949	2.312	1.405
350_C_0.25/0.18	1.988	0.661	0.402	4.473	1.488	0.904	5.916	1.968	1.196
350_C_0.5/0.25	3.245	1.080	0.656	6.460	2.429	1.476	7.429	3.213	1.952
350_C_0.5/0.22	2.920	0.971	0.590	6.460	2.186	1.328	7.429	2.891	1.756
350_C_0.5/0.18	2.486	0.827	0.503	5.592	1.861	1.131	7.396	2.461	1.495
450_C_0/0.25	2.026	0.674	0.410	4.558	1.516	0.921	6.027	2.005	1.219
450_C_0/0.22	1.822	0.606	0.117	4.100	1.364	0.829	5.423	1.804	1.096
450_C_0/0.18	1.551	0.516	0.103	3.491	1.161	0.124	4.617	1.536	0.119
450_C_0.25/0.25	2.575	0.857	0.521	5.794	1.928	1.171	7.429	2.549	1.549
450_C_0.25/0.22	2.306	0.767	0.466	5.188	1.726	1.049	6.860	2.283	1.387
450_C_0.25/0.18	1.963	0.653	0.397	4.416	1.469	0.893	5.841	1.943	1.181
450_C_0.5/0.25	3.230	1.075	0.653	6.460	2.418	1.469	7.429	3.198	1.943
450_C_0.5/0.22	2.906	0.967	0.588	6.460	2.176	1.322	7.429	2.877	1.748
450_C_0.5/0.18	2.463	0.819	0.498	5.541	1.844	1.120	7.328	2.438	1.482
100_T_0/0.25	4.076	1.356	0.824	6.460	3.052	1.854	7.429	4.036	2.452

Table 6.8 continued from previous page

Wall ID	IDR _{RS} [%]								
	Ground type A			Ground type B			Ground type C		
	NC	SD	DL	NC	SD	DL	NC	SD	DL
100_T_0/0.22	3.673	1.222	0.743	6.460	2.749	1.671	7.429	3.636	2.210
100_T_0/0.18	3.132	1.042	0.633	6.460	2.345	1.425	7.429	3.101	1.885
100_T_0.5/0.25	3.770	1.254	0.762	6.460	2.822	1.715	7.429	3.733	2.268
100_T_0.5/0.22	3.393	1.129	0.686	6.460	2.540	1.543	7.429	3.359	2.041
100_T_0.5/0.18	2.890	0.961	0.584	6.460	2.163	1.314	7.429	2.861	1.738
100_T_1/0.25	4.306	1.614	0.981	6.460	3.631	2.206	7.429	4.285	2.918
100_T_1/0.22	4.306	1.453	0.883	6.460	3.269	1.986	7.429	4.285	2.627
100_T_1/0.18	3.721	1.238	0.752	6.460	2.785	1.693	7.429	3.684	2.238
150_T_0/0.25	2.701	0.899	0.546	6.077	2.022	1.229	7.429	2.674	1.625
150_T_0/0.22	2.436	0.810	0.492	5.481	1.824	1.108	7.248	2.412	1.465
150_T_0/0.18	2.083	0.639	0.426	4.687	1.559	0.948	6.198	2.062	1.253
150_T_0.5/0.25	3.730	1.241	0.754	6.460	2.793	1.697	7.429	3.693	2.244
150_T_0.5/0.22	3.355	1.116	0.678	6.460	2.512	1.526	7.429	3.655	2.018
150_T_0.5/0.18	2.855	0.950	0.577	6.425	2.138	1.299	7.429	2.827	1.718
150_T_1/0.25	4.306	1.658	1.008	6.460	3.726	2.267	7.429	4.285	2.998
150_T_1/0.22	4.306	1.492	0.907	6.460	3.358	2.040	7.429	4.285	2.698
150_T_1/0.18	3.819	1.271	0.772	6.460	2.859	1.737	7.429	3.781	2.297
200_T_0/0.25	2.484	0.826	0.502	5.588	1.859	1.130	7.390	2.459	1.494
200_T_0/0.22	2.237	0.744	0.452	5.033	1.674	1.018	6.656	2.214	1.346
200_T_0/0.18	1.909	0.635	0.291	4.296	1.429	0.869	5.682	1.890	1.149
200_T_0.5/0.25	3.649	1.214	0.738	6.460	2.732	1.660	7.429	3.613	2.195
200_T_0.5/0.22	3.281	1.092	0.663	6.460	2.456	1.493	7.429	3.248	1.974
200_T_0.5/0.18	2.791	0.929	0.564	6.280	2.089	1.270	7.429	2.763	1.679
200_T_1/0.25	4.306	1.655	1.005	6.460	3.723	2.262	7.429	4.285	2.992
200_T_1/0.22	4.306	1.489	0.904	6.460	3.349	2.035	7.429	4.285	2.692
200_T_1/0.18	3.809	1.267	0.770	6.460	2.851	1.733	7.429	3.771	2.291
Legend:		IDR < 0.1%			no damage				
		0.1% < IDR < 0.3%			minor damage				
		0.3% < IDR < 0.5%			significant damage				

Table 6.8 continued from previous page

Wall ID	IDR _{RS} [%]								
	Ground type A			Ground type B			Ground type C		
	NC	SD	DL	NC	SD	DL	NC	SD	DL
		IDR >0.5%			structural collapse				

Table 6.9: Inter-story drift according to 2nd generation of Eurocode 8

Wall ID	IDR _{RS} [%]								
	Ground type A			Ground type B			Ground type C		
	NC	SD	DL	NC	SD	DL	NC	SD	DL
250_C_0/0.25	0.846	0.373	0.144	2.165	0.953	0.245	4.277	1.884	0.486
250_C_0/0.22	0.761	0.335	0.137	1.948	0.856	0.222	3.845	1.696	0.436
250_C_0/0.18	0.647	0.286	0.127	1.657	0.733	0.205	3.276	1.443	0.371
250_C_0.25/0.25	0.962	0.422	0.117	2.464	1.083	0.281	4.841	2.143	0.551
250_C_0.25/0.22	0.865	0.381	0.113	2.228	0.981	0.252	4.381	1.927	0.496
250_C_0.25/0.18	0.739	0.326	0.106	1.886	0.833	0.215	3.730	1.642	0.424
250_C_0.5/0.25	1.188	0.522	0.134	3.024	1.335	0.345	6.020	2.624	0.685
250_C_0.5/0.22	1.065	0.472	0.125	2.723	1.205	0.310	5.420	2.374	0.610
250_C_0.5/0.18	0.909	0.401	0.117	2.328	1.025	0.265	4.579	2.027	0.522
350_C_0/0.25	0.775	0.344	0.116	2.000	0.880	0.226	3.926	1.732	0.447
350_C_0/0.22	0.699	0.308	0.111	1.790	0.790	0.203	3.537	1.559	0.403
350_C_0/0.18	0.594	0.262	0.103	1.527	0.673	0.146	3.018	1.326	0.341
350_C_0.25/0.25	0.944	0.416	0.109	2.425	1.069	0.276	4.818	2.104	0.542
350_C_0.25/0.22	0.848	0.374	0.105	2.168	0.955	0.246	4.291	1.888	0.487
350_C_0.25/0.18	0.723	0.319	0.098	1.844	0.817	0.210	3.638	1.604	0.414
350_C_0.5/0.25	1.182	0.520	0.133	3.003	1.330	0.343	5.944	2.604	0.680
350_C_0.5/0.22	1.058	0.465	0.120	2.710	1.192	0.308	5.391	2.369	0.605
350_C_0.5/0.18	0.904	0.398	0.110	2.316	1.020	0.262	4.565	2.012	0.518
450_C_0/0.25	0.737	0.325	0.100	1.882	0.831	0.214	3.723	1.635	0.423
450_C_0/0.22	0.661	0.292	0.096	1.695	0.747	0.192	3.343	1.468	0.380
450_C_0/0.18	0.564	0.248	0.090	1.443	0.636	0.110	2.851	1.253	0.124

Table 6.9 continued from previous page

Wall ID	IDR _{RS} [%]								
	Ground type A			Ground type B			Ground type C		
	NC	SD	DL	NC	SD	DL	NC	SD	DL
450_C_0.25/0.25	0.936	0.412	0.105	2.391	1.057	0.272	4.740	2.086	0.536
450_C_0.25/0.22	0.836	0.370	0.100	2.144	0.943	0.243	4.243	1.863	0.480
450_C_0.25/0.18	0.713	0.314	0.094	1.827	0.802	0.207	3.598	1.586	0.409
450_C_0.5/0.25	1.170	0.519	0.132	2.989	1.327	0.341	5.934	2.603	0.677
450_C_0.5/0.22	1.053	0.462	0.119	2.707	1.187	0.307	5.315	2.355	0.603
450_C_0.5/0.18	0.898	0.395	0.106	2.284	1.005	0.258	4.532	1.981	0.515
100_T_0/0.25	1.471	0.652	0.314	3.798	1.658	0.502	6.646	3.277	0.848
100_T_0/0.22	1.323	0.587	0.296	3.411	1.510	0.475	6.643	2.970	0.762
100_T_0/0.18	1.132	0.543	0.274	2.897	1.279	0.442	5.738	2.536	0.653
100_T_0.5/0.25	1.371	0.599	0.229	3.496	1.537	0.397	6.646	3.055	0.783
100_T_0.5/0.22	1.235	0.543	0.218	3.162	1.396	0.356	6.265	2.760	0.709
100_T_0.5/0.18	1.048	0.460	0.201	2.695	1.181	0.324	5.292	2.334	0.601
100_T_1/0.25	1.759	0.771	0.255	4.513	1.972	0.514	6.646	3.887	1.007
100_T_1/0.22	1.585	0.700	0.243	4.087	1.800	0.464	6.646	3.525	0.902
100_T_1/0.18	1.347	0.593	0.224	3.434	1.535	0.391	6.646	2.994	0.777
150_T_0/0.25	0.979	0.432	0.218	2.504	1.106	0.350	4.935	2.183	0.561
150_T_0/0.22	0.881	0.409	0.207	2.264	0.997	0.333	4.462	1.963	0.509
150_T_0/0.18	0.757	0.378	0.192	1.931	0.851	0.308	3.828	1.688	0.432
150_T_0.5/0.25	1.352	0.594	0.183	3.479	1.536	0.392	6.646	2.998	0.779
150_T_0.5/0.22	1.216	0.536	0.176	3.134	1.370	0.353	6.129	2.693	0.702
150_T_0.5/0.18	1.035	0.454	0.162	2.648	1.169	0.299	5.244	2.313	0.596
150_T_1/0.25	1.802	0.790	0.212	4.679	2.043	0.526	6.646	3.883	1.049
150_T_1/0.22	1.614	0.712	0.200	4.175	1.828	0.471	6.646	3.614	0.932
150_T_1/0.18	1.394	0.613	0.187	3.557	1.554	0.402	6.646	3.075	0.798
200_T_0/0.25	0.904	0.398	0.171	2.315	1.018	0.275	4.565	2.008	0.518
200_T_0/0.22	0.809	0.357	0.163	2.081	0.916	0.261	4.103	1.800	0.465
200_T_0/0.18	0.694	0.305	0.151	1.772	0.784	0.242	3.505	1.545	0.399
200_T_0.5/0.25	1.317	0.584	0.159	3.400	1.498	0.382	6.639	2.958	0.759
200_T_0.5/0.22	1.190	0.523	0.152	3.033	1.343	0.346	6.027	2.633	0.688

Table 6.9 continued from previous page

Wall ID	IDR _{RS} [%]								
	Ground type A			Ground type B			Ground type C		
	NC	SD	DL	NC	SD	DL	NC	SD	DL
200_T_0.5/0.18	1.011	0.445	0.141	2.596	1.145	0.293	5.147	2.255	0.578
200_T_1/0.25	1.801	0.789	0.201	4.634	2.041	0.524	6.646	3.883	1.027
200_T_1/0.22	1.612	0.711	0.182	4.175	1.825	0.470	6.646	3.613	0.929
200_T_1/0.18	1.389	0.611	0.166	3.553	1.550	0.401	6.646	3.071	0.795
Legend:									
		IDR < 0.1%	no damage						
		0.1% < IDR < 0.3%	minor damage						
		0.3% < IDR < 0.5%	significant damage						
		IDR > 0.5%	structural collapse						

Colours in Table 6.8 and Table 6.9 represent different levels of damage, based on limit states of unreinforced masonry (Calvi, 1999), as it is described in the legend under the table. One table contains information regarding all C-type and T-type wall systems, while information regarding the Eurocode 8 generation is divided between the two tables. Thanks to the colour coding of the table information, one can, just by a glance at the tables, observe how less rigorous the 2nd generation of Eurocode 8 appears to be in the context of the rammed earth walls examined by this study. Namely, when 1st generation of Eurocode 8 was used to define the elastic response spectrum, structural collapse was not the case in just a few instances, primarily for ground type A and the shortest return period (limit state Damage Limitation, return period of 225 years).

However, when parametric analysis results overlapped with the elastic response spectrum determined according to the 2nd generation of Eurocode 8, the seismic response changed. As expected, rammed earth walls exhibited the lowest damage rates if ground type A was considered, especially if the shortest return period was considered when mostly minor damage occurred. In the other two ground types, favourable outcomes could be expected only for the shortest return period of 60 years. Moreover, the limit state corresponding to the return period of 475 years (Structural Damage) in ground type A exhibited mostly significant damage, while

it corresponded with the structural collapse in the other two ground types. Also, structural collapse dominated when the longest return period was considered for all ground types.

The difference between the two wall systems could also be observed. Namely, C-wall systems performed marginally better than T-wall systems. That could indicate that parts of construction where T-wall systems occur (a portion of the wall from the door to the connecting wall) are susceptible to higher levels of damage during the seismic event.

As previously stated, the increase in vertical stress intensity reduced seismic capacity, as did the increase in the length of flange walls. Despite that, no such regularity could be observed when the limit states are considered in Table 6.8 and Table 6.9. The reason for that is that the differences between the systems induced by those parameters are not significant enough to influence the changes in limit states.

6.5 Conclusion

Numerical analysis of rammed earth walls representing walls from eastern Croatia was performed using ANSYS Workbench software. In order to build a reliable numerical model, material properties and analysis settings were validated according to the experimental results. In that process, finite element size was also chosen to be $1/5$ of the rammed earth wall layer. Material properties were either determined experimentally or chosen based on literature review. Drucker-Prager's constitutive model was responsible for the non-linear behaviour of the numerical model, while the Cohesive Zone Model induced additional debonding of the layers.

Following the validation, parametric analysis was performed on two wall systems, C-wall and T-wall. Namely, the C-wall consisted of two flange walls at the end and represented the shorter outer wall of the rammed earth house. On the other hand, only one flanged wall is added to the end of the T-wall, which can be considered a portion of the inside wall from the door to the longer outer wall of the house. It should be noted that both wall systems are considered part of a traditional rammed earth house from eastern Croatia, with a three-room layout. By performing

parametric analysis, several parameters were tested:

- Influence of wall length on seismic behaviour of the rammed earth wall
- Necessity of including flange walls while considering rammed earth walls
- Influence of flange wall length on seismic behaviour of rammed earth wall
- Influence of vertical stress intensity on seismic behaviour of rammed earth walls

All parameters were tested on both wall systems. Overall, 18 different geometric dispositions of walls were constructed, and three vertical stress intensities were applied to each numerical model. Vertical stress was determined according to the dimensions of rammed earth houses encountered during the field observation by considering maximum, minimum and average values. In total, 54 numerical models were calculated and analysed in this study.

It was observed that when wall length was increased and flange walls were added, load-bearing capacity also increased. When no flange walls were added, the maximum displacement walls endured increased; however, bearing capacity decreased significantly (26% to 40% in C-walls and 35% to 66% in T-walls, depending on the length). Thus, the flange walls proved necessary when considering the seismic behaviour of rammed earth walls. However, it was determined that shorter flange walls are sufficient between the two considered lengths since the difference is negligible, while the numerical model size and computational time are much higher. Vertical stress, however, did not prove to be highly influential in the bearing capacity of the rammed earth walls. One can attribute that to the low intensity; however, in the case of eastern Croatia rammed earth houses and rammed earth houses in general, that level of vertical stress is expected.

Several parameters have been determined from pushover analysis and bilinear idealisation of the curve. Namely, structural behaviour factors, elastic stiffness, ductility, and inter-story drift were analysed for all 54 numerical models. As previously mentioned, changes in vertical stress had a negligible influence on all parameters determined by the structural capacity and bilinear curve.

Firstly, the structural behaviour factor from 1.99 to 2.43 was determined. In C-walls, systems without flange walls had slightly lower values than those with

flanges. However, in T-walls, no such observation could be made. Flange walls greatly influence the elastic stiffness of C-walls. Specifically, a 35% increase in elastic stiffness was observed for the shortest walls (250 cm), while the difference rose to more than 50% for the other two wall lengths. In T-walls, the influence was minor (18% to 35%) but still not negligible. It should also be mentioned that the length of the flange walls did not significantly influence the reported results. Ductility was influenced by wall length, ranging from ca. 3 to even 6 when C-wall length increased from 250 cm to 450 cm. T-walls exhibited much smaller ductility values than C-walls, but the length also had much impact.

In this part of the analysis, inter-story drift was determined according to the ultimate displacement and denoted as IDR_{du} . The ultimate displacement was the maximum displacement each numerical model had endured. As previously mentioned, walls without flanges endured more significant displacement, *i.e.* a complete displacement of 15 mm that was applied to the top of the numerical model, surpassing the fourth limit state ($IDR > 0.5\%$) that indicates the collapse. Most flanged walls, both C-walls and T-walls, achieved the IDR_{du} between 0.3% and 0.5%, connected to significant structural damage. Those numerical models had material failure before enduring the complete 15 mm of horizontal displacement.

Further seismic analysis was possible when structural capacity curves were transferred to spectral acceleration and displacement. Thus, seismic capacity curves were constructed, and bilinear idealisation was performed for superposition with the elastic response spectrum to determine target displacement. Furthermore, two approaches were used to create the response spectrum: the 1st and 2nd generation of Eurocode 8 that was developed but is still not in force. Three ground types were considered: A (ideal case) and those expected in eastern Croatia (B and C). Also, the elastic response spectrum was calculated for three return periods that are connected with three limit states: Damage Limitation (DL), Significant Damage (SD) and Near Collapse (NC).

Contrary to structural capacity curves determined directly from pushover results, vertical stress greatly impacted the spectral acceleration since, in this context, it was considered a mass from the additional load. Furthermore, seismic capacity curves were first observed without the response spectrum to determine whether they

could withstand the horizontal acceleration of $0.2g$ (design value characteristic for eastern Croatia). It was observed that in C-walls, without flanges, all walls surpass $0.2g$, while for walls with flanges, that depends on the vertical stress intensity, no matter the flange length, which marginally influences the response. However, most T-walls failed to reach the limit of $0.2g$, even though the wall with flanges again performed worse.

Target displacement gathered from the superposition of the curves with the response spectrum was used to determine the inter-story drift of the walls connected to the location and return period (IDR_{RS}). Significant differences between the 1st and 2nd generation of the Eurocode 8 induced discrepancies in the IDR_{RS} results. Namely, if 1st generation of Eurocode 8 was considered, almost none of the analysed rammed earth walls would achieve adequate seismic response since the majority's IDR_{RS} is highly above 0.5%. A few exceptions are C-walls assumed to be built of ground type A and if the shortest return period is considered (225 years).

When 2nd generation of Eurocode 8 was considered, a marginally different picture appeared. Namely, if the longest return period was considered, the structural collapse was determined for all wall systems, the same as for 1st generation of the standard. However, for other return periods, even none and minor damage can be observed, especially for the shortest return period (60 years), corresponding to the Damage Limitation limit state. Also, as expected, when ground type C was considered, almost all wall systems faced structural collapse.

If all numerical results are summed, one can draw a few conclusions. Namely, since walls with flanges proved to be a more critical case regarding seismic behaviour, rammed earth walls should not be considered as free-standing to avoid overestimating their load-bearing capacity. Furthermore, T-walls, reaching from the door frame to the perpendicular wall, should also be considered with flanges. Also, since T-walls appear more critical than C-walls, one should pay extra attention to those places when a complete rammed earth house is considered, especially if the distance between the door and the perpendicular wall is 100 cm or less. The flange wall length for C-walls can be limited to 25% of the wall length, and for T-walls, 50% of the wall length. Since no significant difference in seismic capacity was observed with the increase in length. The vertical stress interval used in this parametric analysis

did not cause significant differences. Thus, all levels would be appropriate, and no reduction is necessary.

Finally, even though the majority of wall systems comprehended by this study can withstand ground accelerations of $0.2g$, superposition with response spectra curves proved that the seismic capacity of rammed earth walls from eastern Croatia should be carefully considered. Namely, according to the current generation of the Eurocode 8, such walls would in almost all cases considered (different return periods and ground types) achieve structural collapse. However, if the 2nd generation of the standard is considered, rammed earth walls can be considered adequate, but that conclusion is mostly limited to the shortest return period of 60 years.

It should be noted that parametric analysis in this study was performed based on experimental results of traditionally built rammed earth walls, characteristic of eastern Croatia. The traditional construction method could influence the strength properties, and material composition could also impact to a degree. Therefore, further analysis should be performed to apply these conclusions to a broader number of cases.

Chapter 7

Concluding remarks

In the past decades, earthen construction (mostly rammed earth and adobe) has passed through a revival on a worldwide scale, and the majority of research has been conducted since the beginning of the 21st century. Moreover, numerous standards and normative documents were written to help engineers and enthusiasts build durable and sustainable earthen structures. However, thanks to the ancient origin of the earthen building technique, the majority of such buildings throughout the world are, in fact, traditionally and empirically built, dating hundreds of years ago. Therefore, to preserve the ancient building fund that is undoubtedly a part of a cultural heritage, one must understand the behaviour of those structures before attempting to create a new, modern earthen construction.

In Croatia, earthen structures are located primarily in eastern parts, *i.e.* Slavonia and Baranja. They are characterised by a traditional building practice and purely empirical techniques spread by word of mouth. Their current state, material composition, characteristic dimensions, and load-bearing capacities are little known. Moreover, even though the horizontal acceleration expected in eastern Croatia is lower than in other parts of the country, earthen structures' seismic capacity has proven problematic. Thus, rammed earth structures from eastern Croatia must also be observed in a seismic context.

Field observation throughout eastern Croatia was conducted, and more than 90 rammed earth houses were noted, with a portion of them thoroughly documented. Houses were photographed and measured with the owner's permission, and material samples for further laboratory testing were collected. This study presents a small

database comprising five rammed earth houses, and the floor plans, characteristic dimensions, layout, and material properties, which are dependent on the amount of collected material, are discussed.

Due to the primitive waterproofing under the rammed earth walls, capillary moisture extended to a height of ca. 1 m in the wall, even though most samples had a moisture content of 2.5 to 3%. Moreover, the granular composition of the material in eastern Croatia rammed earth houses deviated from a portion of large particles (sand and gravel) from the literature recommendation. However, the proportion of fine particles agreed with the recommendations. Plasticity was determined on samples from three houses: two samples were classified as low-plasticity, while the third was classified as medium-plasticity. All samples corresponded to literature recommendations for appropriate rammed earth material. Compressive strength was determined on samples from two houses, which mainly concentrated around 1.5 MPa, even though extremes in both directions were observed as well. Finally, soil water retention behaviour was determined on material collected from one house, whose behaviour agreed with the literature observation.

Further analysis was performed based on observations made on existing rammed earth houses in eastern Croatia. Namely, four rammed earth walls were built using traditional building principles, with material composition resembling collected samples. Dimensions were also determined according to existing houses and scaled due to laboratory limitations to $125 \times 125 \times 25$ cm. Walls were loaded with constant vertical load, and cyclic horizontal displacement was imposed at the top of the wall. The excitation regime was observed not to influence the seismic response significantly. On the contrary, based on experimental results, soil mixture and its uniformity, as well as the duration of the drying period, profoundly affect load-bearing capacity.

One experimentally tested wall, made of lower-performing material, was further used to validate numerical models (E:125) made in ANSYS Workbench software. Material model properties were either experimentally tested or, when the former was impossible, assumed based on the literature review. Following the sensitivity analysis, finite element size was determined in relation to layer height, precisely $1/5$ of the layer. Following the validation, parametric analysis was performed on 54 numerical

models of different geometry and vertical loads. Namely, each of the 18 different geometry systems assumed to be a part of a traditional eastern Croatian rammed earth house was tested with three different vertical stress intensities. Numerical results from pushover analysis were observed in structural and seismic contexts.

It was observed that vertical stress intensities of 0.18 to 0.25 MPa did not significantly affect load-bearing capacity, while the wall system did. If each rammed earth wall is considered a separate unit (*i.e.* without flange walls), lower load-carrying capacity can be achieved, but a larger amount of displacement can be endured, causing a larger IDR. However, a more critical case appears when the wall is considered part of a construction, with flange walls connected to it. Even though higher load-bearing capacity was achieved, lower displacement was endured, thus making the third limit state (structural damage) their final limit state. However, the increased length of the flange walls did not significantly impact the results. Thus, it can be assumed that shorter flange walls are adequate (25% and 50% of the wall length for C-wall and T-wall, respectively). Structural behaviour factor in the range of 1.99 to 2.43 was determined. However, no significant influence of wall length and the presence of flanges on the value was determined.

When seismic acceleration and displacement were overlapped with the elastic response spectrum determined by following two approaches (1st and 2nd generation of Eurocode 8). In this case, increased vertical stress caused the lower seismic acceleration of the wall and flange walls, which again proved critical, reducing the seismic acceleration. Thus, not all observed wall systems could reach the 0.2g of spectral acceleration. However, it should be further examined whether the same conclusion can be applied if a complete house is considered.

Furthermore, by overlapping the bilinear idealised seismic capacity curves with the elastic response spectrum, high discrepancies were observed between the two generations of a standard. A new generation of Eurocode 8 is said to bring significant changes regarding, among others, procedures for determining response spectrum curves. In the context of rammed earth walls observed by this study, this caused significantly different conclusions between the two spectra.

Precisely, according to 1st generation of Eurocode 8, the majority of rammed earth walls in this study did not perform adequately to be built even on ground

type A. Based on the determined target displacement, almost all cases considered had the IDR characterised by collapse. A few exceptions were reserved for C-walls built on the ground type A, with the shortest return period.

The 2nd generation of Eurocode 8 brought marginally different conclusions. For the shortest return period, C-walls achieved minor in both ground types A and B, while in-ground type C, instances of significant damage also appeared. T-walls performed slightly poorer, and majority of wall systems achieved significant damage. For the longer return periods, majority of wall systems showed structural collapse, especially in ground types B and C. Moreover, even though vertical stress intensity had some influence on the behaviour, the utilised interval did not make significant changes to the seismic performance.

Thus, according to the 2nd generation of Eurocode 8, which should be enforced in this and the following years, traditional rammed earth walls modelled after existing rammed earth houses in eastern Croatia should have adequate seismic performance for limit state Damage Limitation (return period 60 years), while for the longest return period (Near Collapse, return period 1600 years) structural collapse can be expected. Also, if ground type C is considered, the majority of wall systems would not perform adequately, while ground type B gives a bit more optimistic conclusion. Moreover, it should be noted that this study is limited to rammed earth walls. Further analysis of the rammed earth houses modelled after existing eastern Croatian rammed earth houses should be performed.

7.1 Scientific contribution

This study was made in the scope of the first research project that deals with the seismic behaviour of rammed earth houses from eastern Croatia (RE-forMS). It comprises the complete research path from observing the existing rammed earth houses in the area followed by laboratory testing and, finally, building numerical models of walls based on the actual constructions for seismic performance analysis. Aims named in the Introduction were focused on building the database of existing rammed earth houses and determining the seismic behaviour of rammed earth structures:

1. To create a database on locations, geometry, load, boundary conditions, and

material composition for physical and numerical models of traditional eastern Croatian rammed earth houses.

2. To evaluate the behaviour of the walls in existing rammed earth houses in eastern Croatia based on the results of destructive testing of physical models loaded with simulated gravity and earthquake loads.
3. To determine the seismic behaviour of rammed earth walls by performing parametric analysis on validated nonlinear numerical models.

The database includes a detailed overview of five rammed earth houses from eastern Croatia, which discusses layout, dimensions, and floor plan. Moreover, depending on the number of collected samples from each house, extensive laboratory testing was performed, and the findings were compared to the literature review and recommendations.

Seismic behaviour was evaluated through experimental and numerical analysis. It was observed that vertical stress intensity has an insignificant influence on load-bearing capacity. Also, rammed earth walls should not be considered as flat walls and separate units that form a whole construction. Instead, at least flange perpendicular walls should be added since the reduction of seismic capacity was observed. Moreover, if the fact that existing rammed earth houses in eastern Croatia were mostly built more than a hundred years ago is considered, it can be assumed they endured at least minor seismic activities. With that in mind, presumably, the 2nd generation of Eurocode 8 gives a better estimate of the rammed earth walls, characterising their seismic performance as adequate for short-term return periods (60 years). However, it was observed that according to the currently enforced version of Eurocode 8, traditionally built rammed earth walls in eastern Croatia would not survive any level of seismic activity without collapsing and similar conclusions were drawn for longer return periods according to 2nd generation of Eurocode 8 as well.

Furthermore, in the Introduction, two hypotheses were set as well:

- **H1:** Rammed earth walls, the likes of which can be found in the eastern Croatian area, can withstand horizontal ground shaking with a minimum ground

acceleration of $0.2g$, which is the design acceleration for the eastern Croatian area.

The first hypothesis **H1** was tested on parametric analysis results, concerning full-scale rammed earth walls. It was observed that longer walls had greater success in achieving the $0.2g$ mark; however, the spectral acceleration reduced with increased vertical stress intensity and flanges added. Thus, for a critical case, which should be applied in the analysis, of a wall considered as a part of a house, it cannot be safe to say that it will achieve the set limit. What is more a portion of the wall extending from the end of a door to a connected perpendicular wall (T-wall system in this study, see Figure 6.1 in page 136) in almost all cases considered failed to reach the $0.2g$. Therefore, when a rammed earth house is analysed as a whole, those portions should be carefully observed, and the wall length from the door to the other wall should not be less than 100 cm.

- **H2:** The structural behaviour factor for rammed earth walls can be greater than 1.5, corresponding to the smallest allowed structural behaviour factor according to the current European standards for designing seismic resistance in masonry and concrete structures.

The second hypothesis **H2** was tested on numerical and experimental results. Namely, in both cases, the structural behaviour factor greater than 2.0 was determined, thus proving that a value greater than 1.5 can be utilised. Values determined in this study correspond to the literature review but were now determined on broader wall types and lengths.

7.2 Recommendations for future work

Since this is the first doctoral dissertation dealing with rammed earth structures from eastern Croatia and a product of the first research project dealing with the same topic, a lot of research ought to be performed in future to get a complete picture of their behaviour, seismic and otherwise. A lot of research has been performed worldwide; however, traditional Croatian rammed earth houses differ from the standards in terms of material composition and floor plan. Also, when reviewing the literature, some gaps were observed.

Firstly, since this study was mainly focused on the seismic performance of traditional rammed earth walls from eastern Croatia, the material characteristics only of used mixtures were evaluated. However, the influence of material composition and sample shape and size was only marginally observed. Further analysis of the influence on mechanical and physical properties could be performed, even though some conclusions can be drawn based on available literature.

Moreover, this study was limited to rammed earth walls. Precisely, walls with and without flange walls. However, openings in walls have proven to impact masonry walls severely, and one can assume it is the same in rammed earth walls. To this day, only one study has been performed on the influence of wall openings on performance. Their presence, position and size should be further examined.

Since rammed earth walls are rarely found as free-standing, especially if they are load-bearing, a complete rammed earth structure should be analysed. This study proved that one should not divide the house into a separate free-standing wall but include at least perpendicular (flange) walls. However, all conclusions in this study were based on walls (with and without flange walls), and it should be checked whether the same conclusions apply to a complete construction or at least a room that forms a house.

The current state of many rammed earth houses in the area is devastating. However, it was observed that owners do not know how to rehabilitate them. Research regarding the procedures for repairing and strengthening such structures should be performed to aid that. Thus, more of the existing houses, which are certainly a part of Croatian cultural heritage, could be preserved and put to further use.

Finally, to enable engineering practices and sustainable building enthusiasts to build rammed earth houses, some sort of normative document must be created with standardised procedures and minimum requirements for the material. Also, rammed earth is just one of the plethora of earthen building techniques, and similar research should be performed if other techniques (*i.e.* adobe, cob, *etc.*) wish to be applied.

Chapter 8

Appendices

Appendix A: Parametric analysis results

In the following figures (Figure 8.1 through Figure 8.35), structural capacity curves determined on 54 numerical models are presented. Curves are colour-coded, depending on the vertical stress intensity, while line style corresponds to the different wall systems. The curve is plotted separately for each numerical model since there is little to no difference between different vertical stresses on the same numerical model. Structural capacity curves of one wall system are followed by bilinear curves determined for each numerical system.

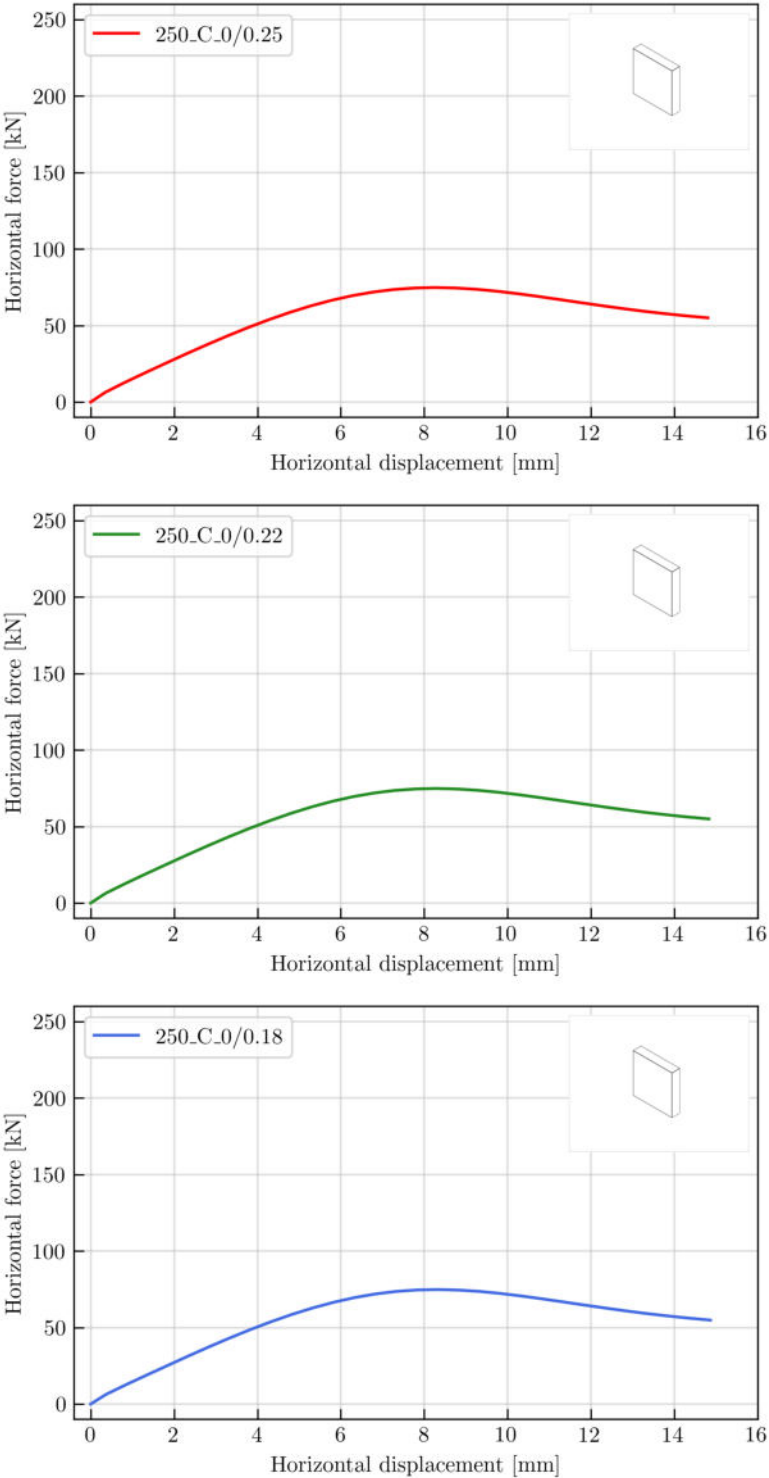


Figure 8.1: Numerical analysis results: 250_C_0

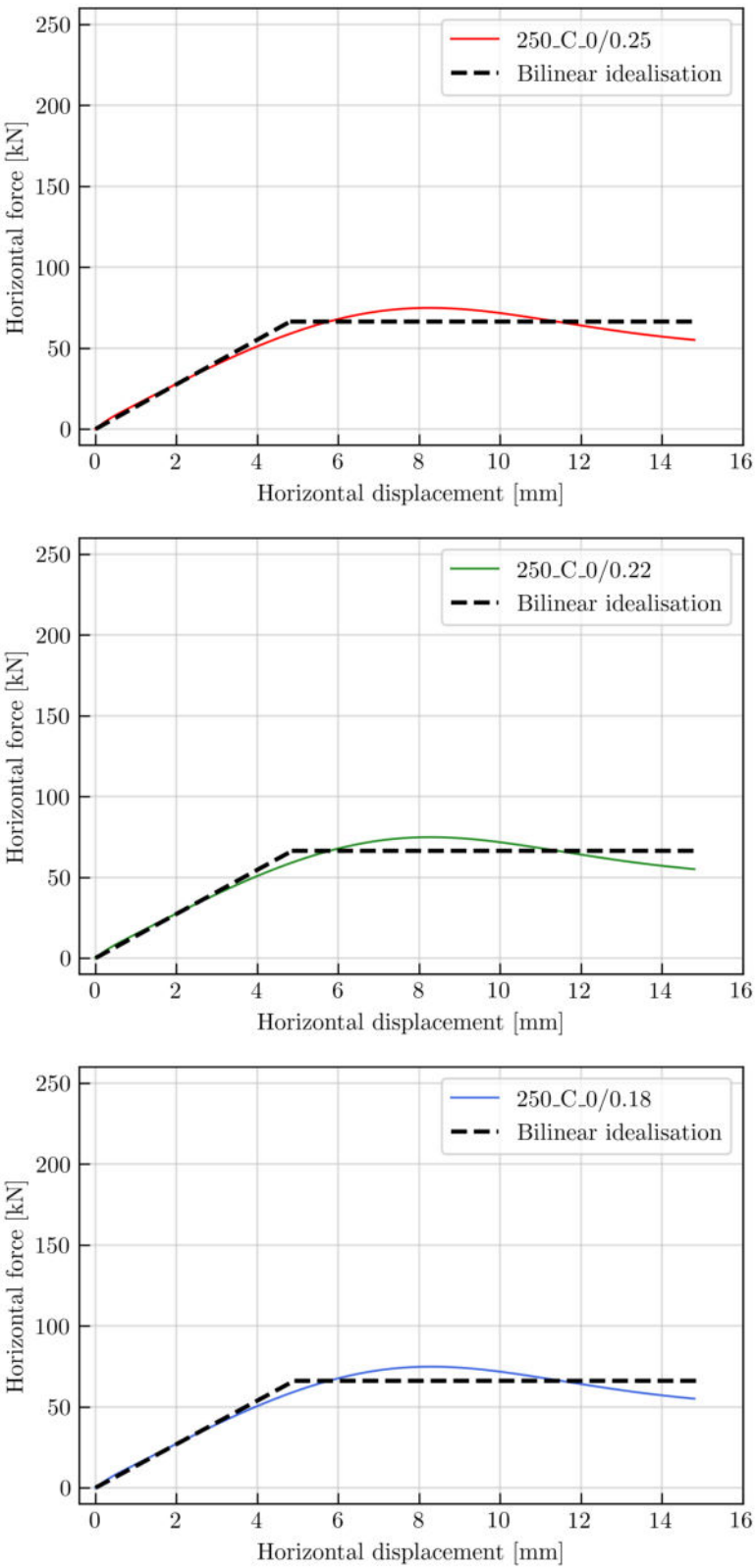


Figure 8.2: Bilinear idealisation: 250_C_0

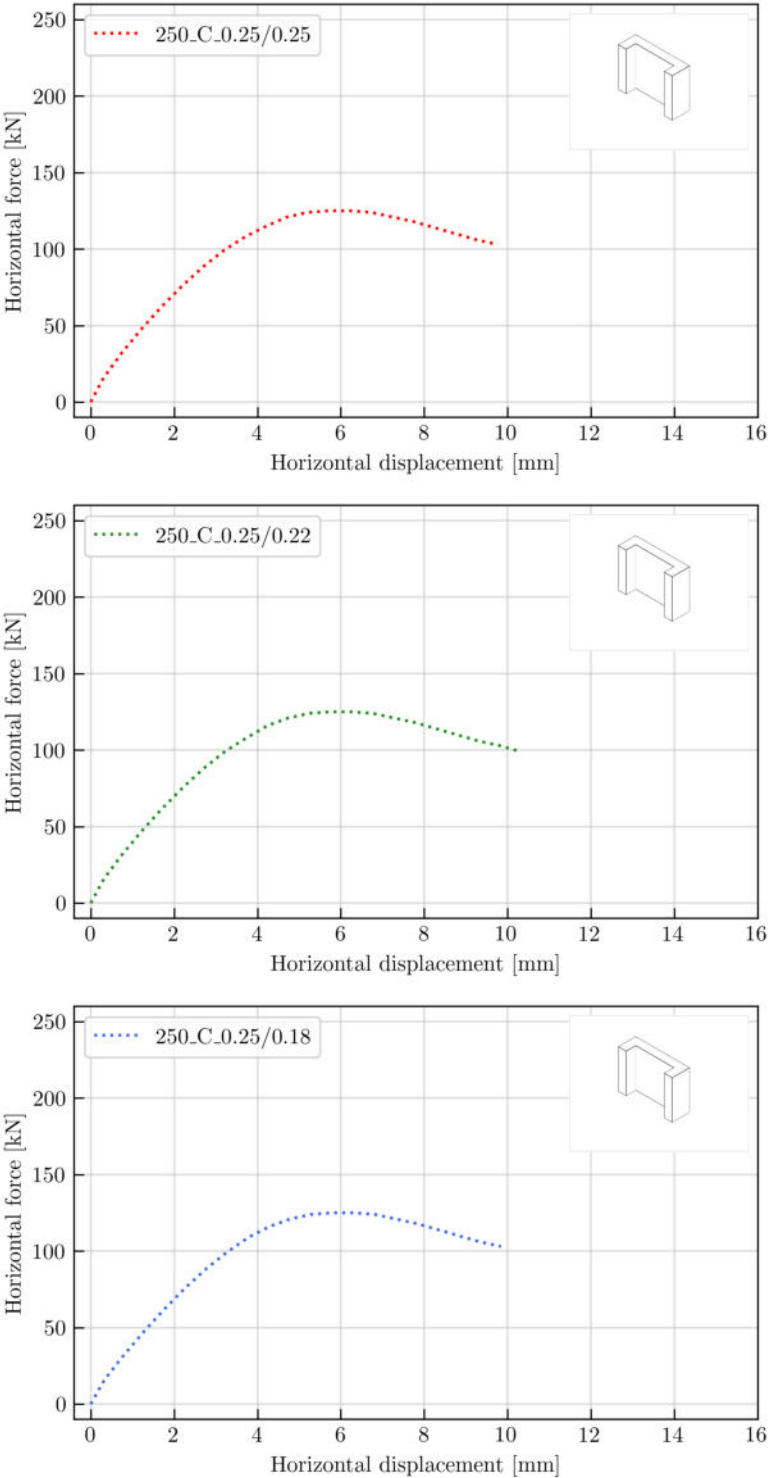


Figure 8.3: Numerical analysis results: 250_C_0.5

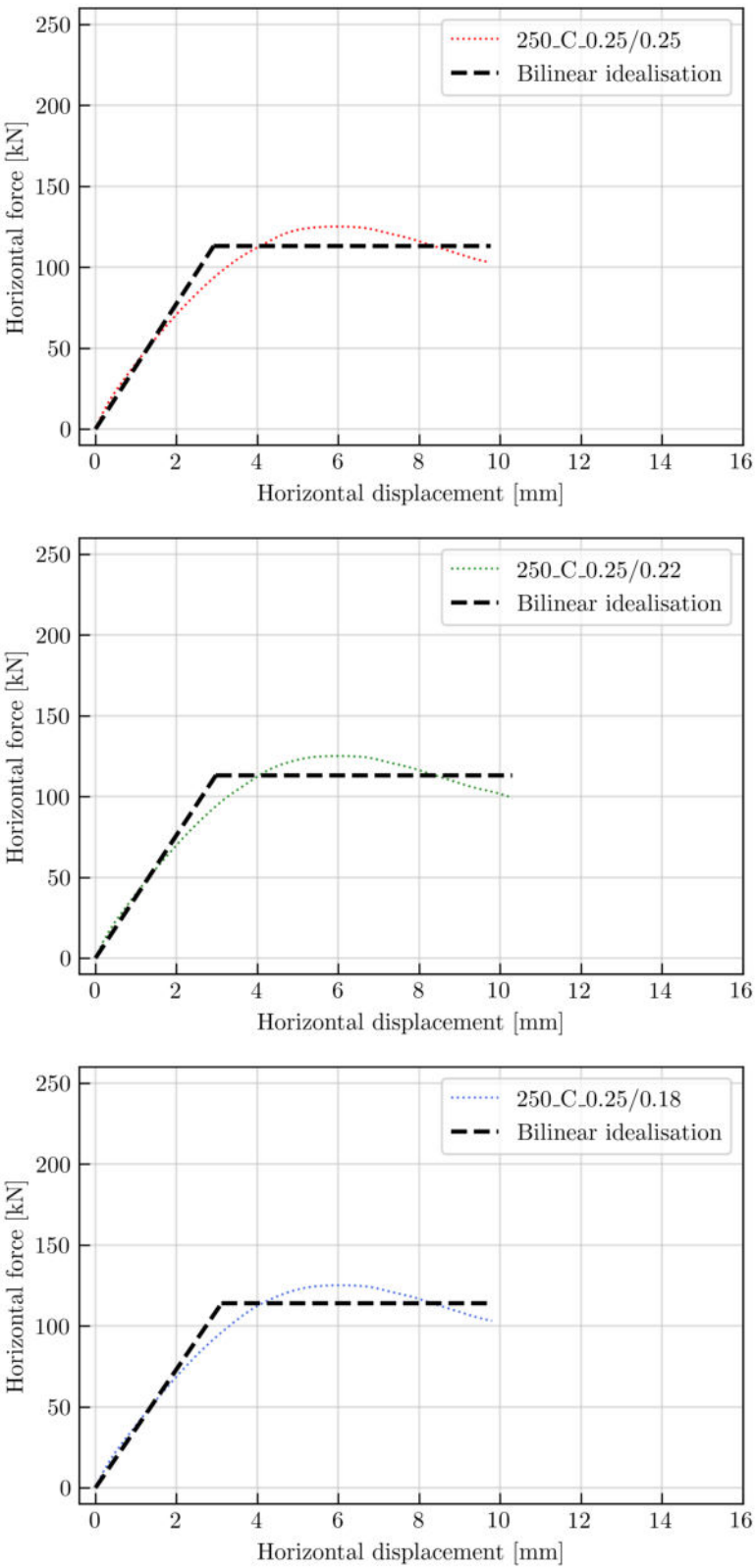


Figure 8.4: Bilinear idealisation: 250_C_0.5

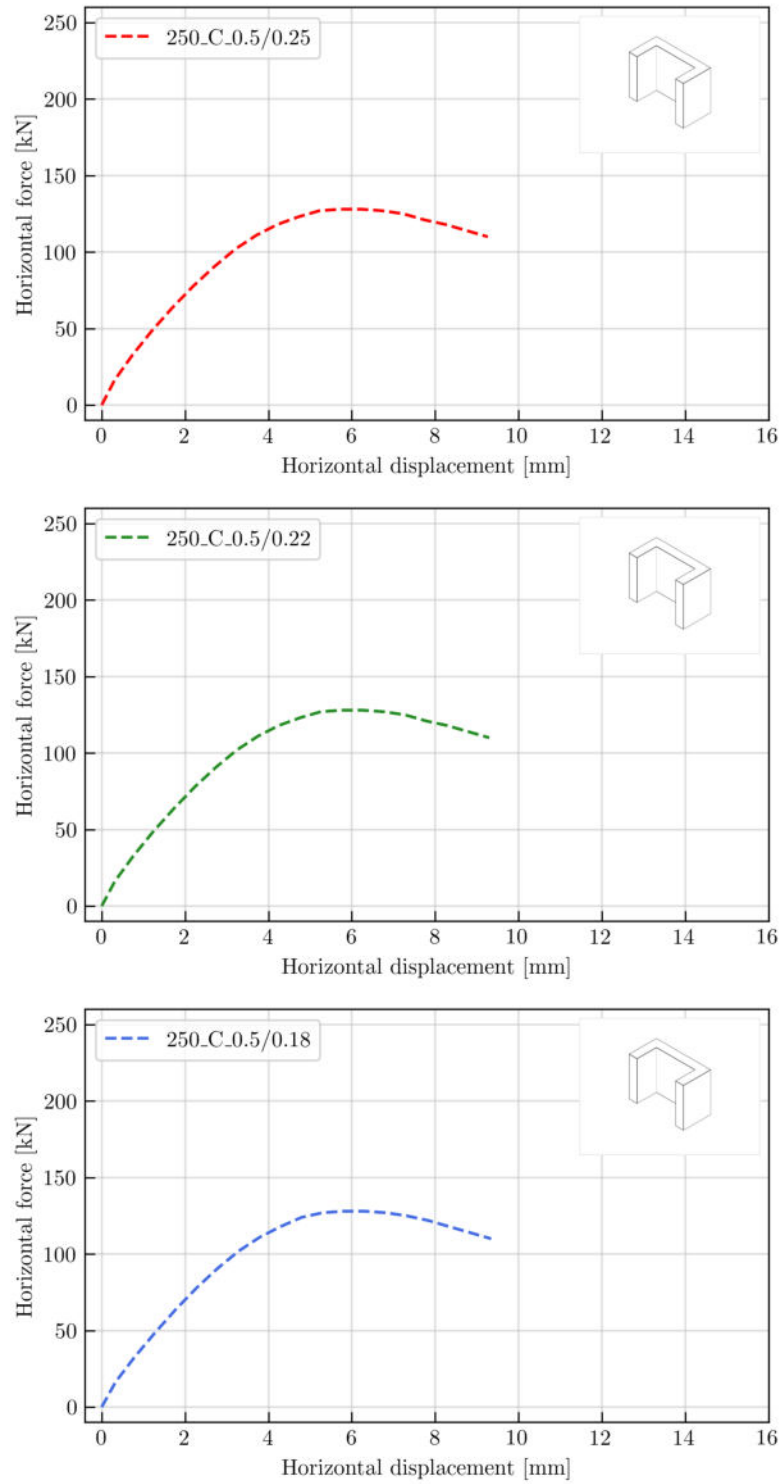


Figure 8.5: Numerical analysis results: 250_C_0.25

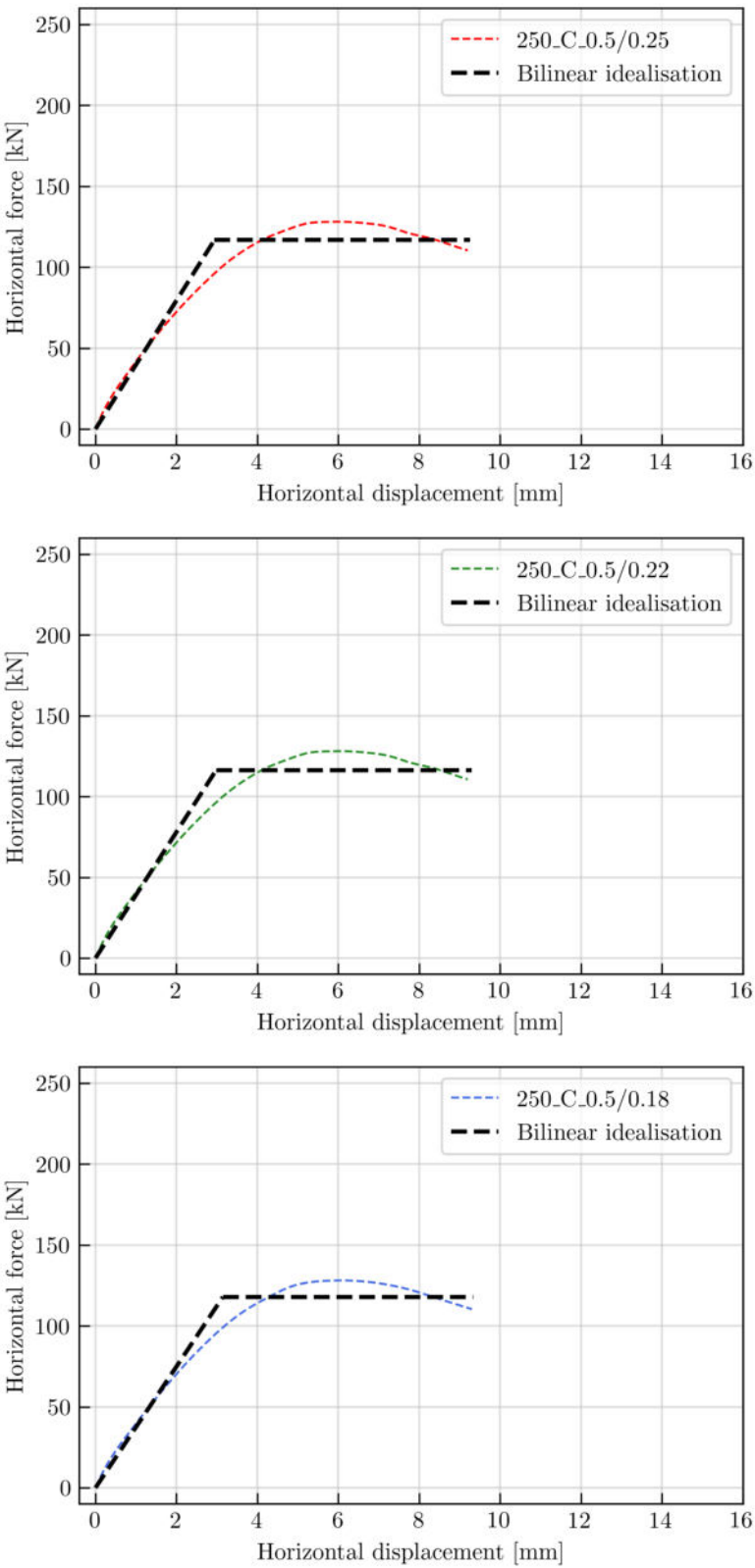


Figure 8.6: Bilinear idealisation: 250_C_0.25

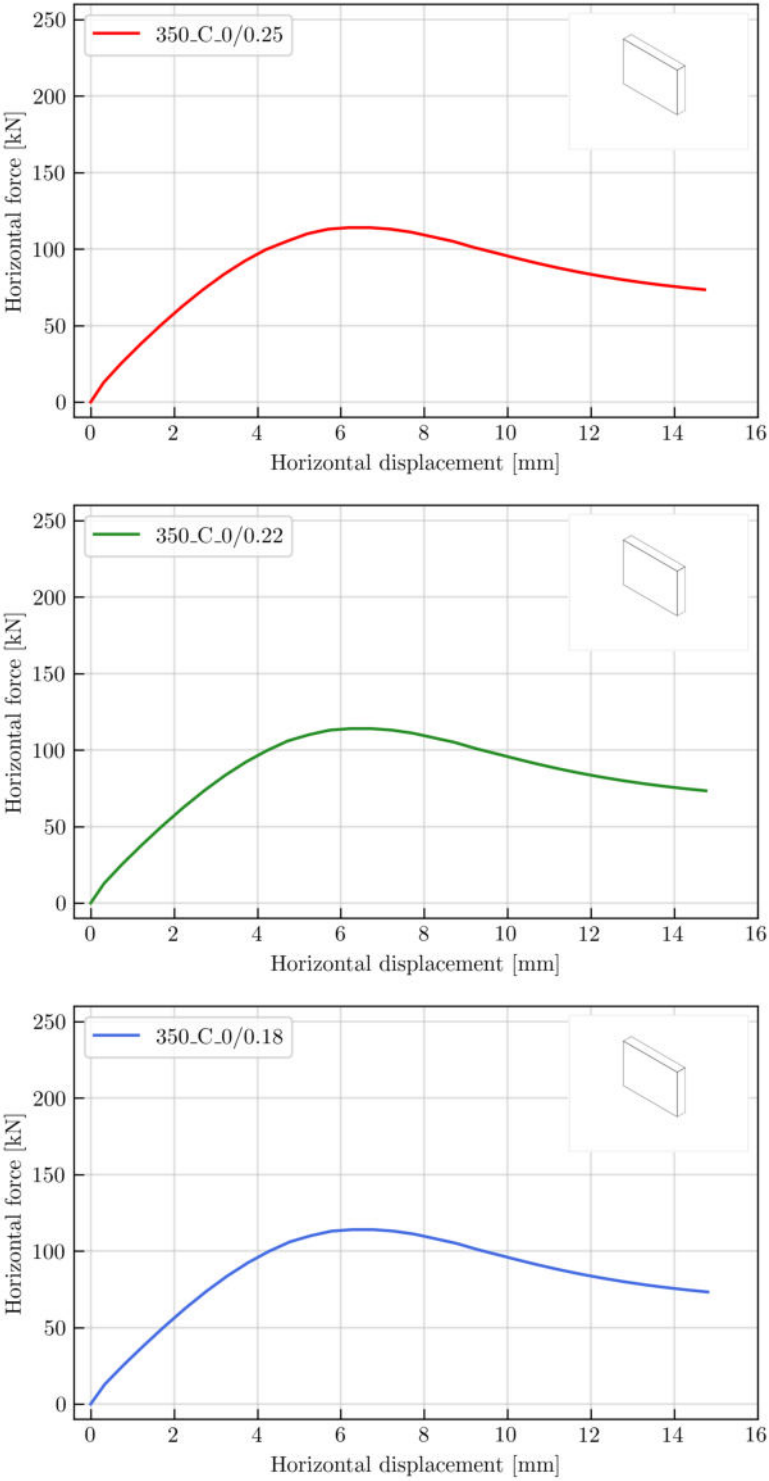


Figure 8.7: Numerical analysis results: 350_C_0

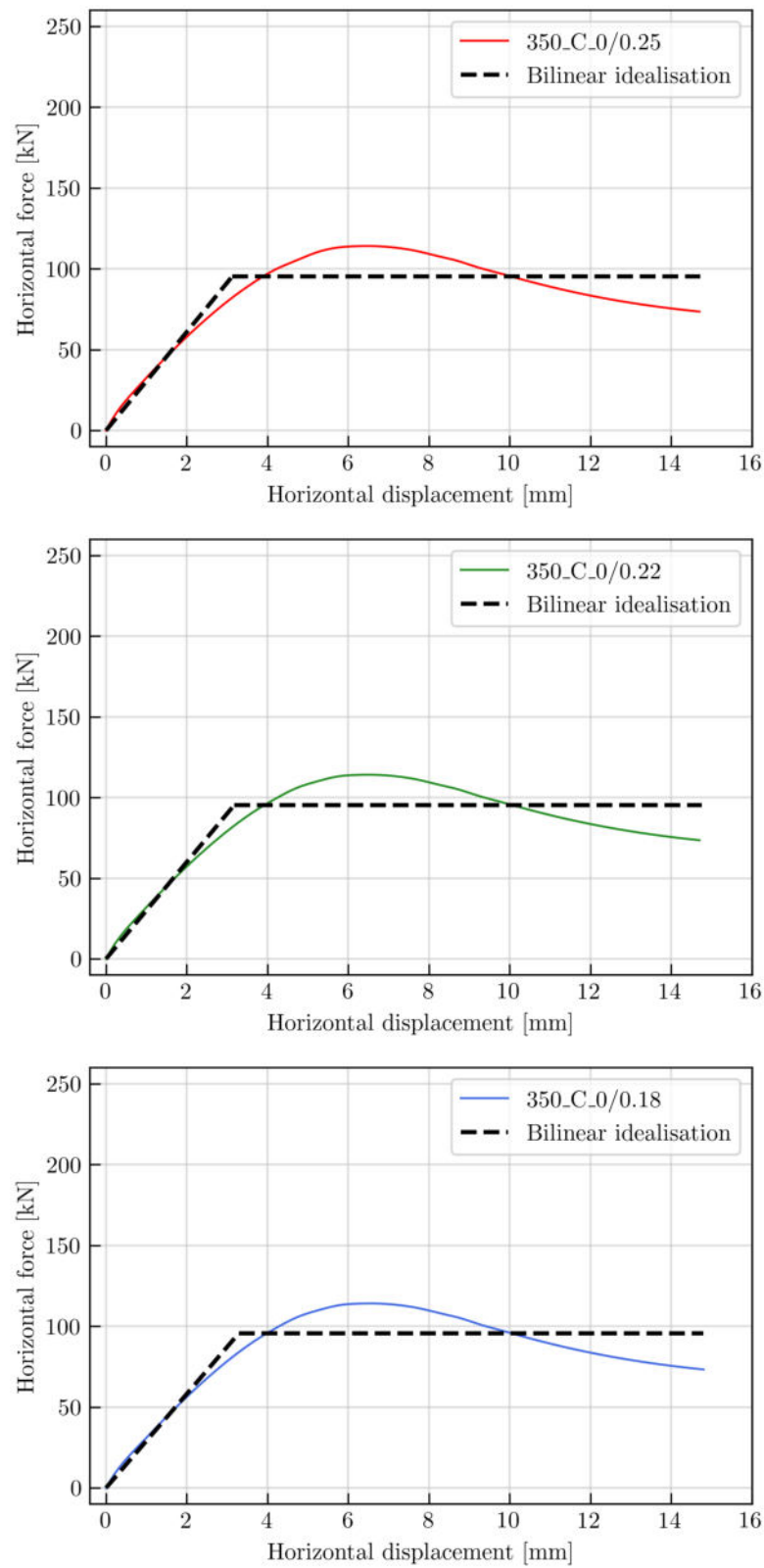


Figure 8.8: Bilinear idealisation: 350_C_0

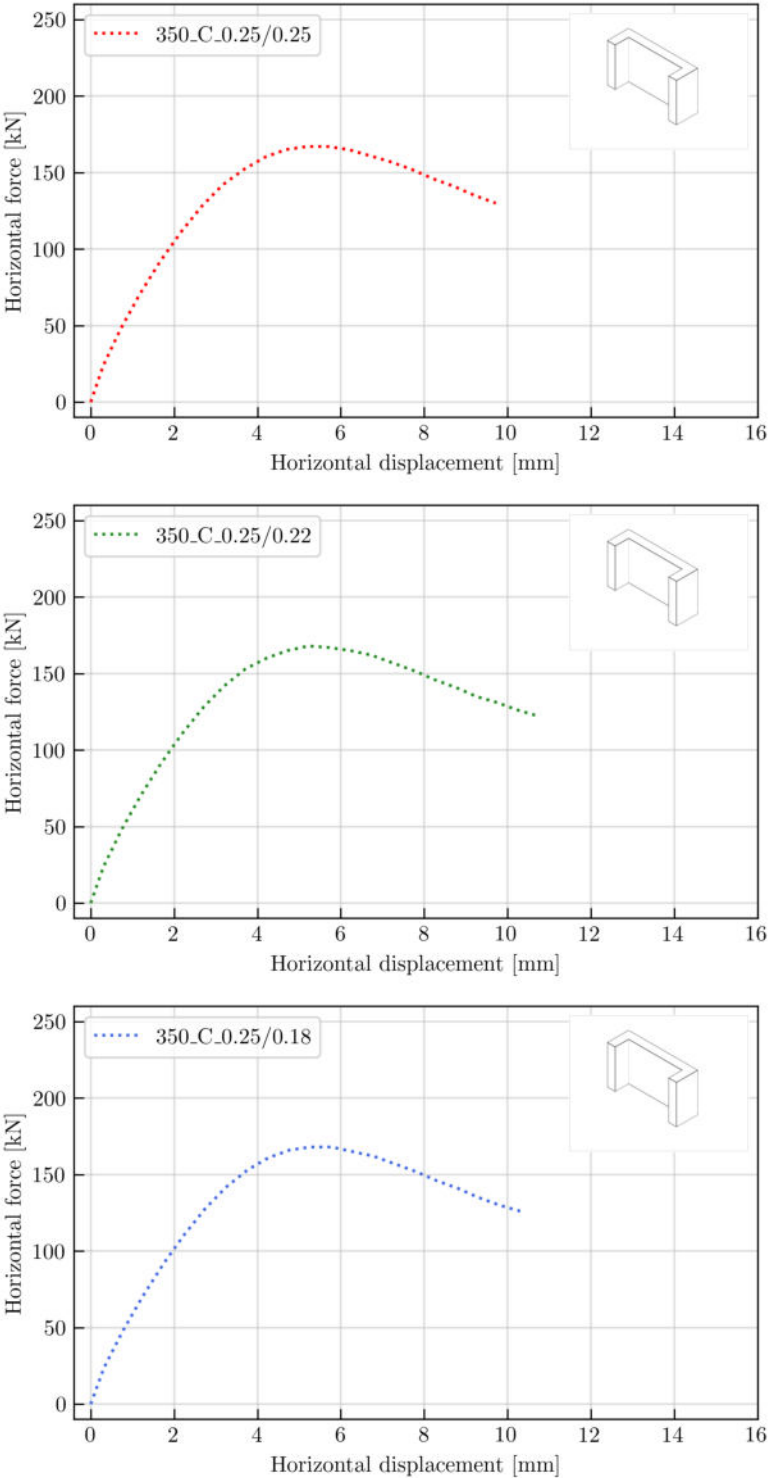


Figure 8.9: Numerical analysis results: 350_C_0.5

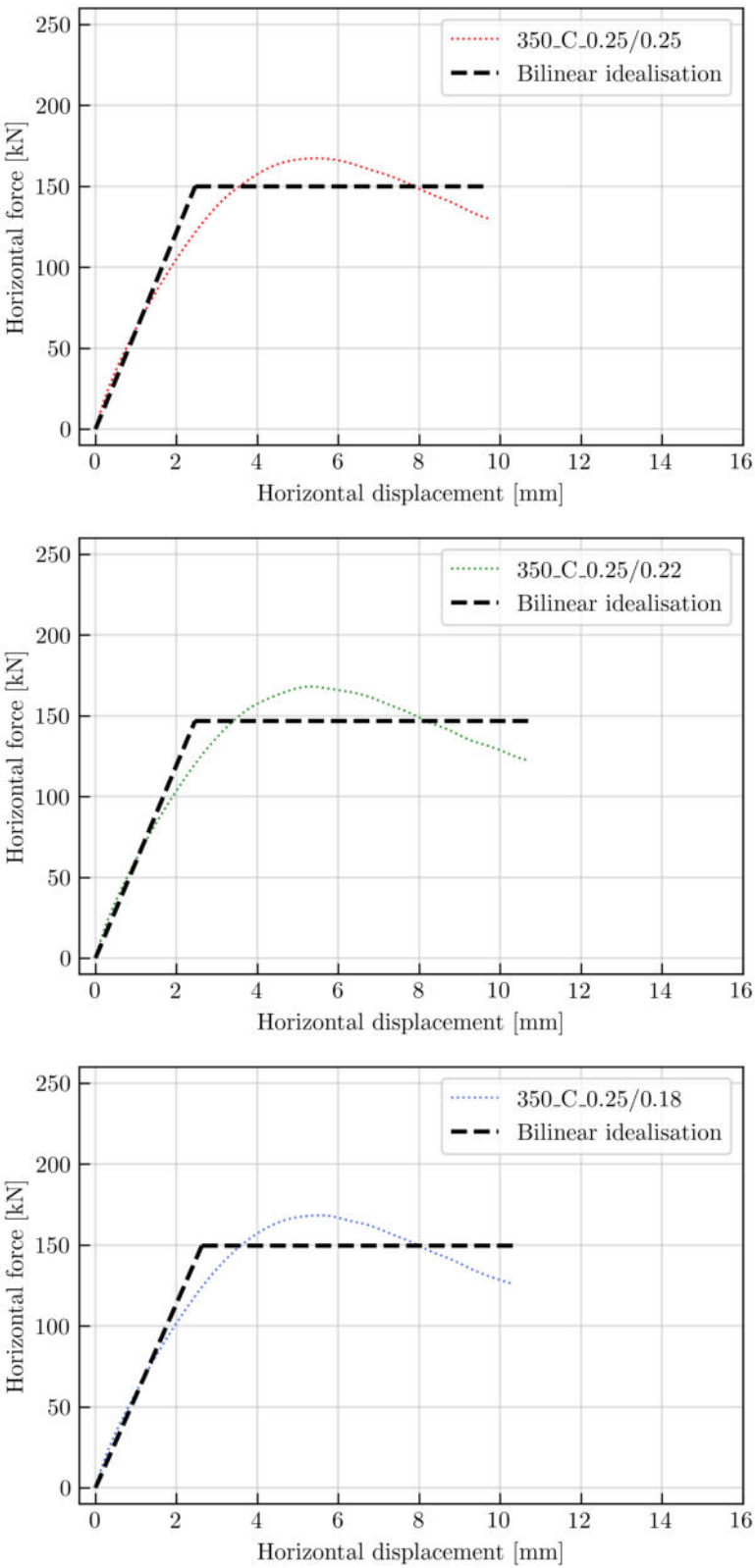


Figure 8.10: Bilinear idealisation: 350_C_0.5

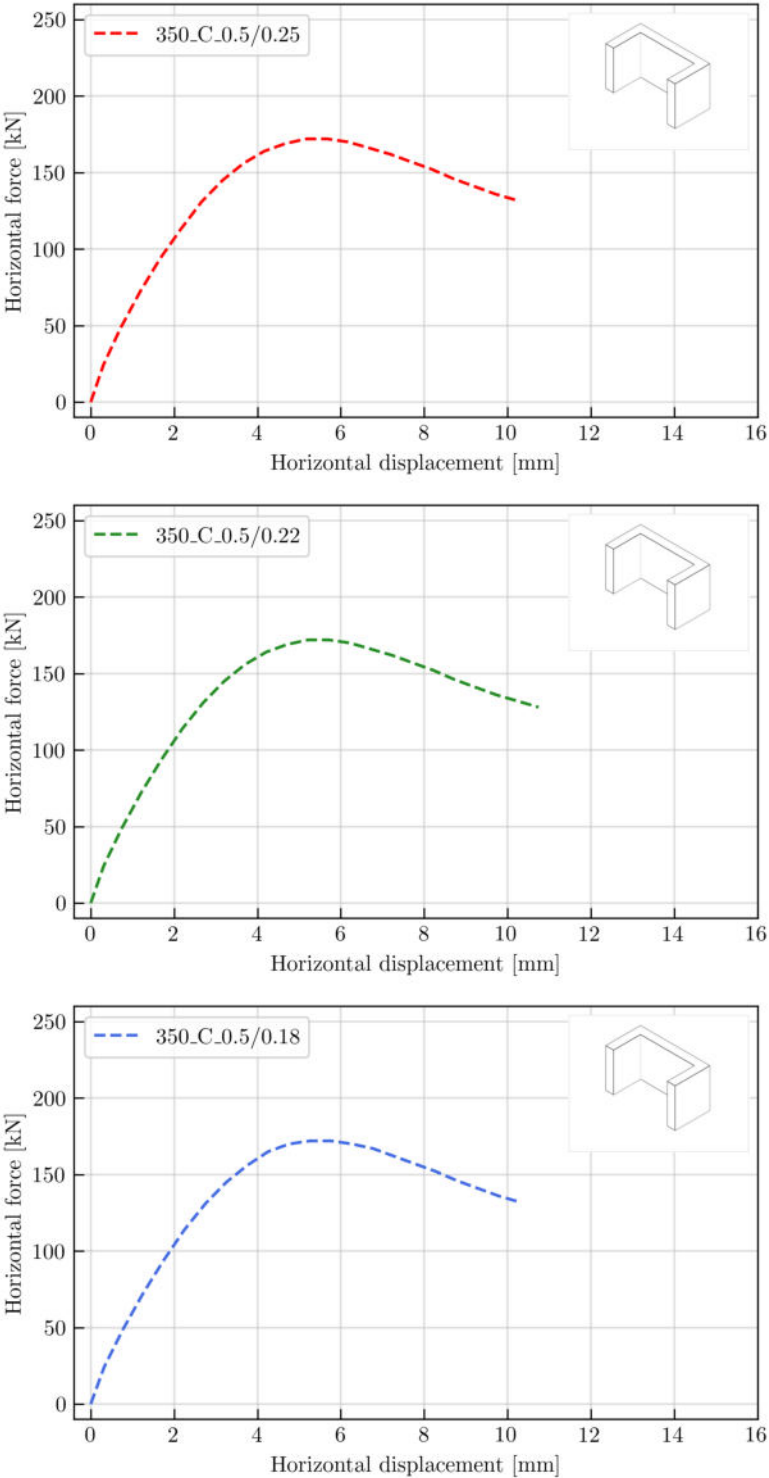


Figure 8.11: Numerical analysis results: 350_C_0.25

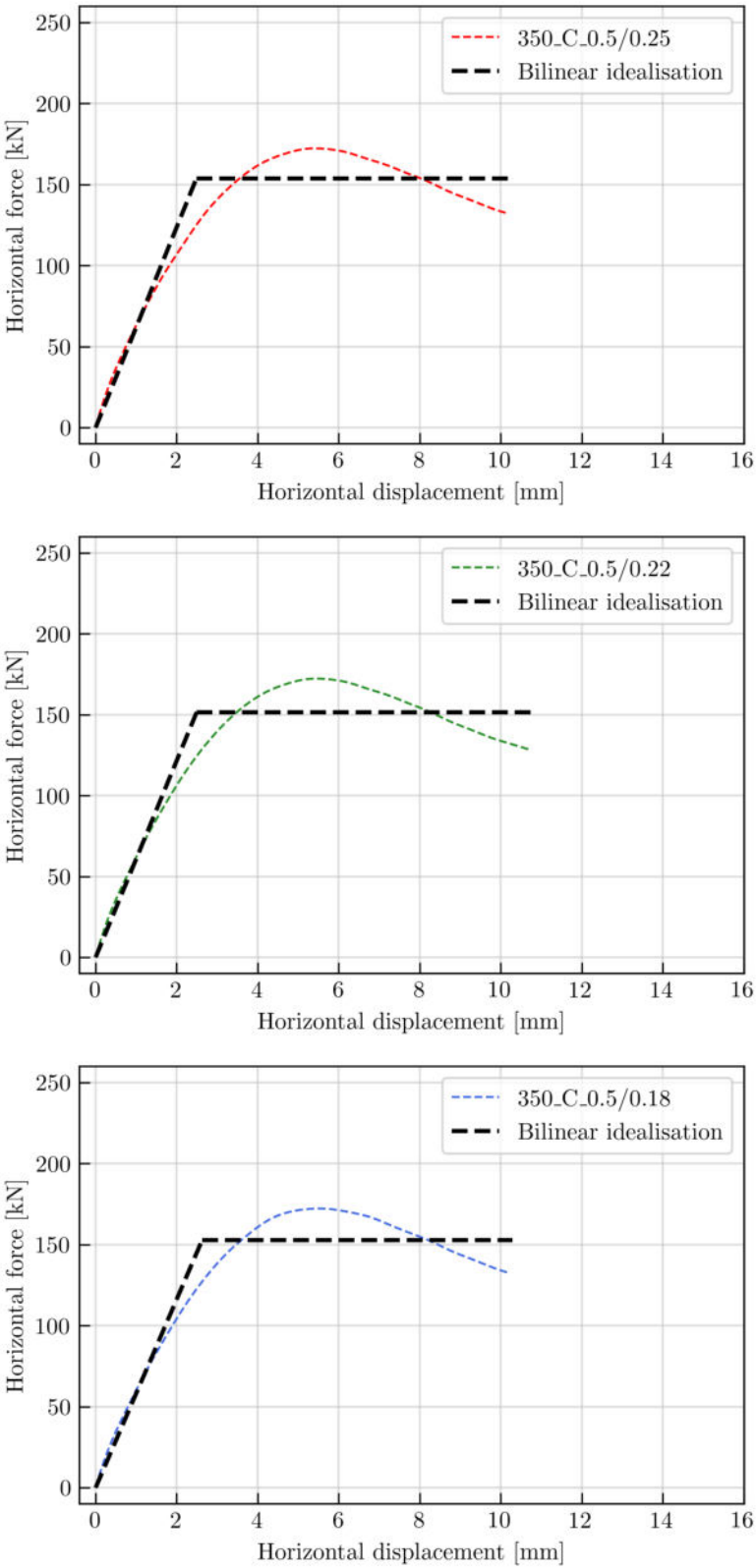


Figure 8.12: Bilinear idealisation: 350_C_0.25

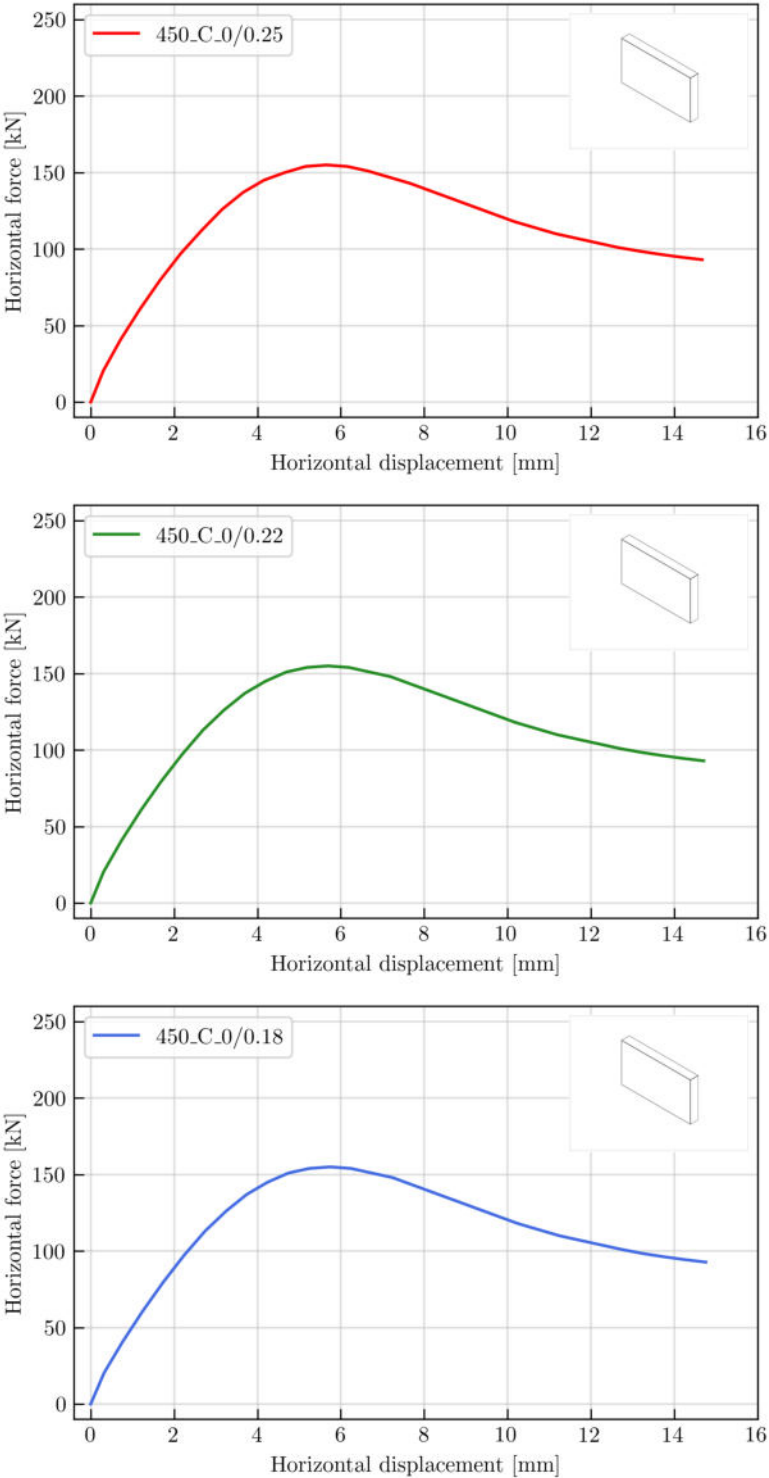


Figure 8.13: Numerical analysis results: 450_C_0

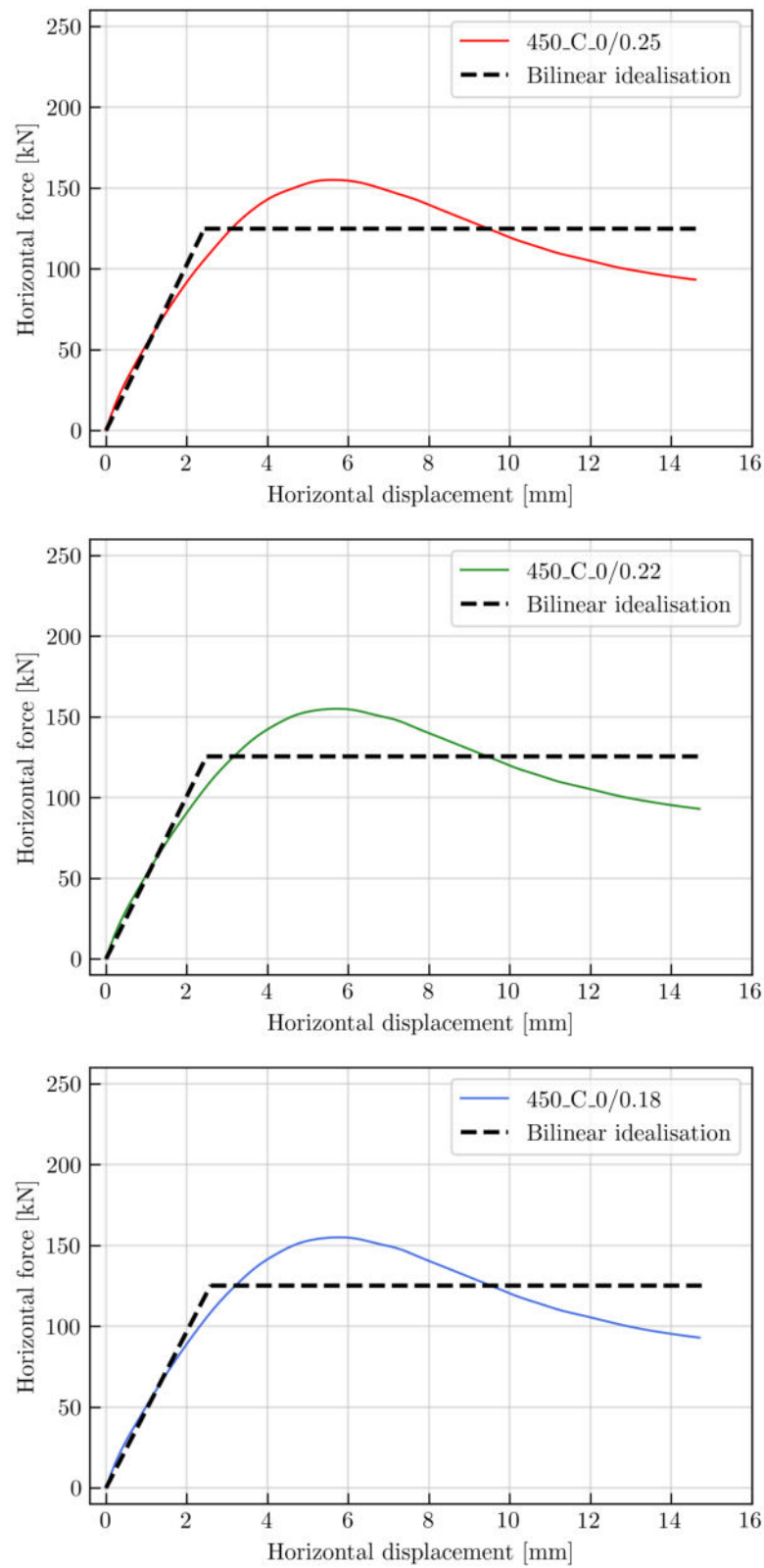


Figure 8.14: Bilinear idealisation: 450_C_0

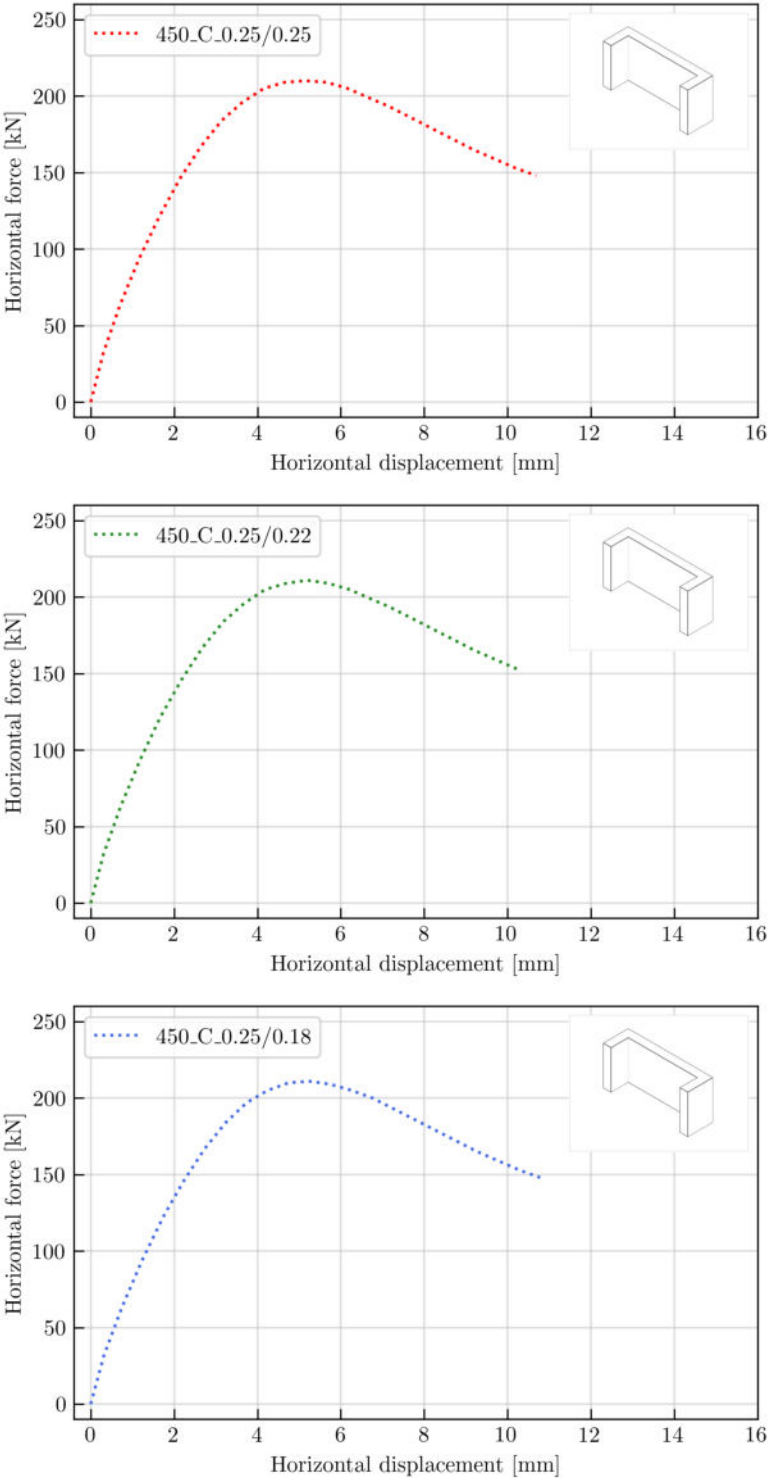


Figure 8.15: Numerical analysis results: 450_C_0.25

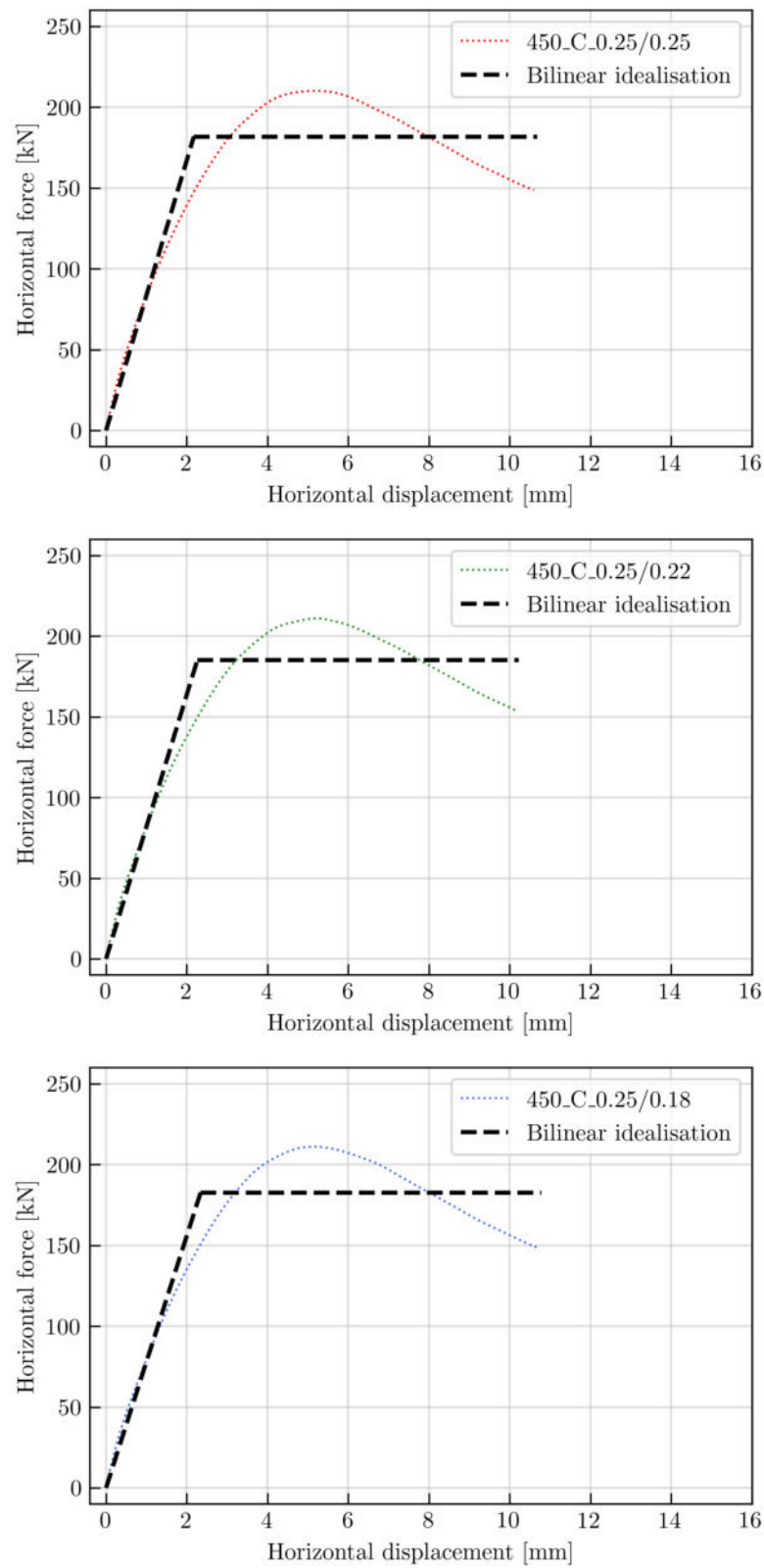


Figure 8.16: Bilinear idealisation: 450_C_0.25

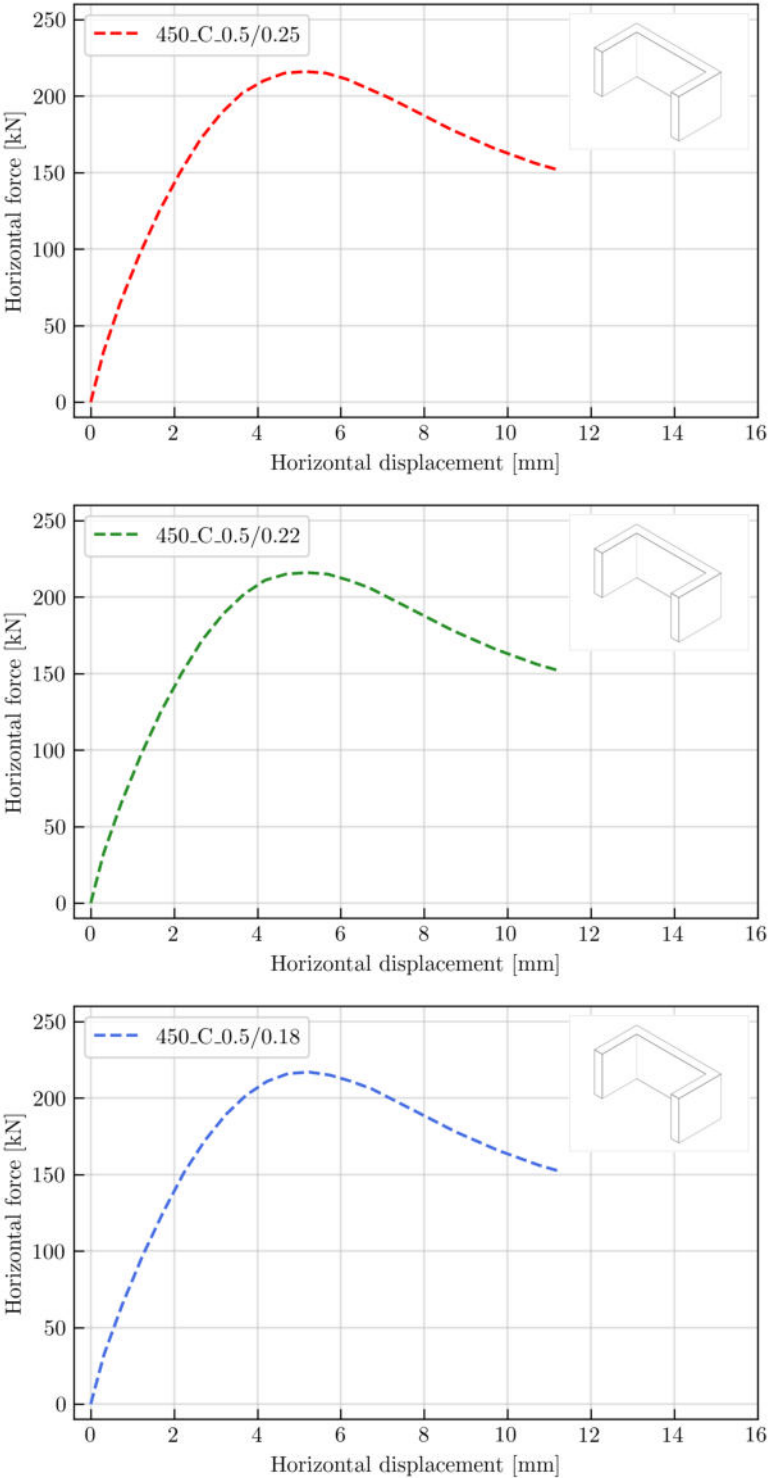


Figure 8.17: Numerical analysis results: 450_C_0.5

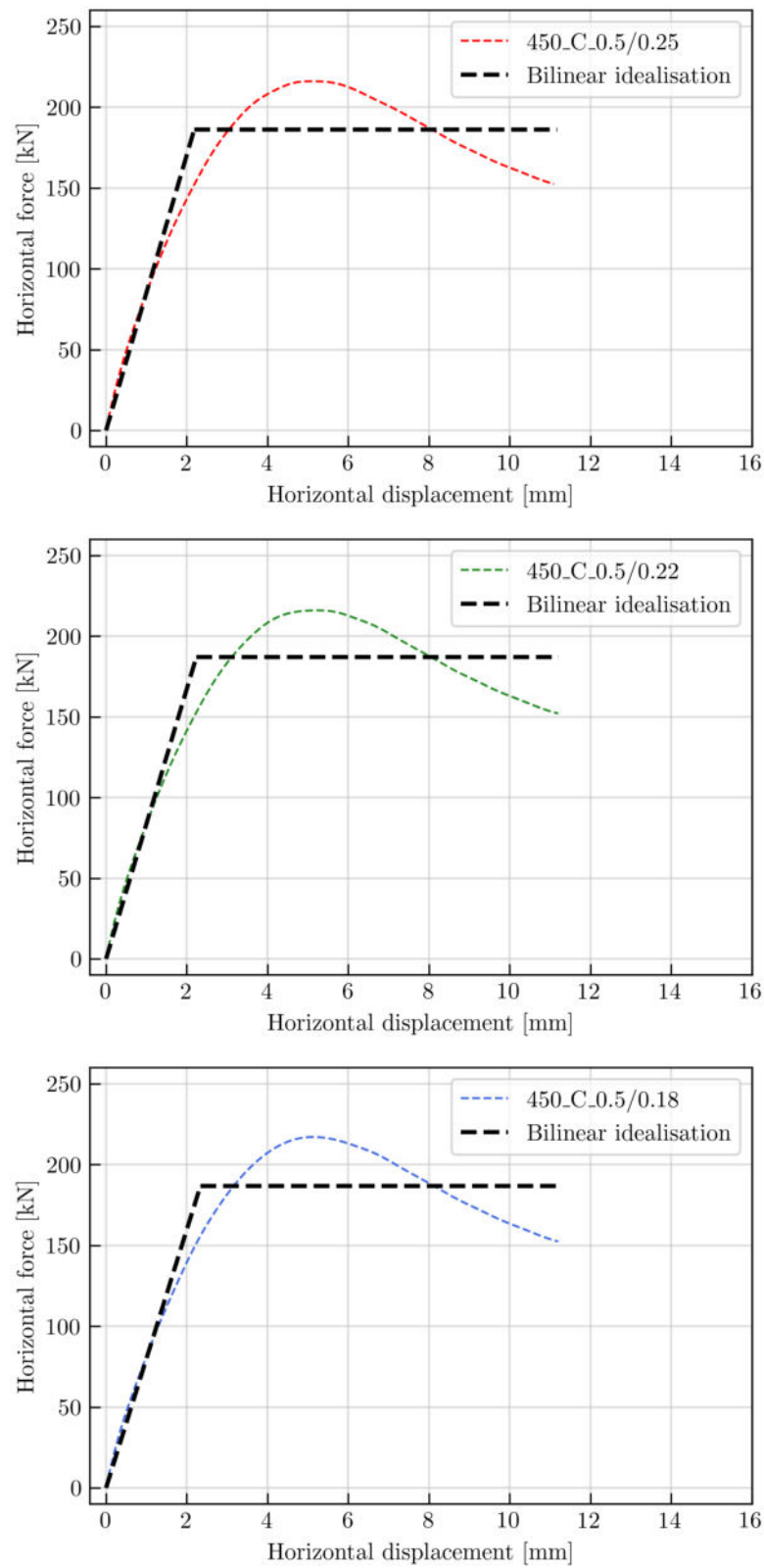


Figure 8.17: Bilinear idealisation: 450_C_0.5

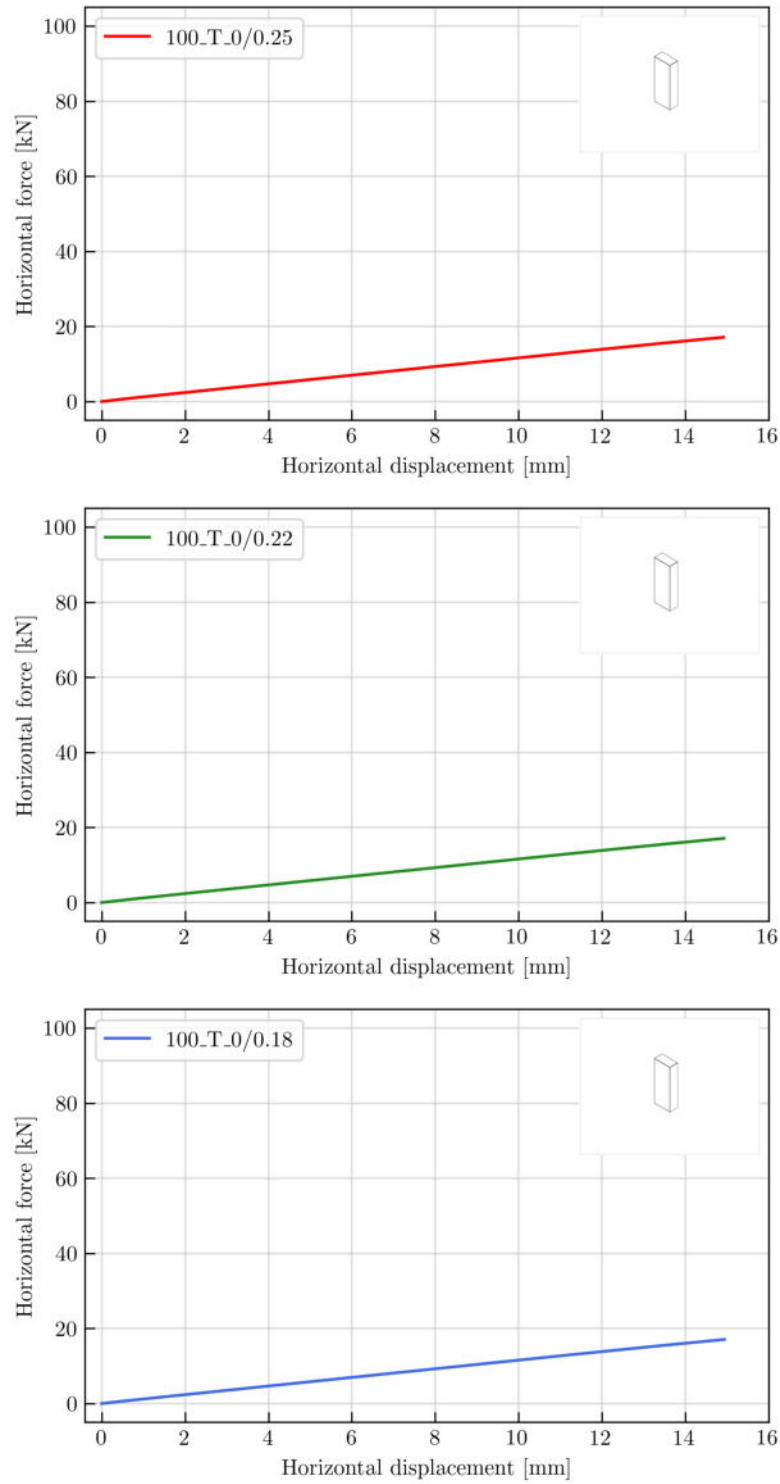


Figure 8.18: Numerical analysis results: 100_T_0

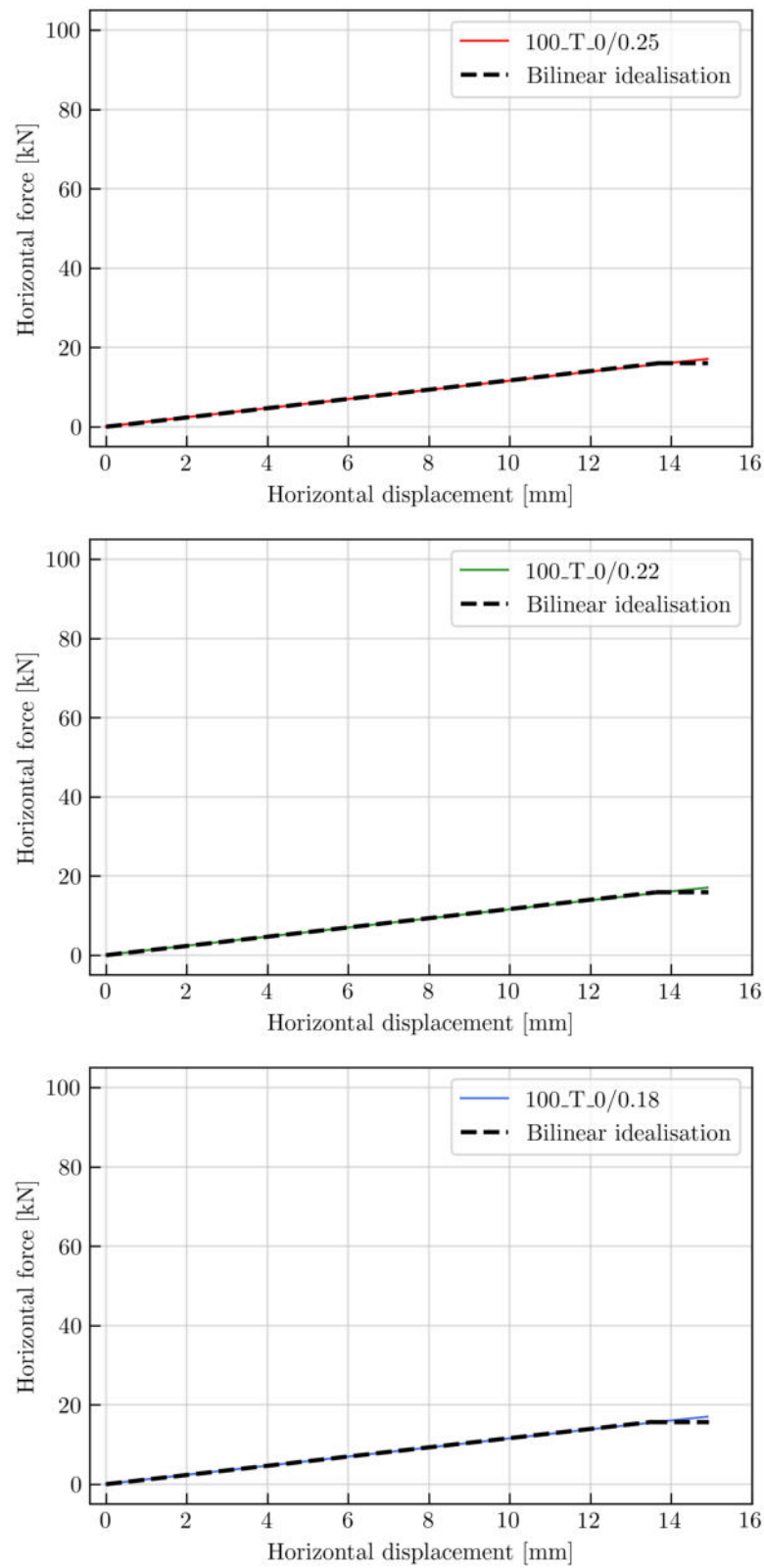


Figure 8.19: Bilinear idealisation: 100_T_0

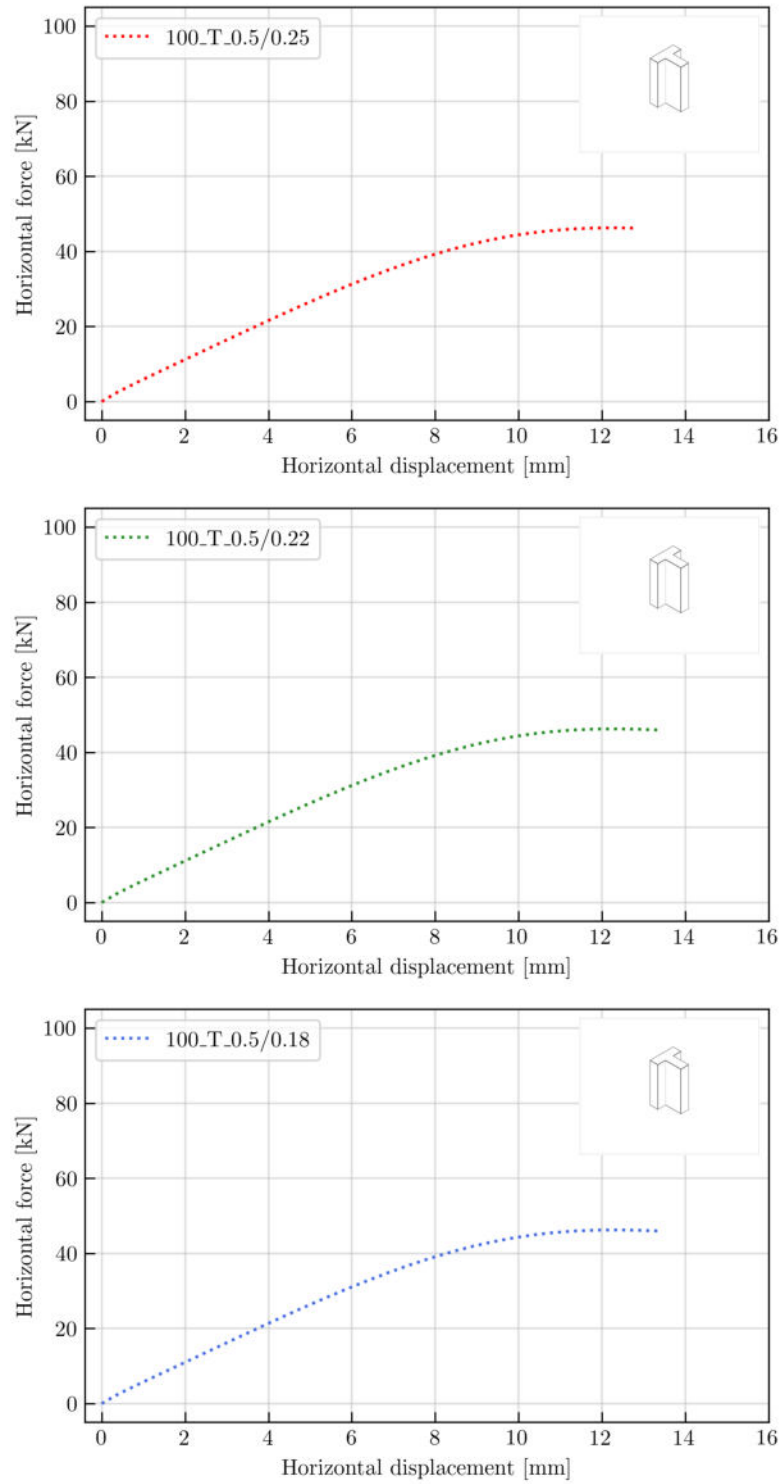


Figure 8.20: Numerical analysis results: 100_T_0.5

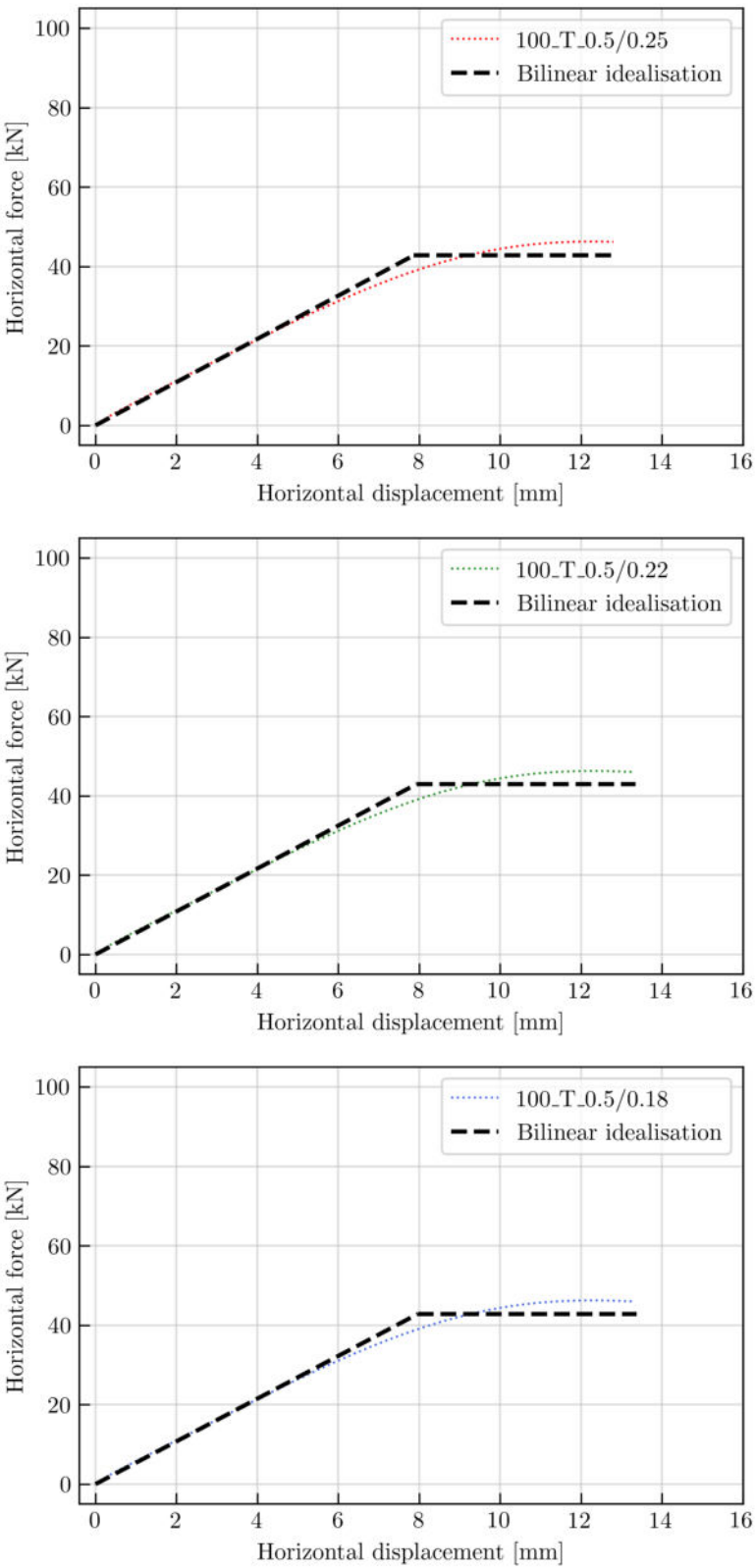


Figure 8.21: Bilinear idealisation: 100_T_0.5

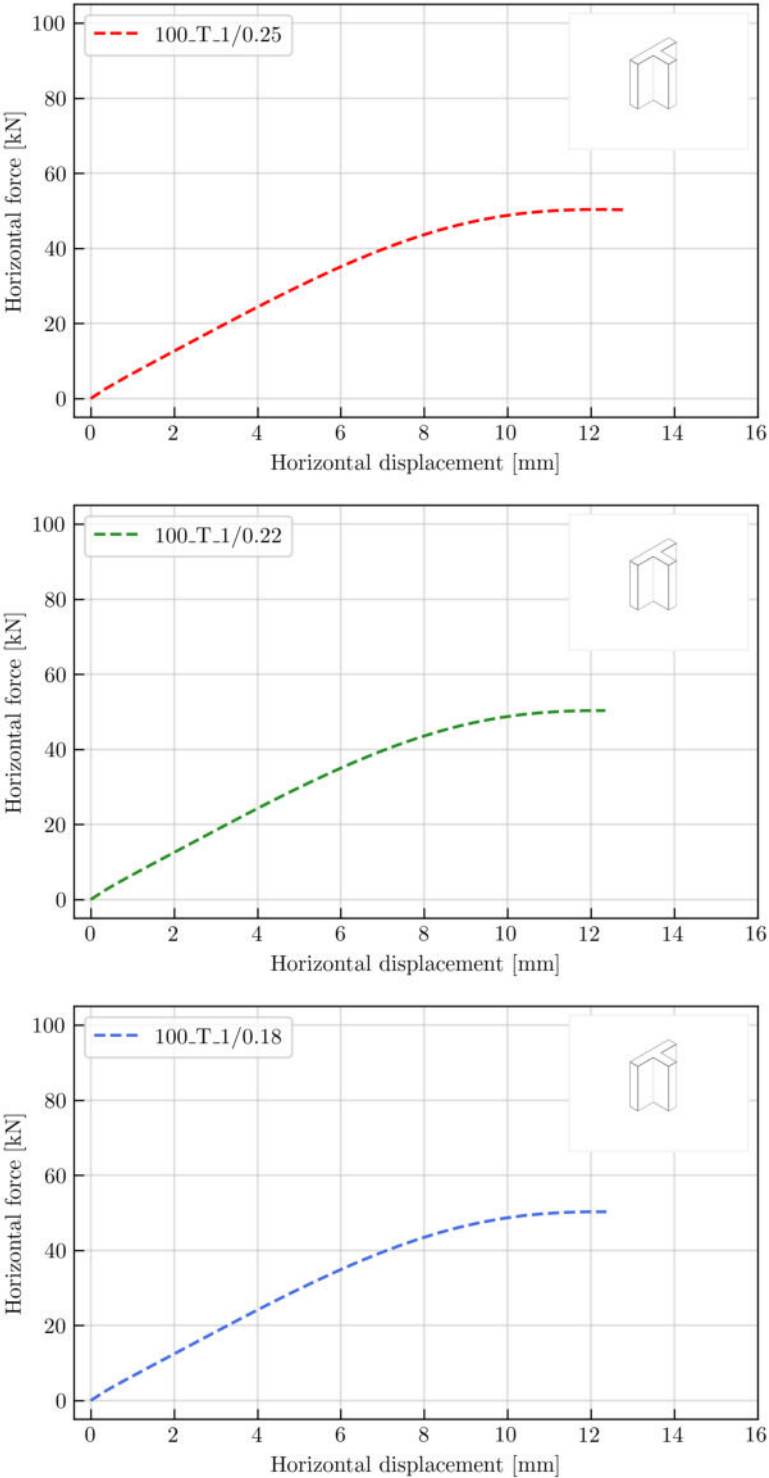


Figure 8.22: Numerical analysis results: 100_T_1

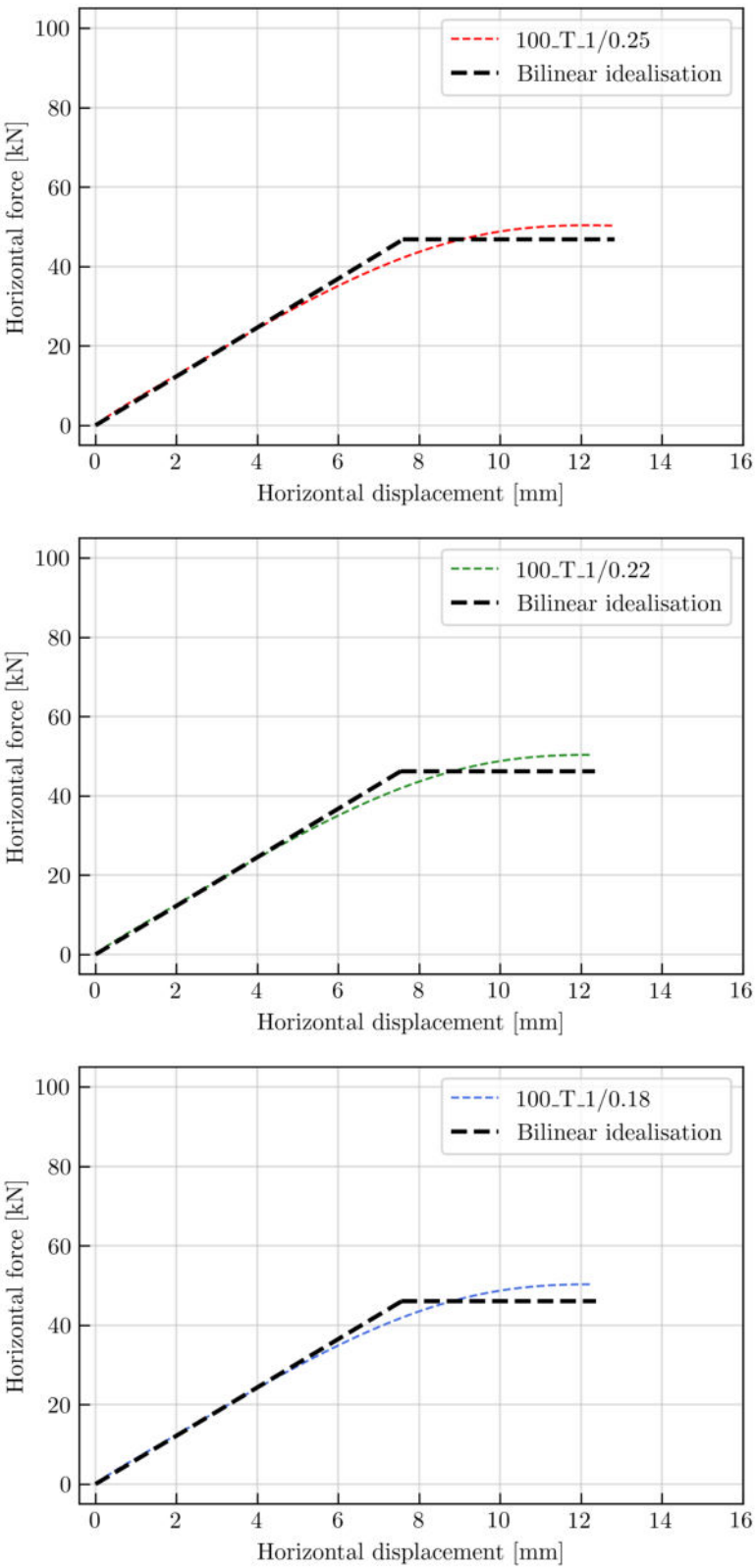


Figure 8.23: Bilinear idealisation: 100_T_1

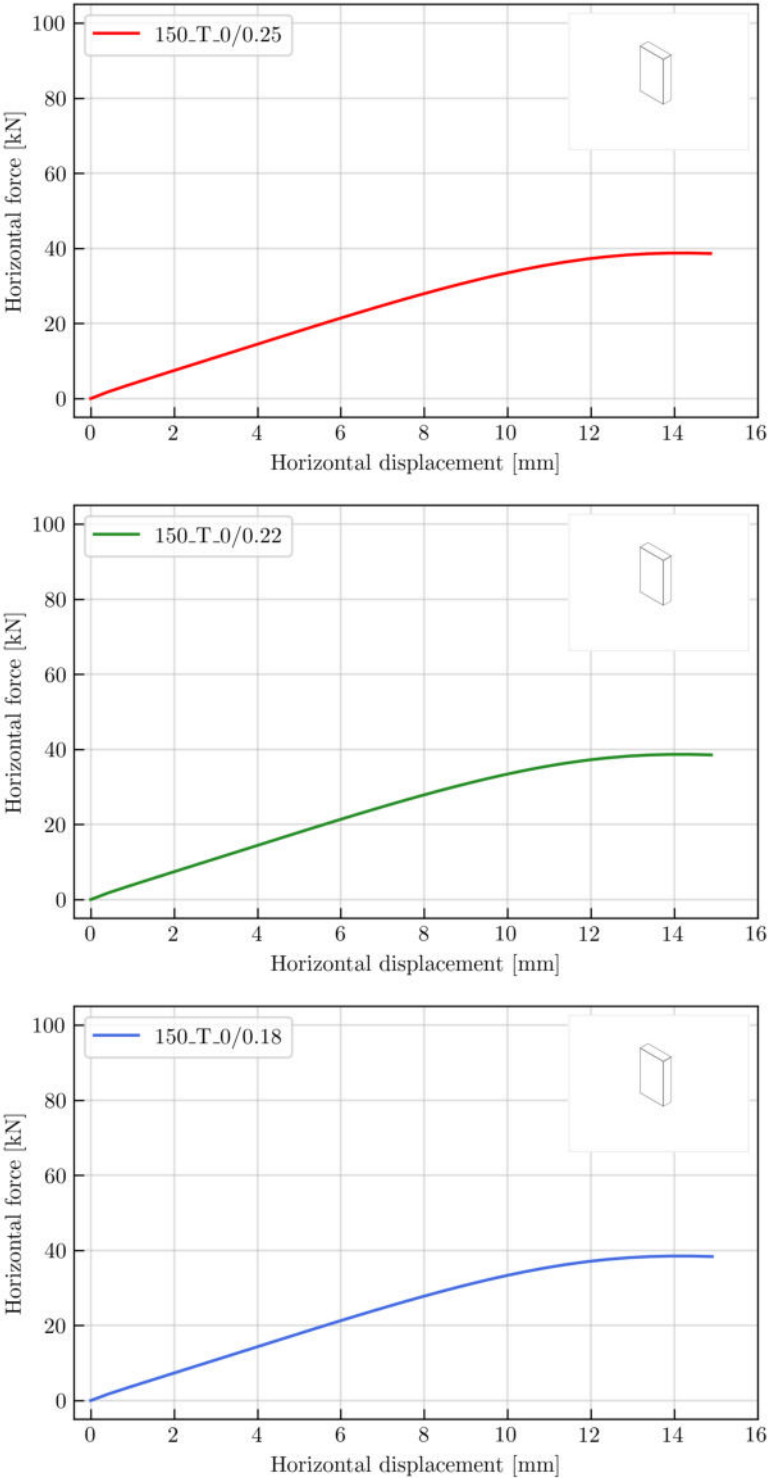


Figure 8.24: Numerical analysis results: 150_T_0

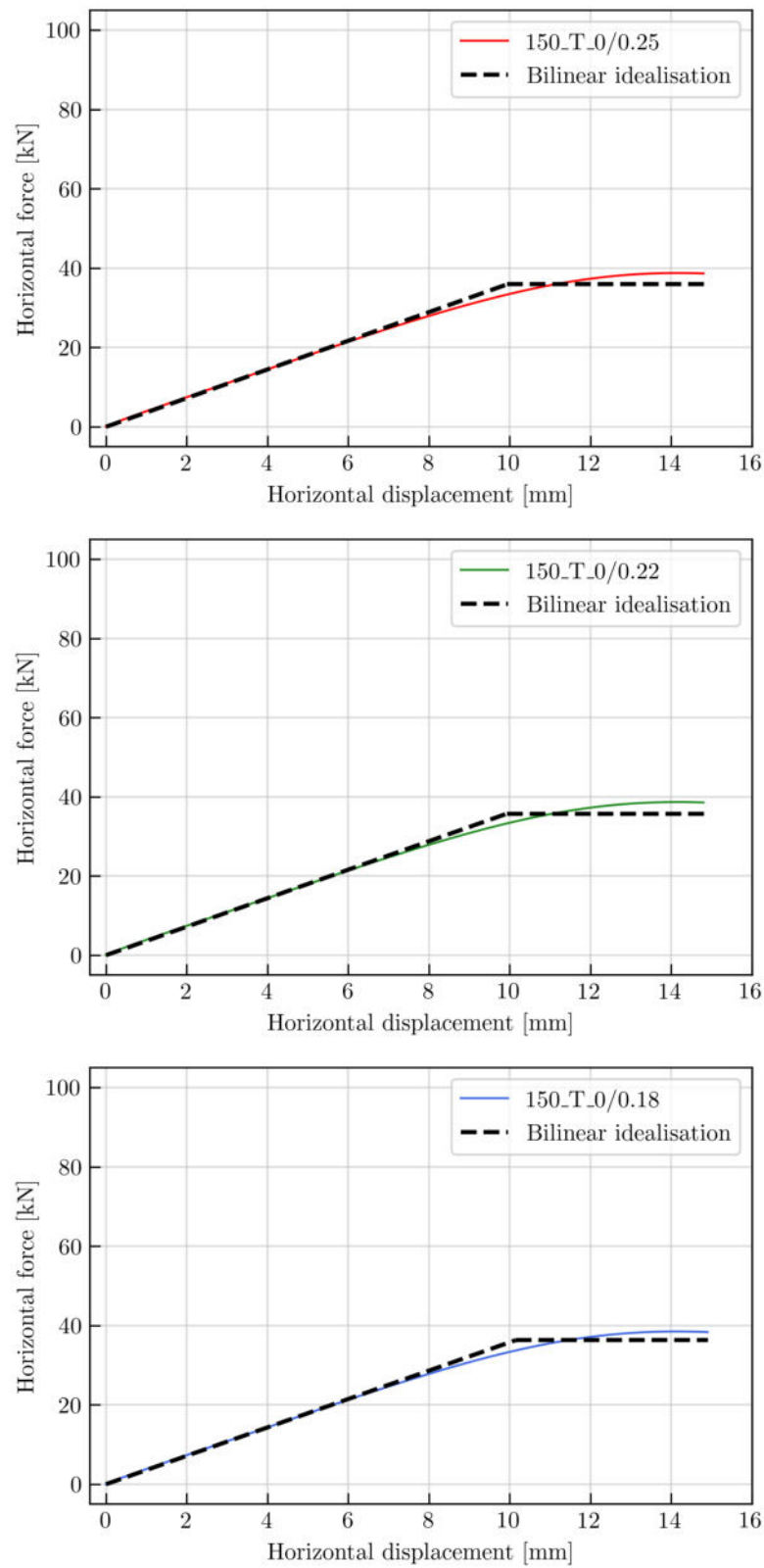


Figure 8.25: Bilinear idealisation: 150_T_0

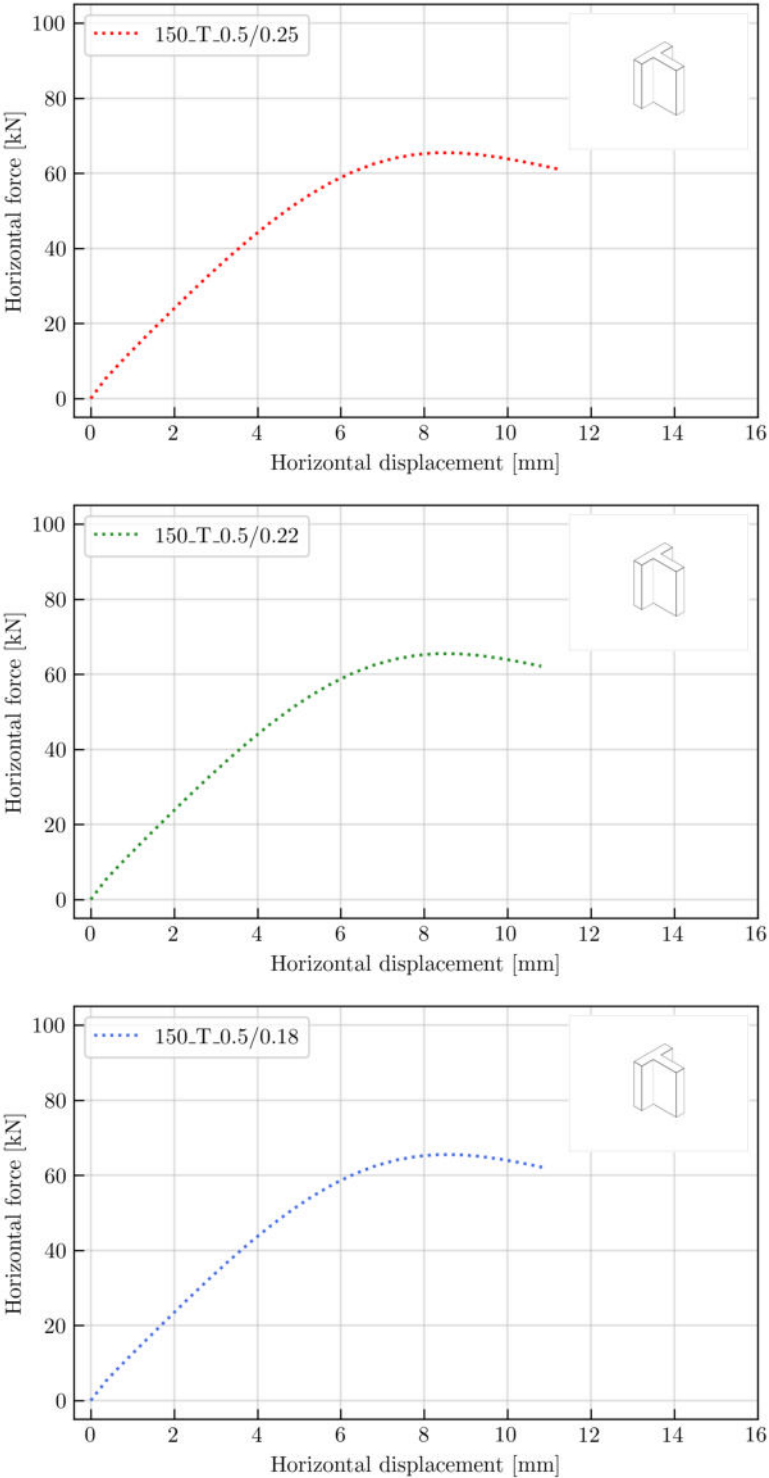


Figure 8.26: Numerical analysis results: 150_T_0.5

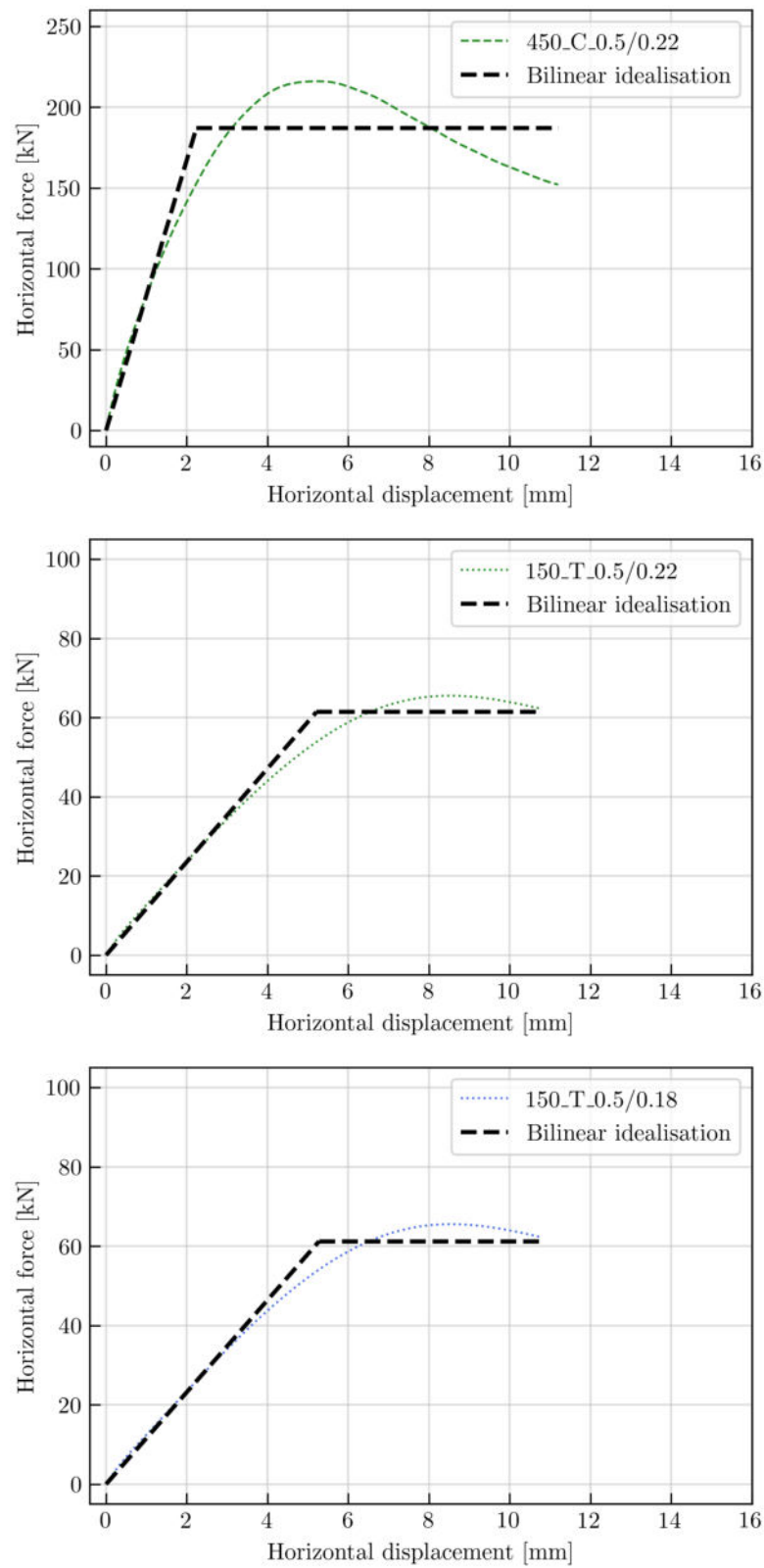


Figure 8.27: Bilinear idealisation: 150_T_0.5

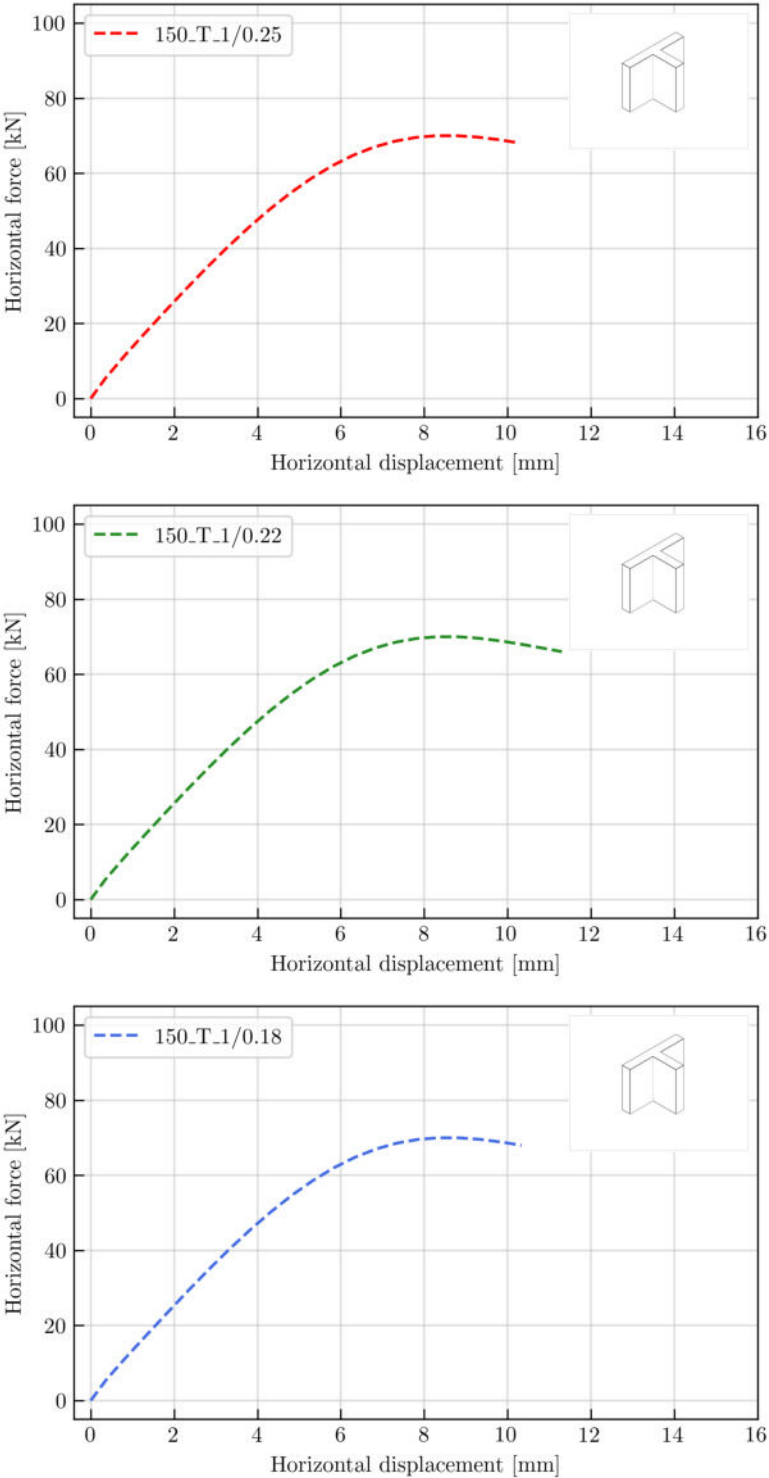


Figure 8.28: Numerical analysis results: 150_T_1

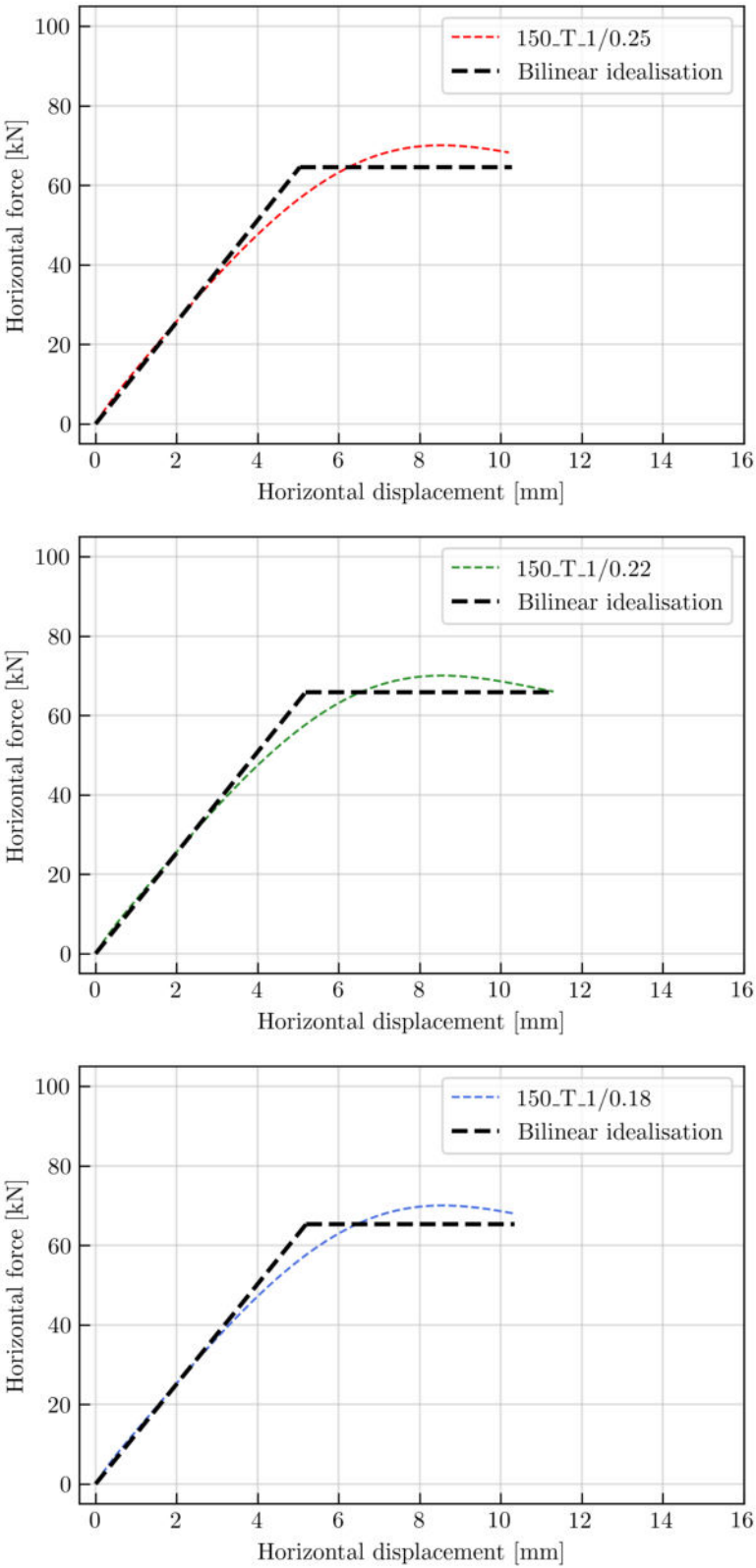


Figure 8.29: Bilinear idealisation: 150_T_1

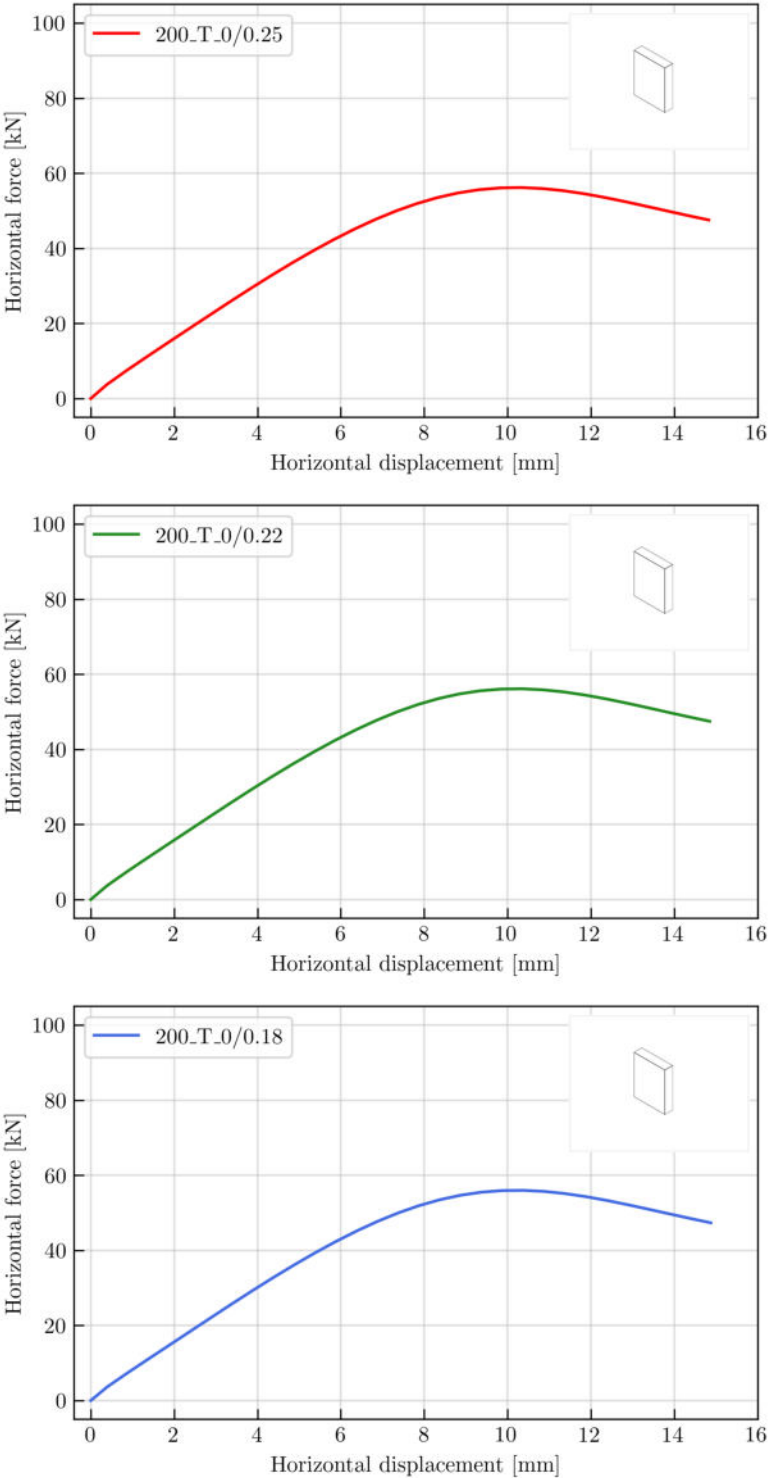


Figure 8.30: Numerical analysis results: 200_T_0

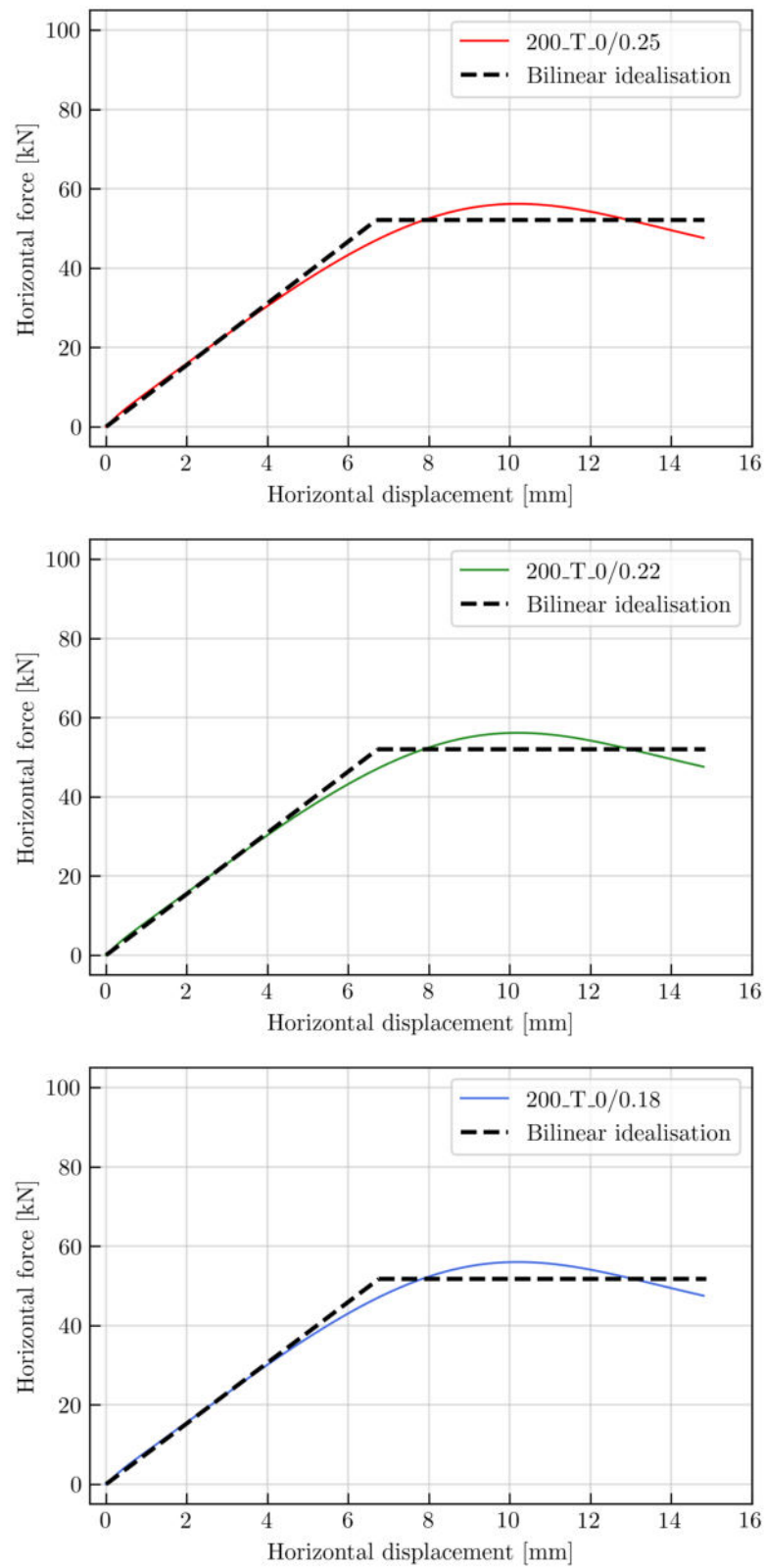


Figure 8.31: Bilinear idealisation: 200_T_0

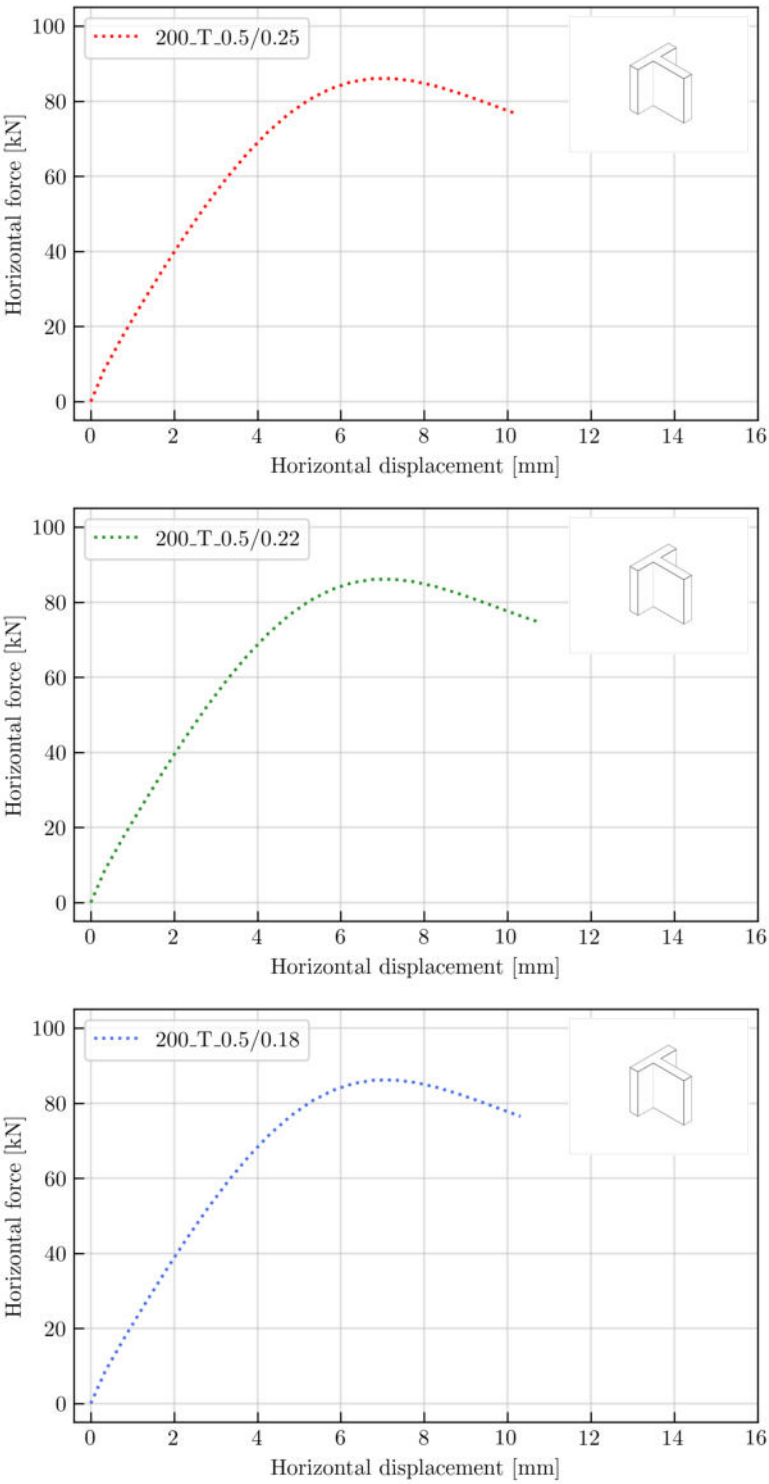


Figure 8.32: Numerical analysis results: 200_T_0.5

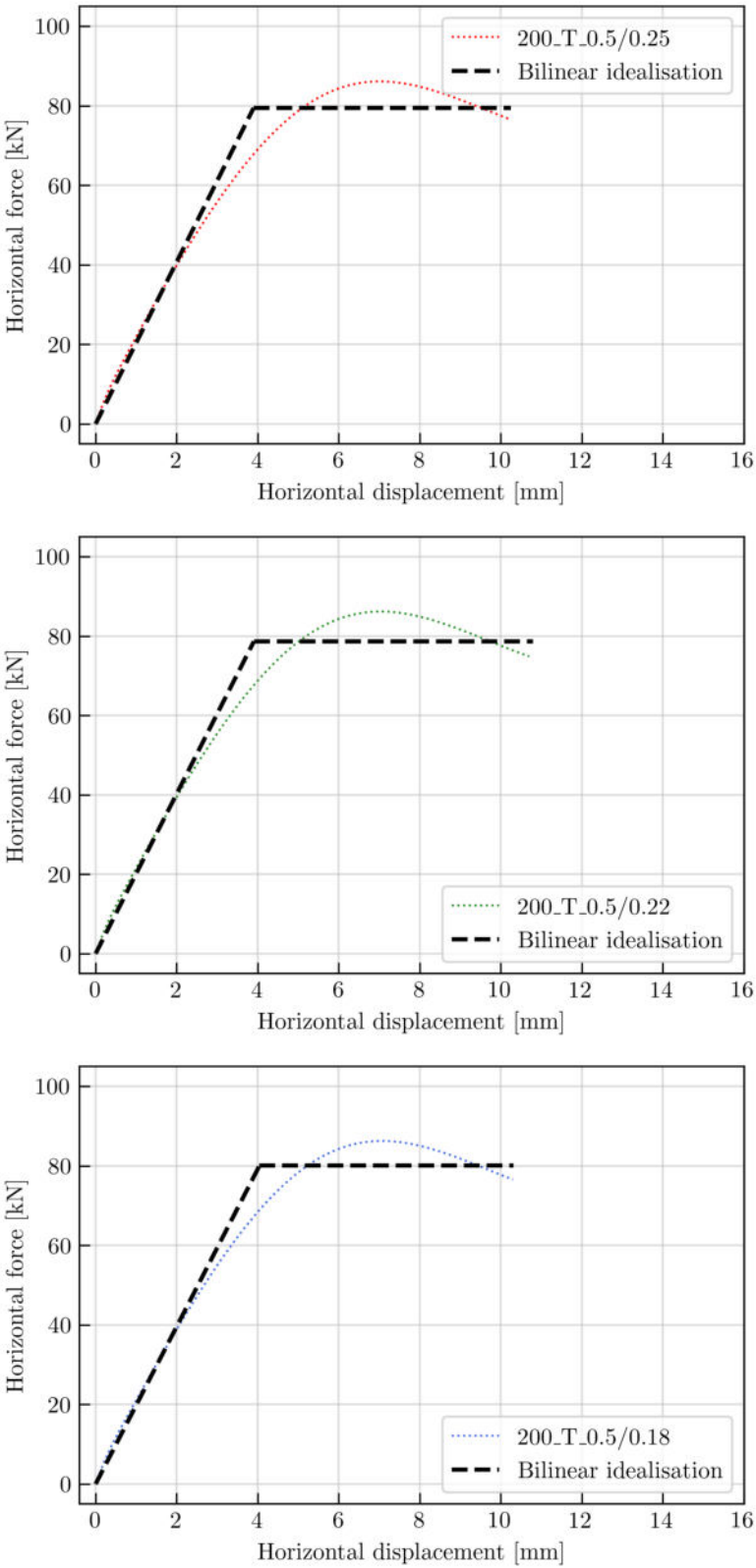


Figure 8.33: Bilinear idealisation: 200_T_0.5

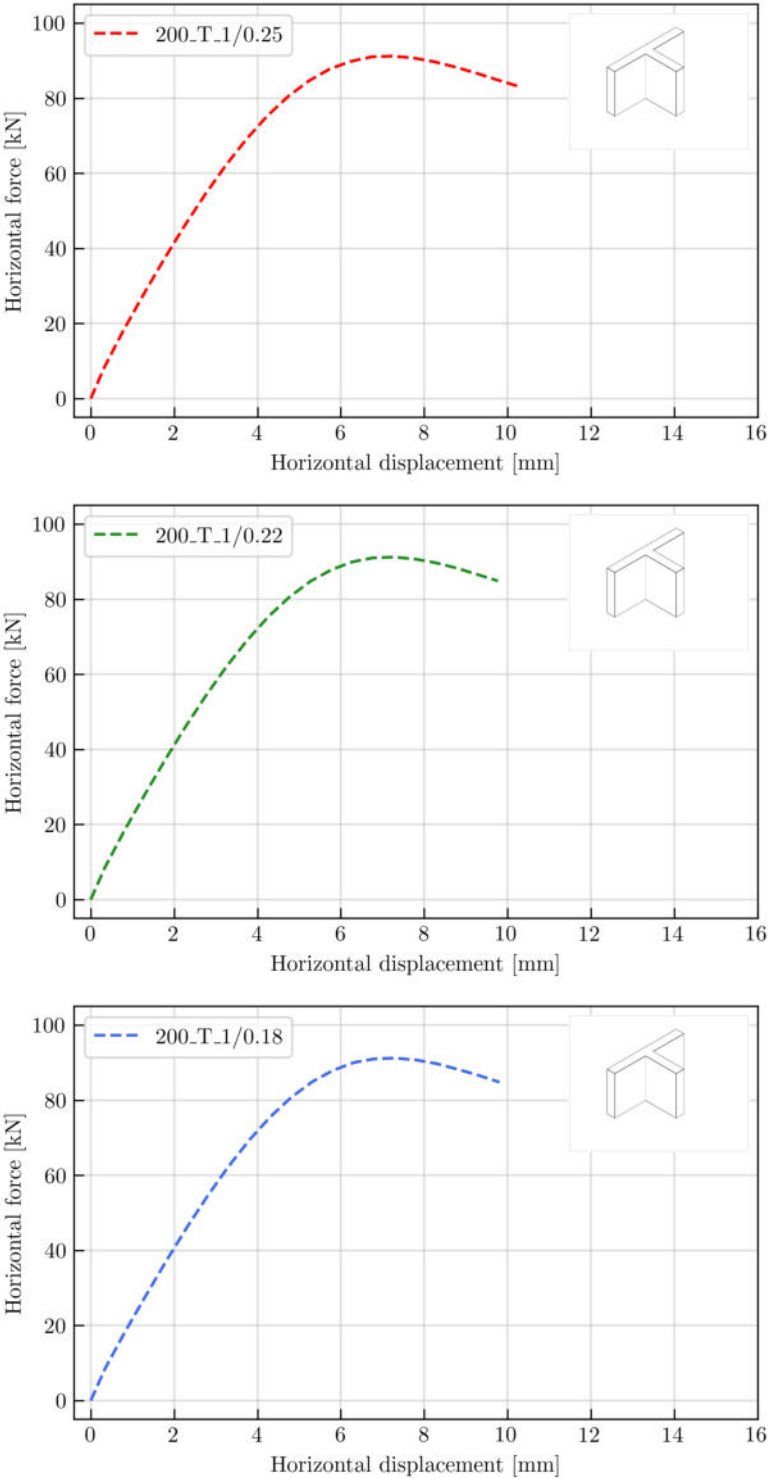


Figure 8.34: Numerical analysis results: 200_T_1

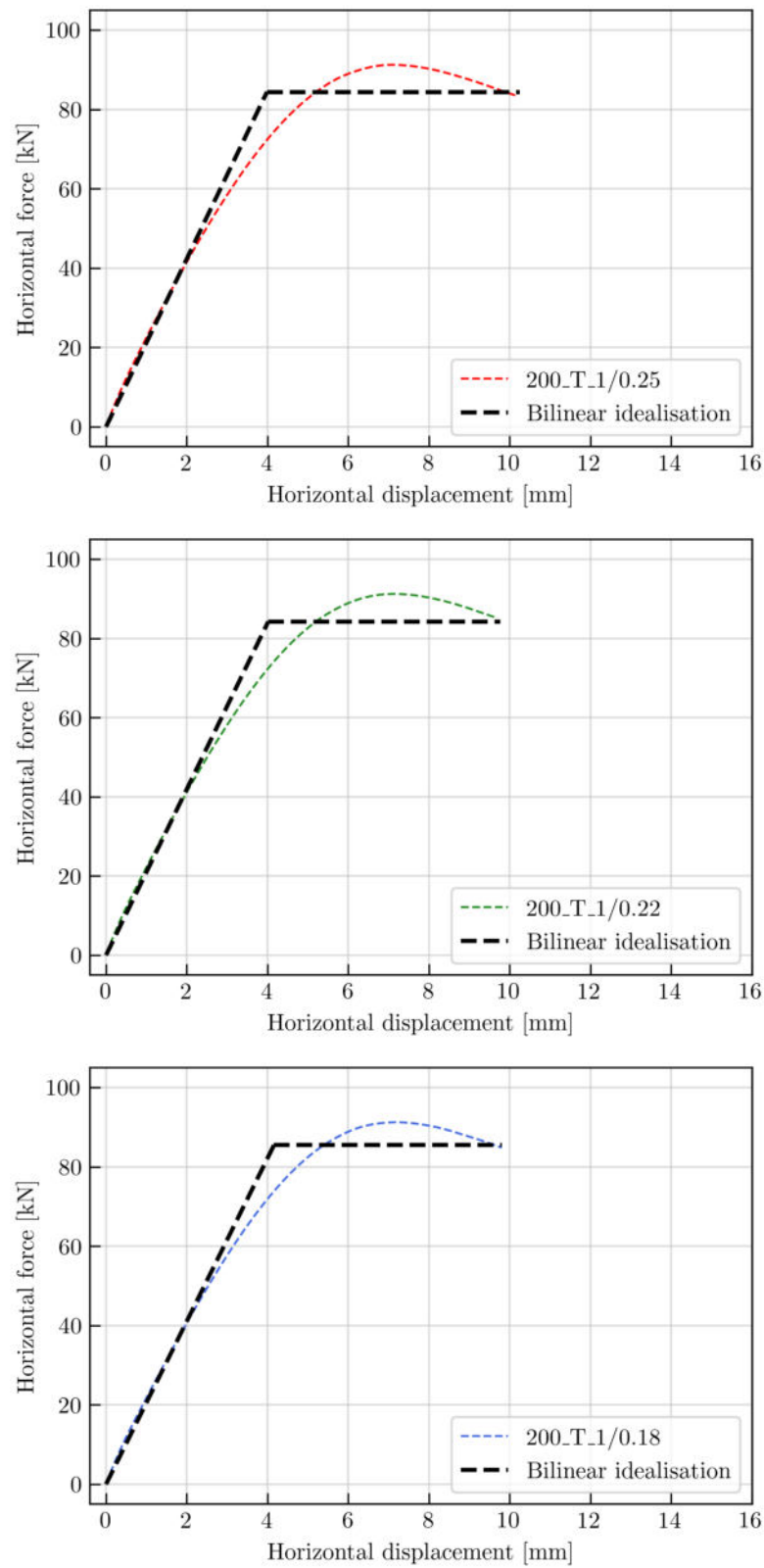


Figure 8.35: Bilinear idealisation: 200_T_1

Appendix B: Seismic capacity

In the following figures (Figure 8.36 through Figure 8.41), seismic capacity curves are shown, with seismic acceleration plotted in g and structural displacement plotted in meters. Different vertical stress is again colour-coded, while the wall system is distinguished by line style. One graph contains three capacity curves, one for each vertical stress imposed (0.18 MPa, 0.22 MPa and 0.25 MPa). On each graph, a thin grey line is plotted at $0.20g$ to ease the comparison of each curve with the amount of design spectral acceleration in eastern Croatia, a minimum of which walls should endure per this study.

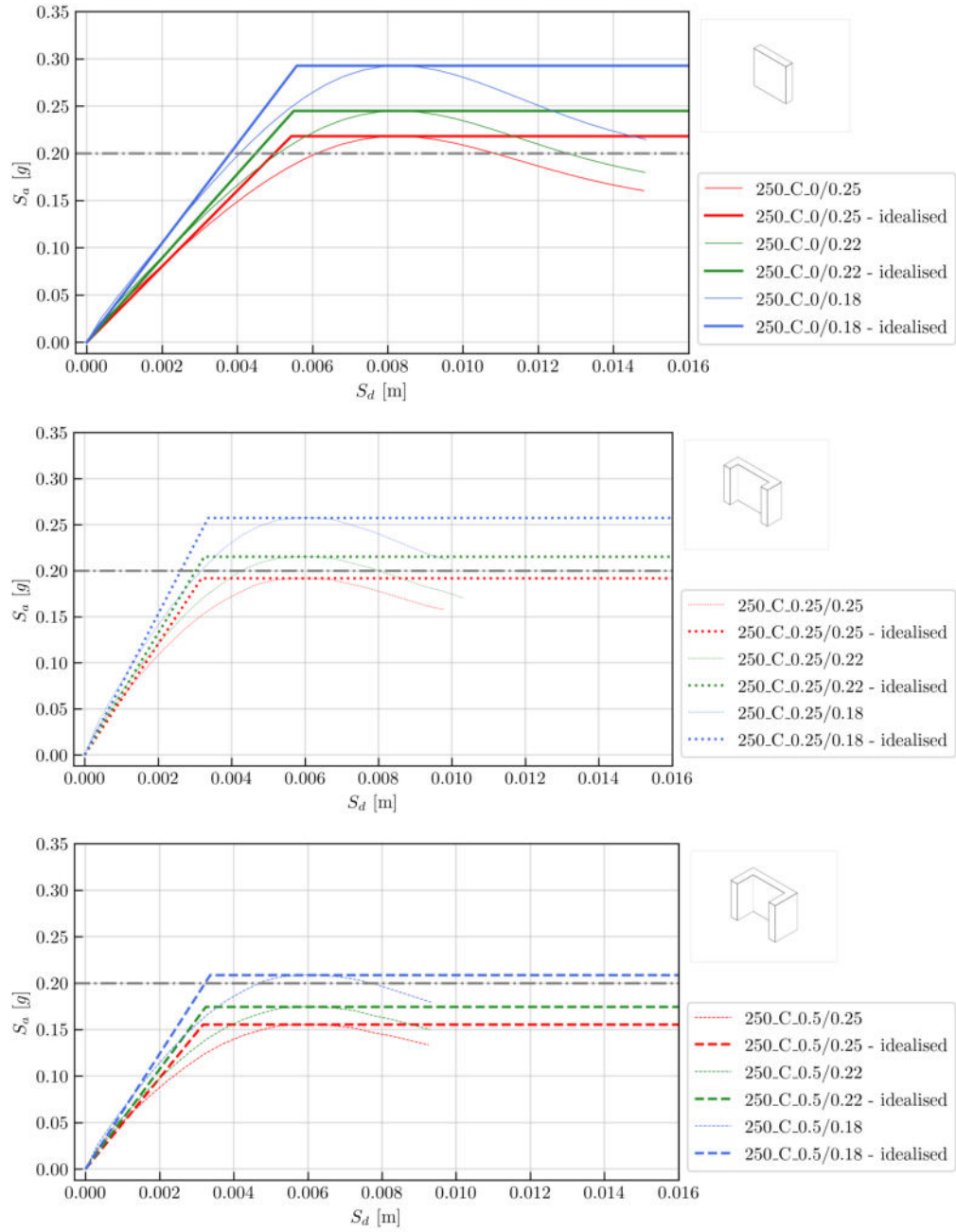


Figure 8.36: Seismic capacity: 250_C

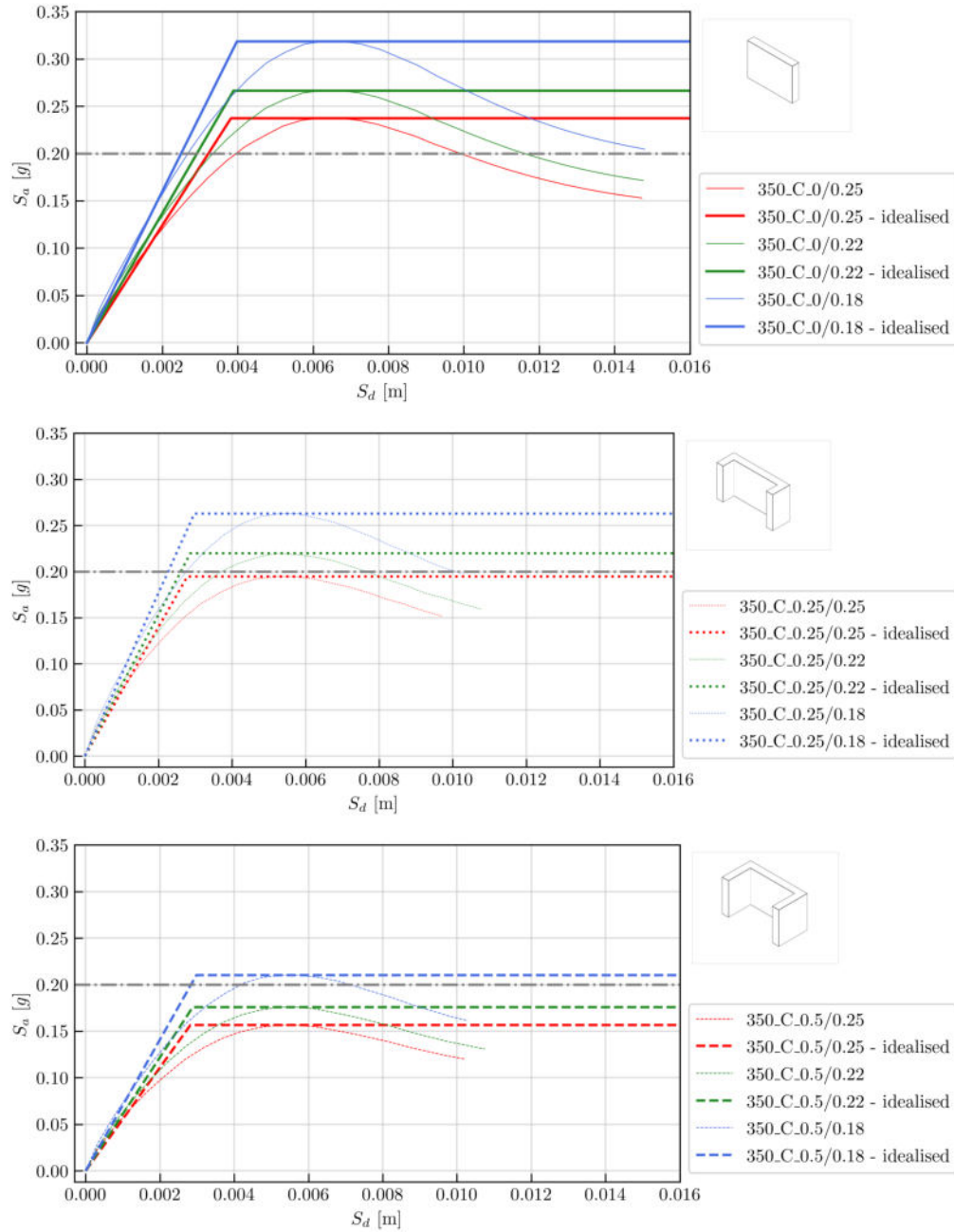


Figure 8.37: Seismic capacity: 350_C

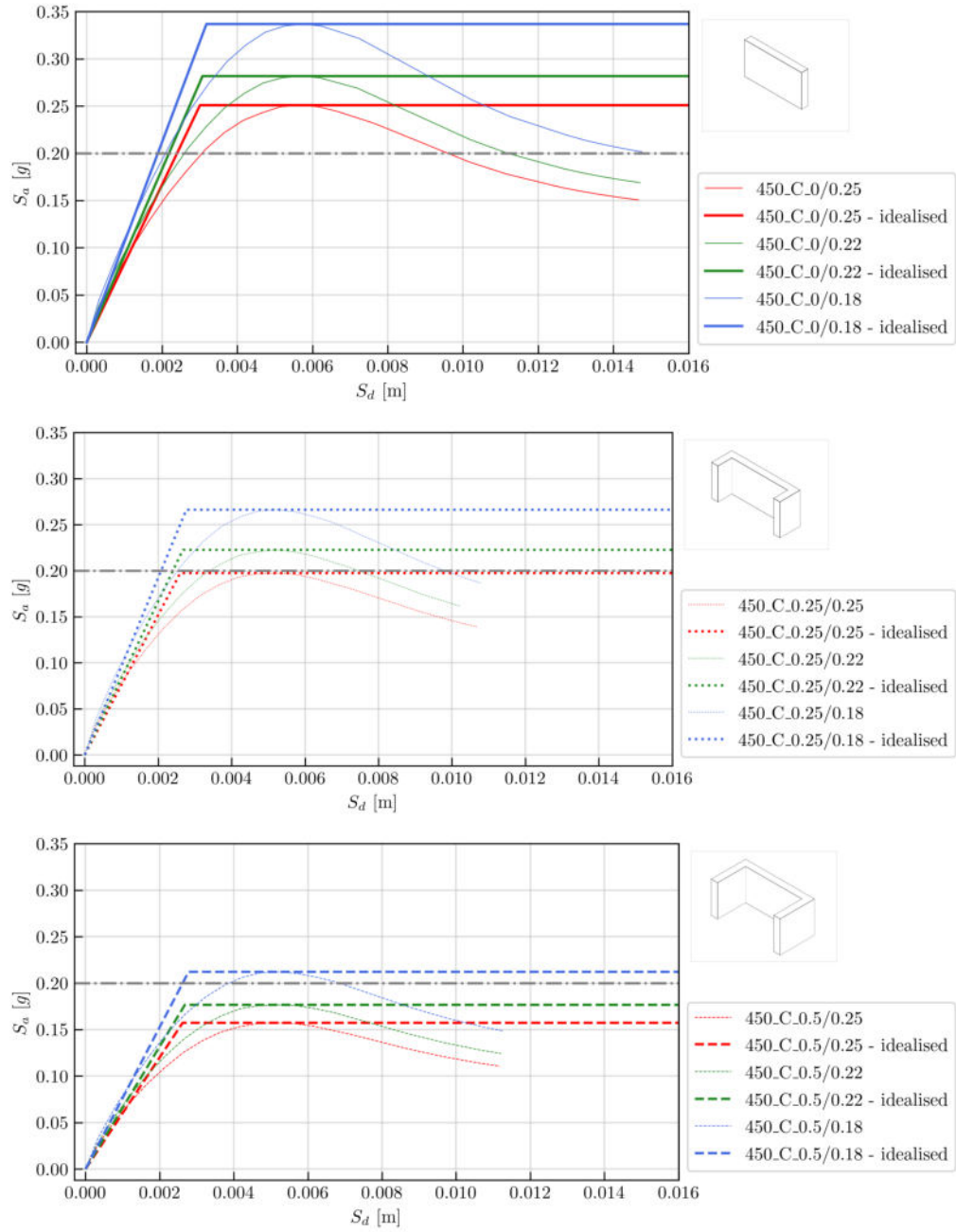


Figure 8.38: Seismic capacity: 350_C

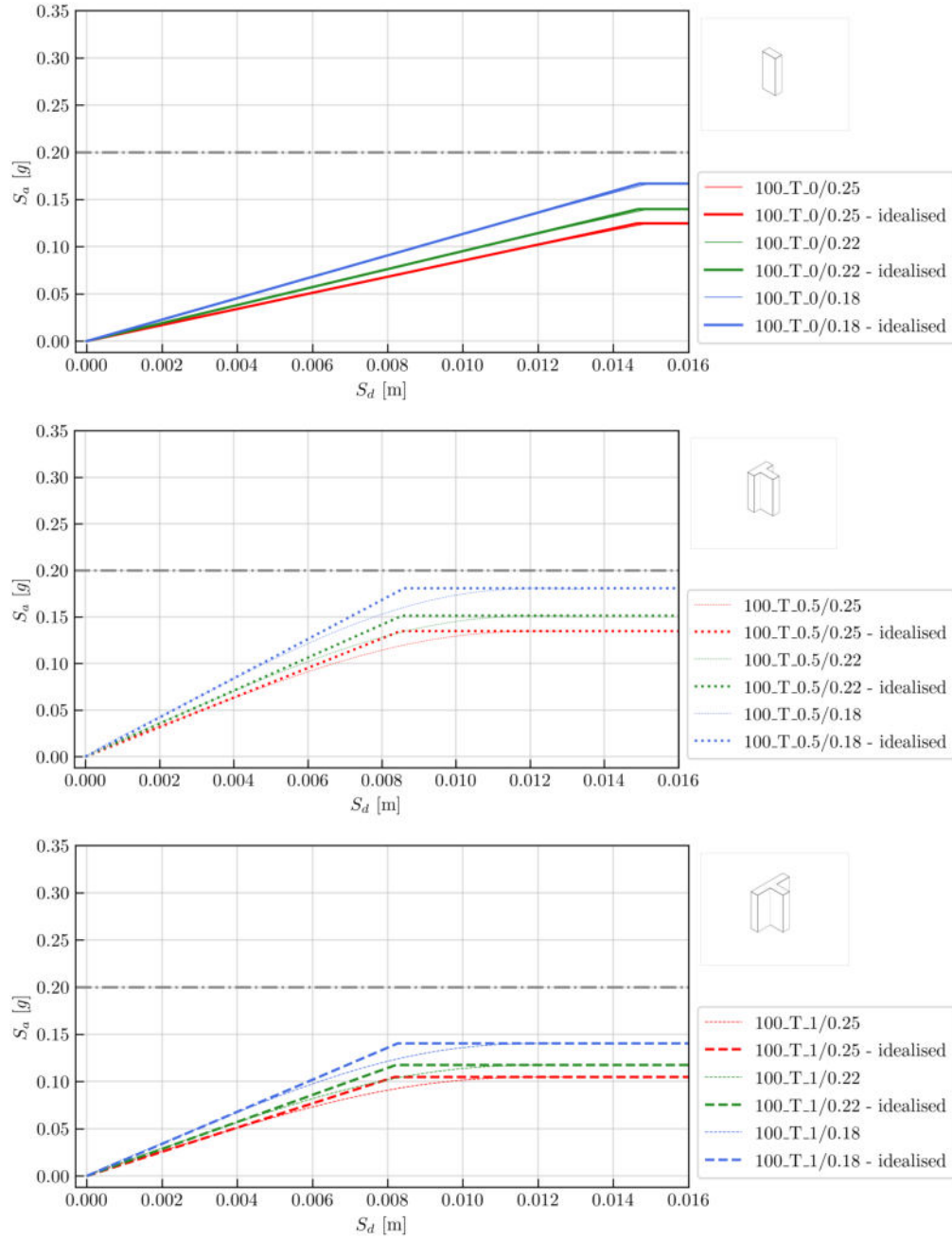


Figure 8.39: Seismic capacity: 100_T

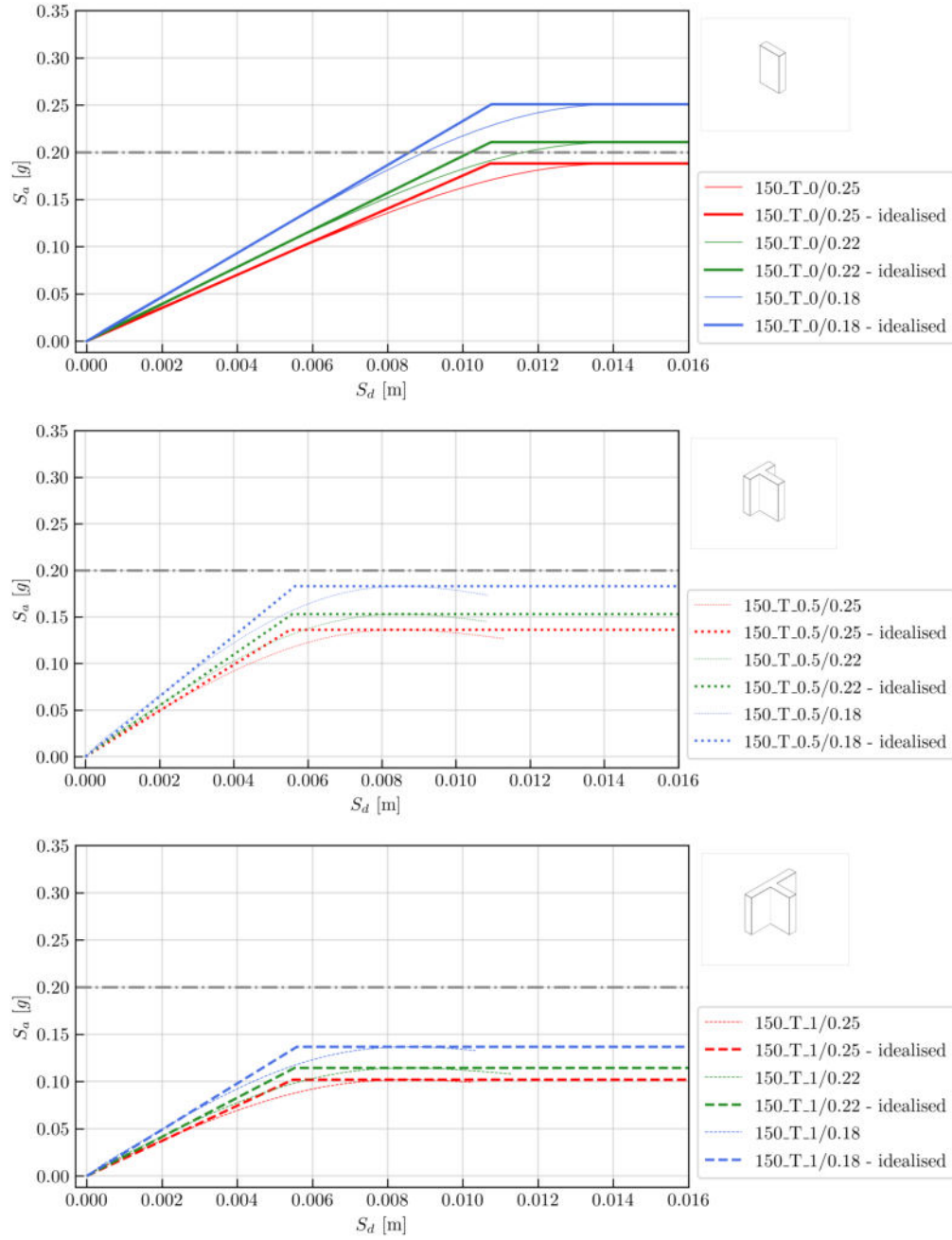


Figure 8.40: Seismic capacity: 150_T

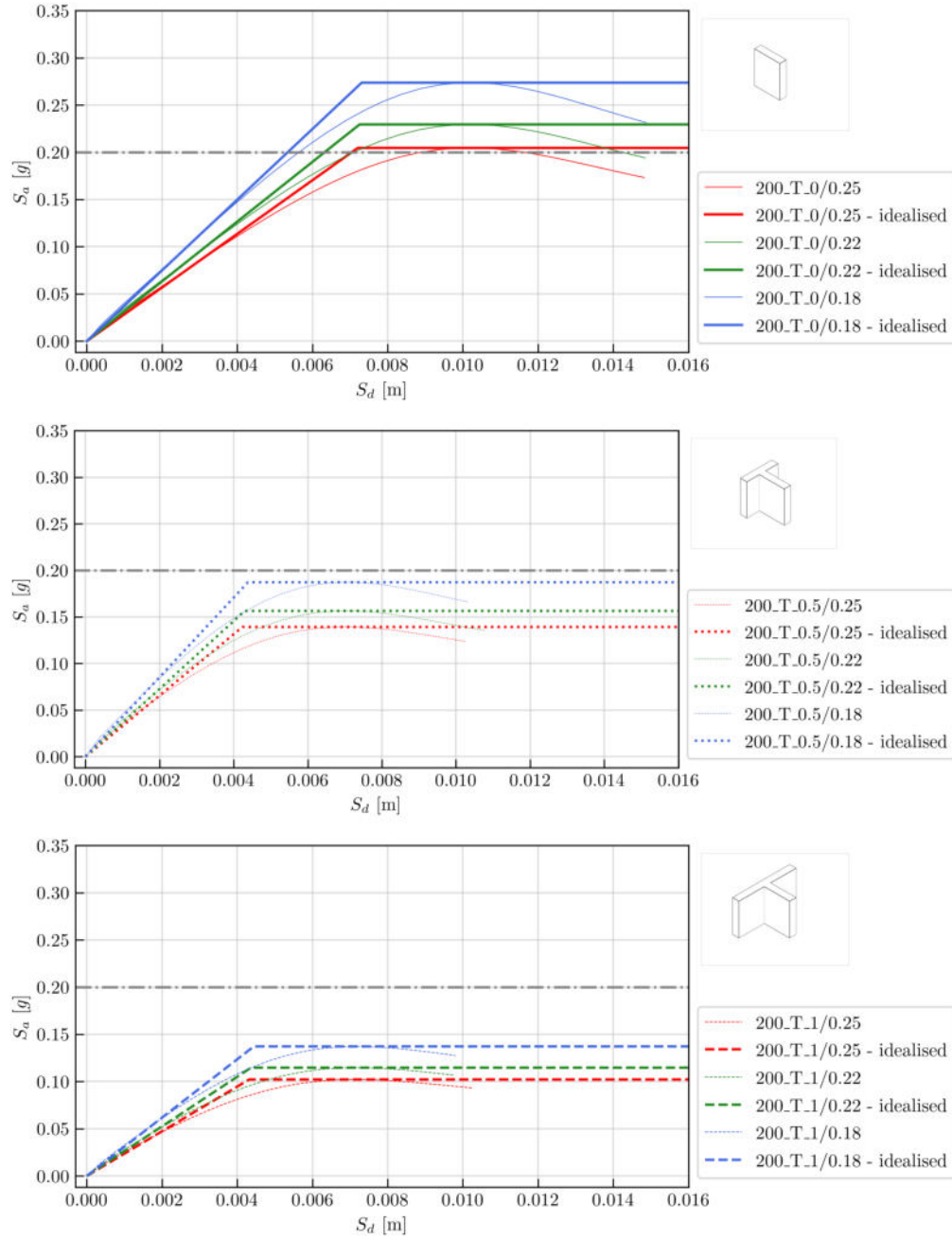


Figure 8.41: Seismic capacity: 200_T

Appendix C: Superposition with response spectrum - current Eurocode 8 (*OLD EC8*)

In the following figures, (Figure 8.42 through Figure 8.59, bilinear idealisation of seismic capacity curves is overlapped with the elastic response spectrum determined according to current Eurocode 8 (EN 1998-1), for three ground types (A, B and C). Bilinear curves are again colour-coded according to the vertical stress intensity, while line styles represent different wall systems. The intersection point of each bilinear curve with the corresponding response spectrum curve is marked with a circular point, coloured the same as a response spectrum curve.

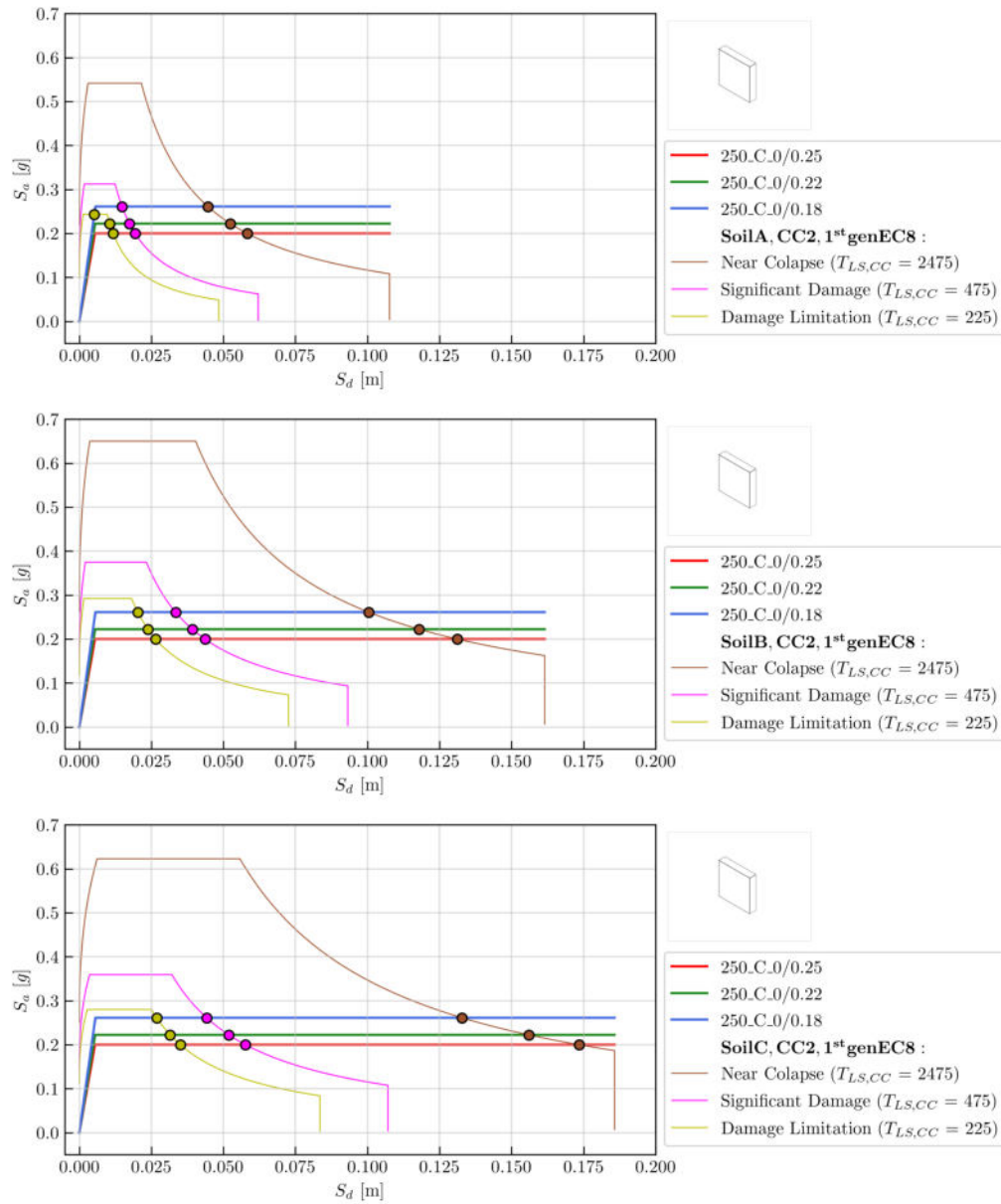


Figure 8.42: Superposition with response spectrum: 250_C_0

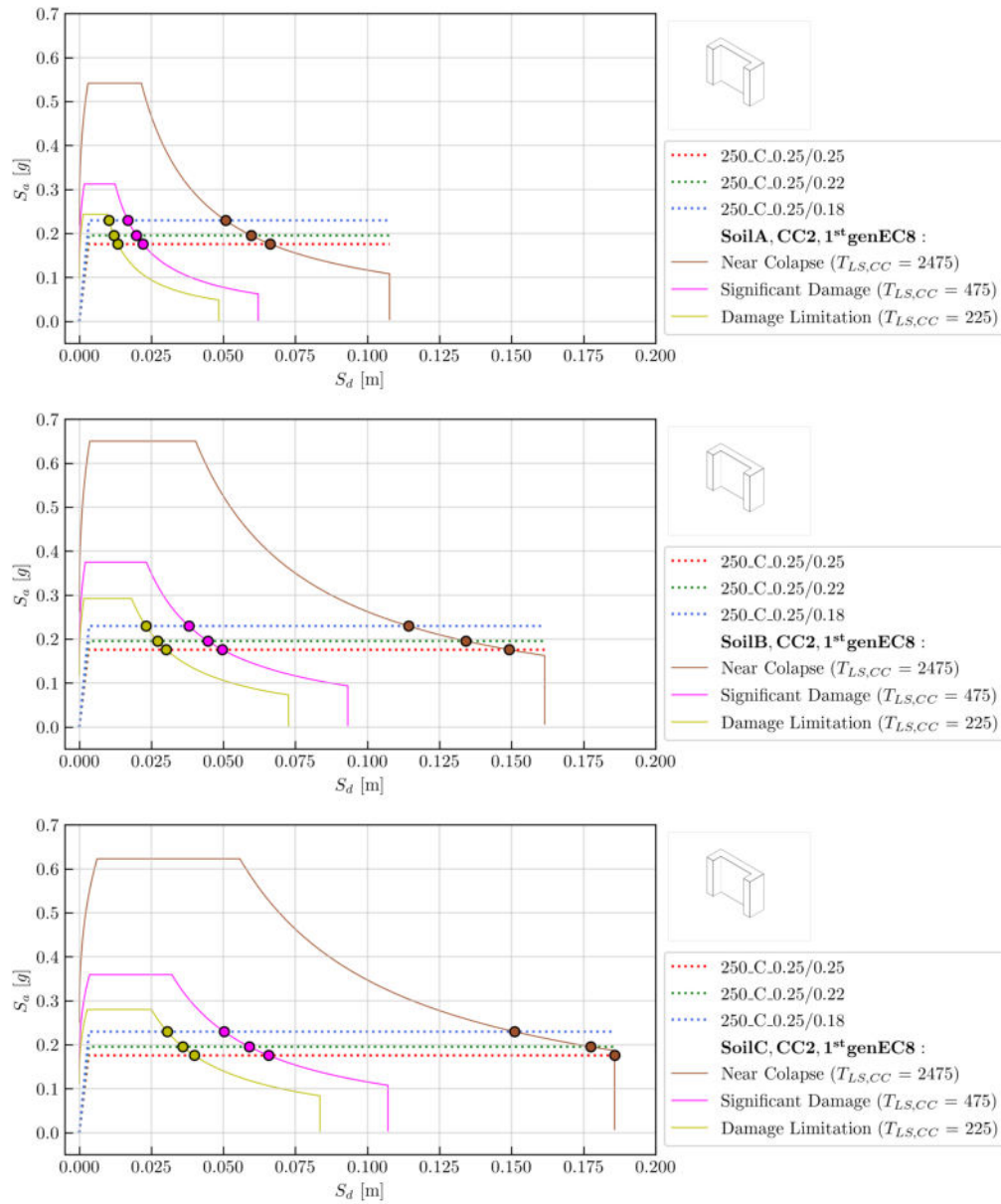


Figure 8.43: Superposition with response spectrum: 250_C_0.25

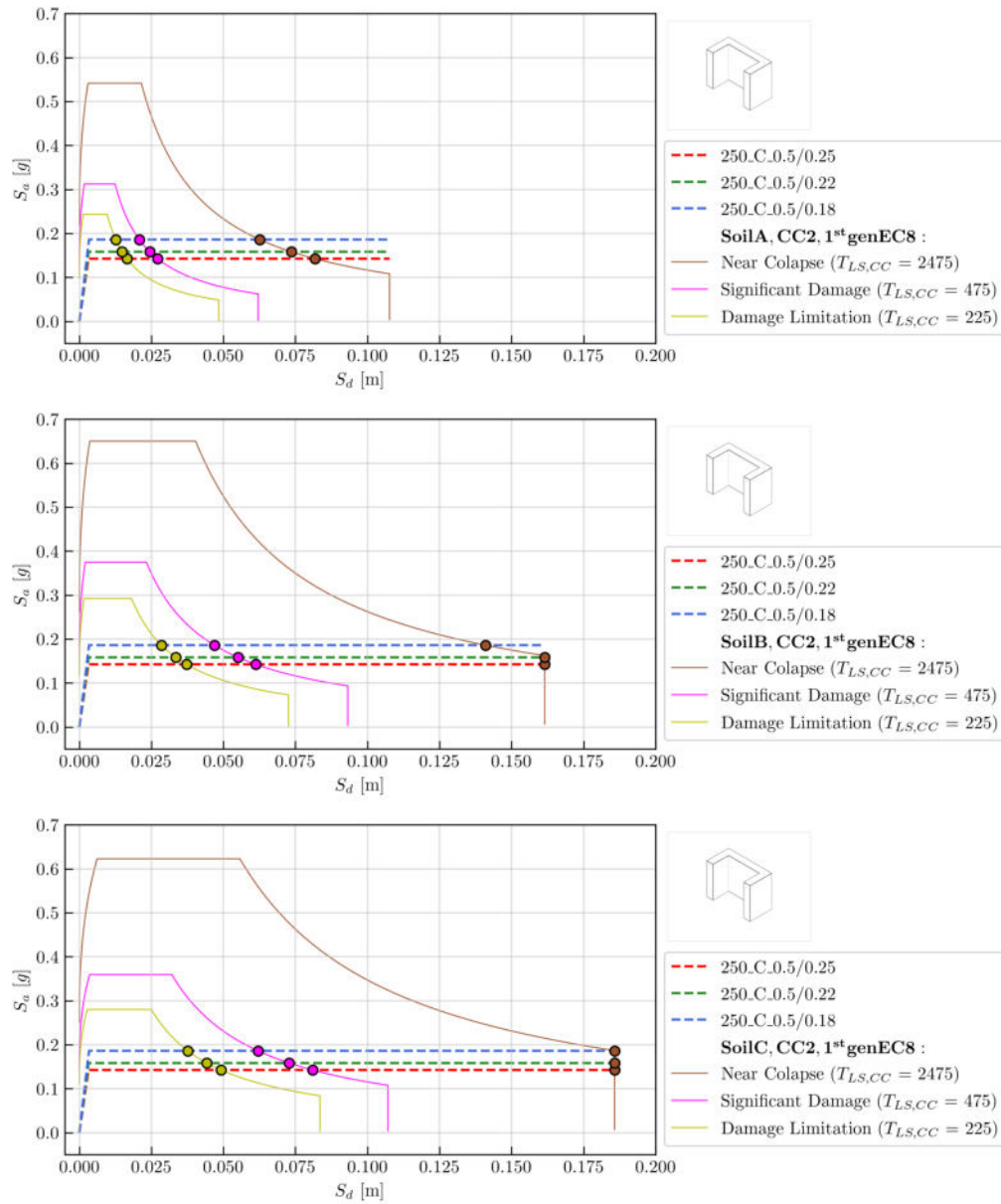


Figure 8.44: Superposition with response spectrum: 250_C_0.5

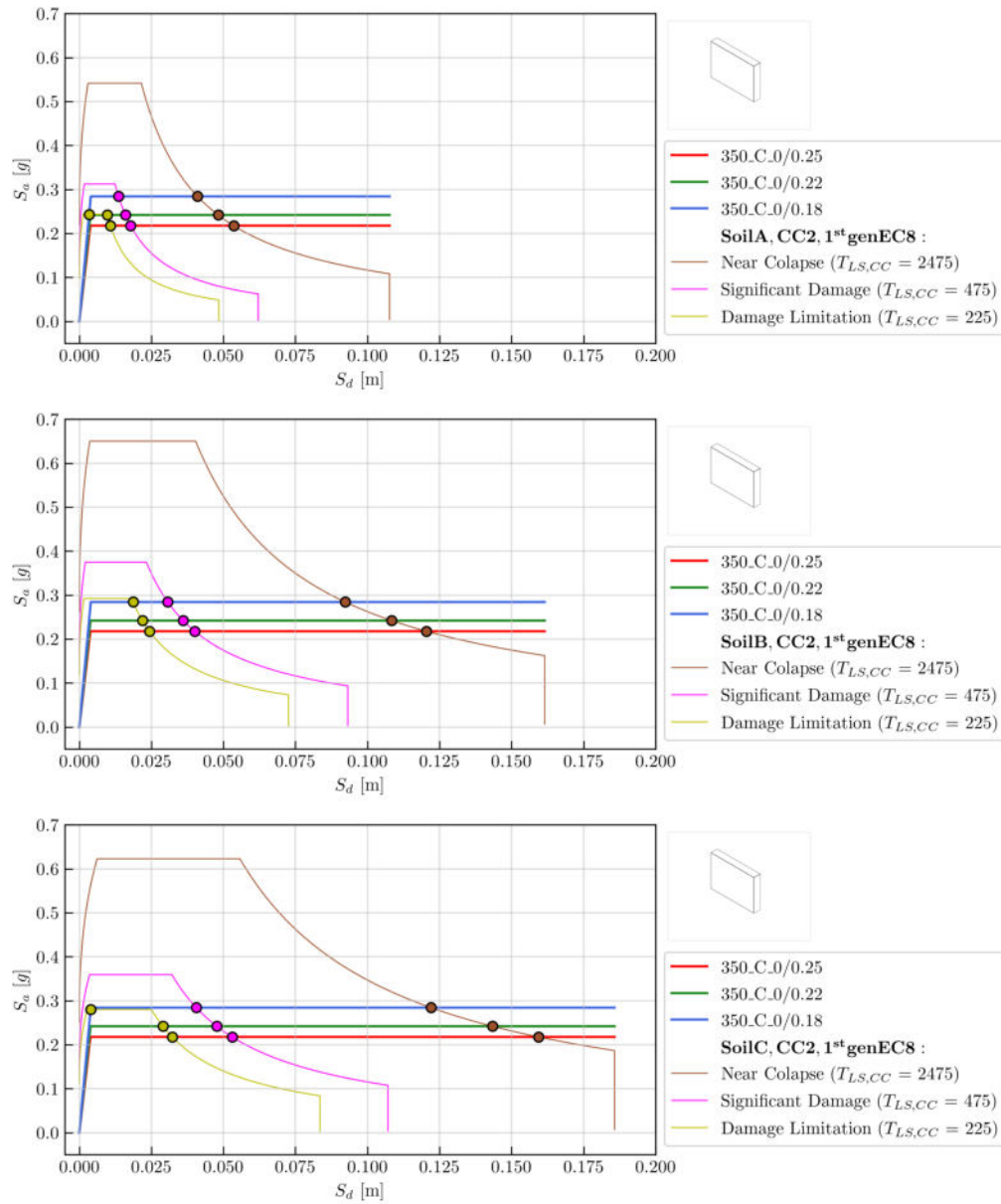


Figure 8.45: Superposition with response spectrum: 350_C_0

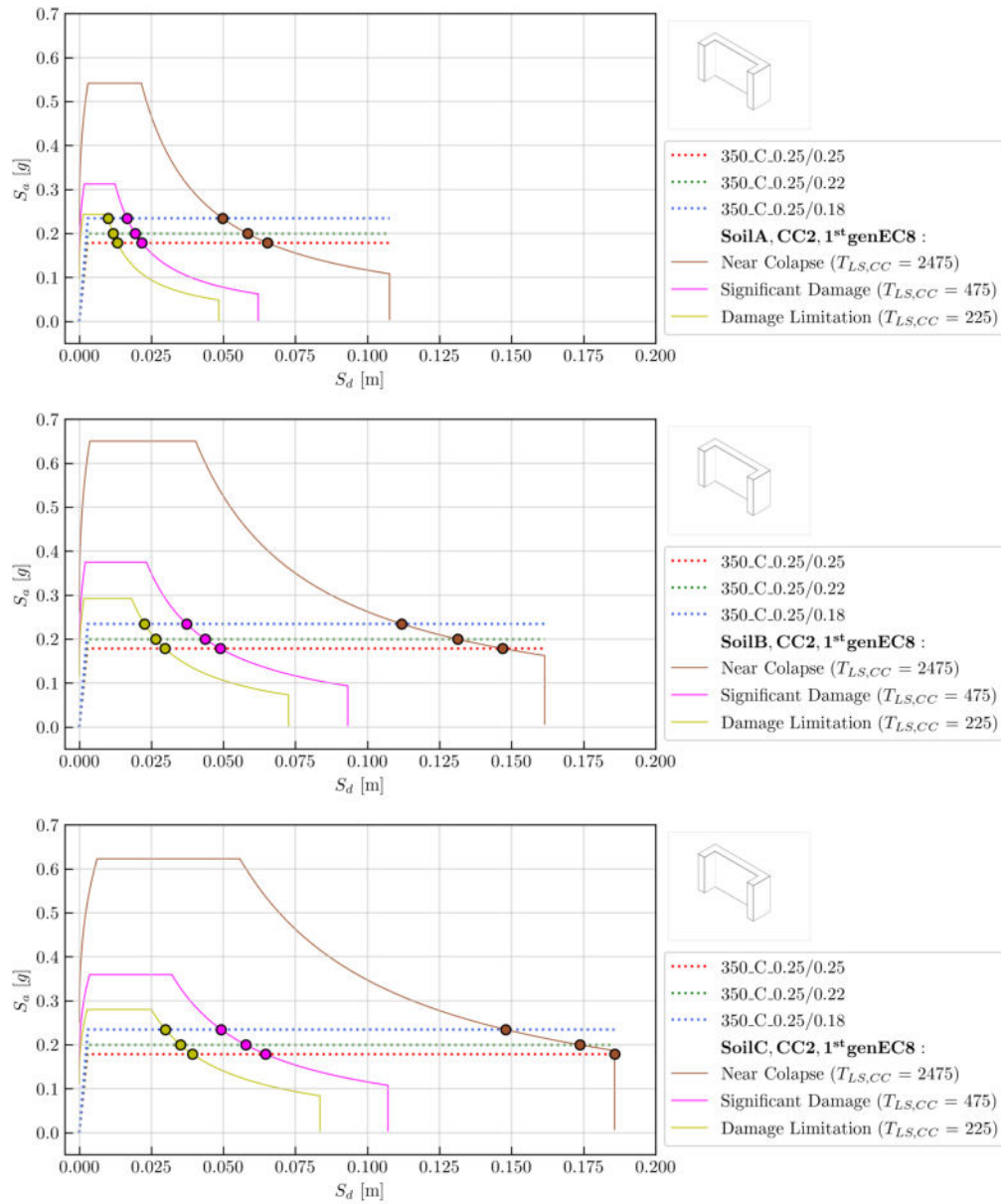


Figure 8.46: Superposition with response spectrum: 350_C_0.25

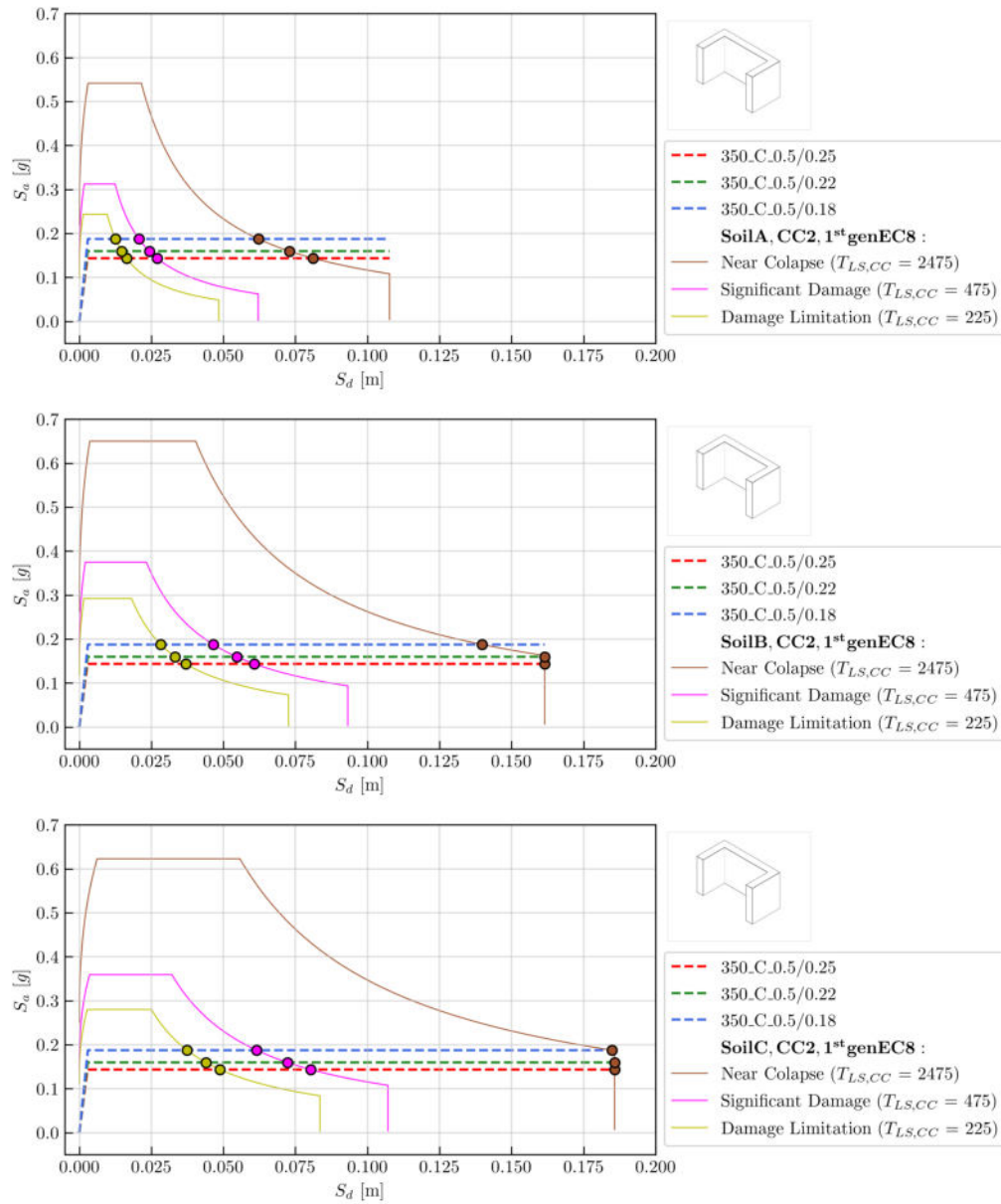


Figure 8.47: Superposition with response spectrum: 350_C_0.5

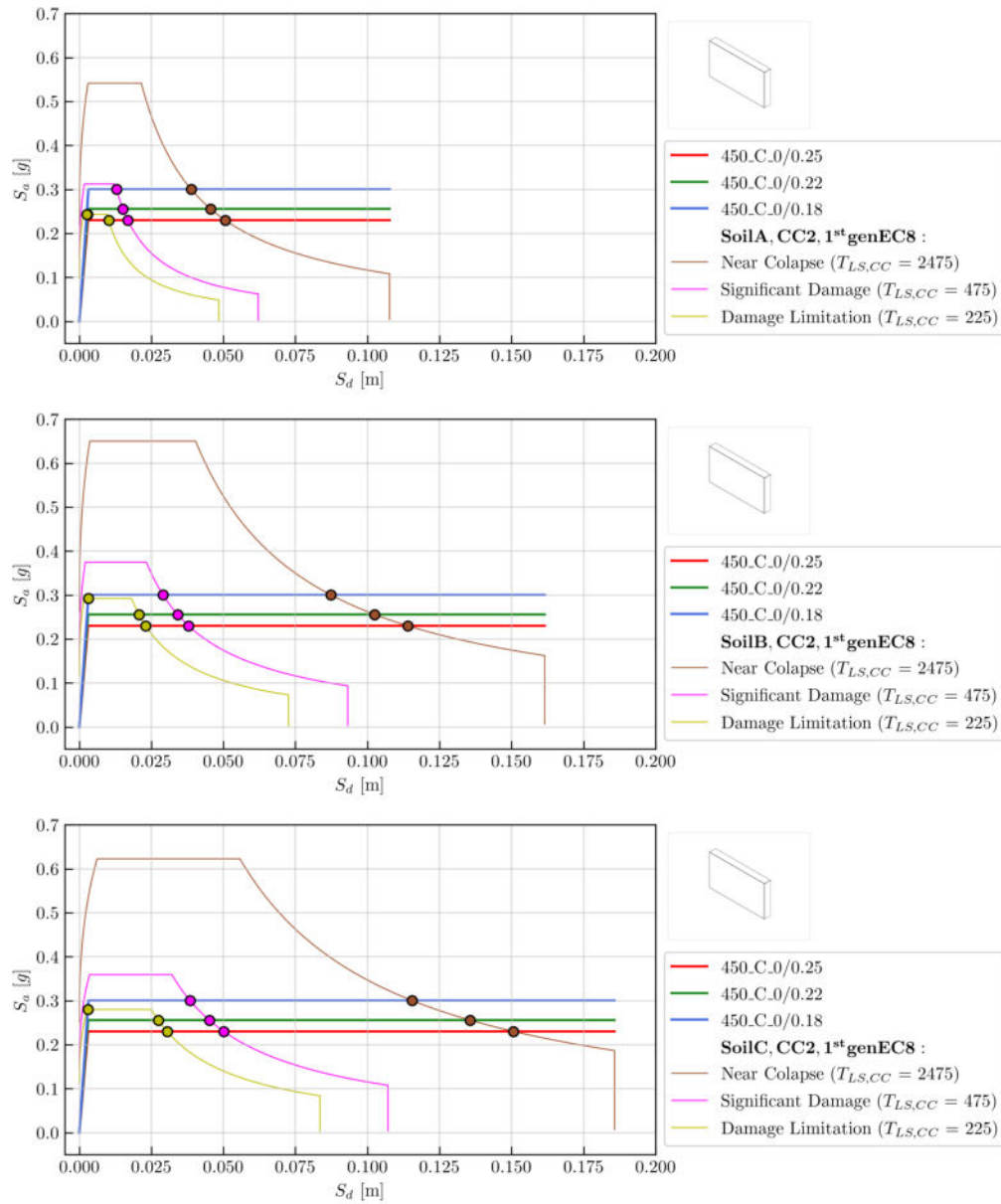


Figure 8.48: Superposition with response spectrum: 450_C_0

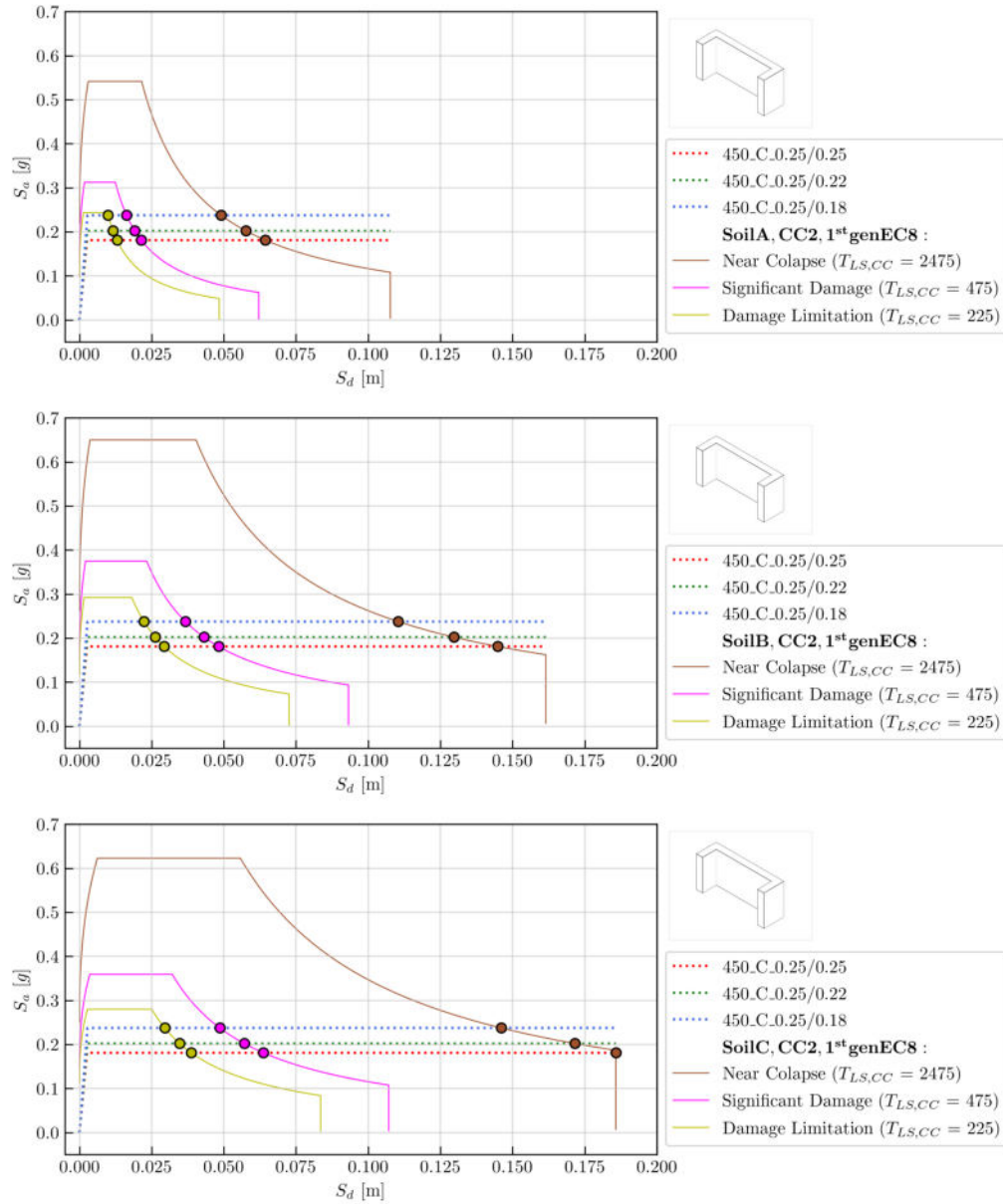


Figure 8.49: Superposition with response spectrum: 450_C_0.25

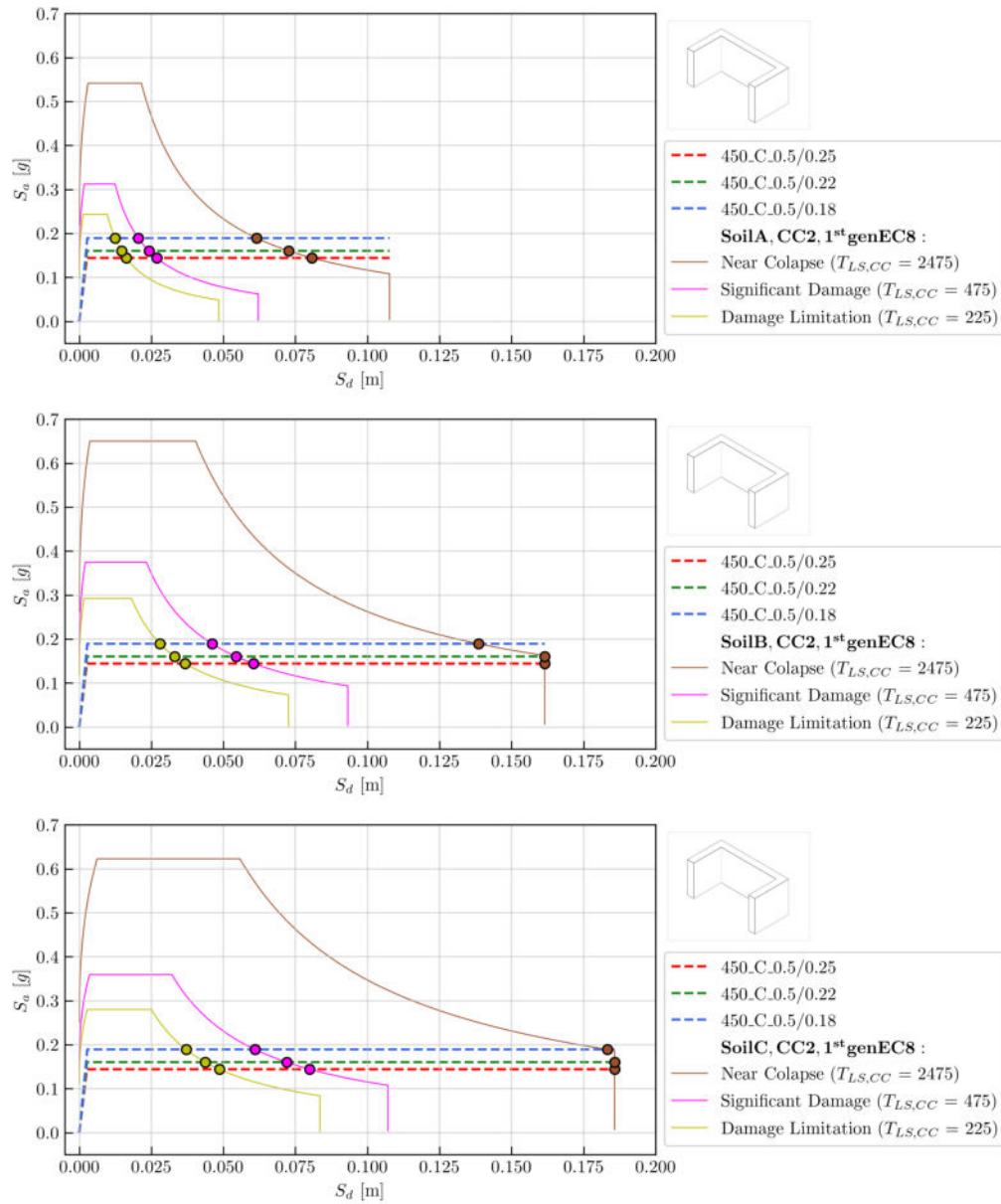


Figure 8.50: Superposition with response spectrum: 450_C_0.5

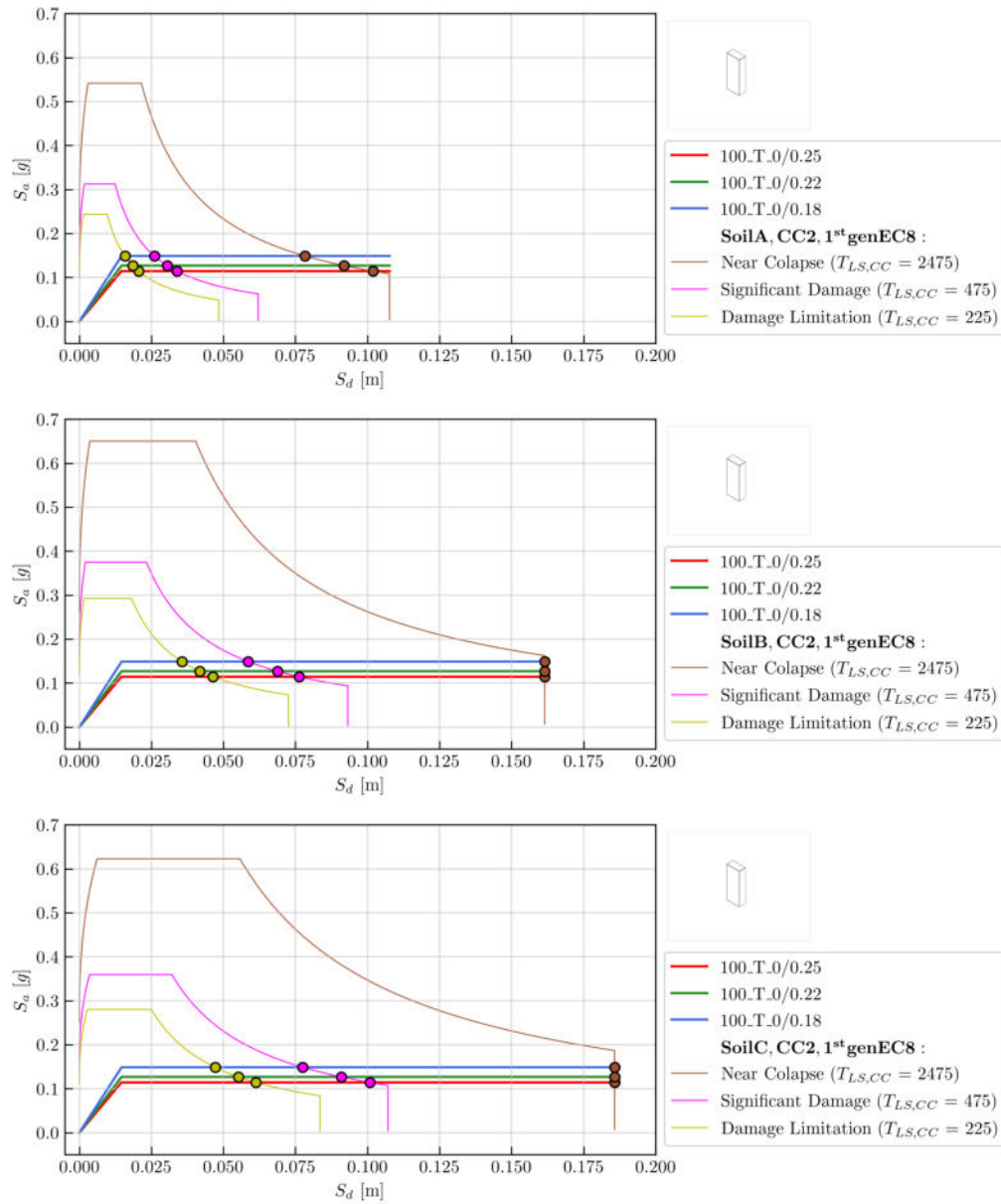


Figure 8.51: Superposition with response spectrum: 100_T_0

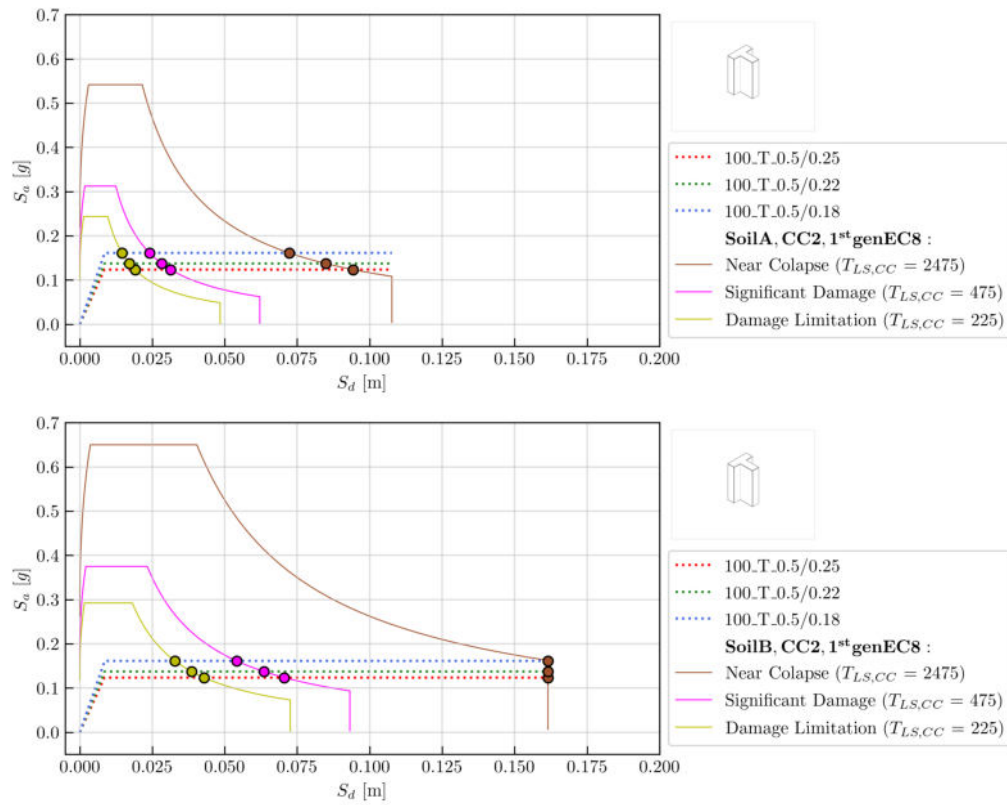


Figure 8.52: Superposition with response spectrum: 100_T_0.5

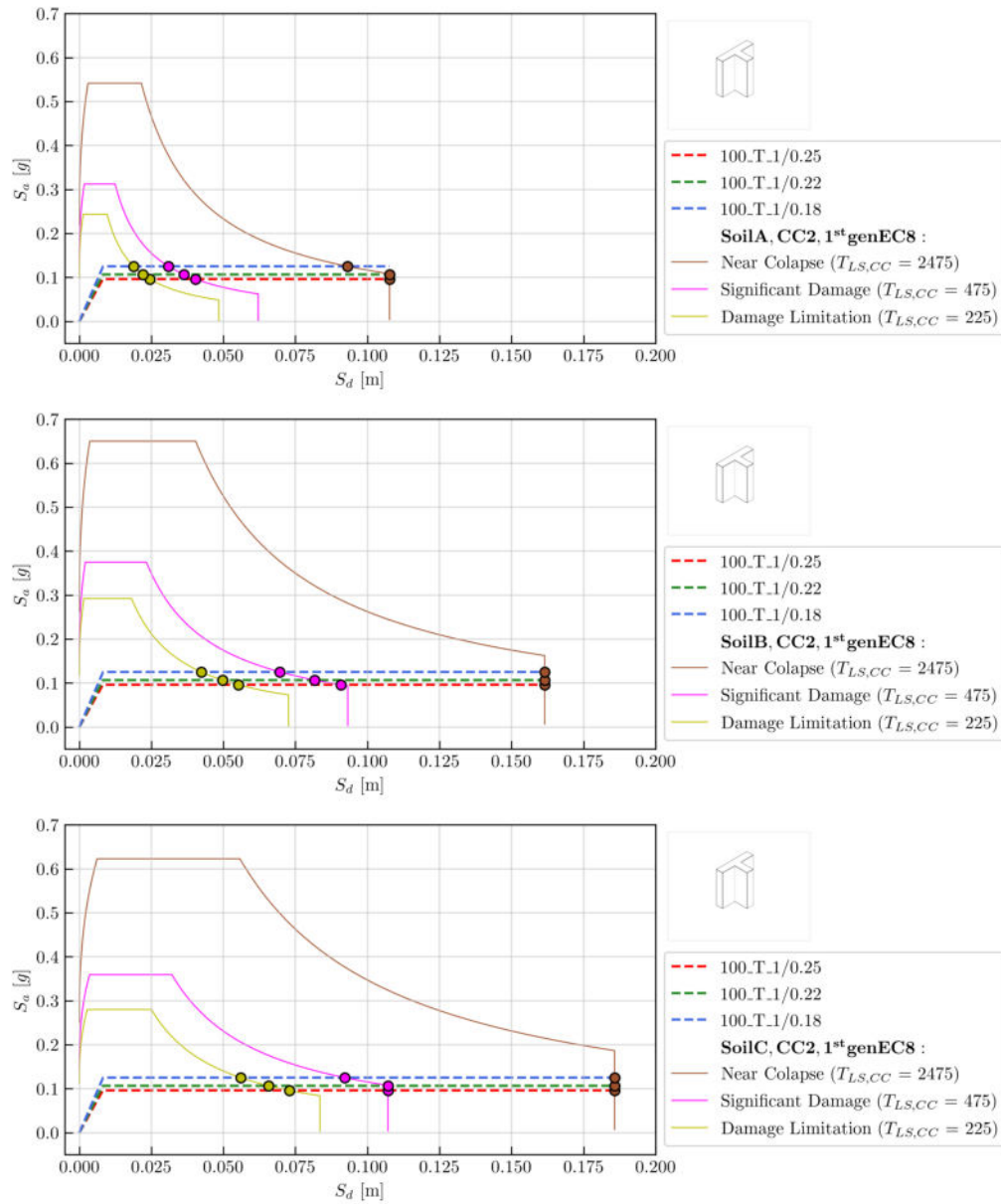


Figure 8.53: Superposition with response spectrum: 100_T_1

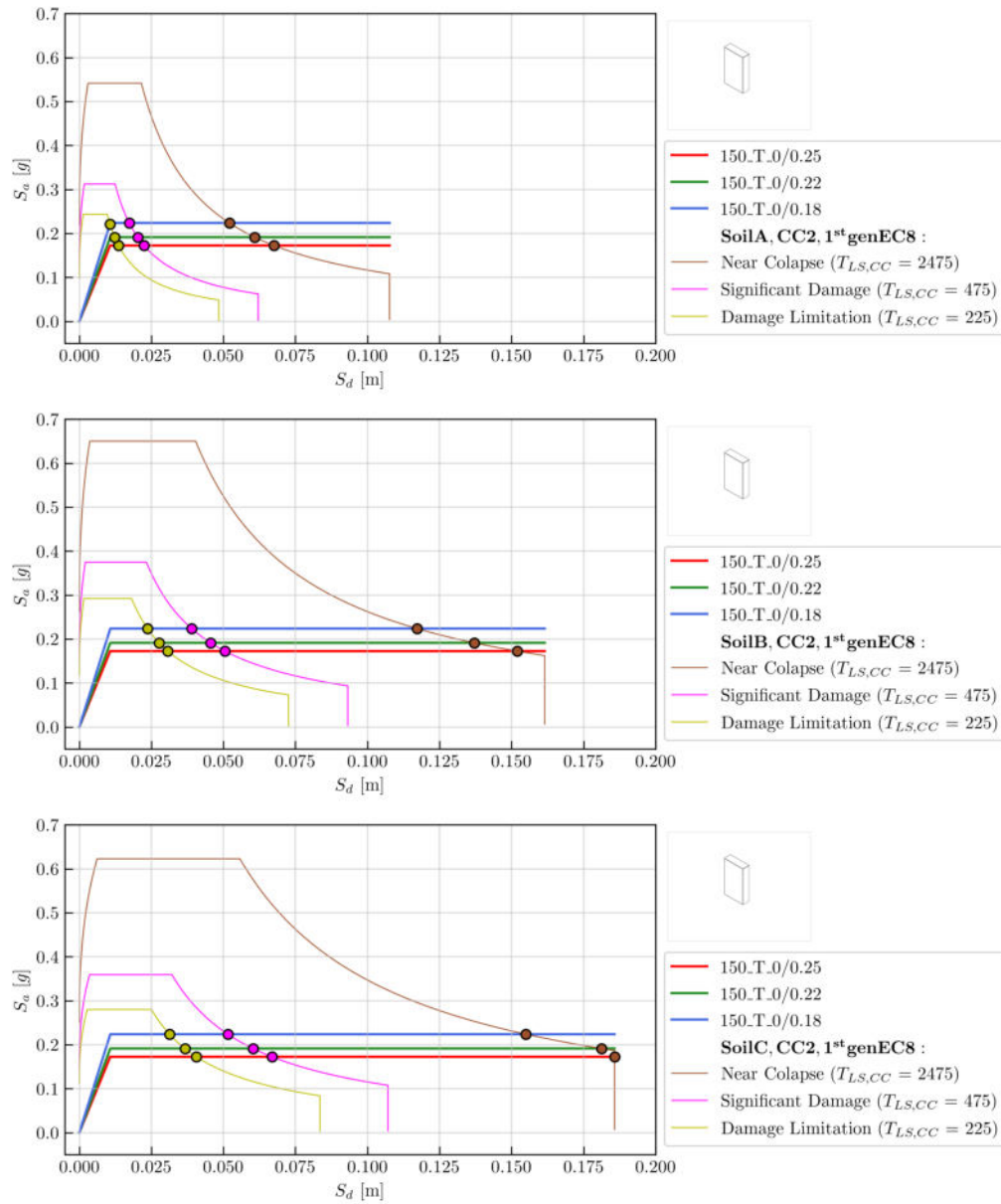


Figure 8.54: Superposition with response spectrum: 150_T_0

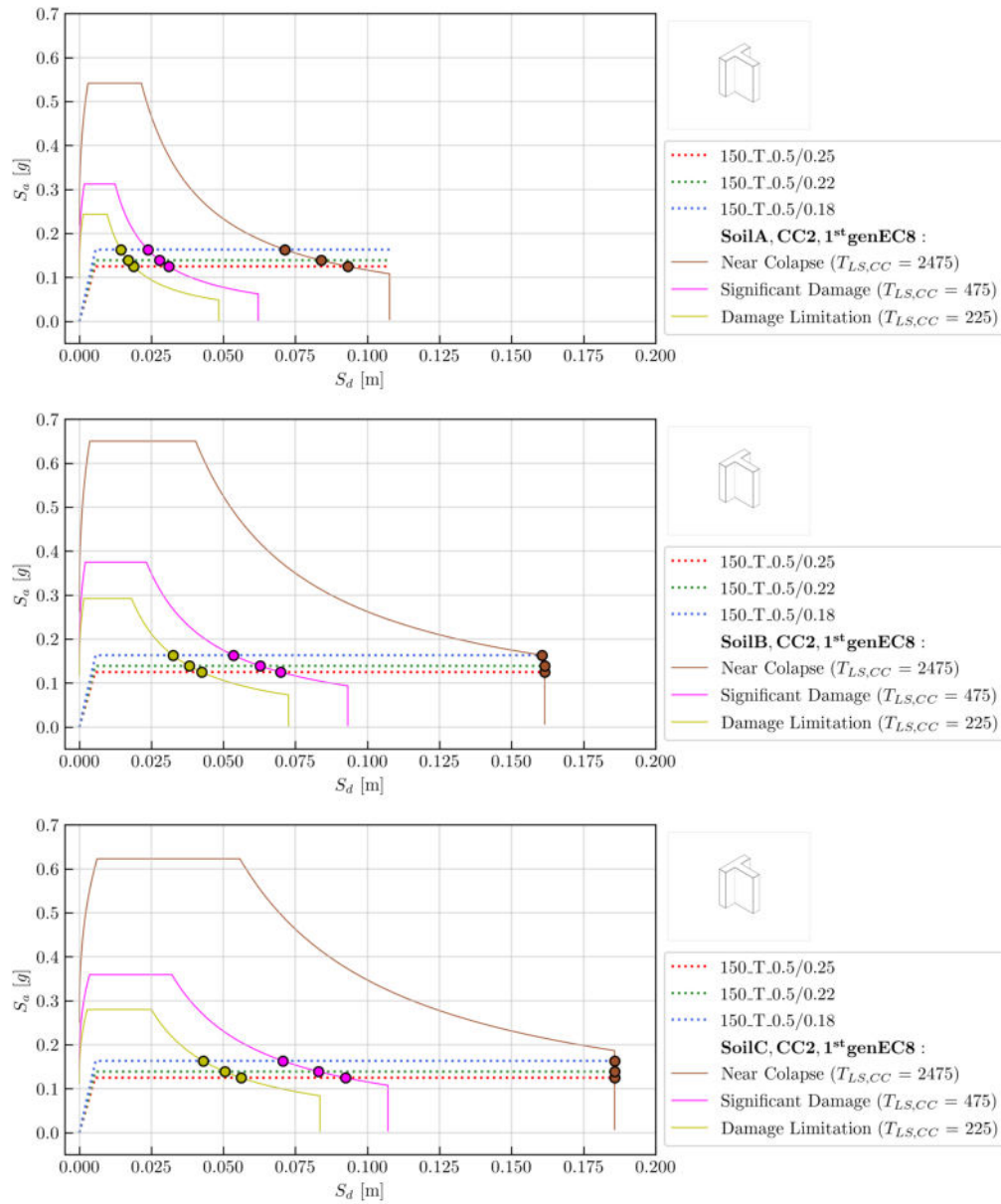


Figure 8.55: Superposition with response spectrum: 150_T_0.5

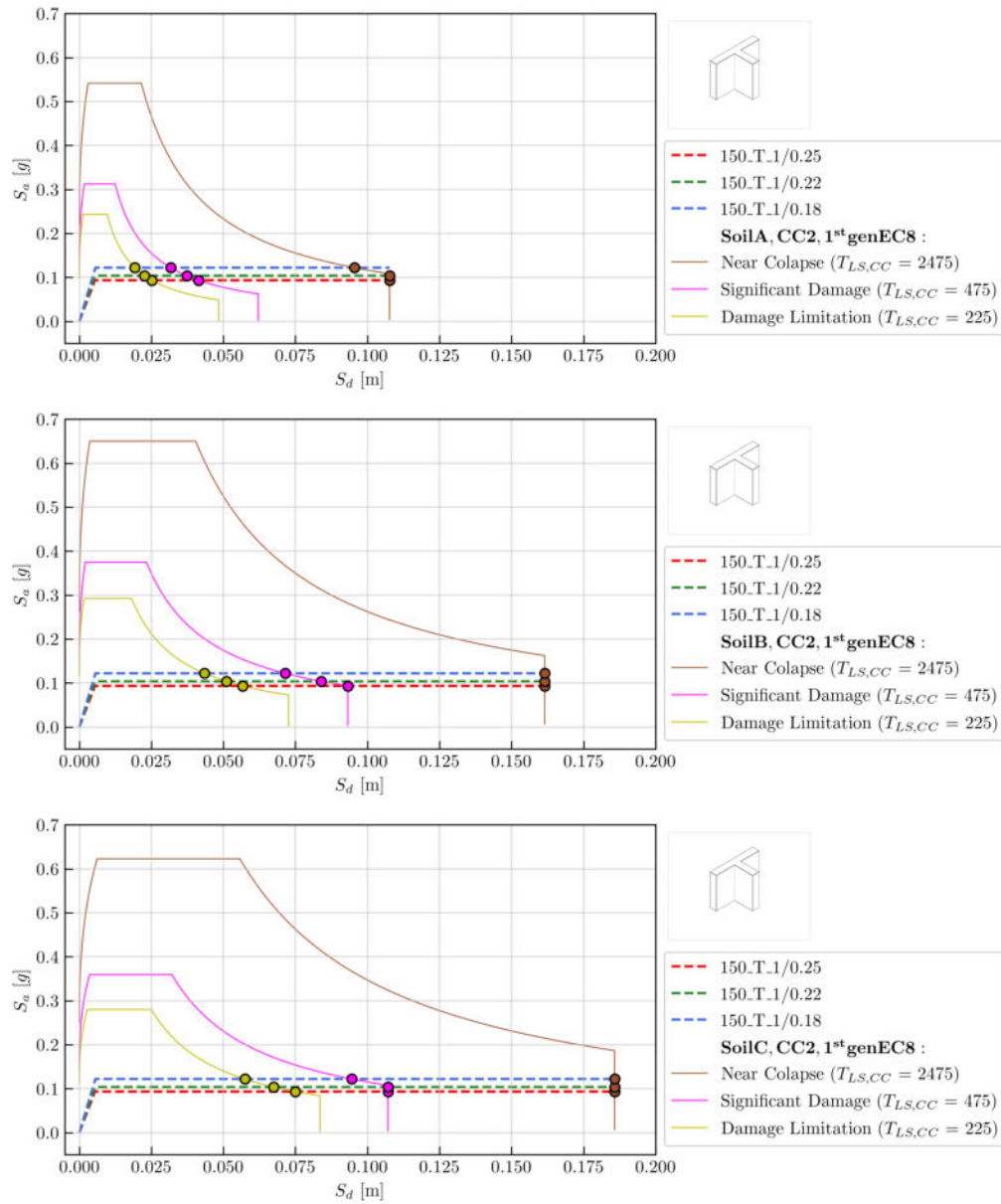


Figure 8.56: Superposition with response spectrum: 150_T_1

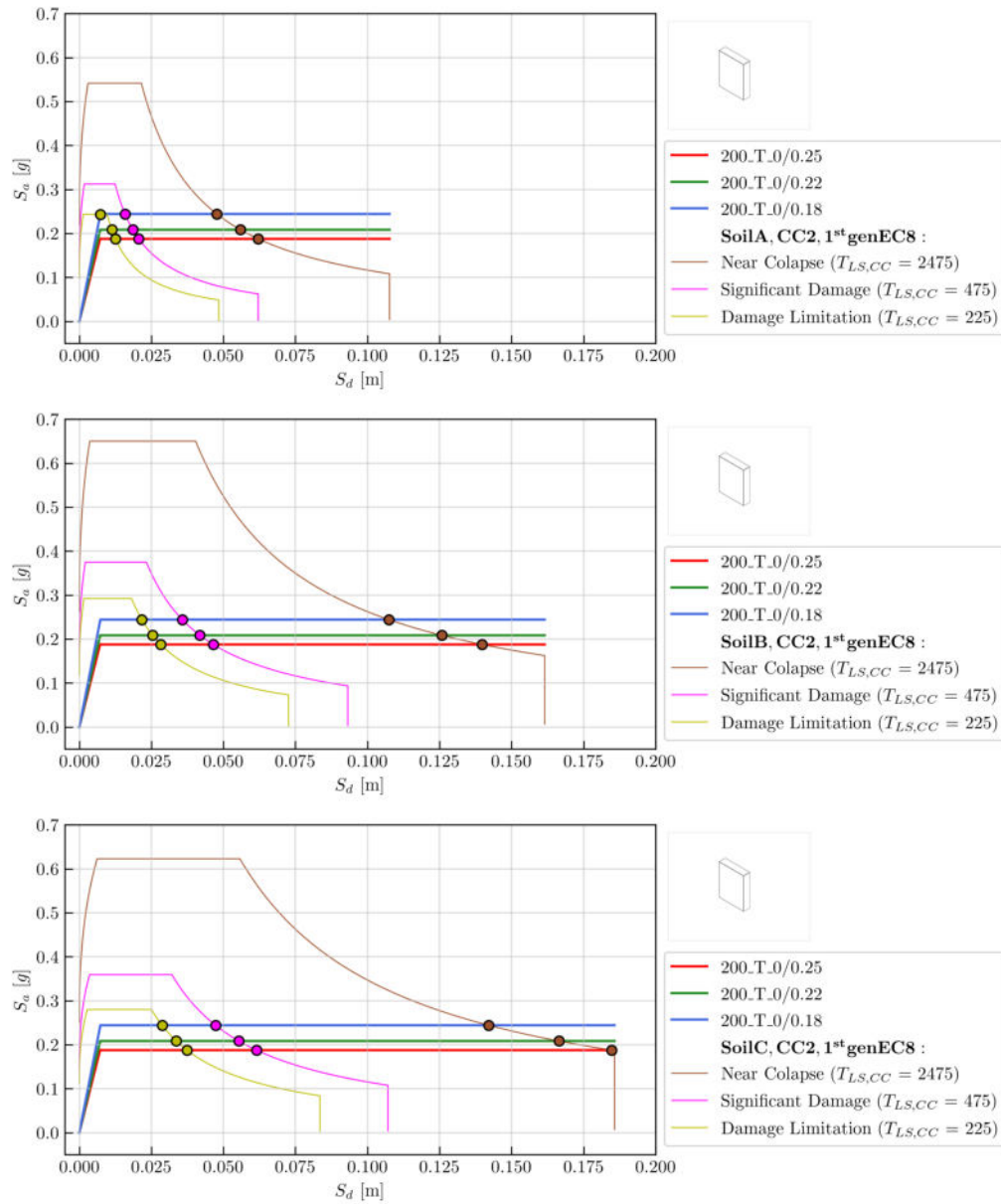


Figure 8.57: Superposition with response spectrum: 200_T_0

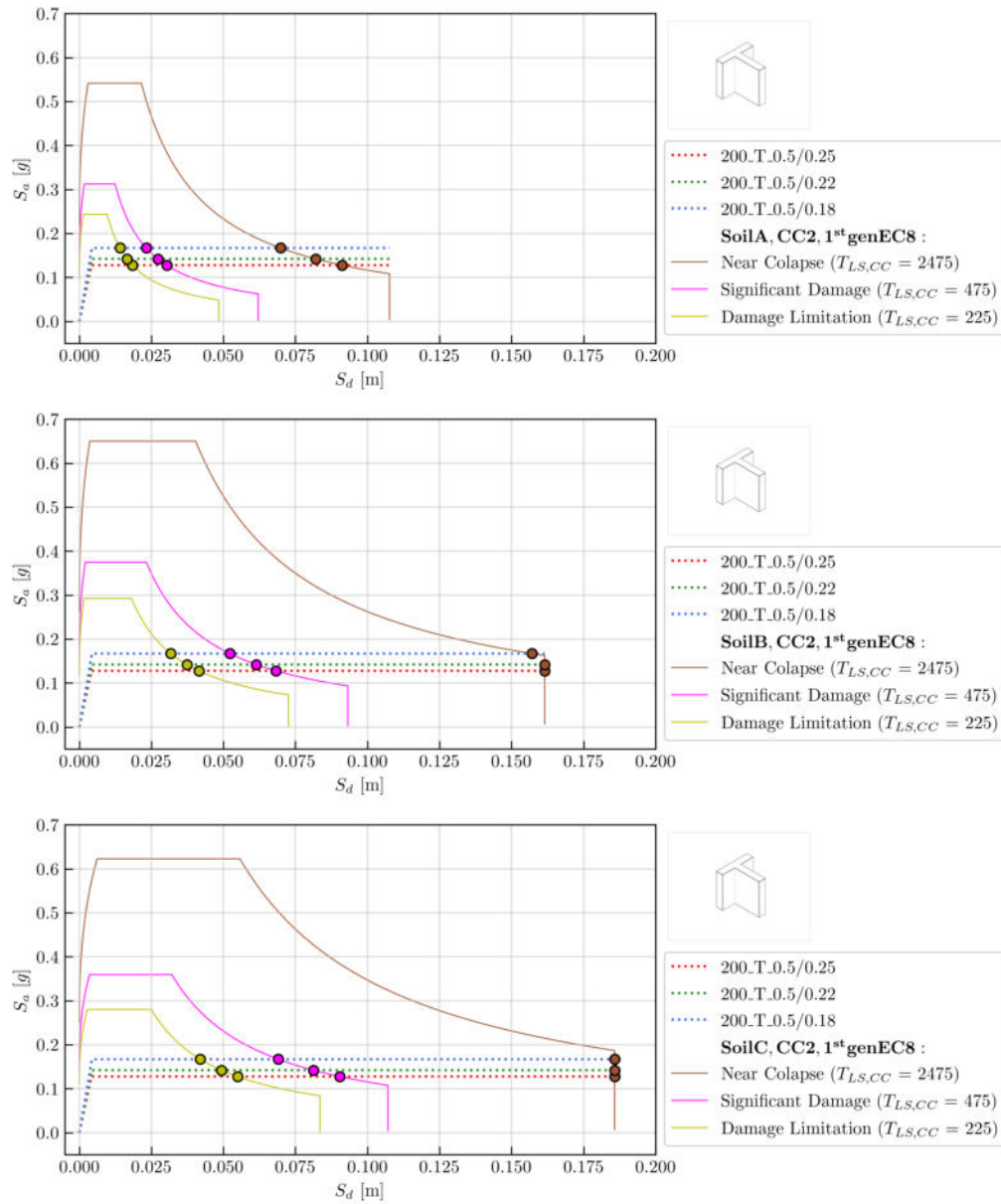


Figure 8.58: Superposition with response spectrum: 200_T_0.5

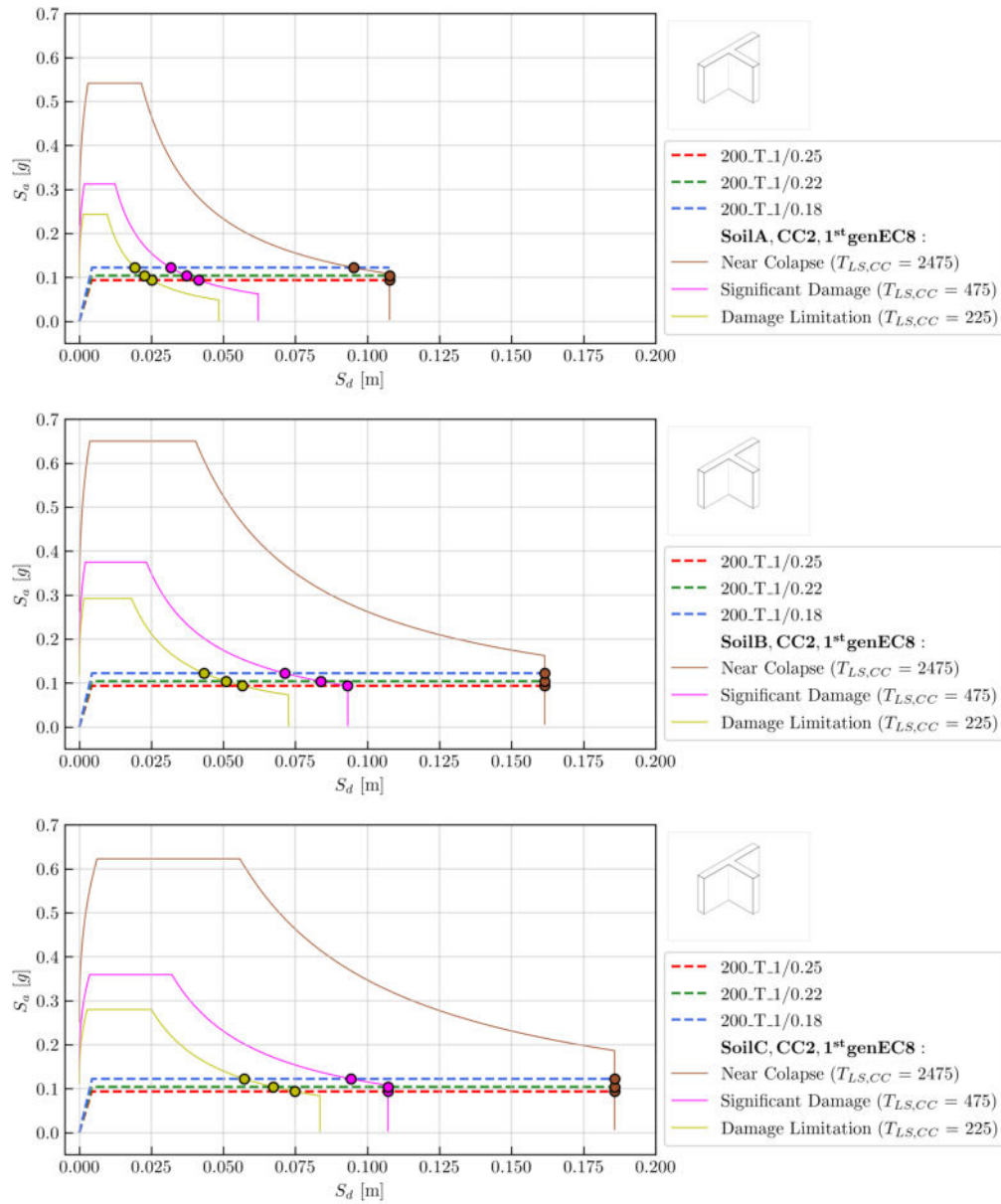


Figure 8.59: Superposition with response spectrum: 200_T_1

Appendix D: Superposition with response spectrum - new generation of Eurocode 8 (*NEW EC8*)

In the following figures, (Figure 8.60 through Figure 8.77, bilinear idealisation of seismic capacity curves is overlapped with the elastic response spectrum determined according to a new generation of Eurocode 8 (Čaušević and Bulić, 2020), for three ground types (A, B and C). Bilinear curves are again colour-coded according to the vertical stress intensity, while line styles represent different wall systems. The intersection point of each bilinear curve with the corresponding response spectrum curve is marked with a circular point, coloured the same as a response spectrum curve.

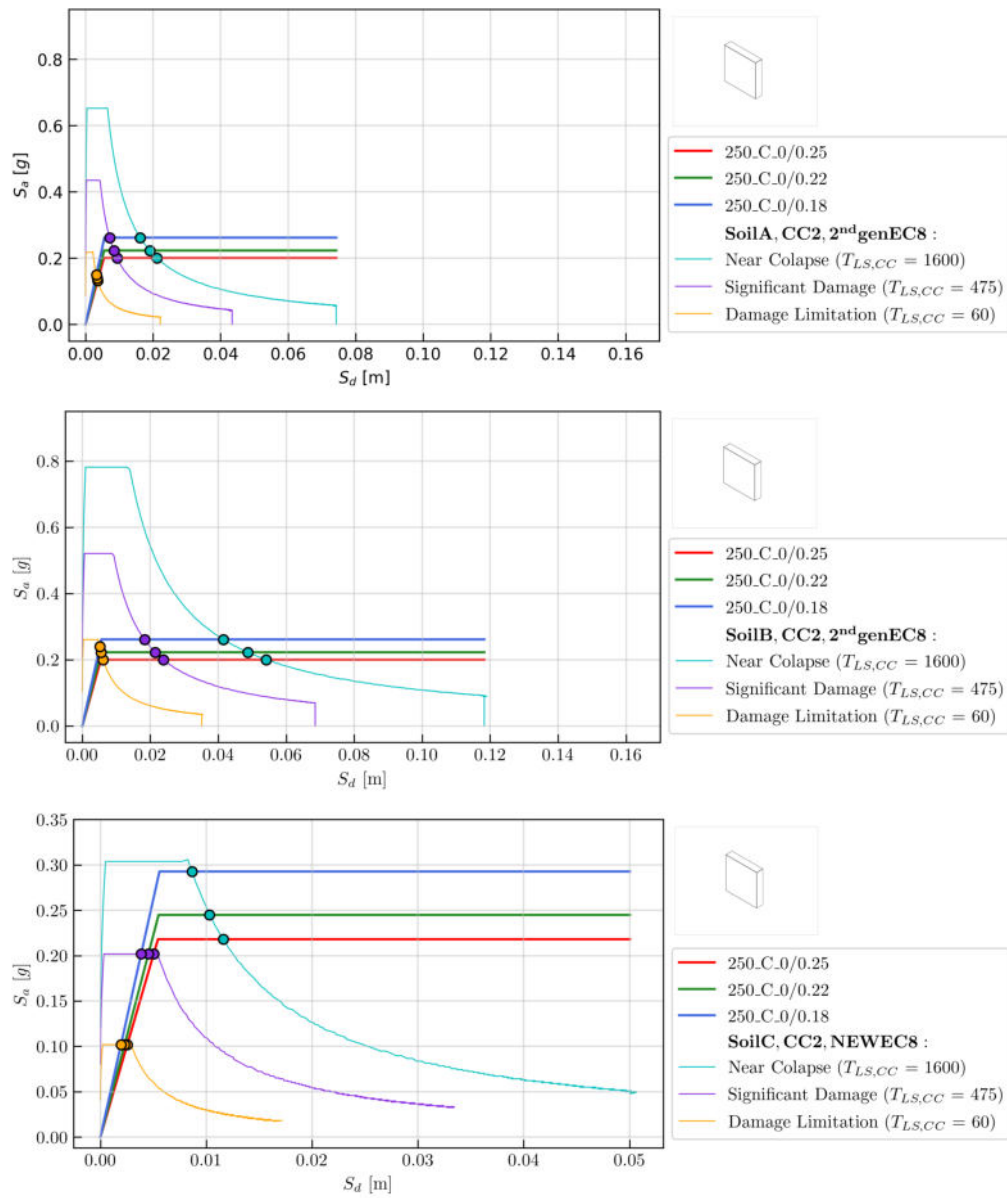


Figure 8.60: Superposition with new response spectrum: 250_C_0

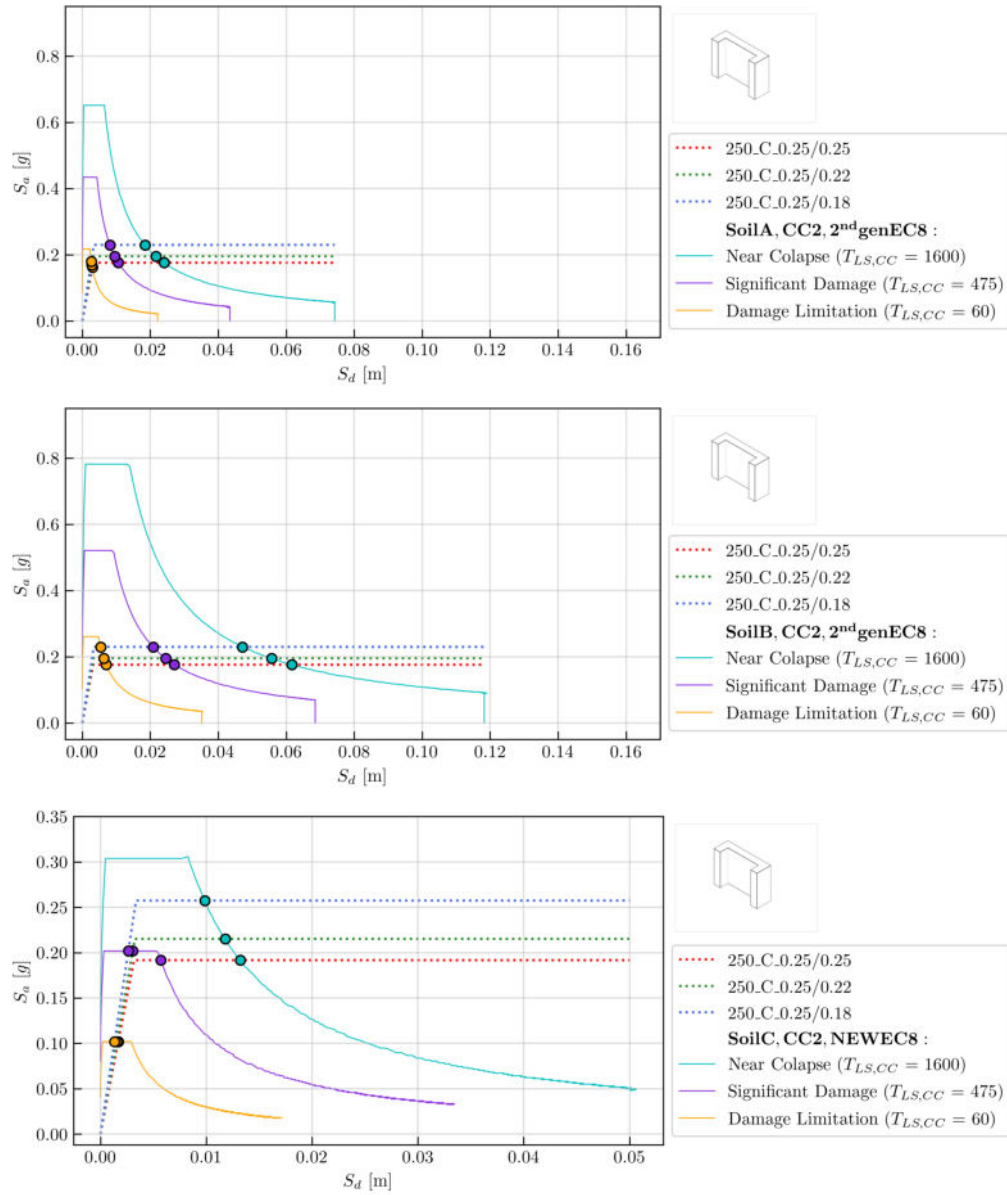


Figure 8.61: Superposition with new response spectrum: 250_C_0.25

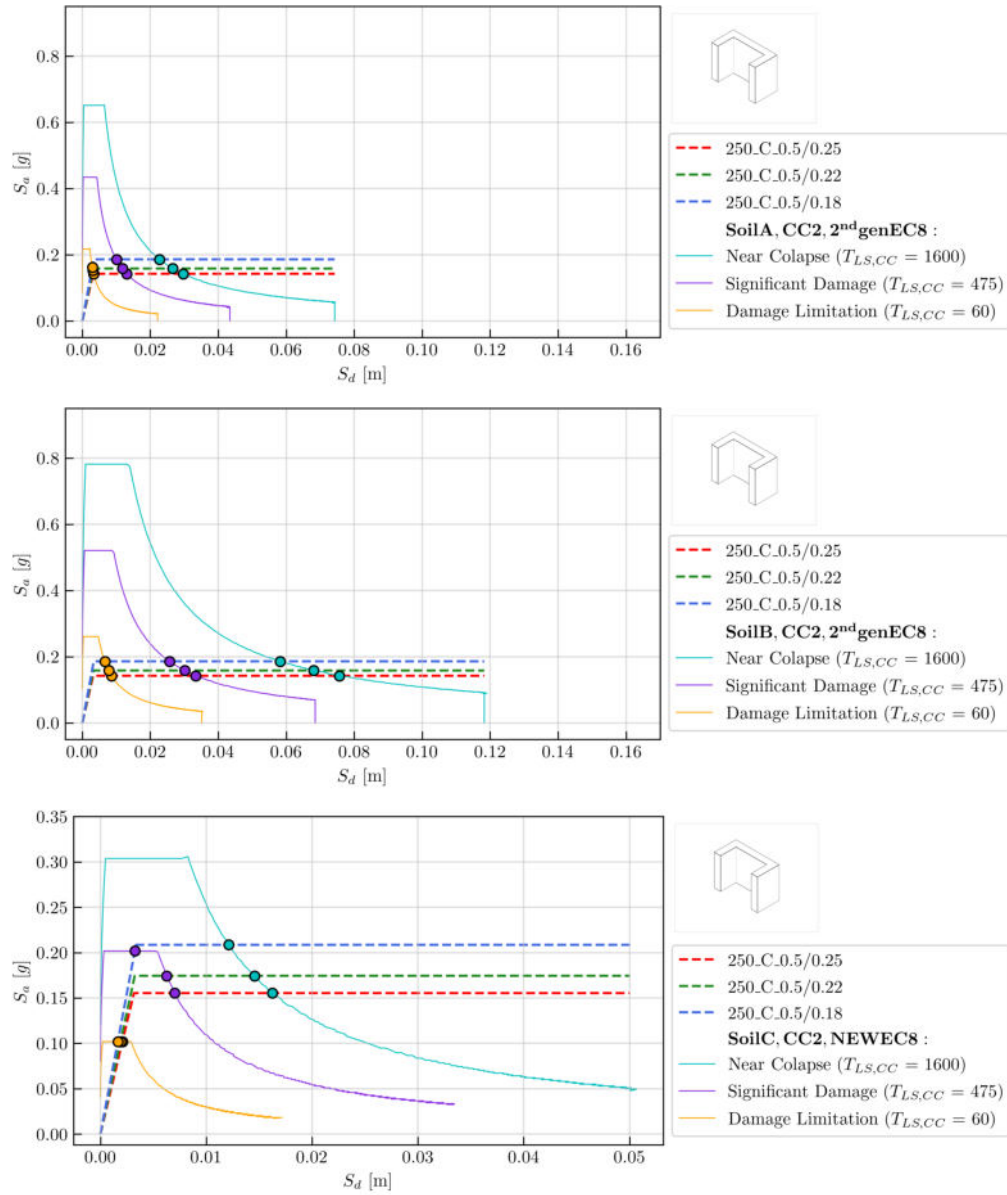


Figure 8.62: Superposition with new response spectrum: 250_C_0.5

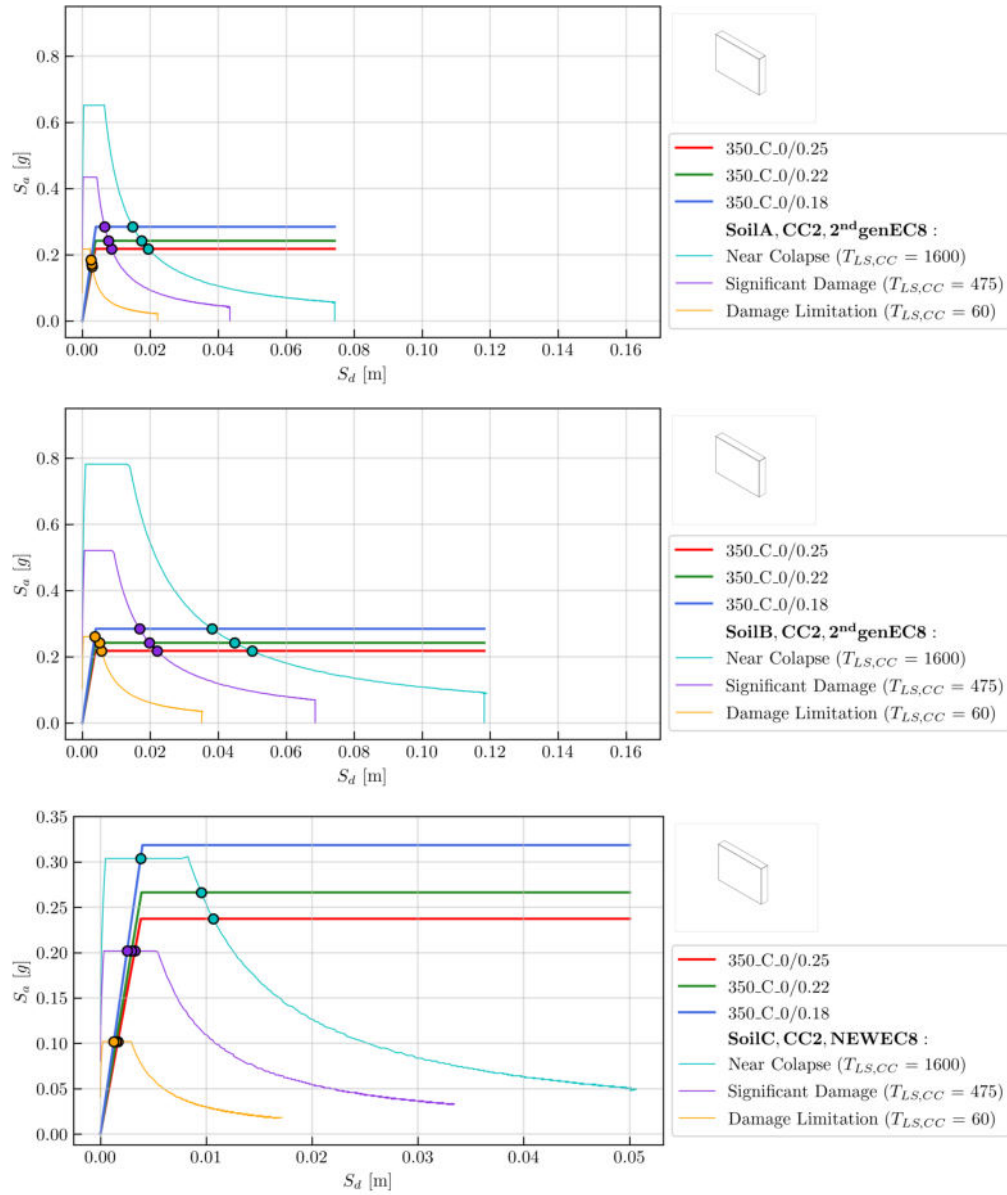


Figure 8.63: Superposition with new response spectrum: 350_C_0

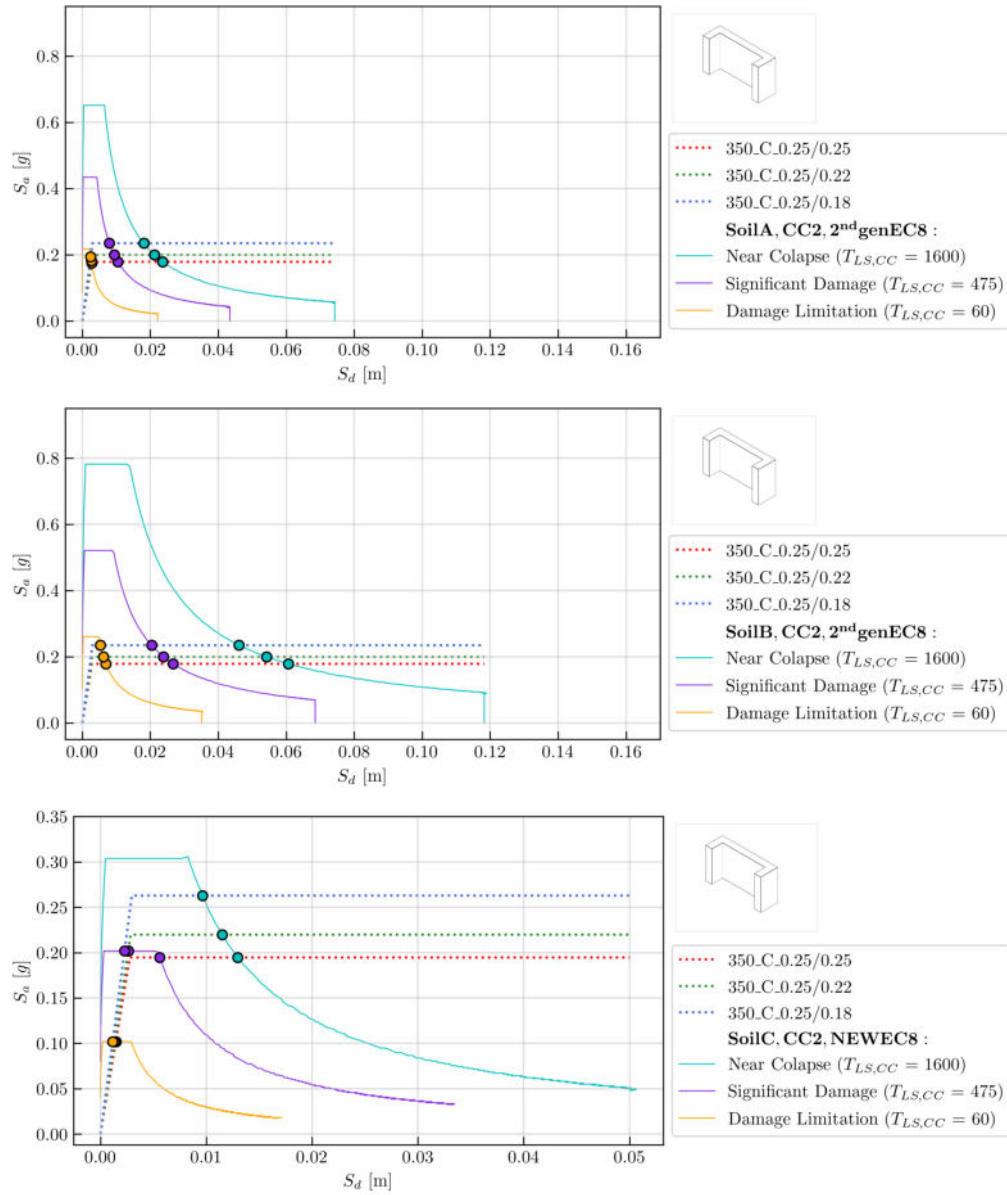


Figure 8.64: Superposition with new response spectrum: 350_C_0.25

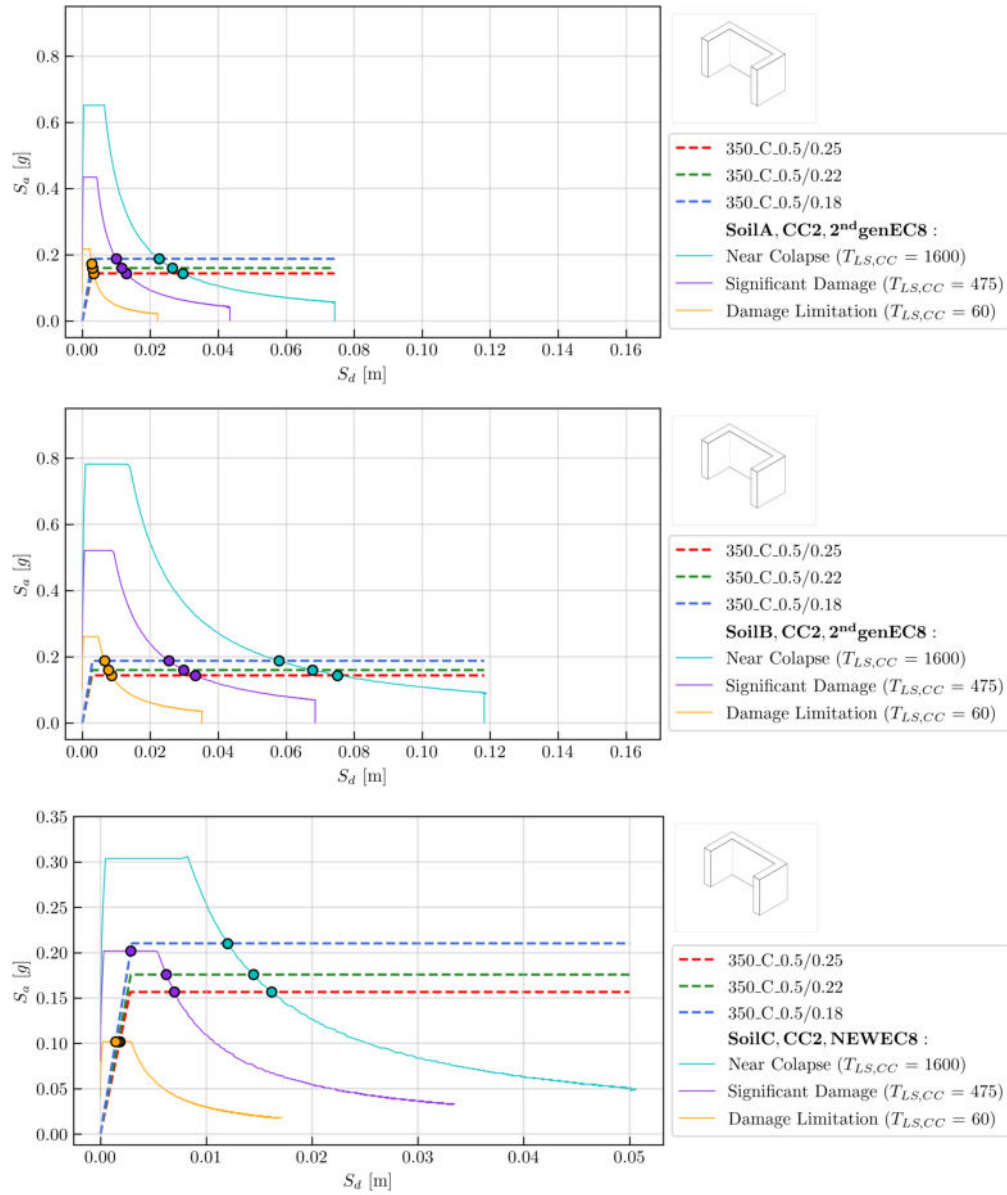


Figure 8.65: Superposition with new response spectrum: 350_C_0.5

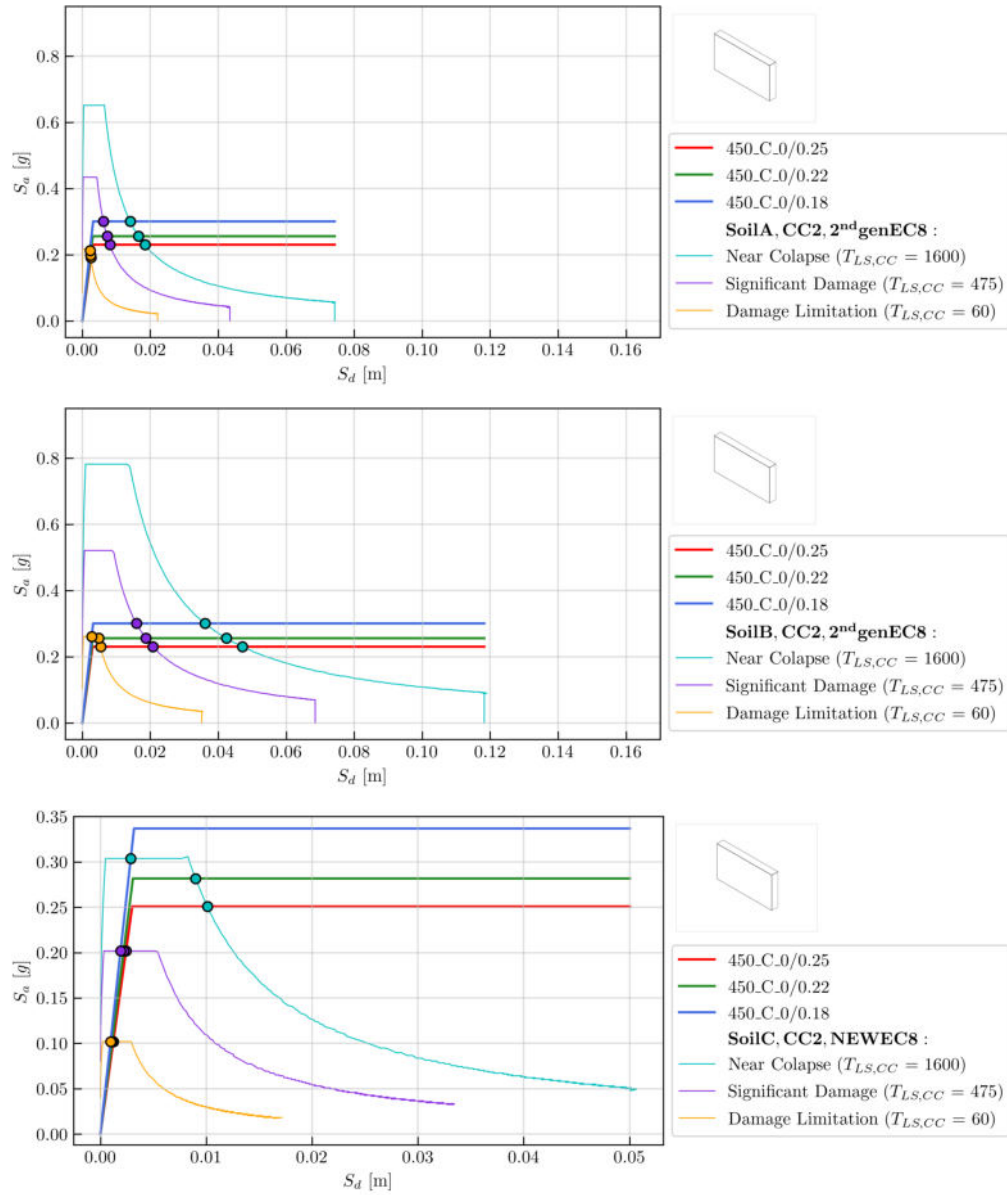


Figure 8.66: Superposition with new response spectrum: 450_C_0

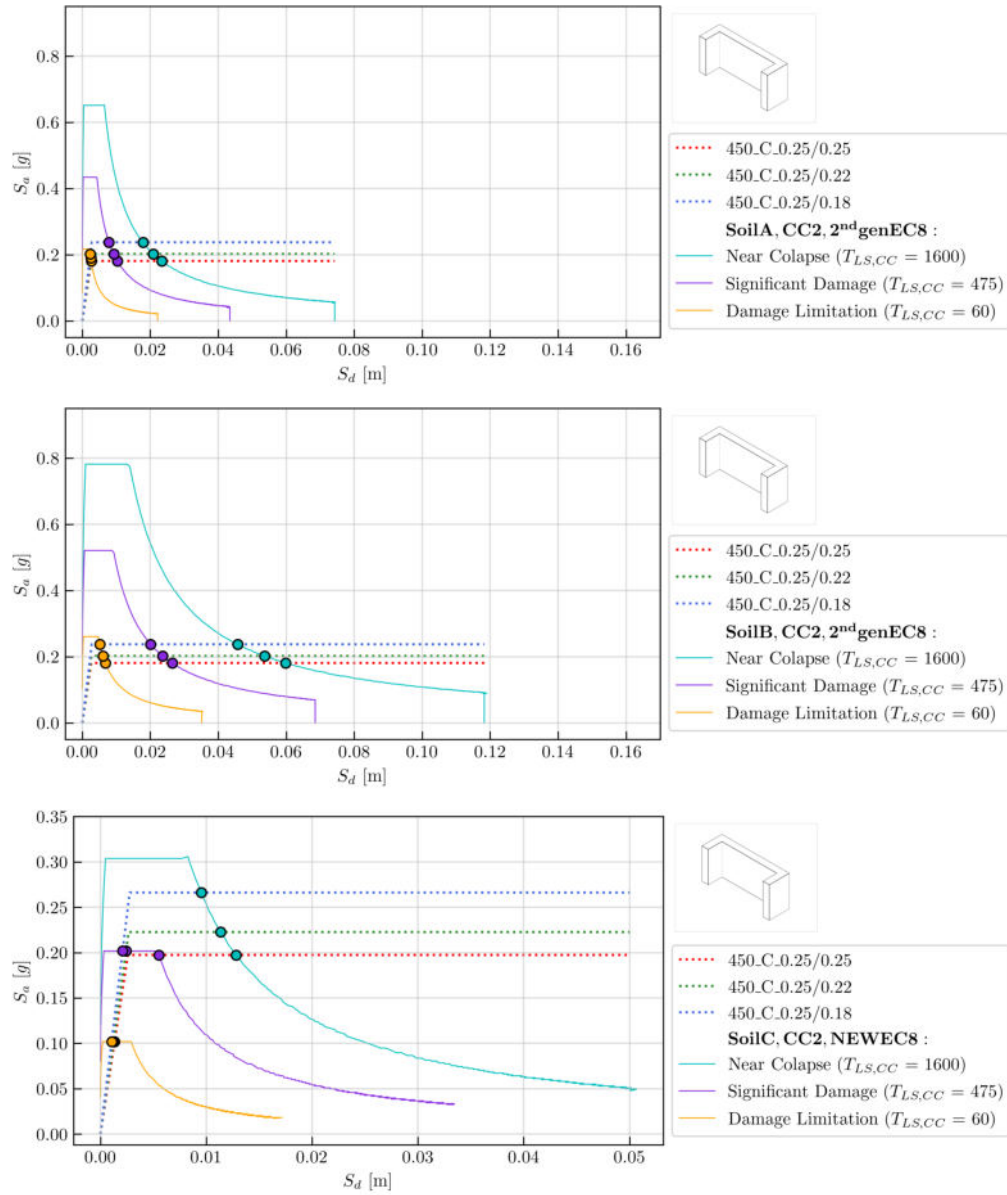


Figure 8.67: Superposition with new response spectrum: 450_C_0.25

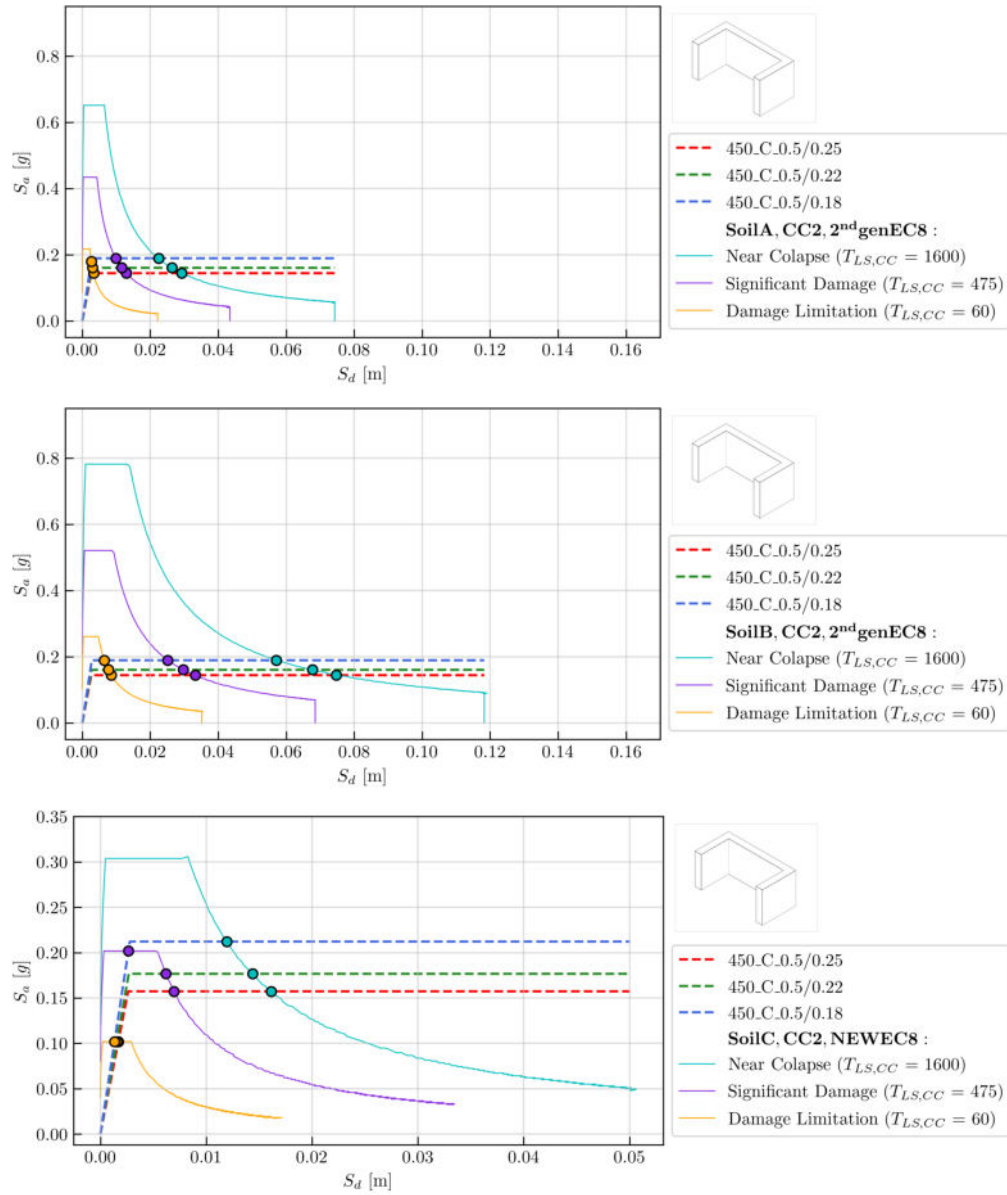


Figure 8.68: Superposition with new response spectrum: 450_C_0.5

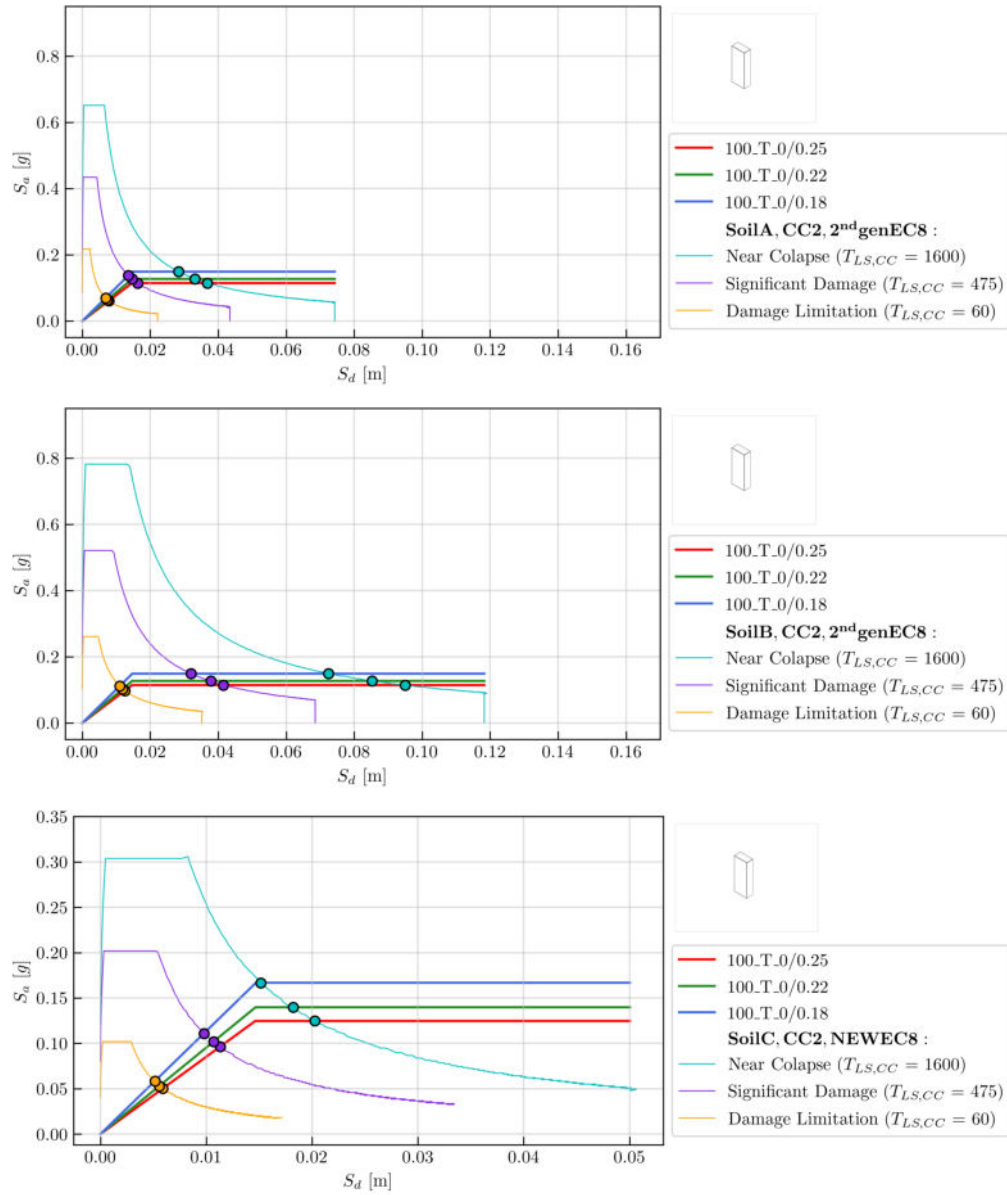


Figure 8.69: Superposition with new response spectrum: 100_T_0

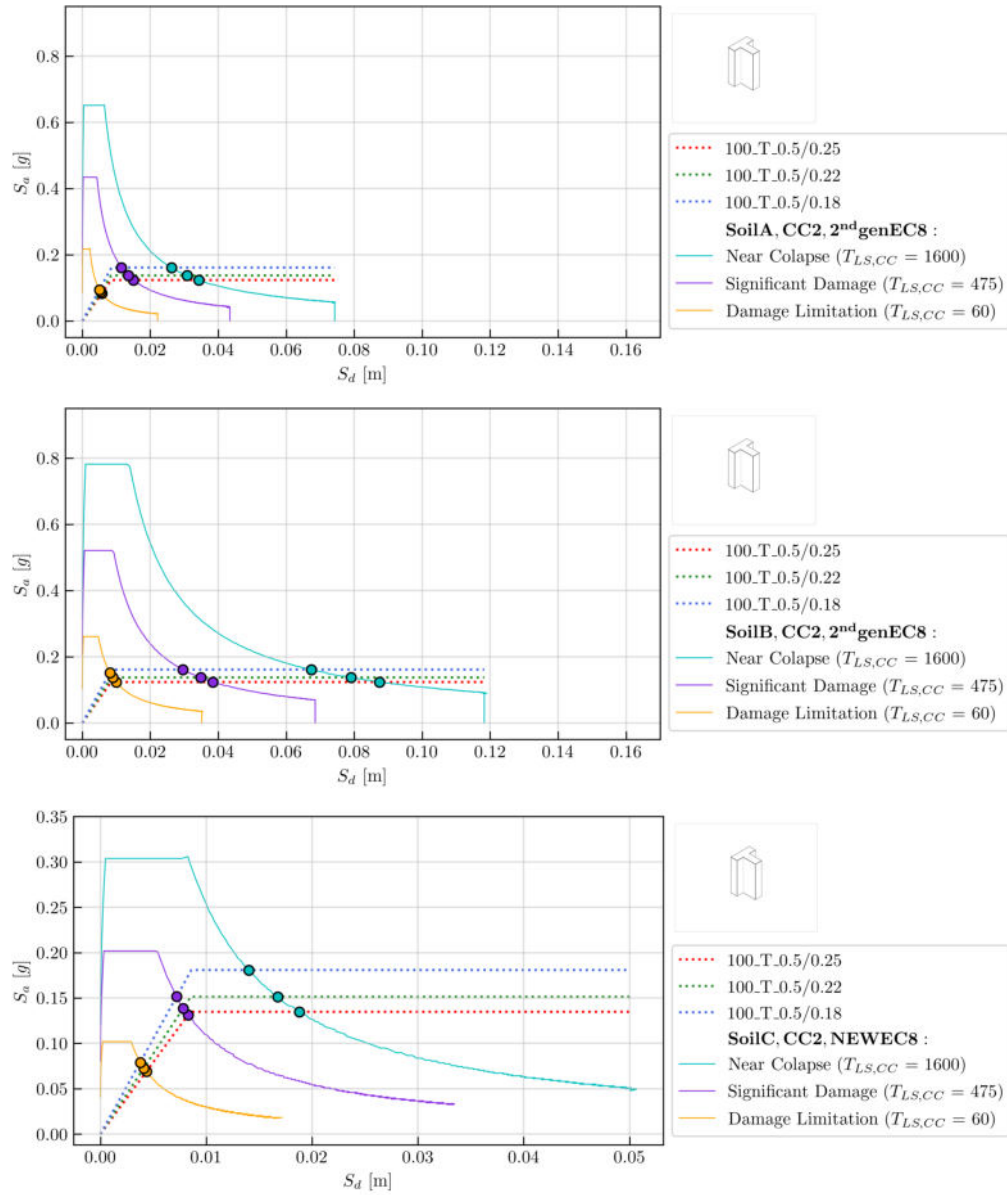


Figure 8.70: Superposition with new response spectrum: 100_T_0.5

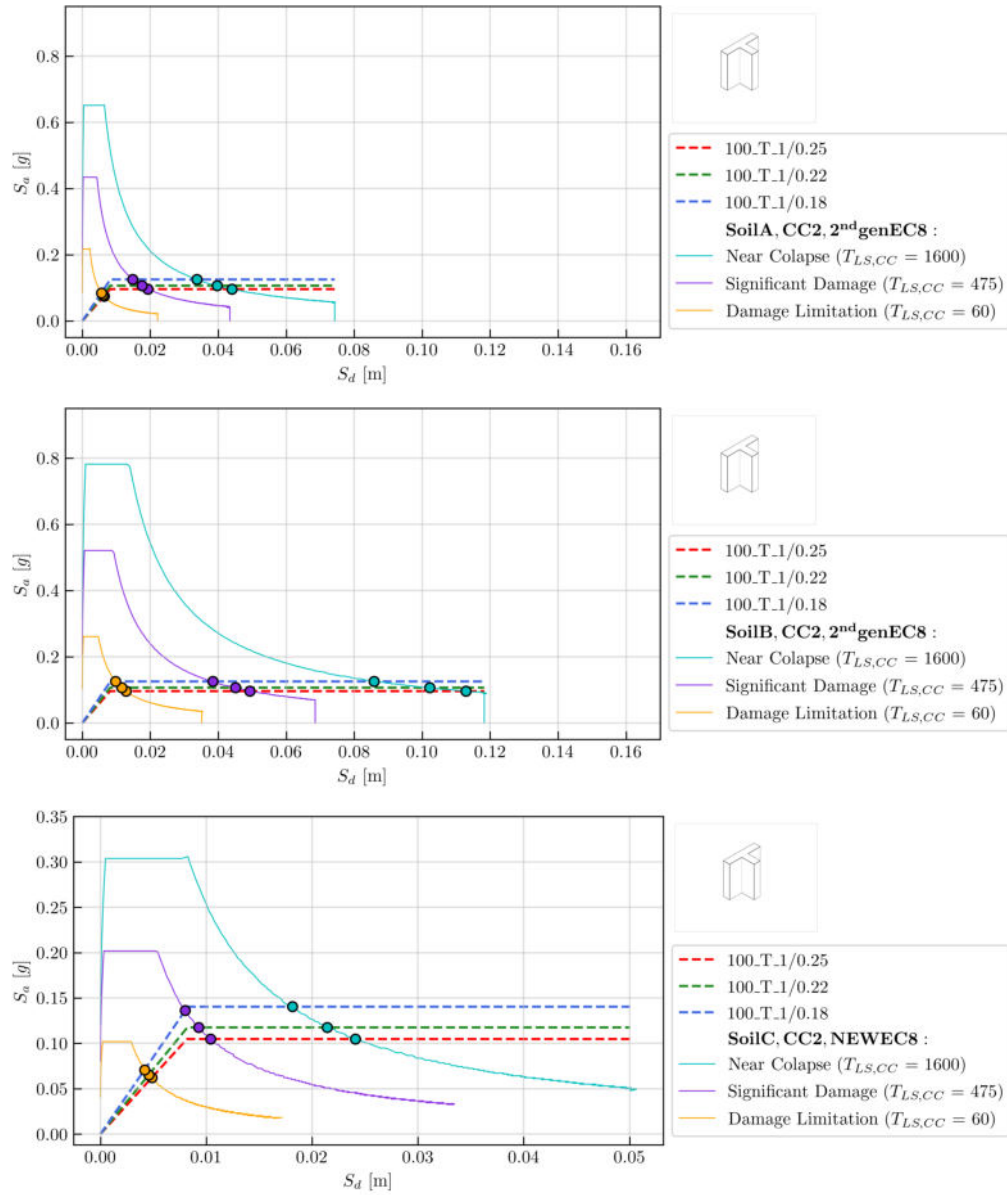


Figure 8.71: Superposition with new response spectrum: 100_T_1

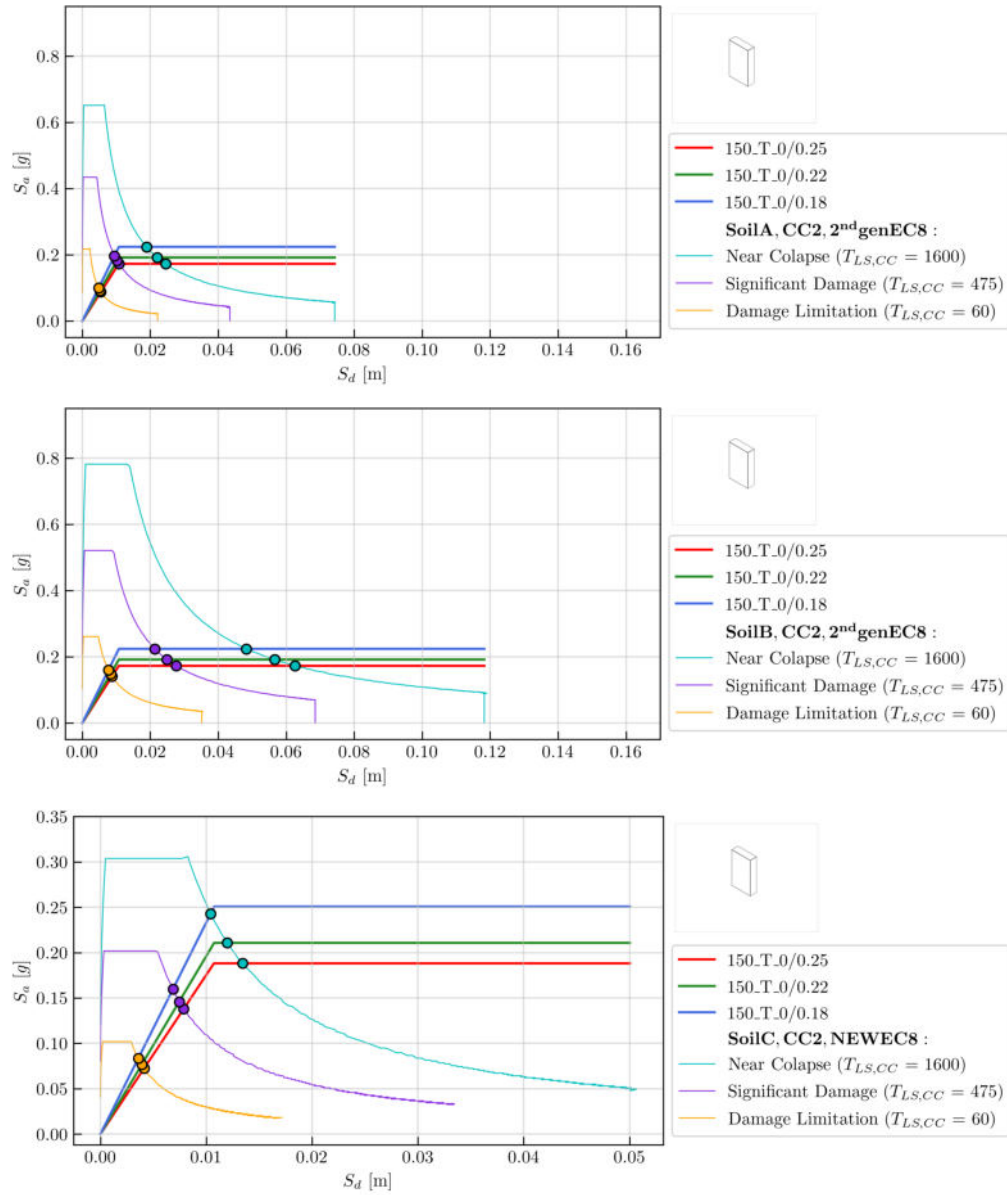


Figure 8.72: Superposition with new response spectrum: 150_T_0

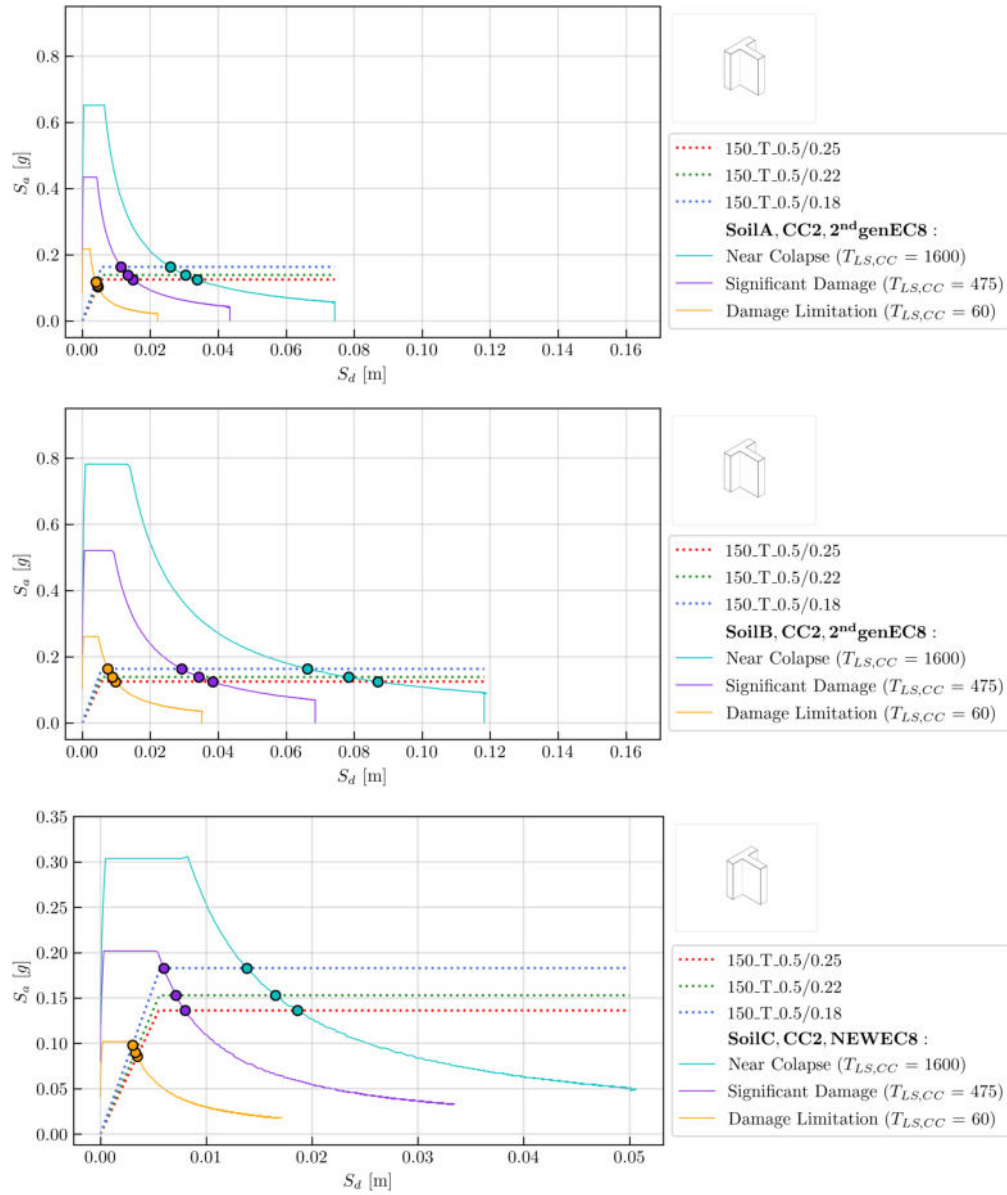


Figure 8.73: Superposition with new response spectrum: 150_T_0.5

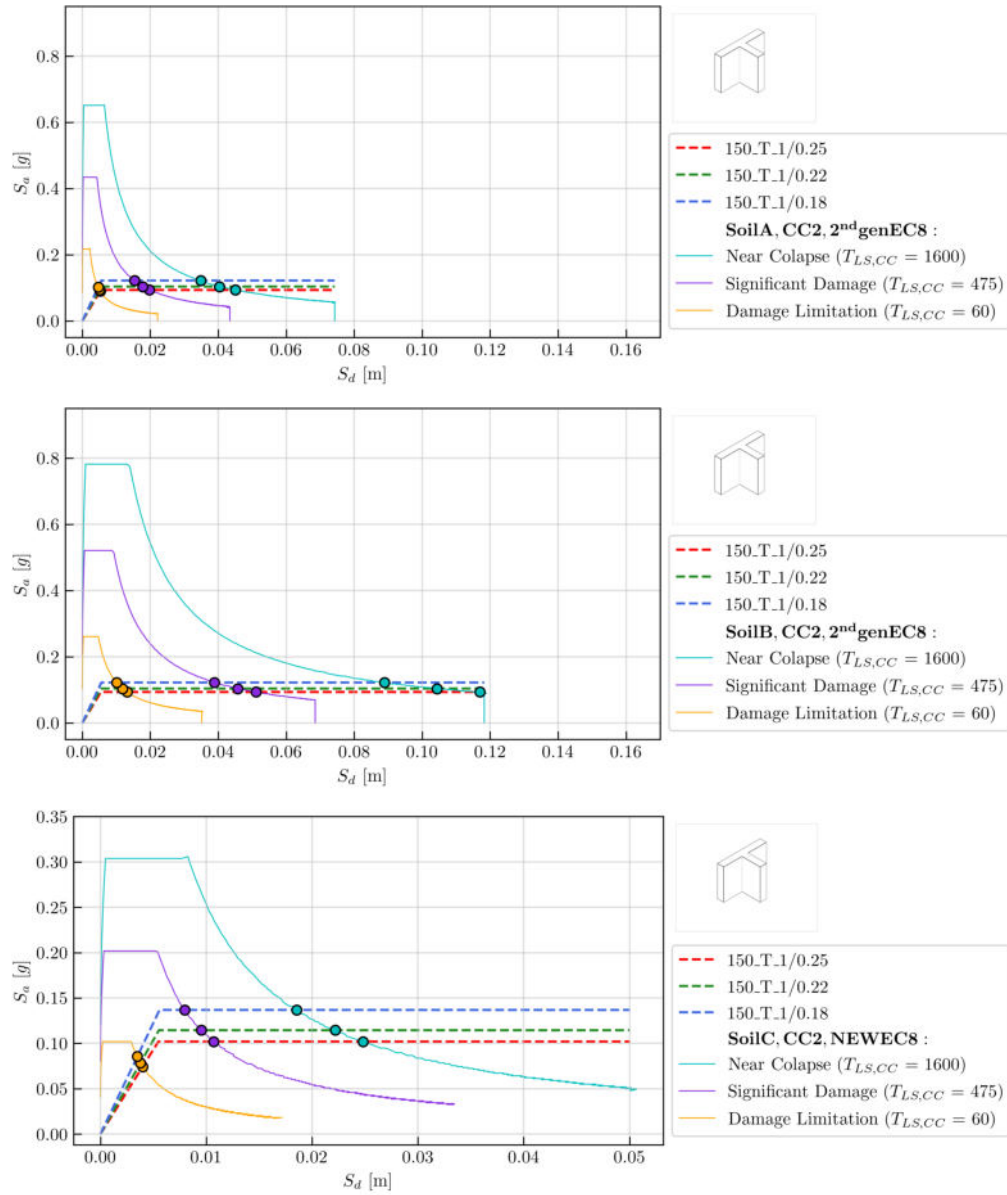


Figure 8.74: Superposition with new response spectrum: 150_T_1

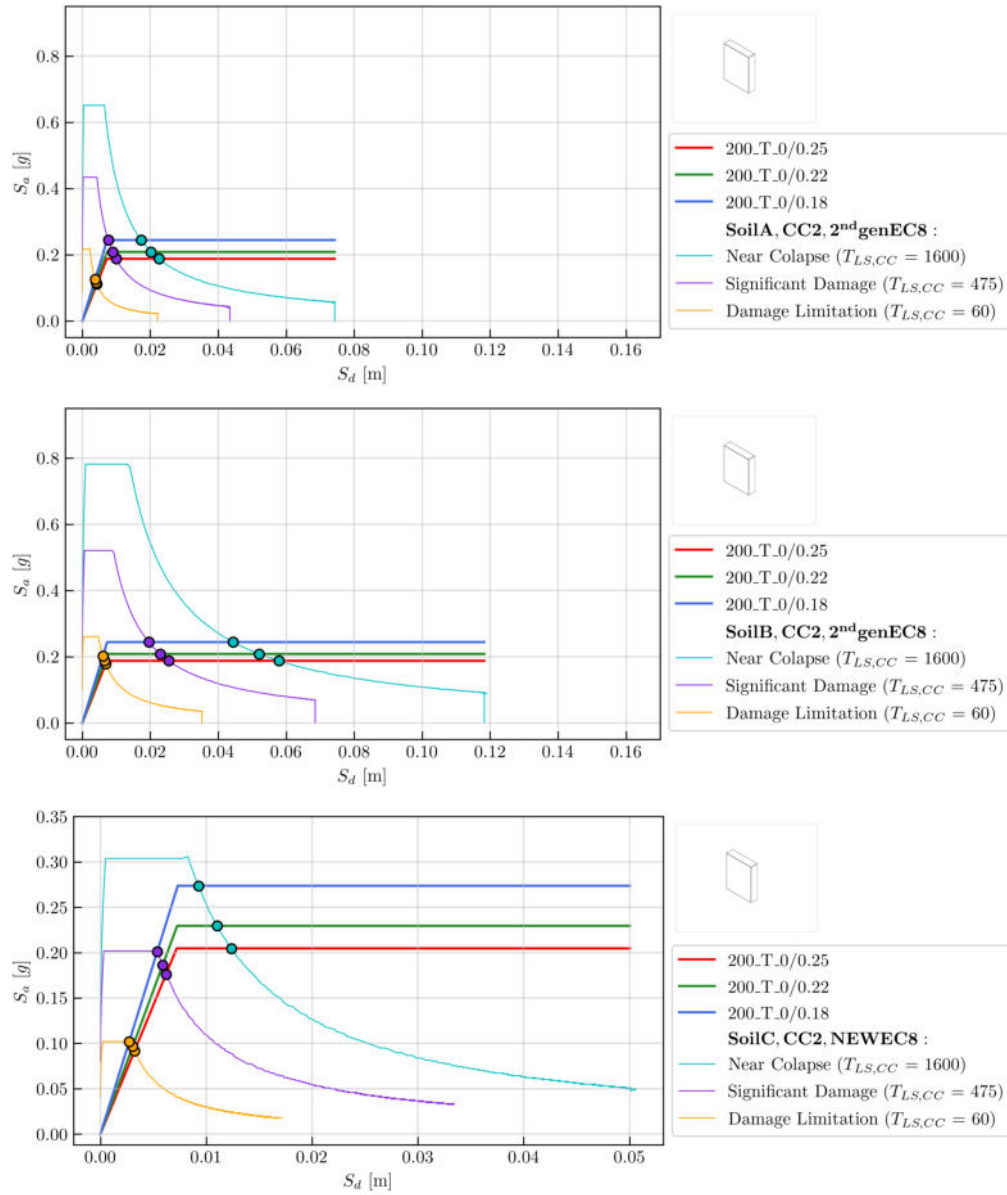


Figure 8.75: Superposition with new response spectrum: 200_T_0

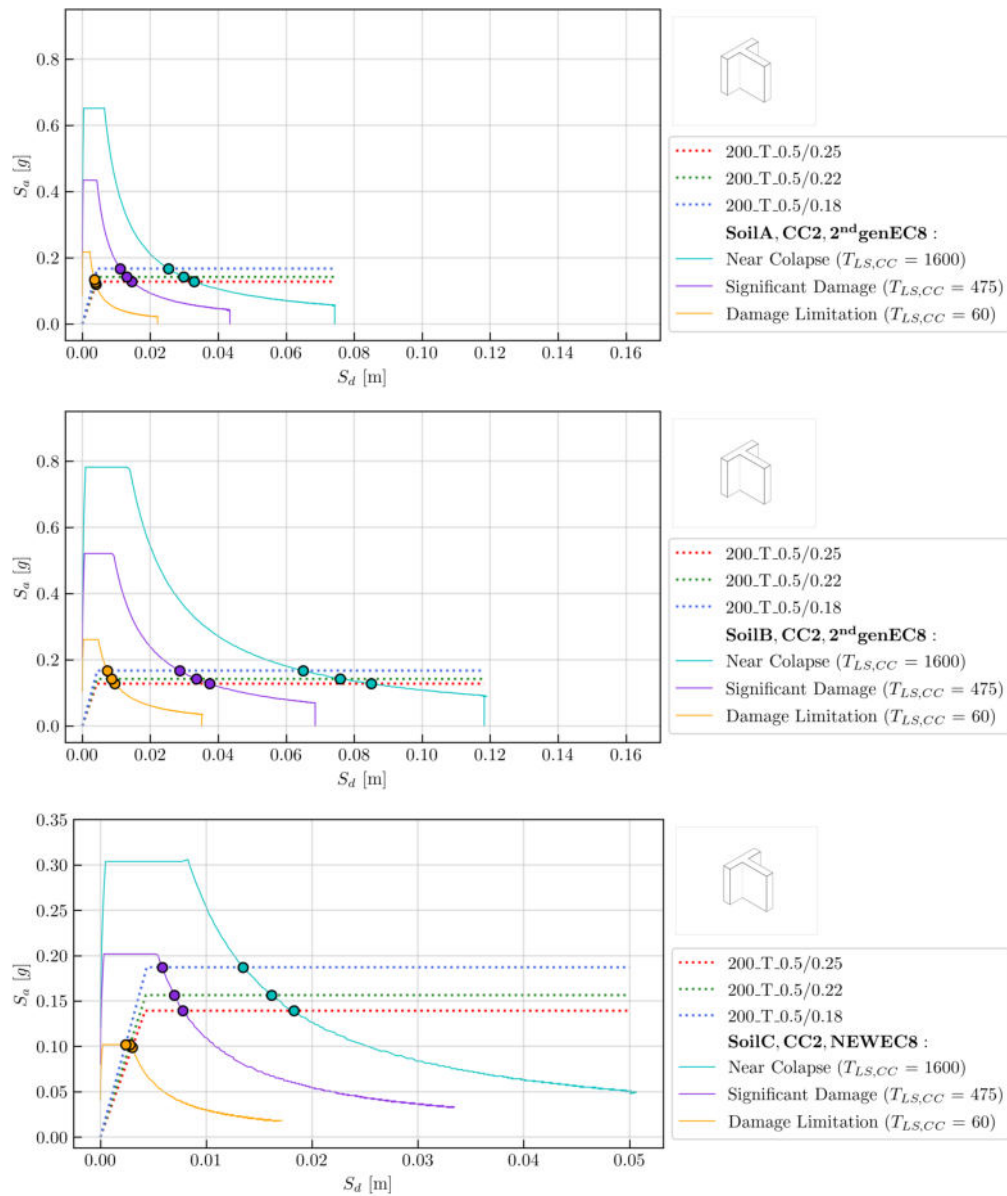


Figure 8.76: Superposition with new response spectrum: 200_T_0.5

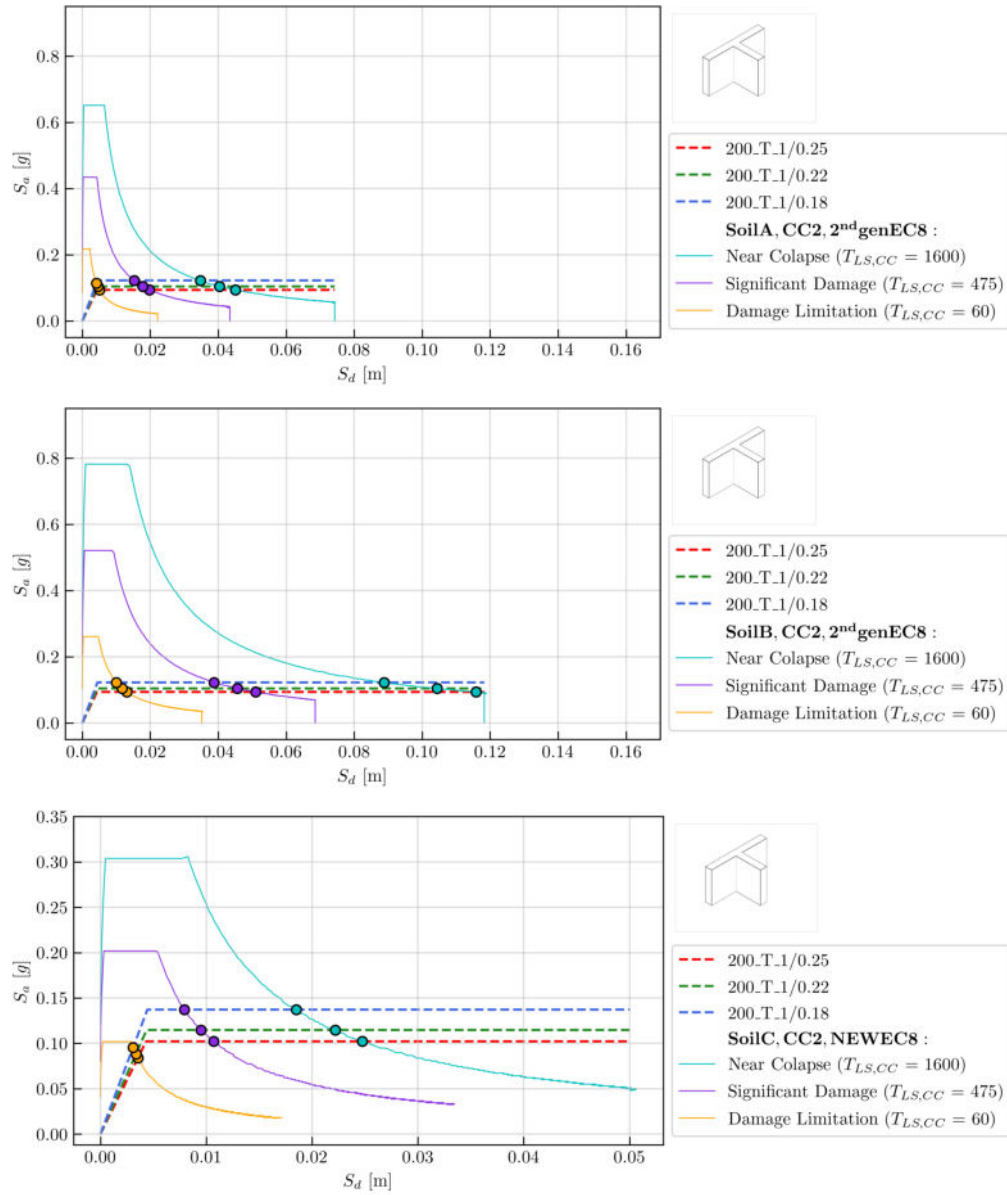


Figure 8.77: Superposition with new response spectrum: 200_T_1

Bibliography

- C. E. 12390-2:2019. *Testing hardened concrete - Part 2: Making and curing specimens for strength tests*. 2019.
- B. 1377-2:1990. *BS 1377-2:1990 British Standard Methods of test for Soils for civil engineering purposes - Part 2: Classification tests*. 1990.
- H. E. I. 14688-2. *Geotehničko istraživanje i ispitivanje – Identifikacija i klasifikacija tla – 2. dio: Načela klasifikacije (ISO 14688-2:2017; EN ISO 14688-2:2018)*. 2018.
- H. E. I. 17892-1:2015. *Geotechnical investigation and testing – Laboratory testing of soil – Part 1: Determination of water content (ISO 17892-1:2015; EN ISO 17892-1:2015)*. 2015.
- H. E. I. 17892-4:2016. *Geotechnical investigation and testing – Laboratory testing of soil – Part 4: Determination of Particle Size Distribution (ISO 17892-4:2016; EN ISO 17892-4:2016)*. 2016.
- B. E. 196-1:2005. *Methods of Testing Cement. Determination of Strength. British Standards Institution*. 2005.
- E. 1998-1. *Eurocode 8 - Design of structures for earthquake resistance. Part 1: general rules, seismic actions and rules for buildings*. 2004.
- A. D. 2487-17. *Standard Practice for Classification of Soils for Engineering Purposes (Unified Soil Classification System)*. 2017.
- A. S. 6836-02. *Standard Test Methods for Determination of the Soil Water Characteristic Curve for Desorption Using a Hanging Column, Pressure Extractor, Chilled Mirror Hygrometer, and/or Centrifuge*. 2008.

- H. N. Abhilash and J.-C. Morel. *Stress–Strain Characteristics of Unstabilised Rammed Earth*, pages 203–214. Springer Singapore, 2019. ISBN 978-981-13-5883-8. doi: 10.1007/978-981-13-5883-8_18.
- H. N. Abhilash, E. Hamard, C. T. S. Beckett, J.-C. Morel, H. Varum, D. Silveira, I. Ioannou, and R. Illampas. Mechanical behaviour of earth building materials. In A. Fabbri, J.-C. Morel, J.-E. Aubert, Q.-B. Bui, D. Gallipoli, and B. V. V. Reddi, editors, *Testing and Characterisation of Earth-based Building Materials and Elements*, State-of-the-Art Report of the RILEM TC 274-TCE, pages 127–180. Springer, 2022. ISBN 978-3-030-83297-1. doi: <https://doi.org/10.1007/978-3-030-83297-1>.
- AIS. *Evaluation and Intervention of Heritage Buildings of One and Two Adobe Floor and Tapia Pisada*. 2002.
- R. Allahvirdizadeh, D. V. Oliveira, and R. A. Silva. Numerical modeling of the seismic out-of-plane response of a plain and trm-strengthened rammed earth subassembly. *Engineering Structures*, 193:43–56, 2019. ISSN 0141-0296. doi: <https://doi.org/10.1016/j.engstruct.2019.05.022>.
- P. J. Alley. *Rammed Earth Construction*. New Zealand Engineering, June 10, 582., 1948.
- ANSYS. Ansys mechanical theory reference. Version: 2022 R1.
- A. ao Brasileira de Normas Técnicas. *NBR 13553: Materiais para emprego em parede monolítica de solo-cimento sem função estrutural*. ABNT Rio de Janeiro, 1996.
- H. Araki, J. Koseki, and T. Sato. Tensile strength of compacted rammed earth materials. *Soils and Foundations*, 56(2):189–204, 2016. ISSN 0038-0806. doi: <https://doi.org/10.1016/j.sandf.2016.02.003>.
- E. Araldi, E. Vincens, A. Fabbri, and J.-P. Plassiard. Identification of the mechanical behaviour of rammed earth including water content influence. *Materials and Structures*, 51(88), 2018. doi: 10.1617/s11527-018-1203-2.

- A. Arrigoni, A.-C. Grillet, R. Pelosato, G. Dotelli, C. T. Beckett, M. Woloszyn, and D. Ciancio. Reduction of rammed earth's hygroscopic performance under stabilisation: an experimental investigation. *Building and Environment*, 115:358–367, 2017a. ISSN 0360-1323. doi: <https://doi.org/10.1016/j.buildenv.2017.01.034>.
- A. Arrigoni, R. Pelosato, G. Dotelli, C. T. Beckett, and D. Ciancio. Weathering's beneficial effect on waste-stabilised rammed earth: a chemical and microstructural investigation. *Construction and Building Materials*, 140:157–166, 2017b. ISSN 0950-0618. doi: <https://doi.org/10.1016/j.conbuildmat.2017.02.009>.
- M. E. Arslan, M. Emiroglu, and A. Yalama. Structural behavior of rammed earth walls under lateral cyclic loading: A comparative experimental study. *Construction and Building Materials*, 133:433–442, 2017. ISSN 0950-0618. doi: <https://doi.org/10.1016/j.conbuildmat.2016.12.093>.
- I. Arto, J. Garrido, and M. L. Gutiérrez-Carrillo. Seismic vulnerability analysis of medieval rammed earth fortifications in southeastern Spain. *Bulletin of Earthquake Engineering*, 18:5827–5858, 2020. ISSN 2352-7102. doi: <https://doi.org/10.1007/s10518-020-00912-1>.
- A. S. Arya. *Guidelines for Earthquake Resistant Design, Construction and Retrofitting of Buildings in Afghanistan*. UNCRD Hyogo Office, Kobe, 2003.
- A. S. Arya, T. Boen, and Y. Ishiyama. *Guidelines for earthquake resistant non-engineered construction*. UNESCO: United Nations Educational, Scientific and Cultural Organization,, 2014. ISBN 978-92-3-000032-5. URL <https://unesdoc.unesco.org/ark:/48223/pf0000229059>.
- J.-E. Aubert, P. Faria, P. Maillard, K. A. J. Ouedraogo, C. Ouellet-Plamondon, and E. Prud'homme. Characterization of earth used in earth construction materials. In A. Fabbri, J.-C. Morel, J.-E. Aubert, Q.-B. Bui, D. Gallipoli, and B. V. Reddi, editors, *Testing and Characterisation of Earth-based Building Materials and Elements*, State-of-the-Art Report of the RILEM TC 274-TCE, pages 17–82. Springer, 2022. ISBN 978-3-030-83297-1. doi: <https://doi.org/10.1007/978-3-030-83297-1>.

- C. Augarde. Soil mechanics and earthen construction: strength and mechanical behaviour. In M. R. Hall, R. Lindsay, and M. Krayenhoff, editors, *Modern Earth Buildings*, Woodhead Publishing Series in Energy, pages 204–221. Woodhead Publishing, 2012. ISBN 978-0-85709-026-3. doi: <https://doi.org/10.1533/9780857096166.2.204>.
- F. Ávila, E. Puertas, and R. Gallego. Characterization of the mechanical and physical properties of unstabilized rammed earth: A review. *Construction and Building Materials*, 270:121435, 2021. doi: <https://doi.org/10.1016/j.conbuildmat.2020.121435>.
- F. Ávila, E. Puertas, and R. Gallego. Mechanical characterization of lime-stabilized rammed earth: Lime content and strength development. *Construction and Building Materials*, 350:128871, 2022. ISSN 0950-0618. doi: <https://doi.org/10.1016/j.conbuildmat.2022.128871>.
- E. C. Avrami, H. Guillaud, and M. Hardy. *Terra Literature Review: An Overview of Earthen Architecture Conservation*. Getty Conservation Institute, 2008.
- V. Baleca, R. Barsotti, S. Bennati, and D. V. Oliveira. Experimental investigation of in-plane loaded timber-framed rammed earth panels. part ii: Cyclic shear-compression tests. *Structures*, 58:104671, 2023. ISSN 2352-0124. doi: <https://doi.org/10.1016/j.istruc.2023.06.002>.
- N. Barrera, D. M. Ruiz, J. C. Reyes, Y. A. Alvarado, and D. Carrasco-Beltrán. Seismic performance of a 1:4 scale two-story rammed earth model reinforced with steel plates tested on a bi-axial shaking table. *Buildings*, 13(12), 2023. ISSN 2075-5309. doi: [10.3390/buildings13122950](https://doi.org/10.3390/buildings13122950).
- R. Barsotti, S. Bennati, and D. V. Oliveira. Experimental investigation of in-plane loaded timber-framed rammed earth panels. part i: Monotonic shear-compression tests. *Structures*, 58:105311, 2023. ISSN 2352-0124. doi: <https://doi.org/10.1016/j.istruc.2023.105311>.
- C. Beckett and C. Augarde. The effect of relative humidity and temperature on the unconfined compressive strength of rammed earth. In C. Mancuso, C. Jommi, and

- F. D’Onza, editors, *Unsaturated Soils: Research and Applications*, pages 287–292. Springer Berlin Heidelberg, 2012.
- C. T. S. Beckett, C. E. Augarde, D. Easton, and T. Easton. Strength characterisation of soil-based construction materials. *Géotechnique*, 68(5):400–409, 2018. doi: 10.1680/jgeot.16.P.288.
- A. Brandis. *Doprinos nelinearnom statičkom potresnom proračunu plitko temeljenih zgrada uzimanjem u obzir međudjelovanja tla i konstrukcije*. PhD thesis, Josip Juraj Strossmayer University of Osijek, Faculty of Civil Engineering and Architecture Osijek, 2022.
- Q. Bui, J. Morel, B. Venkatarama Reddy, and W. Ghayad. Durability of rammed earth walls exposed for 20 years to natural weathering. *Building and Environment*, 44(5):912–919, 2009a. ISSN 0360-1323. doi: <https://doi.org/10.1016/j.buildenv.2008.07.001>.
- Q.-B. Bui and J.-C. Morel. Assessing the anisotropy of rammed earth. *Construction and Building Materials*, 23(9):3005–3011, 2009. ISSN 0950-0618. doi: <https://doi.org/10.1016/j.conbuildmat.2009.04.011>.
- Q.-B. Bui and J.-C. Morel. First exploratory study on the ageing of rammed earth material. *Materials*, 8(1):1–15, 2015. ISSN 1996-1944. doi: 10.3390/ma8010001.
- Q.-B. Bui, J.-C. Morel, S. Hans, and N. Meunier. Compression behaviour of non-industrial materials in civil engineering by three scale experiments: the case of rammed earth. *Materials and Structures*, 42(8):1101–1116, 2009b. ISSN 1871-6873. doi: 10.1617/s11527-008-9446-y.
- Q.-B. Bui, S. Hans, J.-C. Morel, and A.-P. Do. First exploratory study on dynamic characteristics of rammed earth buildings. *Engineering Structures*, 33(12):3690–3695, 2011a. ISSN 0141-0296. doi: <https://doi.org/10.1016/j.engstruct.2011.08.004>.
- Q.-B. Bui, S. Hans, J.-C. Morel, and V. Mollion. Influence of water on the mechanical characteristics of rammed-earth material. *Structural Repairs and Maintenance of Heritage Architecture*, 118(XII):565–576, 2011b. doi: 10.2495/STR110471.

- Q.-B. Bui, J.-C. Morel, S. Hans, and P. Walker. Effect of moisture content on the mechanical characteristics of rammed earth. *Construction and Building Materials*, 54:163–169, 2014a. ISSN 0950-0618. doi: <https://doi.org/10.1016/j.conbuildmat.2013.12.067>.
- Q.-B. Bui, T.-T. Bui, and A. Limam. Assessing the seismic performance of rammed earth walls by using discrete elements. *Cogent Engineering*, 3(1):1200835, 2016. doi: [10.1080/23311916.2016.1200835](https://doi.org/10.1080/23311916.2016.1200835).
- Q.-B. Bui, A. Limam, and T.-T. Bui. Dynamic discrete element modelling for seismic assessment of rammed earth walls. *Engineering Structures*, 175:690–699, 2018. ISSN 0141-0296. doi: <https://doi.org/10.1016/j.engstruct.2018.08.084>.
- Q.-B. Bui, T.-T. Bui, M.-P. Tran, T.-L. Bui, and H.-A. Le. Assessing the seismic behavior of rammed earth walls with an l-form cross-section. *Sustainability*, 11(5), 2019. ISSN 2071-1050. doi: [10.3390/su11051296](https://doi.org/10.3390/su11051296).
- Q.-B. Bui, R. El-Nabouch, L. Miccoli, J.-C. Morel, D. V. Oliveira, R. A. Silva, D. Silveira, H. Varum, and F. Vieux-Champagne. Seismic assessment of earthen structures. In A. Fabbri, J.-C. Morel, J.-E. Aubert, Q.-B. Bui, D. Gallipoli, and B. V. Reddi, editors, *Testing and Characterisation of Earth-based Building Materials and Elements*, State-of-the-Art Report of the RILEM TC 274-TCE, pages 181–210. Springer, 2022. ISBN 978-3-030-83297-1. doi: <https://doi.org/10.1007/978-3-030-83297-1>.
- T.-L. Bui, T.-T. Bui, Q.-B. Bui, X.-H. Nguyen, and A. Limam. Out-of-plane behavior of rammed earth walls under seismic loading: Finite element simulation. *Structures*, 24:191–208, 2020. ISSN 2352-0124. doi: <https://doi.org/10.1016/j.istruc.2020.01.009>.
- T.-T. Bui, Q.-B. Bui, A. Limam, and S. Maximilien. Failure of rammed earth walls: From observations to quantifications. *Construction and Building Materials*, 51: 295–302, 2014b. ISSN 0950-0618. doi: <https://doi.org/10.1016/j.conbuildmat.2013.10.053>.
- T.-T. Bui, Q.-B. Bui, A. Limam, and J.-C. Morel. Modeling rammed earth wall using

- element method. *Continuum Mechanics and Thermodynamics*, 28:523–5368, 2017. ISSN 1432-0959. doi: <https://doi.org/10.1007/s00161-015-0460-3>.
- G. M. Calvi. A displacement-based approach for vulnerability evaluation of classes of buildings. *Journal of Earthquake Engineering*, 3(3):411–438, 1999. doi: 10.1080/13632469909350353.
- E. C. Carvalho. Seismic testing of structures. In P. Bisch, P. Labbe, and A. Pecker, editors, *Proceeding of the 11th European Conference on Earthquake Engineering*, 1998.
- F. Champiré, A. Fabbri, J.-C. Morel, H. Wong, and F. McGregor. Impact of relative humidity on the mechanical behavior of compacted earth as a building material. *Construction and Building Materials*, 110:70–78, 2016. ISSN 0950-0618. doi: <https://doi.org/10.1016/j.conbuildmat.2016.01.027>. URL <https://www.sciencedirect.com/science/article/pii/S0950061816300289>.
- P. Chauhan, A. El Hajjar, N. Prime, and O. Plé. Unsaturated behavior of rammed earth: Experimentation towards numerical modelling. *Construction and Building Materials*, 227:116646, 2019. ISSN 0950-0618. doi: <https://doi.org/10.1016/j.conbuildmat.2019.08.027>.
- P. Chauhan, N. Prime, and O. Plé. Benefit of unsaturated soil mechanics approach on the modeling of early-age behavior of rammed earth building. *Materials*, 15(1), 2022. ISSN 1996-1944. doi: 10.3390/ma15010362.
- T. Chitimbo, F. Abdul-Samad, N. Prime, and O. Plé. Hydro-mechanics coupling on rammed earth material: Drying experiment at structural scale. *Construction Technologies and Architecture*, 1:698–706, 2022. ISSN 2674-1237.
- A. Chourasia, S. Singhal, and P. Bhargava. Damage limitation and structural behaviour factor for masonry structures. *Australian Journal of Structural Engineering*, 22(1):19–28, 2021. doi: 10.1080/13287982.2021.1872978.
- D. Ciancio, P. Jaquin, and P. Walker. Advances on the assessment of soil suitability for rammed earth. *Construction and Building Materials*, 42:40–47, 2013. ISSN 0950-0618. doi: <https://doi.org/10.1016/j.conbuildmat.2012.12.049>.

- D. Ciancio, C. Beckett, and J. Carraro. Optimum lime content identification for lime-stabilised rammed earth. *Construction and Building Materials*, 53:59–65, 2014. ISSN 0950-0618. doi: <https://doi.org/10.1016/j.conbuildmat.2013.11.077>.
- P. CIT 9, Laboratório Nacional de Engenharia Civil Lisbon. *The use of earth as a building material (in Portuguese)*. 1953.
- M. de Obras Públicas y Transportes (MOPT). *Bases para el diseño y construcción con tapial*. Secretaría General Técnica, Madrid, Spain, 1992.
- M. Delgado and I. Guerrero. The selection of soils for unstabilised earth building: A normative review. *Construction and Building Materials*, 21:237–251, 2007. doi: 10.1016/j.conbuildmat.2005.08.006.
- A. Dialmy, M. Rguig, and M. Meliani. Optimization of the granular mixture of natural rammed earth using compressible packing model. *Sustainability*, 15(3), 2023. ISSN 2071-1050. doi: 10.3390/su15032698.
- P. Doat, A. Hays, H. Houben, S. Matuk, and F. Vitoux. *Construire en terre, Grenoble, France: CRATerre—Centre de Recherché et d’Application-Terre*. École d’Architecture de Grenoble, France, 1979.
- R. El Nabouch. *Mechanical behavior of rammed earth walls under Pushover tests*. Phd theses, Université Grenoble Alpes, 2017. URL <https://theses.hal.science/tel-01707009>.
- R. El-Nabouch, Q. B. Bui, P. Perrotin, O. Plé, and J. P. Plassiard. Numerical modeling of rammed earth constructions: analysis and recommendations. *Academic Journal of Civil Engineering*, 33(2):72–79, 2015. doi: 10.26168/icbbm2015.10.
- R. El-Nabouch, Q. Bui, O. Plé, P. Perrotin, C. Poinard, T. Goldin, and J. Plassiard. Seismic assessment of rammed earth walls using pushover tests. *Procedia Engineering*, 145:1185–1192, 2016. ISSN 1877-7058. doi: <https://doi.org/10.1016/j.proeng.2016.04.153>. ICSDEC 2016 – Integrating Data Science, Construction and Sustainability.
- R. El-Nabouch, Q.-B. Bui, O. Plé, and P. Perrotin. Assessing the in-plane seismic performance of rammed earth walls by using horizontal loading tests. *Engineering*

- Structures*, 145:153–161, 2017. ISSN 0141-0296. doi: <https://doi.org/10.1016/j.engstruct.2017.05.027>.
- R. El-Nabouch, Q.-B. Bui, O. Plé, and P. Perrotin. Characterizing the shear parameters of rammed earth material by using a full-scale direct shear box. *Construction and Building Materials*, 171:414–420, 2018. ISSN 0950-0618. doi: <https://doi.org/10.1016/j.conbuildmat.2018.03.142>.
- D. L. e.V. *Lehmbau Regeln - Begriffe Baustoffe Bauteile*. Vieweg+Teubner, 3rd ed. Wiesbaden, Germany, 2009.
- I. O. for Standardization (ISO). *ISO 376 - Metallic materials—Calibration of force-proving instruments used for the verification of uniaxial testing machines*. 2012.
- B. François, L. Palazon, and P. Gerard. Structural behaviour of unstabilized rammed earth constructions submitted to hygroscopic conditions. *Construction and Building Materials*, 155:164–175, 2017. ISSN 0950-0618. doi: <https://doi.org/10.1016/j.conbuildmat.2017.08.012>.
- P. Gerard, M. Mahdad, A. Robert McCormack, and B. François. A unified failure criterion for unstabilized rammed earth materials upon varying relative humidity conditions. *Construction and Building Materials*, 95:437–447, 2015. ISSN 0950-0618. doi: <https://doi.org/10.1016/j.conbuildmat.2015.07.100>.
- L. M. Gil-Martín, M. A. Fernández-Ruiz, and E. Hernández-Montes. Mechanical characterization and elastic stiffness degradation of unstabilized rammed earth. *Journal of Building Engineering*, 56:104805, 2022. ISSN 2352-7102. doi: <https://doi.org/10.1016/j.jobe.2022.104805>.
- M. I. Gomes, M. Lopes, and J. de Brito. Seismic resistance of earth construction in portugal. *Engineering Structures*, 33(3):932–941, 2011. ISSN 0141-0296. doi: <https://doi.org/10.1016/j.engstruct.2010.12.014>.
- M. I. Gomes, T. D. Gonçalves, and P. Faria. Unstabilized rammed earth: Characterization of material collected from old constructions in south portugal and comparison to normative requirements. *International Journal of Architectural Heritage*, 8(2):185–212, 2014. doi: 10.1080/15583058.2012.683133.

GOMmbH. *ARAMIS user manual—hardware*. 2007a.

GOMmbH. *ARAMIS user manual—software*. 2007b.

A. E. Hajjar, P. Chauhan, N. Prime, and O. Plé. Effect of suction on the mechanical characteristics of uniformly compacted rammed earth. *IOP Conference Series: Earth and Environmental Science*, 143(1):012045, 2018. doi: 10.1088/1755-1315/143/1/012045.

M. Hall and Y. Djerbib. Rammed earth sample production: context, recommendations and consistency. *Construction and Building Materials*, 18(4):281–286, 2004. ISSN 0950-0618. doi: <https://doi.org/10.1016/j.conbuildmat.2003.11.001>.

M. Hall, R. Lindsay, and M. Krayenhoff. Overview of modern earth building. In M. R. Hall, R. Lindsay, and M. Krayenhoff, editors, *Modern Earth Buildings*, Woodhead Publishing Series in Energy, pages 3–16. Woodhead Publishing, 2012. ISBN 978-0-85709-026-3. doi: <https://doi.org/10.1533/9780857096166.1.3>.

H. Harris and G. M. Sabnis. *Structural Modeling and Experimental Techniques*. CRC Press, 1999. ISBN 9780367802295. doi: <https://doi.org/10.1201/9780367802295>.

F. Hassan. *Architecture for the Poor – An Experiment in Rural Egypt*. Chicago and London, The University of Chicago Press, 1973.

M. Heinsdorf. Code or standard? Available online: www.csemag.com/articles/code-or-standard, July 2015. (Accessed: the 6th of December 2023).

H. Houben and H. Guillard. *Earth Construction: A comprehensive guide*. London: Intermediate Technology Publications, 1994. ISBN 185339193X.

S. Hračov, S. Pospíšil, A. Garofano, and S. Urushadze. In-plane cyclic behaviour of unfired clay and earth brick walls in both unstrengthened and strengthened conditions. *Materials and Structures*, 49:3293–3308, 2016. ISSN 1871-6873. doi: 10.1617/s11527-015-0720-5.

B. S. Institution. *BS 1377-4:1990 British Standard Methods of test for Soils for civil engineering purposes - Part 4: Compaction-related tests*. 1990.

- S. d. C. Instituto Nacional de Normalización. *Estructuras - Intervención de construcciones patrimoniales de tierra cruda - Requisitos del proyecto estructural (Structural design—retrofitting of historic earth buildings — requirements for the structural design planning)*. 2013.
- A. International. *Standard Guide for Design of Earthen Wall Building Systems: ASTM E2392/E2392 - 10*. West Conshohocken, PA, ASTM International, 2010.
- A. International. *Standard Test Methods for Cyclic (Reversed) Load Test for Shear Resistance of Vertical Elements of the Lateral Force Resisting Systems for Buildings ASTM E2126-19*. West Conshohocken, PA, ASTM International, 2019.
- ISO. *Standardisation and Related Activities - General Vocabulary: ISO Guide 2*. ISO, Geneva, Switzerland, 2004.
- P. Jaquin. History of earth building techniques. In M. R. Hall, R. Lindsay, and M. Krayenhoff, editors, *Modern Earth Buildings*, Woodhead Publishing Series in Energy, pages 307–323. Woodhead Publishing, 2012. ISBN 978-0-85709-026-3. doi: <https://doi.org/10.1533/9780857096166.3.307>.
- P. Jaquin and C. Augarde. *EARTH BUILDING: History, science and conservation*. IHS BRE Press, 2012. ISBN 978-1-84806-192-7.
- P. A. Jaquin. *Analysis of historic rammed earth construction*. PhD thesis, Durham University, 2008.
- P. A. Jaquin, C. E. Augarde, D. Gallipoli, and D. Toll. The strength of unstabilised rammed earth materials. *Géotechnique*, 59(5):487–490, 2009. ISSN 1751-7656. doi: <https://doi.org/10.1680/geot.2007.00129>.
- R. C. Jonathan Knappett. *Craig’s Soil Mechanics*. Spon Press, Taylor and Francis Group, 8th ed., 2012. ISBN 978-0-203-86524-8.
- J. Kaluder, I. Kraus, A. Perić, and L. Kraus. Shear strength of reproduced soil mixtures based on samples from rammed earth walls from eastern croatia. *Applied Sciences*, 12(22), 2022. ISSN 2076-3417. doi: 10.3390/app122211708.

- J. Keable and R. Keable. *Rammed Earth Structures: A Code of Practice*. Practical Action Publishing, 1996. ISBN 9781853397271.
- L. Keefe. *Earth Building: Methods and Materials, Repair and Conservation*. Taylor and Francis, London, UK, 1st ed., 2005. doi: <https://doi.org/10.4324/9780203342336>.
- M. Kosarimovahhed and V. Toufigh. Sustainable usage of waste materials as stabilizer in rammed earth structures. *Journal of Cleaner Production*, 277:123279, 2020. ISSN 0959-6526. doi: <https://doi.org/10.1016/j.jclepro.2020.123279>.
- A. Kossa. Analytical strain solution for the drucker-prager elastoplasticity model with linear isotropic hardening. *Periodica Polytechnica Mechanical Engineering*, 56:27–31, 2012. doi: 10.3311/pp.me.2012-1.05.
- A. Koutous and E. Hilali. Reinforcing rammed earth with plant fibers: A case study. *Case Studies in Construction Materials*, 14:e00514, 2021. ISSN 2214-5095. doi: <https://doi.org/10.1016/j.cscm.2021.e00514>.
- A. Koutous and E. Hilali. Compression stress-strain curve of rammed earth: Measuring and modelling. *Results in Engineering*, 18:101012, 2023. ISSN 2590-1230. doi: <https://doi.org/10.1016/j.rineng.2023.101012>.
- T. Krahn. *Essential Rammed Earth Construction: The Complete Step-by-Step Guide*. New Society Publishers, 2019. ISBN 9780865718579.
- I. Kraus, A. Perić, J. Kaluđer, L. Kraus, P. Krolo, M. Domazetović, D. Iljkić, I. Varga, I. Brkanić Mihić, and M. Grubišić. Rammed earth for modelling and standardization in seismically active areas: the re-forms project. In C. Arion, A. Scupin, and Țiganescu, editors, *3rd EUROPEAN CONFERENCE ON EARTHQUAKE ENGINEERING SEISMOLOGY*, 2022.
- P. Labbé and R. Paolucci. Developments relating to seismic action in the eurocode 8 of next generation. In C. Arion, A. Scupin, and Țiganescu, editors, *3rd EUROPEAN CONFERENCE ON EARTHQUAKE ENGINEERING SEISMOLOGY*, 2022.

- D. M. Liley and J. Robinson. Ultimate strength of rammed earth walls with openings. *Proceedings of the Institution of Civil Engineers - Structures and Buildings*, 110(3):278–287, 1995. doi: 10.1680/istbu.1995.27872.
- H. Lin, S. Zheng, S. D. Lourenço, and P. Jaquin. Characterization of coarse soils derived from igneous rocks for rammed earth. *Engineering Geology*, 228:137–145, 2017. ISSN 0013-7952. doi: <https://doi.org/10.1016/j.enggeo.2017.08.003>.
- K. Liu, Y. A. Wang, and M. Wang. Experimental and numerical study of enhancing the seismic behavior of rammed earth buildings. In *Advanced Construction Technologies*, volume 919 of *Advanced Materials Research*, pages 925–931. Trans Tech Publications Ltd, 6 2014. doi: 10.4028/www.scientific.net/AMR.919-921.925.
- Q. Liu and L. Tong. Engineering properties of unstabilized rammed earth with different clay contents. *Journal of Wuhan University of Technology-Mater. Sci. Ed.*, 32:914–920, 2017. doi: 10.1007/s11595-017-1690-y.
- F. Loccarini, G. Ranocchiali, T. Rotunno, and M. Fagone. Experimental and numerical analyses of strengthened rammed earth masonry arches. *Computers Structures*, 239:106329, 2020. ISSN 0045-7949. doi: <https://doi.org/10.1016/j.compstruc.2020.106329>.
- S. Lončar-Vicković and D. Stober. *Tradicijska kuća Slavonije i Baranje*. Ministarstvo turizma Republike Hrvatske, Sveučilište Josipa Jurja Strossmayera u Osijeku, Građevinski fakultet Osijek, 2011. URL https://mint.gov.hr/UserDocsImages/arhiva/150514_Slavonija_Baranja.pdf.
- A. E. Losini, T. Chitimbo, L. Létévé, M. Wolostyn, A. C. Grillet, and N. Prime. Hygrothermal characterization of rammed earth according to humidity variations. *E3S Web of Conferences*, 382, 2023. doi: <https://doi.org/10.1051/e3sconf/202338223004>.
- V. Maniatidis and P. Walker. *A Review of Rammed Earth Construction for DTi Partners in Innovation Project ‘Developing Rammed Earth for UK Housing’*. Natural Building Technology Group, Department of Architecture Civil Engineering, University of Bath, Bath, UK, 2003.

- V. Maniatidis and P. Walker. Structural capacity of rammed earth in compression. *Journal of Materials in Civil Engineering*, 20(3):230–238, 2008. doi: 10.1061/(ASCE)0899-1561(2008)20:3(230).
- P. G. McHenry. *Adobe and Rammed Earth Buildings. Design and Construction*. A Wiley-Interscience Publication, New York, USA, 1984.
- L. Miccoli, U. Müller, and P. Fontana. Mechanical behaviour of earthen materials: A comparison between earth block masonry, rammed earth and cob. *Construction and Building Materials*, 61:327–339, 2014. ISSN 0950-0618. doi: <https://doi.org/10.1016/j.conbuildmat.2014.03.009>.
- L. Miccoli, D. V. Oliveira, R. A. Silva, U. Müller, and L. Schueremans. Static behaviour of rammed earth: experimental testing and finite element modelling. *Materials and Structures*, 48:3443–3456, 2015. ISSN 1871-6873. doi: <https://doi.org/10.1617/s11527-014-0411-7>.
- L. Miccoli, A. Drougkas, and U. Müller. In-plane behaviour of rammed earth under cyclic loading: Experimental finite element modelling. *Engineering Structures*, 125:144–152, 2016. ISSN 0141-0296. doi: <https://doi.org/10.1016/j.engstruct.2016.07.010>.
- L. Miccoli, U. Müller, and S. Pospíšil. Rammed earth walls strengthened with polyester fabric strips: Experimental analysis under in-plane cyclic loading. *Construction and Building Materials*, 149:29–36, 2017. ISSN 0950-0618. doi: <https://doi.org/10.1016/j.conbuildmat.2017.05.115>.
- T. Michiels, R. Napolitano, S. Adriaenssens, and B. Glisic. Comparison of thrust line analysis, limit state analysis and distinct element modeling to predict the collapse load and collapse mechanism of a rammed earth arch. *Engineering Structures*, 148:145–156, 2017. ISSN 0141-0296. doi: <https://doi.org/10.1016/j.engstruct.2017.06.053>.
- G. F. Middleton. *Earth Wall Construction*. Bull. 5, North Ryde, NSW Australia, CSIRO Division of Building, Construction and Engineering, 4th ed., 1995 (revised 1987 by Schneider, L. M.).

- G. Minke. *Construction manual for earthquake-resistant houses built of earth*. GATE BASIN at GTZ GmbH, 2001.
- G. Minke. *Building with Earth: Design and Technology of a Sustainable Architecture*. Birkhäuser Basel, 2006. doi: <https://doi.org/10.1007/3-7643-7873-5>.
- A. Mirjalili, A. Eslami, and R. Morshed. Experimental investigation into the effect of vertical loading on in-plane cyclic behavior of adobe walls. *Construction and Building Materials*, 264:120706, 2020. ISSN 0950-0618. doi: <https://doi.org/10.1016/j.conbuildmat.2020.120706>.
- G. Misseri and L. Rovero. Rammed earth as bi-modulus material: experimental and analytical investigations through euler-bernoulli and timoshenko beam models. *Int. J. Masonry Research and Innovation*, 7(5), 2022.
- H. W. Morris. Natural disasters and earth buildings: resistant design and construction. In M. R. Hall, R. Lindsay, and M. Krayenhoff, editors, *Modern Earth Buildings*, Woodhead Publishing Series in Energy, pages 481–537. Woodhead Publishing, 2012. ISBN 978-0-85709-026-3. doi: <https://doi.org/10.1533/9780857096166.1.3>.
- B. Mužíková, T. Otcovská Plaček, and P. Pavel. Modulus of elasticity of unfried rammed earth. *Acta Polytechnica CTU Proceedings*, 15:63–68, 2018. doi: <https://doi.org/10.14311/APP.2018.15.0063>.
- U. Nations. Transforming our world: The 2030 agenda for sustainable development. Technical report, United Nations, 2015.
- T.-D. Nguyen, T.-T. Bui, A. Limam, T.-L. Bui, and Q.-B. Bui. Evaluation of seismic performance of rammed earth building and improvement solutions. *Journal of Building Engineering*, 43:103113, 2021. ISSN 2352-7102. doi: <https://doi.org/10.1016/j.jobbe.2021.103113>.
- J. Norton. *Building with Earth. A handbook*. Intermediate Technology Publications, London, UK, 2nd ed., 1997.

- H. Nowamooz and C. Chazallon. Finite element modelling of a rammed earth wall. *Construction and Building Materials*, 25(4):2112–2121, 2011. ISSN 0950-0618. doi: <https://doi.org/10.1016/j.conbuildmat.2010.11.021>.
- S. N. Z. (NZS). *NZS 4297: Engineering Design of Earth Buildings*. Wellington, New Zealand, 1998a.
- S. N. Z. (NZS). *NZS 4298: Materials and Workmanship For Earth Buildings, incorp. Amend. No. 1*. Wellington, New Zealand, 1998b.
- S. N. Z. (NZS). *NZS 4299: Earth Buildings Not Requiring Specific Design, incorp. Amend. No. 1*. Wellington, New Zealand, 1998c.
- E. B. A. of Australia (EBAA). *Building with Earth Bricks and Rammed Earth in Australia*. Wangaratta, Australia, EBAA, 2004.
- B. of Indian Standards (BIS). *IS 2110: Code of Practice for In Situ Construction of Walls in Buildings with Soil-cement*. Indian Standards, New Delhi, 1980, reaff. 1998.
- B. of Indian Standards (BIS). *IS 13827: Improving Earthquake Resistance of Earthen Buildings - Guidelines*. Indian Standards, New Delhi, 1993, reaff. 1998.
- N. B. of Standards and Metrology. *NBC 204:1994 Guidelines for earthquake resistant building construction: earthen building*. Nepal National Building Code, 2015.
- C. I. D. of the Regulation and Licensing. *New Mexico Earthen Building Materials Code, CID-GCB-NMBC-14.7.4*. Santa Fe NM., 2006.
- S. B. C. of the Republic of Kyrgyzstan/Gosstroj of Kyrgyzstan. *RBN-2-87: Building of low-storied houses with stabilised rammed earth*. Republic Building Norms, Frunse (Bischkek), Republic of Kyrgyzstan, 1988.
- C. C. of Tuscan. *Uniform Administrative Code Amendment for Earthen Material and Straw Bale Structures*. Tucson/Pima County, Arizona -appendix chapter 71 - Earthen materials and structures, 1997.
- S. A. of Zimbabwe. *SAZS 724: Rammed Earth Structures*. Zimbabwe Standard Code of Practice, Harare, Zimbabwe, 2001.

- J. Ortega, G. Vasconcelos, H. Rodrigues, and M. Correia. Assessment of the influence of horizontal diaphragms on the seismic performance of vernacular buildings. *Bulletin of Earthquake Engineering*, 16:3871–3904, 2018. ISSN 1573-1456. doi: <https://doi.org/10.1007/s10518-018-0318-8>.
- M. Pakand and V. Toufigh. A multi-criteria study on rammed earth for low carbon buildings using a novel anp-ga approach. *Energy and Buildings*, 150:466–476, 2017. ISSN 0378-7788. doi: <https://doi.org/10.1016/j.enbuild.2017.06.004>.
- G. Pavić. *Unaprjedenje metodologije procjene potresnog rizika za zgrade*. PhD thesis, Josip Juraj Strossmayer University of Osijek, Faculty of Cifil Engineering and Architecture Osijek, 2023.
- A. Pelé-Peltier, A. Fabbri, J.-C. Morel, E. Hamard, and M. Lhenry. A similitude relation to assessing the compressive strength of rammed earth from scale-down samples. *Case Studies in Construction Materials*, 16:e00921, 2022. ISSN 2214-5095. doi: <https://doi.org/10.1016/j.cscm.2022.e00921>.
- A. Perić, I. Kraus, J. Kaluđer, and L. Kraus. Experimental campaigns on mechanical properties and seismic performance of unstabilized rammed earth—a literature review. *Buildings*, 11(8), 2021. ISSN 2075-5309. doi: [10.3390/buildings11080367](https://doi.org/10.3390/buildings11080367).
- A. Perić Fekete, I. Kraus, M. Grubišić, and T. Dokšanović. In-plane seismic performance of rammed earth walls: an eastern croatia reconnaissance based study. *Bulletin of Earthquake Engineering*, 22:1359–1385, 2024. ISSN 1573-1456. doi: [10.1007/s10518-023-01826-4](https://doi.org/10.1007/s10518-023-01826-4).
- S. Petry and K. Beyer. Scaling unreinforced masonry for reduced-scale seismic testing. *Bulletin of Earthquake Engineering*, 12:2557–2581, 2014. ISSN 1573-1456. doi: [10.1007/s10518-014-9605-1](https://doi.org/10.1007/s10518-014-9605-1).
- H. Porter, J. Blake, N. K. Dhami, and A. Mukherjee. Rammed earth blocks with improved multifunctional performance. *Cement and Concrete Composites*, 92:36–46, 2018. ISSN 0958-9465. doi: <https://doi.org/10.1016/j.cemconcomp.2018.04.013>.

- H. Rahardjo, A. Satyanaga, H. Mohamed, S. C. Yee Ip, and R. S. Shah. Comparison of soil–water characteristic curves from conventional testing and combination of small-scale centrifuge and dew point methods. *Geotechnical and Geological Engineering*, 37:659–672, 2019. doi: [10.1007/s10706-018-0636-2](https://doi.org/10.1007/s10706-018-0636-2).
- M. Ramezanpour, A. Eslami, and H. Ronagh. Seismic performance of stabilised/unstabilised rammed earth walls. *Engineering Structures*, 245:112982, 2021. ISSN 0141-0296. doi: <https://doi.org/10.1016/j.engstruct.2021.112982>.
- L. N. Reddi, A. K. Jain, and H. B. Yun. Soil materials for earth construction: properties, classification and suitability testing. In M. R. Hall, R. Lindsay, and M. Krayenhoff, editors, *Modern Earth Buildings*, Woodhead Publishing Series in Energy, pages 155–171. Woodhead Publishing, 2012. ISBN 978-0-85709-026-3. doi: <https://doi.org/10.1533/9780857096166.1.3>.
- B. V. V. Reddy, J.-C. Morel, P. Faria, P. Fontana, D. V. Oliveira, I. Serclerat, P. Walker, and P. Maillard. Codes and standards on earth construction. In A. Fabbrì, J.-C. Morel, J.-E. Aubert, Q.-B. Bui, D. Gallipoli, and B. V. Reddy, editors, *Testing and Characterisation of Earth-based Building Materials and Elements*, State-of-the-Art Report of the RILEM TC 274-TCE, pages 243–259. Springer, 2022. ISBN 978-3-030-83297-1. doi: <https://doi.org/10.1007/978-3-030-83297-1>.
- J. C. Reyes, L. E. Yamin, W. M. Hassan, J. D. Sandoval, C. D. Gonzalez, and F. A. Galvis. Shear behavior of adobe and rammed earth walls of heritage structures. *Engineering Structures*, 174:526–537, 2018. ISSN 0141-0296. doi: <https://doi.org/10.1016/j.engstruct.2018.07.061>.
- J. C. Reyes, J. P. Smith-Pardo, L. E. Yamin, F. A. Galvis, J. D. Sandoval, C. D. Gonzalez, and J. F. Correal. In-plane seismic behavior of full-scale earthen walls with openings retrofitted with timber elements and vertical tensors. *Bulletin of Earthquake Engineering*, 17(11):4193–4215, 2019. doi: <https://doi.org/10.1007/s10518-019-00601-8>.
- A. Romanazzi, D. V. Oliveira, R. Silva, A. Barontini, and N. Mendes. Performance of rammed earth subjected to in-plane cyclic displacement. *Materials and Structures*, 55, 2022a. doi: <https://doi.org/10.1617/s11527-022-01894-z>.

- A. Romanazzi, D. V. Oliveira, R. Silva, P. X. Candeias, A. C. Costa, and A. Carvalho. Out-of-plane shake table test of a rammed earth sub-assembly. *Bulletin of Earthquake Engineering*, 20:8325–8356, 2022b. ISSN 1573-1456. doi: <https://doi.org/10.1007/s10518-022-01525-6>.
- A. Romanazzi, D. Oliveira, R. Silva, and A. Barontini. Effectiveness of a trm solution for rammed earth under in-plane cyclic loads. *Construction and Building Materials*, 407:133551, 2023. ISSN 0950-0618. doi: <https://doi.org/10.1016/j.conbuildmat.2023.133551>.
- SADCSTAN. *SADC harmonized standard for rammed earth structures – code of practice THC 03, SAZS 724*. African Organization for Standardization, 2014.
- M. Saidi, A. S. Cherif, B. Zeghmami, and E. Sediki. Stabilization effects on the thermal conductivity and sorption behavior of earth bricks. *Construction and Building Materials*, 167:566–577, 2018. ISSN 0950-0618. doi: <https://doi.org/10.1016/j.conbuildmat.2018.02.063>.
- M. Savor Novak, J. Atalić, M. Uroš, S. Prevolnik, and M. Nastev. Seismic risk reduction in croatia: mitigating the challenges and grasping the opportunities. In A. M. Ivanković and S. Lakušić, editors, *Future Trends in Civil Engineering 2019*, 2019.
- C. A. Schrader. Rammed earth construction: A re-emerging technology. In *6th Natural Passive Solar Conference held in 1981*, 1981.
- H. Schroeder. Moisture transfer and change in strength during the construction of earthen buildings. *Informes de la Construcción*, 63(523):107–116, 2011.
- H. Schroeder. Modern earth building codes, standards and normative development. In M. R. Hall, R. Lindsay, and M. Krayenhoff, editors, *Modern Earth Buildings*, Woodhead Publishing Series in Energy, pages 72–109. Woodhead Publishing, 2012. ISBN 978-0-85709-026-3. doi: <https://doi.org/10.1533/9780857096166.1.72>.
- H. Schroeder. *Sustainable Building with Earth*. Springer Cham, 2016. ISBN 978-3-319-37388-1. doi: <https://doi.org/10.1007/978-3-319-19491-2>.

- B. Sen and R. Saha. Experimental and numerical investigation of mechanical strength characteristics of natural fiber retrofitted rammed earth walls. *Geotextiles and Geomembranes*, 50(5):970–993, 2022. ISSN 0266-1144. doi: <https://doi.org/10.1016/j.geotexmem.2022.06.004>.
- L. SENCICO, Technical Building Standard. *Adobe. Reglamento Nacional de Construcciones (Adobe.National Building Standards of Peru)*. 2000.
- T. A. Shittu. Earth building norms and regulation: A review of nigerian building codes. In *LEHM 2008: Proceedings of the 5th International Conference on Earth Building*, pages 40–47, Weimar, Germany, 2008. Dachverband Lehm e.V.
- K. C. Shrestha, T. Aoki, M. Miyamoto, P. Wangmo, and Pema. In-plane shear resistance between the rammed earth blocks with simple interventions: Experimentation and finite element study. *Buildings*, 10(3), 2020a. ISSN 2075-5309. doi: [10.3390/buildings10030057](https://doi.org/10.3390/buildings10030057).
- K. C. Shrestha, T. Aoki, M. Miyamoto, P. Wangmo, Pema, J. Zhang, and N. Takahashi. Strengthening of rammed earth structures with simple interventions. *Journal of Building Engineering*, 29:101179, 2020b. ISSN 2352-7102. doi: <https://doi.org/10.1016/j.jobbe.2020.101179>.
- R. Silva, D. Oliveira, L. Schueremans, P. B. Lourenço, and T. Miranda. Modelling the structural behaviour of rammed earth components. *Civil-Comp Proceedings*, 106, 2014a. doi: [doi:10.4203/ccp.106.112](https://doi.org/10.4203/ccp.106.112).
- R. Silva, D. Oliveira, L. Schueremans, T. Miranda, and J. Machado. Effectiveness of the repair of unstabilised rammed earth with injection of mud grouts. *Construction and Building Materials*, 127:861–871, 2016a. ISSN 0950-0618. doi: <https://doi.org/10.1016/j.conbuildmat.2016.10.064>.
- R. Silva, D. Oliveira, L. Schueremans, T. Miranda, and J. Machado. Effectiveness of the repair of unstabilised rammed earth with injection of mud grouts. *Construction and Building Materials*, 127:861–871, 2016b. ISSN 0950-0618. doi: <https://doi.org/10.1016/j.conbuildmat.2016.10.064>.

- R. A. Silva, D. V. Oliveira, T. Miranda, N. Cristelo, M. C. Escobar, and E. Soares. Rammed earth construction with granitic residual soils: The case study of northern Portugal. *Construction and Building Materials*, 47:181–191, 2013. ISSN 0950-0618. doi: <https://doi.org/10.1016/j.conbuildmat.2013.05.047>.
- R. A. Silva, P. Jaquin, D. V. Oliveira, T. F. Miranda, L. Schueremans, and N. Cristelo. *Conservation and New Construction Solutions in Rammed Earth*, pages 77–108. Springer Berlin Heidelberg, 2014b. ISBN 978-3-642-39686-1. doi: 10.1007/978-3-642-39686-1_3.
- R. A. Silva, D. V. Oliveira, L. Miccoli, and L. Schueremans. Modelling of rammed earth under shear loading. In F. P. na M. Chávez, editor, *SAHC2014 – 9th International Conference on Structural Analysis of Historical Constructions*, 2014c.
- R. A. Silva, N. Mendes, D. V. Oliveira, A. Romanazzi, O. Domínguez-Martínez, and T. Miranda. Evaluating the seismic behaviour of rammed earth buildings from Portugal: From simple tools to advanced approaches. *Engineering Structures*, 157:144–156, 2018. ISSN 0141-0296. doi: <https://doi.org/10.1016/j.engstruct.2017.12.021>.
- D. Thompson, C. Augarde, and J. P. Osorio. A review of current construction guidelines to inform the design of rammed earth houses in seismically active zones. *Journal of Building Engineering*, 54:104666, 2022. ISSN 2352-7102. doi: <https://doi.org/10.1016/j.jobbe.2022.104666>.
- J. Tinsley and S. Pavía. Thermal performance and fitness of glacial till for rammed earth construction. *Journal of Building Engineering*, 24:100727, 2019. ISSN 2352-7102. doi: <https://doi.org/10.1016/j.jobbe.2019.02.019>.
- D. G. Toll. A framework for unsaturated soil behaviour. *Géotechnique*, 40(1):31–44, 1990. doi: 10.1680/geot.1990.40.1.31.
- D. G. Toll and B. H. Ong. Critical-state parameters for an unsaturated residual sandy clay. *Géotechnique*, 53(1):93–103, 2003. doi: 10.1680/geot.2003.53.1.93.
- M. Tomaževič. *Earthquake-resistant design of masonry buildings*. Imperial College Press, London, 2006. ISBN 9781848160835.

- M. Tomažević. Shear resistance of masonry walls and eurocode 6: shear versus tensile strength of masonry. *Materials and Structures*, 42:889–907, 2009. ISSN 1871-6873. doi: <https://doi.org/10.1617/s11527-008-9430-6>.
- V. Toufigh and E. Kianfar. The effects of stabilizers on the thermal and the mechanical properties of rammed earth at various humidities and their environmental impacts. *Construction and Building Materials*, 200:616–629, 2019. ISSN 0950-0618. doi: <https://doi.org/10.1016/j.conbuildmat.2018.12.050>.
- D. D. Tripura and K. D. Singh. Characteristic properties of cement-stabilized rammed earth blocks. *Journal of Materials in Civil Engineering*, 27(7), 2014. doi: [https://doi.org/10.1061/\(ASCE\)MT.1943-5533.0001170](https://doi.org/10.1061/(ASCE)MT.1943-5533.0001170).
- S. I. und Architekten-Verein SIA. *Regeln zum Bauen mit Lehm/Lehmbau-Atlas*. D 0111 + D 0112, Zurich, Switzerland, 1994.
- P. Walker. *Australian Earth Building Handbook - HB 195*. SAI Global Limited, Standards Australia, Sydney, Australia, 2002. ISBN 9781849770958.
- P. Walker, R. Keable, J. Martin, and V. Maniatidis. *Rammed earth: design and construction guidelines*. BRE Bookshop, 2005. ISBN 1-86081-734-3.
- P. Wangmo, K. C. Shrestha, M. Miyamoto, and T. Aoki. Assessment of out-of-plane behavior of rammed earth walls by pull-down tests. *International Journal of Architectural Heritage*, 13(2):273–287, 2019. doi: 10.1080/15583058.2018.1433903.
- P. Wangmo, K. C. Shrestha, and T. Aoki. Exploratory study of rammed earth walls under static element test. *Construction and Building Materials*, 266:121035, 2021. ISSN 0950-0618. doi: <https://doi.org/10.1016/j.conbuildmat.2020.121035>.
- B. V. Wilding and K. Beyer. Force–displacement response of in-plane loaded unreinforced brick masonry walls: the critical diagonal crack model. *Bulletin of Earthquake Engineering*, 15:2201–2240, 2017. doi: 10.1007/s10518-016-0049-7.
- L. Xu, K. K. Wong, A. Fabbri, F. Champiré, and D. Branque. Loading-unloading shear behavior of rammed earth upon varying clay content and relative humidity conditions. *Soils and Foundations*, 58(4):1001–1015, 2018. ISSN 0038-0806. doi: <https://doi.org/10.1016/j.sandf.2018.05.005>.

- M. Čaušević and M. Bulić. Proposal of response spectra in the second generation of eurocode en 1998-1-1 for seismic areas and comparison with the existing standard en 1998-1: 2004. *GRADEVINAR*, 72(10):2895–904, 2020. doi: 10.14256/JCE.2838.2019.
- M. Čaušević, S. Mitrović, and M. Bulić. Determination of seismic load for buildings using different response spectra and application on different methods of analysis. *Cogent Engineering*, 10(1):2220494, 2023. doi: 10.1080/23311916.2023.2220494.
- Španiček. Špiljski stanovi i gospodarski prostori u lesu na području baranje. *Studia Ethnologica*, 4:69–92, 1992.
- Z. Živković. *Hrvatsko tradicijsko graditeljstvo*. Ministarstvo kulture Republike Hrvatske, Uprava za zaštitu kulturne baštine, 2013.

